Dissertation at the
Graduate School of Systemic Neurosciences at the
Ludwig-Maximilians-Universität München

Graduate School of
Systemic Neurosciences
LMU Munich

The role of direction-selective visual interneurons T4 and T5 in *Drosophila* orientation behavior

Submitted by

Armin Bahl

21st of November 2014

First reviewer (supervisor)

Prof. Dr. Alexander Borst

Second reviewer

Prof. Dr. Andreas Herz

Date of oral defense

Munich, 27th of February 2015

For my family
and friends.

SUMMARY

In order to safely move through the environment, visually-guided animals use several types of visual cues for orientation. Optic flow provides faithful information about ego-motion and can thus be used to maintain a straight course. Additionally, local motion cues or landmarks indicate potentially interesting targets or signal danger, triggering approach or avoidance, respectively. The visual system must reliably and quickly evaluate these cues and integrate this information in order to orchestrate behavior. The underlying neuronal computations for this remain largely inaccessible in higher organisms, such as in humans, but can be studied experimentally in more simple model species. The fly *Drosophila*, for example, heavily relies on such visual cues during its impressive flight maneuvers. Additionally, it is genetically and physiologically accessible. Hence, it can be regarded as an ideal model organism for exploring neuronal computations during visual processing.

In my PhD studies, I have designed and built several autonomous virtual reality setups to precisely measure visual behavior of walking flies. The setups run in open-loop and in closed-loop configuration. In an open-loop experiment, the visual stimulus is clearly defined and does not depend on the behavioral response. Hence, it allows mapping of how specific features of simple visual stimuli are translated into behavioral output, which can guide the creation of computational models of visual processing. In closed-loop experiments, the behavioral response is fed back onto the visual stimulus, which permits characterization of the behavior under more realistic conditions and, thus, allows for testing of the predictive power of the computational models.

In addition, *Drosophila*'s genetic toolbox provides various strategies for targeting and silencing specific neuron types, which helps identify which cells are needed for a specific behavior. We have focused on visual interneuron types T4 and T5 and assessed their role in visual orientation behavior. These neurons build up a retinotopic array and cover the whole visual field of the fly. They constitute major output elements from the medulla and have long been speculated to be involved in motion processing.

This cumulative thesis consists of three published studies: In the first study, we silenced both T4 and T5 neurons together and found that such flies were completely blind to any kind of motion. In particular, these flies could not perform an optomotor response anymore, which means that they lost their normally innate following responses to motion of large-field moving patterns. This was an important finding as it ruled out the contribution of another system for motion vision-based behaviors. However, these flies were still able to fixate a black bar. We could show that this behavior is mediated by a T4/T5-independent flicker detection circuitry which exists in parallel to the motion system.

In the second study, T4 and T5 neurons were characterized via two-photon imaging, revealing that these cells are directionally selective and have very similar temporal and orientation tuning properties to direction-selective neurons in the lobula plate. T4 and T5 cells responded in a contrast polarity-specific manner: T4 neurons responded selectively to ON edge motion while T5 neurons responded only to OFF edge motion. When we blocked T4 neurons, behavioral responses to moving ON edges were more impaired than those to moving OFF edges and the opposite was true for the T5 block. Hence, these findings confirmed that the contrast polarity-specific visual motion pathways, which start at the level of L1 (ON) and L2 (OFF), are maintained within the medulla and that motion information is computed twice independently within each of these pathways.

Finally, in the third study, we used the virtual reality setups to probe the performance of an artificial microcircuit. The system was equipped with a camera and spherical fisheye lens. Images were processed by an array of Reichardt detectors whose outputs were integrated in a similar way to what is found in the lobula plate of flies. We provided the system with several rotating natural environments and found that the fly-inspired artificial system could accurately predict the axes of rotation.

DEUTSCHE ZUSAMMENFASSUNG

Um sich gerichtet und sicher in der Umgebung zu bewegen nutzen visuell geleitete Tiere verschiedene visuelle Reize zur Orientierung. Zum einen bietet der durch die Bewegung entstehende optische Fluss ausreichend Informationen um die Richtung der aktuellen Eigenbewegung zu ermitteln. Zum anderen deuten lokale Bewegungsreize oder die Wahrnehmung von Landmarken auf potentiell interessante Ziele hin und können dazu führen, dass das Tier sich auf die entsprechenden Objekte zubewegt. Dieselben Reize signalisieren möglicherweise aber auch Gefahr und sollten also zur gegenteiligen Verhaltensantwort führen, zur Flucht. Das visuelle System muss dabei schnell und zuverlässig die Situation bewerten und folglich alle Signale aus der Umgebung integrieren, daraus eine Entscheidung fällen und letztendlich die richtige Verhaltensantwort initiieren. Die Rechenoperationen, welche solchen Verarbeitungen zugrunde liegen, bleiben jedoch in höheren Organismen, wie zum Beispiel beim Menschen, weitgehend unzugänglich. Sie können allerdings auch an einfachen Modellen untersucht werden. Die Fliege *Drosophila*, zum Beispiel, ist eines davon. Während ihrer beindruckenden Flugmanöver verlässt sich die Fliege auf optische Informationen aus der Umgebung, ist gleichzeitig allerdings experimentell zugänglich.

In meiner Doktorarbeit habe ich mehrere voll-automatisierte Verhaltensapparaturen entworfen und gebaut, welche es erlauben, genaue Messungen des Laufverhaltens von Fliegen in einer künstlichen virtuellen Umgebung durchzuführen. Hier sind open-loop und sowie closed-loop Experimente möglich: In open-loop Experimenten ist der visuelle Stimulus klar definiert und unabhängig von der Verhaltensantwort. Damit lässt sich genau ermitteln, wie eine bestimmte Eigenschaft eines visuellen Reizes in ein Verhalten übersetzt wird. Aus solchen Beziehungen lassen sich Computermodelle der visuellen Verarbeitung genieren. In closed-loop Experimenten hingegen wird die Verhaltensantwort auf den visuellen Reiz rückgekoppelt. Dies lässt Studien des Systems unter natürlicheren Bedingungen zu und kann benutzt werden um die Vorhersagekraft der Modelle zu testen.

Weiterhin bietet *Drosophila* eine unglaubliche Vielzahl von genetischen Manipulationsmöglichkeiten. Diese ermöglichen ein gezieltes Ausschalten von bestimmen Nervenzelltypen, womit man deren Notwendigkeit für ein bestimmtes Verhalten untersuchen kann. Ich habe mich auf die Charakterisierung von visuellen Interneuronentypen T4 und T5 konzentriert um deren Rolle bei visuellem Orientierungsverhalten zu ermitteln. Diese Zellen bilden eine retinotope Struktur und decken das gesamte visuelle Feld der Fliege ab. Sie sind wesentliche Ausgangselemente der Medulla und werden seit langem für wichtige Elemente des Bewegungssehsystems gehalten.

Diese kumulative Dissertation besteht aus drei veröffentlichten Studien: In der ersten Studie habe ich sowohl T4 als auch T5 Zellen blockiert und gefunden, dass solche Fliegen vollständig blind für jede Art von Bewegung waren. Insbesondere waren die Fliegen nicht mehr im Stande eine optomoto-

rische Reaktion auszuführen, also der Bewegung eines Großfeldmusters zu folgen. Dies war ein wichtiges Ergebnis, da es zeigte, dass es kein anderes, möglicherweise redundantes System für die Verarbeitung von Bewegungsreizen gibt. Allerdings waren diese bewegungsblinden Fliegen immer noch in der Lage einen schwarzen Balken zu fixieren. Ich konnte zeigen, dass dieses Verhalten auf einem T4/T5-unabhängigen System beruht, welches lokale Helligkeitsänderungen erkennt und welches parallel zum Bewegungssehsystem implementiert ist.

In der zweiten Studie wurden die T4 und T5 Neuronen im Zwei-Photonen-Mikroskop charakterisiert und es wurde gefunden, dass diese Zellen bereits richtungsselektive Antworten aufweisen, deren Tuningeigenschaften (Muster Orientierung und zeitliche Kontrastfrequenz) sehr denen von richtungsselektive Zellen in der Lobula Platte ähneln. Weiterhin reagierten die Zellen spezifisch für Kontrastpolarität: T4 Neurone reagierten selektiv auf die Bewegung von hellen Kanten (ON), während T5 Zellen auf die Bewegungen von dunklen Kanten (OFF) reagierten. Als wir die Zellen genetisch blockierten waren entsprechende Defizite im Verhalte offensichtlich: Blockierten wir T4 Neurone, war die Verhaltensantwort auf helle Kanten mehr beeinträchtigt als auf dunkle Kanten, und beim T5 Block war dies genau umgekehrt. Diese Arbeit liefert also weitere Hinweise darauf, dass die Aufspaltung des Bewegungssehsystems in spezifische Kanäle für Kontrastpolarität, welche auf der Ebene der Lamina bei L1 (ON) bzw. L2 (OFF) beginnt, bis zu T4, bzw. T5 Zellen aufrechterhalten wird. Die Berechnung der Richtungsselektivität sollte also zweifach und kanalspezifisch zwischen L1 und T4, bzw. zwischen L2 und T5 stattfinden.

In der dritten Studie war ich am Testen eines Mikroprozessors beteiligt. Das System wurde mit einer Kamera und sphärischen Fischaugenlinse ausgestattet, die Bilder von einem Feld von Reichardt Detektoren analysiert und deren Ausgabewerte wurden so verschalten, wie man dies in der Lobula Platte der Fliege vorfindet. Das System wurde in der Mitte einer virtuellen Umgebung befestigt. Wir zeigten verschiedene virtuelle Räume, welche entlang unterschiedlicher Drehachsen rotierten und fanden, dass das künstliche, durch Fliegen inspirierte System die Rotationsachen sehr präzise vorhersagen konnte.

ACKNOWLEDGEMENTS

First and foremost, I would like to thank Axel who has been an inspiring supervisor throughout the time of my PhD. I very much enjoyed a unique kind of intellectual and experimental freedom which allowed me to develop, test and follow up my own ideas and to venture slightly off the beaten track in the department. It is such kind of working environment which makes scientific work so enjoyable.

Certainly, this work would have not been possible without the many inspiring discussions with many colleagues and friends in our department, in many other laboratories around the world as well as outside the scientific community. I very much want to thank Hubert Eichner, Franz Weber, and Friedrich Förstner (who shared the P7 office experience with me), Väinö Haikala, Johannes Plett, Marion Hartl and Christopher Schnaitmann, all of whom accompanied me during the first years of my PhD. I am also thankful to Reinhardt Wolf (University of Würzburg) and Vivek Jayaraman (Janelia Research Campus) for giving technical advice when I started to develop the virtual environment setups. Furthermore, I want to thank Aljoscha Leonhardt (also in P7), Georg Ammer, Matthias Meier, Etienne Serbe, and Alexander Arenz for infinitely many and very fruitful discussions without which many of my ideas would have needed so much longer to be born or, perhaps, would have never come up. I am also grateful to Stefan Prech, Romina Kutlesa, Christian Theile, and Wolfgang Essbauer for electrical engineering, help with the experiments, and fly work, and to everybody else in the department for making the last years an unforgettable time. Further, I would also like to thank Aljoscha Leonhardt, Alison Barker, Sebastian Philipp, and Katrin Vogt for carefully reading this thesis and making helpful comments. Finally, I want to thank my entire family, all my friends, and my girlfriend Katrin who patiently accepted my often crazy workload and without whom I might not have overcome the sometimes challenging episodes of the PhD.

And, of course, I am grateful to all those little flies for their constant running efforts which have produced so many hundreds of hours of highly valuable behavioral data.

CONTENTS

LIST OF FIGURES

1 INTRODUCTION

1.1 SYSTEMS NEUROSCIENCE

When we move through the environment, our nervous system performs rapid and precise computations in order to transform the varying sensory signals from the outside world into a meaningful internal representation. In the case of vision, this means that light enters our eyes and is directed onto the retina stimulating photoreceptors. This initiates a biochemical and electrical cascade and information processing by the neuronal networks in the retina and deeper brain structures. Eventually, some neurons in the brain will respond specifically to certain, potentially complex, features. For example, such complex features can be motion of the complete field of view which signals an involuntary deviation from a desired path. Hence, direction-selective neurons can be used to trigger an appropriate course correction maneuver. On the other hand, neurons responding to the orientation, shape or speed of an object can signal an interesting target or an enemy and could evoke a directed modification of the current course.

Importantly, any behavioral action in response to such stimuli alters the visual scene and, therefore, the brain has to update its representation. This stimulus-response loop creates an infinite number of fascinating questions which we are studying in the field of visual systems neuroscience: How do photoreceptors work? How is direction-selectivity computed? What are the neuronal networks that extract the relevant features from a complex visual scene? How does the nervous system orchestrate behavior? What are the differences and similarities between different species?

However, the human brain with its 10^{11} neurons, intricate connectivity and network plasticity is far too complex to approach and answer such questions at a satisfying level of detail. Instead, simple organisms such as worms, flies, fish or mice are better systems which are not only far less complex but also offer various tools for experimentally accessing and manipulating brain functions.

1.2 DROSOPHILA AS A MODEL ORGANISM

Originally introduced to the laboratory by William Castle in 1901 (Greenspan, 2008), *Drosophila* had its breakthrough when Thomas Hunt Morgan (Morgan, 1910) discovered the *white* gene which allowed him to link Gregor Mendel's theories of inheritance to a cellular structure, the chromosome. This finding opened the gates for modern genetics

and *Drosophila* quickly became a standard model organism for genetics, development, behavior, learning, and for the study of neuronal circuits.

The use of *Drosophila* in the lab offers several advantages: They are small, easy to breed, clean, harmless, they have a short generation time of about 10 days and don't raise ethical concerns (Jennings, 2011). Their brains are rather simple and consist of about 300 000 neurons with mostly genetically hard-wired development (Simpson, 2009). Yet, *Drosophila* has a sufficiently complex behavioral repertoire (Borst, 2013; Dickson, 2008). These facts, as well as the large variety of genetic tools for selective cellular manipulations, combined with today's technologies for neurophysiology make *Drosophila* ideal for the study of neural circuits in vision.

1.3 FLY VISUAL BEHAVIORS

Some of the most intriguing features of flies are their breathtaking aerobatic maneuvers during flight. For example, when a male house fly chases its female mating partner, it experiences turning speeds around its body axis of more than $2500\,^\circ\,s^{-1}$ and up to $65\,cm\,s^{-1}$ in forward velocity (Land and Collett, 1974). During this amazingly virtuosic flight, the fly must quickly compute the direction of motion of the surround, determine the position of the female and use this information to precisely control its wing and body movements in order to eventually succeed in the mating attempt.

In order to understand the mechanisms underlying this superposition of complex behaviors, flies have long been studied in a controlled laboratory environment. Naturalistic behavior is inherently closed-loop, meaning that a visual stimulus elicits a behavioral response that, in turn, alters the stimulus. As this situation makes it difficult to reveal the mechanisms underlying any sensory processing, behavioral studies in the lab are often done in open-loop configuration where the behavioral response can be measured directly as function of the stimulus and without the behavior affecting the stimulus. This approach has led to a separation of fly visual behaviors into several groups, which has permitted precise investigation of each type of behavior and has accumulated detailed knowledge about their neuronal implementations. Yet, little is known about the ecology of *Drosophila* in the wild, which sometimes makes it difficult to interpret a certain behavioral response studied solely in the lab (but see Dickinson, 2014).

1.3.1 Optomotor response

In a naturalistic environment, full-field rotatory motion implies a deviation from a straight course. Most seeing animals respond with a following response of their body, head or eyes, a behavior often referred to as optomotor response. Such full-field rotatory motion cues occur under multiple circumstances. In the case of a flying fly, a gust of wind might push the fly to the left, which results in a rightward motion stimulus. A syn-directional turning response would compensate for this involuntary movement and would bring the fly back on course. But such course deviations may also result

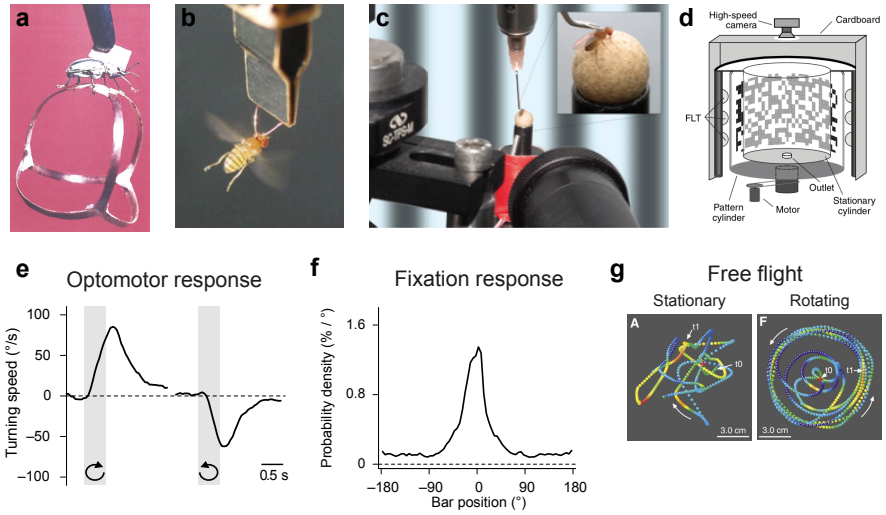

Figure 1: Insect visual behaviors. (**a**) *Cholorphanus* on a "Y-maze" globe. (**b**) Flying *Drosophila* on a torque-meter. (**c**) Walking *Drosophila* on an air-suspended ball. (**d**) Setup for free flight experiments. (**e**) Optomotor behavior in response to clockwise and counterclockwise rotation of a full-field pattern. (**f**) Fixation response. The fly, in control of the azimuthal position of a single black bar, stabilizes the object in its frontal visual field. (**g**) Free flight trajectories of a single fly when the surround is stationary or rotating. **a** modified from Hassenstein (1991), **b** taken from Buchner and Wu (2009), **d** and **g** taken from Mronz and Lehmann (2008), **e** and **f** modified from Bahl *et al.* (2013). Photo in **c** taken by Robert Schorner (MPIN).

from unbalanced forces during behavior. For example, one of the wings might be slightly stronger than the other or one leg could be weaker than the other legs, which would lead to a constant turning bias during flight or walking. The optomotor response counteracts such a bias, and hence, it can generally be considered as a course stabilizing visual feedback system.

Devices for open-loop studies

The first steps to investigate the mechanisms of this course control system in insects were performed by Bernhard Hassenstein and Werner Reichardt (Hassenstein, 1951; Hassenstein and Reichardt, 1956): In their experiments, they took the beetle *Cholorphanus* and placed it on a straw-made "Y-maze globe" on which the animal could walk freely even though it was tethered to a rod (Fig. 1a). When they stimulated the animal with a rotating cylinder, they observed a robust turning of the beetle in the direction of pattern rotation. Hassenstein and Reichardt realized that in order to do so, the beetle must be able to compute the direction of motion and that this is a non-trivial operation. With a set of clever simplifications of the stimulus they were able to design a simple model for motion detection which became known as the Hassenstein-Reichardt correlator (HRC), or as the Reichardt detector.

Moreover, these experiments laid the ground for a new systematic way of thinking in biology and encouraged many talented physicists and engineers to develop a variety of sophisticated devices in order to systematically dissect orientation behavior in insects. One of the key inventions was the so called torque-meter, a device which could amplify the force of the turning tendency of a tethered flying fly and which allowed a more precise investigation of the optomotor response for rotation along the vertical (yaw) body axis (Fermi and Reichardt, 1963; Götz, 1964) (Fig. 1b,e). The technique was then refined in order to measure responses for rotations along the transverse

(pitch) and longitudinal (roll) body axis with similar results (Blondeau and Heisenberg, 1982). Later, it became possible to measure the difference between the two wing beat amplitudes during flight, which turned out to be a precise measure of the behavior as well (Götz, 1987). Moreover, flies not only turn their body in response to a moving pattern, they also follow rotations by head movements, making the head yet another indicator of optomotor behavior (Hengstenberg, 1988).

Walking flies in open-loop were first measured on a tread compensator with tremendous technical effort: A miniature metal sledge was attached to the fly. The fly was then allowed to walk freely on a big sphere while the movement and orientation of the sledge could be detected by a differential transformer. This signal was then used to control a set of servo motors which rotated the ball such that the fly would keep its position and orientation no matter where it walked and turned (Götz and Wenking, 1973). The study of walking flies was then simplified greatly by placing a tethered fly on a small air-suspended ball whose rotational axis could be detected optically (Buchner, 1976), a technique which is still used in today's open-loop fly walking assays (Lott *et al.*, 2007; Seelig *et al.*, 2010) (Fig. 1c).

Properties of the optomotor response

All these devices and different behavioral modalities have provided a coherent picture of the dynamics of the optomotor response in flies (Borst *et al.*, 2010). 1) Flies turn in the direction of pattern movement. 2) The response becomes stronger with increasing contrast. 3) If presented with a sinusoidal grating which moves at different velocities (v) the response of the fly increases until a velocity optimum is reached, then it decreases again. 4) The velocity tuning curve is shifted to higher velocities when the pattern wavelength (λ) becomes larger, i.e. the response of the fly depends on temporal frequency ($f = v/\lambda$) rather than speed.

Freely behaving flies

The optomotor response has also been studied in freely moving flies. First walking experiments were done by Götz (1970) where groups of flies were placed in transparent tubes and stimulated with a translatory cylinder. Surprisingly, flies did not walk in the direction of the moving pattern, as would have been expected from the optomotor response, but rather against it. This apparent conflict between the open- and closed-loop optomotor response was then later investigated in detail by Götz (1975) and explained by a superposition of the given motion stimulus with self-initiated rotatory and translatory optic flow. The idea of placing large groups of flies in a translatory environment in order to probe their optomotor abilities has recently been revived (Zhu *et al.*, 2009). Freely flying flies are much more difficult to study, yet, recent high-speed cameras allow tracking of flight trajectories under controlled visual stimulation and confirm that motion cues lead to a constant following reaction and a curved flight path also during naturalistic behavior (Mronz and Lehmann, 2008) (Fig. 1d,g).

1.3.2 Fixation response

Closed-loop fixation experiments

Flies not only orient based on the full-field rotation of the surround. They also use visual landmarks for finding their way through complex environments or for heading towards an object of interest. Similarly to the optomotor response, fixation behavior has been studied extensively in the lab.

Reichardt and Wenking (1969) extended the torque-meter system such that it could be used to instantaneously control the position of a black bar in the surround of the fly. This setup made artificial closed-loop experiments possible. It turned out that flies reliably bring the bar to the front and keep it there (Fig. 1f). Under these well-controlled conditions, it became possible to systematically dissect the behavior. When using a rotating stripe in open-loop, Reichardt (1973) realized that progressive (front-to-back) bar motion elicits a stronger turning response than regressive (back-to-front) bar motion, which introduces a turning bias towards the bar and would bring it to the front in a closed-loop fixation experiment.

Fixation mechanism

This finding initiated a detailed theory of pattern-induced orientation and it turned out that the apparent asymmetry could be explained by a superposition of two systems: one symmetric motion system which computes the direction of stripe motion and which initiates a syn-directional turning response and a separate position system which determines the location of the stripe and elicits turning towards it (Poggio and Reichardt, 1973). The latter system was later attributed to a tendency to turn towards local flicker (Pick, 1974, 1976). Other studies have argued against the hypothesis that the response asymmetry originate from flicker responses and that it is rather an intrinsic property of motion vision (Wehrhahn, 1981; Wehrhahn and Hausen, 1980). In contrast, more recent work has investigated the detailed steering dynamics of flying flies during figure-ground discrimination and concluded that fixation behavior and motion rely on separate processing streams (Aptekar *et al.*, 2012). However, flies were shown to operantly learn a fixation strategy even if their torque is coupled incorrectly to the stripe position (Heisenberg and Wolf, 1984; Wolf and Heisenberg, 1986), and hence, fixation behavior might not necessarily need to be a reflex and might therefore not be accessible in open-loop experiments.

Freely behaving flies

Fixation behavior has also been studied in freely walking and flying flies. Wehner (1972) developed a cylindrical arena where flies could walk freely and interact with a pattern or with one or more stripes on the walls. When two stripes were close together (less than 65°), flies preferred the sector in between. When the stripes were separated by larger angles, either one of the stripes was fixated (Horn, 1978; Horn and Wehner, 1975). This was true for a black stripe on a white background as well as for bright stripes on a dark background. Further separation of the stripes by 180° led to robust back and forth walking and flies alternated between fixation and anti-fixation (Bülthoff, 1982; Bülthoff *et al.*, 1982; Götz, 1980). This scenario became popular as "Buridan's paradigm", named after the French philosopher Jean Buridan who formulated a paradox of free will: An equally hungry and thirsty donkey is placed between a bale of hay and a bucket of water and dies because it cannot decide between the two equally attractive nutrients.

Fixation behavior of freely flying flies has been studied in an arena with a central elongated vertical bar and multiple high-speed cameras on top tracking the detailed flight path of the fly (Maimon *et al.*, 2008). Interestingly, the behavior depended on the length of the bar: A long bar was attractive and flies circulated around it in close proximity while flies avoided the bar if it was short.

1.3.3 Landing and escape response

A quickly expanding visual scene or an approaching object are good indicators of an imminent collision, and controlled landing or directed escape are essential for animal survival. The landing response of flies was first systematically analyzed by Goodman (1960) who designed a sophisticated apparatus to either move a dark disk towards a tethered fly or to show a distant disk with decreasing luminance. The flies responded with a stereotypic pattern of leg movements when the disk approached and positioned their legs in a well-controlled manner once the disk was near enough. However, this also happened when the luminance of a non-moving disk was quickly reduced, indicating that the landing response depends on local luminance change rather than motion.

Visual cues for the behavior

Later, Borst (1986) investigated the detailed time course of the behavior for different kinds of visual stimuli. He found that the landing response, once initiated, always follows the same dynamics and that the response latency depends on the properties of the visual stimulus. Expansion avoidance reactions were observed in flies presented with patterns of fast expanding optic flow. A quantification of the behavior revealed that the latency for the landing response depends on contrast, spatial wavelength and speed of the pattern in a similar fashion as has been found for the optomotor response. Thus, the landing response relies on similar or even the same mechanisms as motion vision (Borst and Bahde, 1986). When the focus of expansion was shifted to locations other than in the frontal field of view, flies responded differently: Instead of performing a landing response, they robustly turned away from the focus of expansion with amplitudes even larger than those found for rotatory motion stimuli (Tammero *et al.*, 2004). However, when a vertical bar was placed in the center of expansion, flies tolerated the stimulus and even turned towards the center of expansion (Reiser and Dickinson, 2010).

Freely behaving flies

In order to study escape responses under more natural conditions, flies were placed on a platform and filmed while they were stimulated with a rapidly approaching dark dot (Card and Dickinson, 2008). This experiment revealed an elaborate motor planning and a directed jump away from the region of potential danger. Similar responses were found during free flight (Muijres *et al.*, 2014): Whenever a fly passed a cross of two IR lasers in the center of an area, a quickly enlarging disk was presented while monitoring the behavior at 7500 fps. Flies responded with rapid directed banked turns, a maneuver that consists of a fast body rotation followed by an active counter-rotation and requires just a few wing strokes.

1.3.4 Other visual behaviors

Phototaxis and color vision

Freely walking and flying *Drosophilae* have an innate preference for light. Because this robust phototactic response requires only a single lamp for stimulation, it was one of the first fly behaviors studied in the lab (Carpenter, 1905). Later, flies were given the chance to choose between two sources of light of different spectral compositions, which revealed that they are able to

discriminate colors covering the visual spectrum from green to UV, but with a preference for UV (Schümperli, 1973).

Color vision, in the classical sense, relies on the ability of the animal to distinguish light of different spectral compositions independently of intensity. In order to prove color vision for *Drosophila*, Menne and Spatz (1977) designed a learning essay in which flies could be conditioned differentially to yellow and blue lights of the same intensities. It was found that flies were able to discriminate the colors later in the test. Conversely, flies neither respond with an optomotor response when the moving pattern consists of stripes of different colors which are matched in their intensities (Yamaguchi *et al.*, 2008), nor are they able to fixate an edge between two intensity-matched colored areas (Y. Zhou *et al.*, 2012).

Polarization vision

Besides having a certain intensity or color, light can vary in its degree of polarization, which is yet another kind of information that animals, especially insects, utilize for navigation (Wehner, 2001). In nature, polarized light is created under several conditions: When unpolarized sun light enters the sky, it interacts with the molecules in the atmosphere and scatters in various directions. Light remaining on a straight line from the sun stays unpolarized. Yet, when it scatters perpendicularly it becomes polarized. This creates a vector field of concentric circles around the straight line from the sun, providing a celestial compass for orientation. Moreover, if unpolarized light is reflected from shiny surfaces, such as a lake, the reflection at certain angles becomes polarized, which could be a potential cue for finding water. *Drosophila* can make use of both kinds of polarization cues as it robustly aligns with the electric vector of the polarized light in the lab (Velez *et al.*, 2014; Wernet *et al.*, 2012; Wolf *et al.*, 1980) as well as in authentic outdoor experiments (Weir and Dickinson, 2012). Generally, polarization vision can considered extremely relevant for navigating in resource-poor environments as it allows traveling long distances on a direct path.

1.4 MAPPING AND MANIPULATING NEURONAL CIRCUITS

During the past hundred years of *Drosophila* research, a variety of tools have been developed which have equipped *Drosophila* researchers with a very powerful armory that is increasingly used to map and manipulate the neuronal circuits controlling a variety of visually-guided behaviors (Simpson, 2009).

1.4.1 Neurogenetics

Mutagenesis

After Morgan (1910) had established that genetic information is located on the chromosomes *Drosophila* became a genetic workhorse. Large numbers of mutant flies could be created by treating flies with x-rays Muller (1928) or with chemicals such as ethyl methanesulfonate (EMS) (Alderson, 1965). The progeny which survived such treatments was initially characterized and

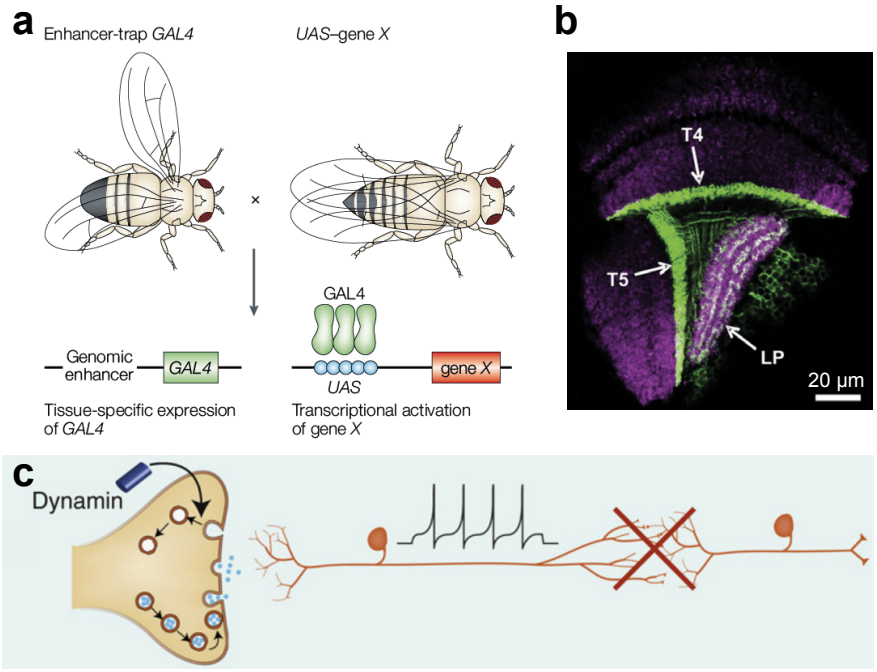

Figure 2: Fly genetics. (**a**) Gal4-UAS system. A fly (here the male, left) from the driver line carries the gene for the transcription factor Gal4 which is expressed only in a specific subset of neurons. Another fly (here the female, right) carries the effector gene *X* whose transcription requires activation via Gal4. Their offspring will express gene *X* in the desired neuronal subset. (**b**) GFP expression pattern of T4/T5-Gal4. (**c**) Shibire^{ts} is a temperature-sensitive mutated form of dynamin. When expressed in neurons, it blocks cellular output at elevated temperatures. **a** taken from St Johnston (2002), **b** taken from Schnell *et al.* (2012), **c** taken from Borst (2009).

named according to their behavioral deficits and their anatomical abnormalities.

A classical behavioral screening approach was developed by Seymour Benzer (Benzer, 1967): He designed a countercurrent device which allowed him to separate large groups of mutant flies according to their ability to perform phototactic behavior, a strategy which proved to be ideal for behavioral phenotyping. The approach was later generalized to more complex visual behaviors, including the optomotor and fixation response, and it became possible to causally link these behaviors to certain groups of neurons in the fly brain (Heisenberg and Götz, 1975; Heisenberg *et al.*, 1978).

Gal4/UAS System

The biggest step towards more directed circuit manipulation happened when it became possible to insert transposable pieces of DNA (P-elements) into a random location of the genome of *Drosophila* (Rubin and Spradling, 1982). The piece of DNA, a transgene, could end up in a genomic region that is translated only in a subset of neurons and consequently, it would only be expressed in this neuronal subpopulation. Brand and Perrimon (1993) used this approach and inserted a P-element containing the yeast transcription factor gene for Gal4 in the genome of *Drosophila*, resulting in a fly strain expressing Gal4 only in a subset of neurons (driver line). Gal4 has no molecular partner in the fly and therefore has no effect on the function of the cells in which it is expressed. In another fly, they inserted a P-element containing an upstream activation sequence (UAS) followed by a certain

gene of interest (reporter or effector line). This gene sequence is available in every cell in the fly but it is never translated as the fly does not have the appropriate transcription factor.

However, the situation changes if driver and reporter lines are crossed: In the offspring, Gal4 can bind to UAS and initiate the transcription of the desired gene in a defined subset of neurons (Fig. 2a). Given a specific driver line, the huge advantage of using such a binary expression system is that almost any protein can be expressed in virtually any group of neurons. As the success of the Gal4-UAS system relies on the abundance of specific driver lines, large libraries have been established which allow efficient search for expression patterns of interest (for example, see Jenett *et al.*, 2012). Recently, it has become possible to significantly improve how transgenic fly lines are created. First, directing the transgene to dedicated locations in the genome ensures that the insertion will not disrupt important other genes and that it can be efficiently transcribed (Pfeiffer *et al.*, 2010), and second, chaining multiple UASs allowed boosting transgene expression levels by as much as 20-fold (Pfeiffer *et al.*, 2012).

Intersectional strategies

The specificity of the Gal4 expression pattern can be further enhanced by applying several intersectional strategies (Venken *et al.*, 2011). One of them is to split the Gal4 protein into its two functional components, the DNA binding-domain (DBD) and the activation domain (AD) and to create independent driver lines for each (Luan *et al.*, 2006). This results in different expression patterns for the Gal4-DBD and Gal4-AD driver lines but if they are brought together, functional Gal4 will reconstitute only in the region where both lines have overlapping expression patterns. Further, it is possible to use a flip-out technique in which a stop codon right after the UAS sequence prevents the translation of the transgene. The stop codon is marked with a certain base sequence, the FRT site, which allows a temperature sensitive flippase to recognize and remove it, leading to a mosaic-like expression pattern (Golic and Lindquist, 1989).

Moreover, Gal80 has been used to effectively suppress transgene expression during development. Gal80 is another yeast-specific protein which binds to the transcriptional activation domain of Gal4 and inhibits its activity. The gene for Gal80 has been placed under the control of *Drosophila*'s ubiquitous tubulin promotor, allowing pan-neuronal expression. Thermounstable forms of tubulin Gal80 exist which lose their inhibitory effect on Gal4 when the temperature is mildly increased (McGuire *et al.*, 2003). Hence, Gal4 activation of the UAS domain and the expression of the desired effector protein can be triggered at any time point during development. Similarly to the concepts developed for the Gal4/UAS system, targeted transgene expression can be achieved by using the LexA/LexOP system or the Q system. In the former, LexA from the driver line binds to the LexA operator (LexOp) (Lai and T. Lee, 2006) while in the latter, the activator QF binds to the QF upstream activating sequence (QUAS) (Potter *et al.*, 2010). A combination of these systems with the Gal4/UAS system allows expression of different genes in distinct neuronal subpopulations.

Important reporters and effectors

Various reporter and effector lines exist which can be grouped according to their scope of application, namely visualizers, indicators, blockers and activators. The most important visualizer is the green fluorescent protein

(GFP) (Chalfie *et al.*, 1994) because it is essential for the initial characterization of the Gal4 expression pattern of the driver line (Fig. 2b).

Indicators are proteins which change their florescence depending on the internal state of the cell and can be used to assess neuronal activity with imaging. Genetically-encoded calcium indicators depend on the intracellular calcium level and thereby provide an indirect measure of neuronal activity. Various such indicators exist (TN-XXL, for example; Mank *et al.*, 2008) but the currently most widely used ones are a set of GCaMPs (Nakai *et al.*, 2001) which offer a superb signal-to-noise ratio and are constantly improved (Akerboom *et al.*, 2012; Chen *et al.*, 2013). However, assessing neuronal activity via GCaMPs has two significant disadvantages: First, calcium levels in the cell build up and decrease slowly. Hence, even the currently fastest GCaMP6f variant achieves only rough single AP resolution. Second, hyperpolarization might not be detectable as in this case calcium levels remain largely unchanged. Here, genetically-encoded voltage indicators might help in the future (Cao *et al.*, 2013).

In order to assess the functional roles of a neuron in the circuit, a long list of blockers exists. One strategy is to cause genetically controlled cell death through expression of cell toxins such as Ricin which irreversibly inhibits protein synthesis (Hidalgo *et al.*, 1995) or genes such as *hid* which interferes with the cellular machinery for apoptosis (Grether *et al.*, 1995). One of the first potent tools for blocking neuronal transmission without killing the cell was Tetanus Toxin Light Chain (TNT). TNT cleaves the synaptic vesicle protein synaptobrevin which is necessary for synaptic vesicle release. Hence, cells lose their ability to signal activity to their postsynaptic partners (Sweeney *et al.*, 1995). Another prominent tool for silencing neuronal output is shibire^{ts} which is a dominant-negative thermo-unstable form of dynamin, a protein that is an essential element of the vesicle recycling machinery (Kitamoto, 2001) (Fig. 2c). When shibire^{ts} is expressed in a neuron, synaptic transmission is intact as long as the temperature remains below 29 °C (permissive). However, above 29 °C (restrictive) vesicle recycling stops working, which leads to neurotransmitter depletion and hence defective synaptic transmission. The effect of shibire^{ts} can be reversed by lowering the temperature again. This conditional property makes shibire^{ts} an ideal tool for the study of the functional significance of defined neuronal subsets independently of developmental effects likely to be caused by other effectors. Neurons can also be manipulated by introducing ion channels. For example, a neuron can be silenced by expression of an inward rectifying potassium channel K_{ir} that constantly hyperpolarizes the cell (Baines *et al.*, 2001).

Alternatively, it is possible to activate a cell by introducing a cation channel such as TrpA1 (Hamada *et al.*, 2008). TrpA1 is temperature-dependent and opens reversibly beyond 26 °C, which provides temporal control of neuronal activity via temperature regulation.

Optogenetics

An alternative approach for manipulating neuronal activity is the use of optogenetics where genetically expressed light-gated ion channels are visually stimulated with high temporal precision (for a review, see Fenno *et al.*, 2011). One of these is Channelrhodopsin-2 (Chr2), a light-gated cation channel (Nagel *et al.*, 2003), which can effectively depolarize neurons upon illumination with blue light (Boyden *et al.*, 2005; Nagel *et al.*, 2005). These

channels are intensively studied and constantly improved, and variants with distinct light absorption spectra exist (for example, red-shifted ReaChR or Chrimson; Inagaki *et al.*, 2014; Klapoetke *et al.*, 2014) as well as bistable forms which can be rapidly switched between the open and closed state by short pulses of light (Berndt *et al.*, 2009). Recently, directed mutations in the gene for Channelrhodopsin-2 generated blue-light-sensitive chloride channels which can efficiently hyperpolarize neurons and inhibit spiking (Berndt *et al.*, 2014; Wietek *et al.*, 2014). Such channels are promising tools and they appear to be superior to halorhodopsins, yellow light-gated chloride pumps, which have been used for optical shunting of neural activity (Gradinaru *et al.*, 2008).

1.4.2 Neuroanatomy

An important prerequisite for understanding of how neuronal circuits operate is detailed knowledge about the anatomy, location and connectivity of the neurons in the brain. The first anatomical drawings of the visual system of flies were created in the beginning of the 20th century by Cajal and Sánchez (1915) using Camillo Golgi's silver staining technique. Later, this technique was systematically applied in order to create precise atlases of the *Calliphora* brain (Strausfeld, 1976) as well as the brain of *Drosophila* (Bausenwein *et al.*, 1992; Fischbach and Dittrich, 1989). Today, a more directed approach is to use a binary expression system, such as the Gal4/UAS system, in combination with a flip-out strategy. This makes it possible to drive GFP expression in single neurons which can then be anatomically characterized via fluorescence microscopy.

Connectomics

Even though these anatomical maps have proven to be essential in the identification of neurons of interest, they could only provide a rough estimate about connectivity between neurons because synaptic connections are beyond the resolution limit of light microscopy. Here, electron microscopy (Knoll and Ruska, 1932) allows a much finer resolution of local structures. In order to obtain a three dimensional data set, a large block of tissue is serially cut and each slice is manually transferred to the scanning chamber of the electron microscope. The resulting images are then aligned and stacked in a high-resolution volume in which it is possible to trace single axons or to count the number of synaptic connections between pairs of neurons. This has been done for a part of the visual system of *Drosophila*, resulting in fine anatomy and connectivity maps (Meinertzhagen and O'Neil, 1991; Shinomiya *et al.*, 2014; Takemura *et al.*, 2013, 2011, 2008). The manual step of sectioning can be automated by techniques such as serial block-face scanning electron microscopy where the blocks of tissue are automatically sliced in the chamber of the electron microscope (Denk and Horstmann, 2004).

1.4.3 Neurophysiology

However, knowing the connectome is just the first step. In order to understand the information flow in the brain, one also needs to know the neuronal response properties and how the nerve cells communicate, i.e. via which re-

ceptor types a neuron receives input and whether it uses an excitatory or inhibitory neurotransmitter.

Neurotransmitter systems

Drosophila's visual system relies on several different neurotransmitter systems: acetylcholine, GABA, glutamate, aspartate, taurine, dopamine, serotonin, octopamine, and histamine. In order to reveal which cells use acetylcholine as a transmitter, for example, it is possible to drive GFP expression stochastically only in cholinergic neurons. This can be done by using a Gal4 line which is under the control of the "Cha" promotor. This promotor controls expression of choline acetyltransferase and the vesicular acetylcholine transporter (S. V. Raghu *et al.*, 2011). Similarly, one can study the glutamateric system by using a Gal4-line under the control of the promotor for the vesicular glutamate transporter "dvGlut" (S. V. Raghu and Borst, 2011). Acetylcholine is considered to be the major excitatory neurotransmitter in the fly brain. Glutamate however, can have an excitatory or inhibitory effect. Therefore, one also needs to know the receptor types of the postsynaptic targets. Here, it is possible to apply brain-wide immunolabeling techniques or to use single-cell transcript profiling in order to obtain a complete list of genes expressed in the cell (for example, see Takemura *et al.*, 2011).

Electrophysiology

Cellular activity can be best assessed via electrophysiological recordings which offer the most direct measure with high temporal resolution. Thanks to the relatively large size of some cells in the *Calliphora* brain, extracellular or sharp electrode recordings have accumulated a tremendous amount of data about neuronal response properties (for example, see Douglass and Strausfeld, 1996; Hausen, 1976) and, via paired-recordings, connectivity (Haag and Borst, 2001, 2004). On the other hand, the small size of neurons in the *Drosophila* brain has long been an obstacle for electrophysiology. Only in recent years has reliable whole-cell patch clamp techniques permitted recordings in the olfactory system (Wilson *et al.*, 2004) and in the visual system (Joesch *et al.*, 2008). These techniques have rapidly advanced and today allow recordings even during tethered flight (Maimon *et al.*, 2010; Tuthill *et al.*, 2014).

Two-photon microscopy

However, most of the cells in the fly brain are too small for electrophysiology. Here, two-photon imaging (Denk *et al.*, 1990) has been developed as an alternative for assessing neuronal activity in the *Drosophila* visual system (Reiff *et al.*, 2010) and can even be applied during behavior (Seelig *et al.*, 2010; Seelig and Jayaraman, 2013). In principle, a femtosecond-pulsed laser transmits light of $\approx$ 1000 nm into a specimen containing fluorescent proteins, such as, for example activity-dependent GCaMP. A single photon does not have enough energy to excite the fluorophore, and hence, the probe is mostly non-fluorescent. Only in the small spot of focus two coincident low-energy photons can overcome the necessary threshold for excitation. Hence, two-photon imaging hardly interferes with out-of-focus cells, does not stimulate photorecepetors and is therefore ideal for imaging single neurons in a visual system.

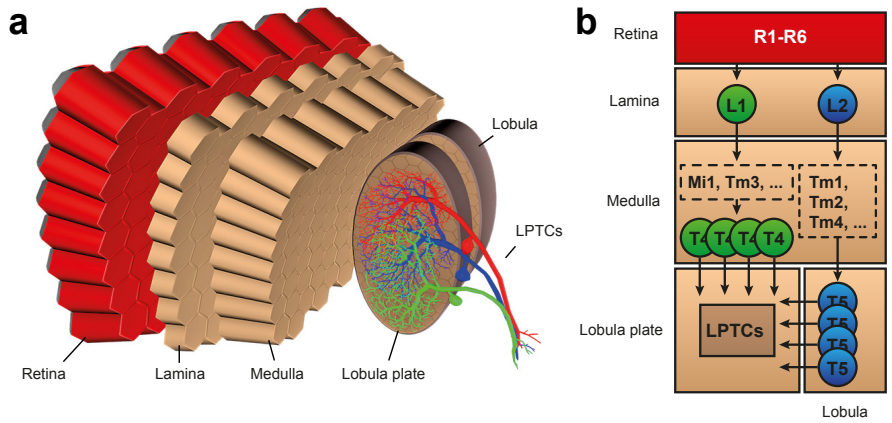

Figure 3: Schematic of the visual system of *Drosophila*. (**a**) The fly visual system consists of several anatomical layers known as retina, lamina, medulla, lobula and lobula plate. The lobula plate houses several types of lobula plate tangential cells (LPTCs) of which the three horizontal system cells are shown here. (**b**) In each lamina column photoreceptors R1–R6 synapse onto lamina neurons L1 and L2 and form parallel pathways for motion detection of ON and OFF signals, respectively. The outputs of both pathways converge onto T4 and T5 which, in turn, synapse onto the dendrites of LPTCs. **a** and **b** modified from Bahl *et al.* (2013).

1.5 STRUCTURE AND PHYSIOLOGY OF THE VISUAL SYSTEM

The central nervous system of the adult *Drosophila* consists of two major parts, the head and the thoracic ganglion. While the thoracic ganglion is dedicated to motor control, the head ganglion, or the brain, is involved in sensory processing and evaluation. The brain of *Drosophila* consists of three parts which build up a densely-packed structure of ≈ 300 000 neurons: the central brain and two optic lobes. The central brain is involved in tasks such as, for example, visual learning (Ofstad *et al.*, 2011). The optic lobes are processing visual information and direct their output to the central brain and to the thoracic ganglion in order to control visually-guided and potentially experience-based behaviors.

The optic lobe of *Drosophila* consists of ≈ 60 000 neurons (Hofbauer and Campos-Ortega, 1990) and can be divided into several neuropiles: retina, lamina, medulla and the lobula complex which separates into lobula and lobula plate (Fig. 3). Retinotopy is maintained throughout the columnar structure of the visual system down to the direction-selective lobula plate tangential cells which have complex and wide receptive fields. Recording from these cells and simultaneous circuit manipulation has become a valuable technique for dissecting the motion processing circuitry.

1.5.1 Retina

Drosophila's compound eye is formed by ≈ 750 hexagonal facets or ommatidia which build up an evenly spaced mosaic with an interommatidial an-

gle of $\approx 5°$ (Land, 1997). It samples almost the entire visual hemisphere excluding only an area of about 20° in the back of the fly (Buchner, 1971).

Photoreceptors

Each of the ommatidias houses six outer photoreceptors (R1–R6) surrounding a stack of two inner photoreceptors (R7 and R8). Photoreceptors R1–R6 contain Rhodopsin-1 (Rh1), a broad-band photopigment. Ommatidia in the central area of the eye are separated into two types, pale (p) and yellow (y), depending on the photopigment present in the inner photoreceptors (Franceschini *et al.*, 1981). In p-type ommatidia R7 cells contain UV-absorbing photopigment Rhodopsin-3 (Rh3) and R8 cells contain Rhodopsin-5 (Rh5), a blue sensitive photopigment. In y-type ommatidia photoreceptors R7 contain another UV-absorbing photopigment, Rhodopsin-4 (Rh4), while photoreceptors R8 contain the green sensitive photopigment Rhodopsin-6 (Rh6). Approximately 30 % of the ommatidia belong to the p-type and 70 % to the y-type. Both types are distributed stochastically in the retina. A third class of ommatidia is located along the dorsal rim area of the eye where both photoreceptors R7 and R8 contain UV-sensitive Rh3 (Feiler *et al.*, 1992).

Photoreceptor types and visual behavior

Early studies have revealed several mutations resulting in photoreceptors deficits (Harris *et al.*, 1976). For example, flies with the *ora* mutation (*outer rhabdomeres absent*) have strongly degenerated photoreceptors R1–R6 and show a severe performance reduction in several visual orientation behaviors including the optomotor and fixation response, which indicates a major role for R1–R6 in these behaviors (Heisenberg and Buchner, 1977). The same held true for flies carrying a mutation in the *ninaE* gene (*neither inactivation nor afterpotential E*) which is required for the synthesis of photopigment Rh1 (O'Tousa *et al.*, 1985). Similar deficits could be observed in flies in which R1–R6 output was silenced with shibire^{ts} (Rister *et al.*, 2007). R1–R6 have also been shown to be sufficient for visual behavior because flies with impaired R7 and R8 photoreceptors have an unchanged optomotor response (Yamaguchi *et al.*, 2008) and an intact edge-fixation performance (Y. Zhou *et al.*, 2012). However, flies without functional R1–R6 are not blind because they can still perform wavelength-specific phototaxis (Gao *et al.*, 2008), suggesting R7/R8 to be involved in color discrimination (Schnaitmann *et al.*, 2013; Yamaguchi *et al.*, 2010). Moreover, it has been shown that polarization vision is mediated via two systems, a dorsal and a ventral one. While the former system consists of specialized photoreceptors R7/R8 in the dorsal rim area, the latter system requires an interaction of inner and outer photoreceptors in the ventral region of the eye (Wernet *et al.*, 2012).

Phototransduction

The visual pigments are located in the rhabdomere, a densely packed structure of microvilli attached to the photorecepetor where light is converted into an electrical signal by an intricate biochemical cascade (Hardie and P. Raghu, 2001): Upon illumination rhodopsin is photoisomerized into metarhodopsin which catalyzes the phosphorylation of a trimeric G-protein. Metarhodopsin is converted back into rhodopsin by long-wavelength light and is ready for absorbing the next photon. The activated G-protein dissociates and releases its G_α-subunit which activates phospholipase C which, in turn, hydrolyzes PIP_2 to DAC and $InsP_3$. Via a still unknown mechanism, this leads to an opening of calcium permeable transient receptor potential (TRP) channels and non-selective TRP-like cation channels which depolarize the photoreceptor.

Recent work has shown that the depletion of PIP_2 leads to a rapid contraction of the photoreceptor membrane and suggests that such a mechanical force might trigger the channel opening (Hardie and Franze, 2012). Phospholipase C is encoded by the *norpA* gene (*no receptor potential A*) and is a key element in the phototransduction cascade because a mutation in that locus renders flies completely blind (Bloomquist *et al.*, 1988). Phototransduction in flies is very fast: Upon a short light pulse the depolarization in the photoreceptor is detectable already after a few milliseconds and quickly decays back to resting levels (Hardie, 1991), which explains the incredible temporal flicker resolution of the fly eye at values larger than 200 Hz (Autrum, 1950). All photoreceptors use histamine as a neurotransmitter and hence provide an inhibitory signal to their postsynaptic targets (Hardie, 1989).

Neuronal superposition

The photoreceptors within one ommatidium are spatially separated in flies and point at different locations in space. Thus, a simple convergence of their outputs into the subsequent lamina cartridge would decrease visual acuity. Nature has solved that problem by using the principle of neuronal superposition which maintains resolution and increases sensitivity at the same time (Braitenberg, 1967; Kirschfeld, 1967): Photoreceptors R1–R6 from within one ommatidium project into distinct neighboring cartridges of the lamina in such a way that the photoreceptors with the same optical axis project into the same lamina cartridge. Hence, the functional unit for light processing is not the ommatidium itself but rather the lamina cartridge which is therefore also called the neuro-ommatidium. The projection for R7 and R8 cells is more simple: They project directly into the subjacent cartridge passing the lamina and synapse onto medulla cells. Yet, R7 and R8 axons are gap junction-coupled to the R6 axon within the same cartridge at the level of the lamina (Shaw *et al.*, 1989; Wardill *et al.*, 2012).

1.5.2 Lamina

12 cell types

The first neuropil, the lamina, consists of ≈ 6000 cells (Hofbauer and Campos-Ortega, 1990) which can be divided into 12 neuron types (Fischbach and Dittrich, 1989). Eight of these are columnar: five lamina monopolar cells (L1–L5), two centrifugal cells (C2 and C3) as well as T1. The other four types are multi-columnar: One lamina intrinsic neuron (Lai) and one lamina tangential neuron (Lat) as well as two lamina wide-field neurons (Lawf1 and Lawf2). L1–L5 neurons have their somata and input dendrites in the lamina and provide a feed-forward signal to different layers of the medulla. C2, C3 and T1 neurons have their somata and dendrites in the medulla and are thought to provide a feedback signal to the lamina. The input and output of Lai neurons is confined just to the lamina while Lawf1 and Lawf2 receive their input in the medulla and provide multi-columnar feedback projections to the lamina. Finally, Lat projects from the ipsilateral central brain to the outer region of the lamina. At least L1 and L2 are coupled via gap-junctions (Joesch *et al.*, 2010), suggesting that the lamina constitutes an intricate network of synaptic and electrical connections. Single-cell transcript profiling has identified L1 to be glutamatergic and both L2 and L4 to be cholinergic while the transmitter systems used by the other lamina neurons are currently unknown (Takemura *et al.*, 2011).

Lamina monopolar cells L1–L3

Lamina monopolar cells L1–L3 have been studied extensively and, due

to their sufficiently large size, can be recorded with sharp microelectrodes (Laughlin and Hardie, 1978; Laughlin and Osorio, 1989). They are non-spiking neurons receiving histaminergic input from photoreceptors R1–R6 (Gengs *et al.*, 2002). L1–L3 respond with a transient hyperpolarization upon illumination and depolarize when luminance decreases (Clark *et al.*, 2011; Reiff *et al.*, 2010; Silies *et al.*, 2013). L1 and L2 are key players in motion vision as blocking the output of both cells at the same time abolishes the optomotor response (Rister *et al.*, 2007; Tuthill *et al.*, 2013). This has also been found in electrophysiological recordings from lobula plate tangential cells which become unresponsive upon L1 and L2 blockade (Joesch *et al.*, 2010).

ON and OFF pathways

Moreover, when L1 and L2 were blocked separately, lobula plate tangential cells responded only to one polarity of motion in a direction-selective manner: When L1 was blocked, they only responded to dark-edge (OFF) motion while in a L2 block only a response to bright-edge (ON) motion was detectable, implying that L1 and L2 constitute two major input lines for independent ON and OFF motion detection pathways, respectively (Joesch *et al.*, 2010). This early split in motion vision has been investigated in behavioral experiments as well with similar results (Clark *et al.*, 2011). L2 has also been shown to control walking speed (Katsov and Clandinin, 2008) and to be necessary for the escape response (de Vries and Clandinin, 2012). Moreover, responses in L2 depend on the size of the stimulus and are best characterized by an excitatory center and an inhibitory surround receptive field, suggesting a lamina preprocessing mechanism which could alter the response dynamics selectively only to dark-edge motion (Freifeld *et al.*, 2013).

Lamina monopolar cells L3 and L4

L3 has been speculated to form the major input pathway to a color processing system (Gao *et al.*, 2008) and to mediate fixation behavior (Rister *et al.*, 2007). However, recently L3 has been found to play a role during processing of OFF motion stimuli as well (Shinomiya *et al.*, 2014; Silies *et al.*, 2013). Even though L4 does not receive direct photoreceptor input, its responses to light increments and decrements resembles those of L1–L3 neurons (Meier *et al.*, 2014; Silies *et al.*, 2013). This could be explained by its reciprocal connections with L2, a circuit motif which has been speculated to tune motion computation differentially to progressive and regressive motion (Takemura *et al.*, 2011). Blocking the output of L4 neurons and simultaneous recordings from lobula plate tangential cells revealed a drastic response reduction to OFF edge, but not to ON edge motion, corroborating the role of L4 in the OFF motion pathway (Meier *et al.*, 2014).

Feedback projections

Finally, responses of lamina neurons are shaped by feedback neurons: Lawf2 is accessible via whole-cell patch clamp recordings and shows a pronounced spiking response upon flicker stimulation but is not direction-selective. Blocking its output during behavioral experiments revealed that Lawf2 suppresses low-frequency signals for motion detection (Tuthill *et al.*, 2014). Virtually nothing is known about the physiology and function of the other neurons in the lamina and only recently a behavioral screen has revealed surprisingly little contribution of these neurons to various visually-guided behaviors (Tuthill *et al.*, 2013).

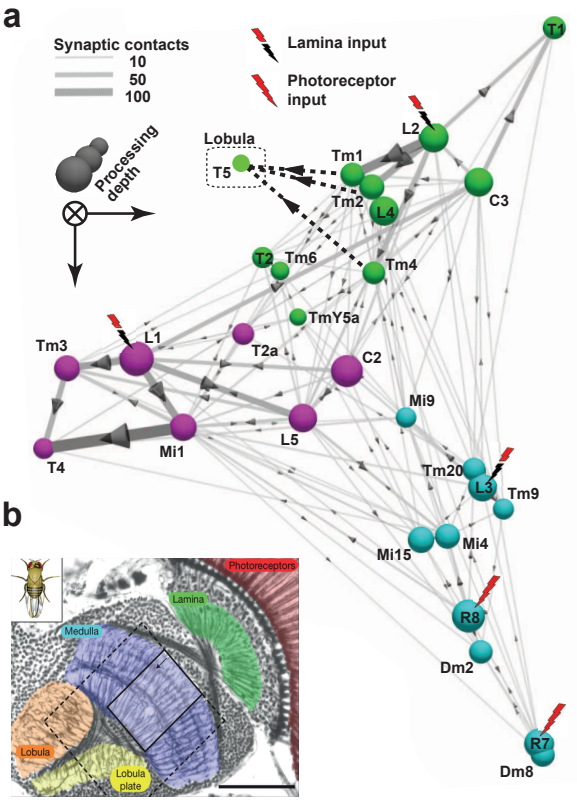

Figure 4: Medulla connectome. (**a**) Connectivity diagram of lamina and medulla neurons thought to be involved in motion detection. Diameter of circles symbolizes processing depth. Lines and arrows indicate the number of synaptic contacts and is an indicator of connectivity strength. Cluster analysis revealed three different pathways emerging postsynaptically to L1 (magenta), L2 (green) and L3/R7/R8 (cyan). (**b**) The black square indicates the reconstructed medulla region (37 µm x 37 µm). **a**, **b** modified from Takemura *et al.* (2013).

1.5.3 Medulla

The second neuropil, the medulla, consists of ≈ 60 mostly columnar neuron types, forming a dense neural network of ≈ 40 000 neurons (Hofbauer and Campos-Ortega, 1990). The medulla can be divided into 10 separate layers (M1–M10) where lamina neurons make synaptic connections with different types of medulla neurons (Fischbach and Dittrich, 1989; Takemura *et al.*, 2008). Almost all medulla neurons receive their input from within these layers. They can be grouped according to their shape and target projection pattern.

Cell types

Local medulla intrinsic (Mi) neurons target cells within the medulla while trans-medulla (Tm) neurons project onto neurons in the lobula. On the other hand, trans-medulla Y-cells bifurcate and synapse onto neurons in the lobula and, additionally, onto neurons in the lobula plate. Another group of cells is formed by the columnar bushy T cells (T2, T3, T4 and T5) which target different layers of the lobula (T2 and T3) and of the lobula plate (T4 and T5). While T2, T3 and T4 neurons receive input from within the medulla, T5 gets input from the lobula. T4 and T5 cells are further divided into four subtypes each (T4a–d and T5a–d) which target layers 1–4 of the lobula plate (Bausenwein and Fischbach, 1992).

Connectivity clusters

Recent developments in electron microscopy have created detailed connectivity maps (Fig. 4), which revealed clusters of connectivity within the medulla network (Shinomiya *et al.*, 2014; Takemura *et al.*, 2013). One cluster was found between L1, Mi1, Tm3 and T4 neurons, another between L2, L4, Tm1, Tm2, Tm4 and T5 cells and yet another between L3, R7, R8, Tm9 and

T5 neurons. It is currently well-established that the L1–Mi1–Tm3–T4 and L2–L4–Tm1–Tm2–Tm3–T5 clusters correspond to the ON and OFF motion pathway, respectively.

Physiological characterization

Due to the small size of neurons in the medulla it has rarely been possible to establish electrophysiological recordings (Douglass and Strausfeld, 1996) and only with the recent advent of two-photon imaging in *Drosophila* has it become feasible to obtain reliable data of their visual response properties. One of the few medulla neurons characterized so far is Tm2 (Meier *et al.*, 2014): When presented with moving dark and bright edges, Tm2 neurons responded transiently only to the moving dark edge, yet, independently of its direction of motion. Similarly, when probed with flickering bars, a response only to the darkening phase of the bar was apparent. This, however, strongly depended on the size of the bar, leading to no detectable response for full-field flicker, which indicated a significant role for lateral inhibition. Moreover, blocking the output of Tm2 and recording from lobula plate tangential cells revealed a reduction of the response only to moving OFF edges but not to moving ON edges.

Another study recently applied pan-neuronal imaging to the medulla and probed the visual system with dark and bright flashing dots of different sizes. This revealed a clear separation of layers responding selectively to brightness increments and others to brightness decrements, which matches the projection regions of L1 and L2, respectively (Strother *et al.*, 2014). They also imaged Mi1 and Tm1 directly: Mi1 responded selectively to brightness increments of the dot independently of size. In contrast, Tm1 responded selectively to brightness decrements, however, only if the dot was small, which demonstrates that Tm1 is laterally inhibited.

Recently, Mi1, Tm3, Tm1 and Tm2 neurons were recorded from via electrophysiolgical whole-cell patch clamp (Behnia *et al.*, 2014). It was found that Mi1 and Tm3 depolarize selectively to brightness increments and hyperpolarize to brightness decrements while Tm1 and Tm2 neurons did the opposite. Polarity-specific rectification was present in these cells but weak. These three studies implicate that the split of ON and OFF motion signals starting at L1 and L2, respectively, is maintained in the medulla and that the flow of information matches the one suggested by the anatomy.

T4 and T5 cells

Finally, T4 and T5 neurons have been shown to be the major output elements of the medulla because silencing these cells completely abolishes direction-selective responses in lobula plate tangential cells (Schnell *et al.*, 2012). However, it has been unclear whether the lack of direction-selectivity in lobula plate tangential cells would translate directly into an inability to perform an optomotor response because other pathways might play a role in this behavior as well. Moreover, it has remained speculative whether T4 and T5 neurons themselves are direction-selective (Douglass and Strausfeld, 1996) and how the split of ON and OFF motion signals is carried on to the different T4 and T5 subtypes or whether, alternatively, direction-selectivity is computed postsynaptically within lobula plate tangential cells.

1.5.4 Lobula complex

The final neuropil in the fly optic lobe is called the lobula complex where large-field neurons integrate columnar input from the medulla. In dipteran flies the lobula complex is further divided into lobula and lobula plate which both have a similarly-layered anatomical structure.

Lobula plate

The lobula plate is the most well-studied neuropil in the fly as it was recognized early that the structure is electrically highly active and contains many direction-selective elements, the lobula plate tangential cells (Hausen, 1976, 1982a,b; Hengstenberg, 1982). Relatively easy access to this neuropil and the large size of lobula plate tangential cells permitted thorough investigations of the lobula plate network (for review, see Borst and Haag, 2002). Lobula plate tangential cells are large neurons with a magnificent dendritic tree spanning the whole lobula plate. They respond with depolarization upon motion stimuli in their preferred direction and with hyperpolarization for motion in the other (null) direction. They are tuned to different directions of motion and form groups of vertical system (VS) cells as well as horizontal system (HS) cells.

Tangential cells and optic flow fields

Moreover, detailed mapping of their spatial receptive fields in *Calliphora vicina* revealed that each lobula plate tangential cells has a different preferred optic flow pattern. Interestingly, these patterns resemble the optic flow as seen by the fly when it rotates along certain body axes, and hence, each lobula plate tangential cells encodes a different axis of fly ego-motion (Krapp *et al.*, 1998; Krapp and Hengstenberg, 1996). It is thought that these complex receptive fields are shaped further by axonal gap-junctions which couple lobula plate tangential cells in a chain-like manner (Haag and Borst, 2004).

Lobula plate in Drosophila

Most of the findings appear to be transferable to *Drosophila* (Fischbach and Dittrich, 1989; Scott *et al.*, 2002). Deoxyglucose mapping of the *Drosophila* visual system revealed a four-layered structure where each layer is responsive only to one of the four cardinal directions of motion: Layer 1 is selective for front-to-back, layer 2 for back-to-front, layer 3 for upward and layer 4 for downward motion on the ipsilateral side (Buchner *et al.*, 1984). In *Drosophila*, three HS cells (HSN, HSE, HSS) have been identified whose dendritic trees reside in the anterior region of the lobula plate (layers 1 and 2) where HSN covers the dorsal, HSE the medial and HSS the ventral part of the hemisphere (Heisenberg *et al.*, 1978; Schnell *et al.*, 2010). The six known VS cells (VS 1-6) have their dendrites covering the entire lobula plate (Heisenberg *et al.*, 1978).

Direction-selectivity of tangential cells

When stimulated with gratings moving in preferred or null direction at various velocities, the direction-selective responses of lobula plate tangential cells share many properties with optomotor behavior, including that the response strength is tuned to temporal frequency rather than velocity. Yet, the optimal frequency is around 1 Hz for lobula plate tangential cell recordings (Joesch *et al.*, 2008) while it is around 3–10 Hz for the optomotor response (Götz and Wenking, 1973). This discrepancy was resolved by performing electrophysiological recordings and two-photon imaging from lobula plate tangential cells in tethered flying or walking flies (Chiappe *et al.*, 2010; Maimon *et al.*, 2010): When the fly moved, the gain of the cell increased and the optimum shifted to higher temporal frequencies getting closer to those

found in behavioral experiments. Importantly, these effects could be mimicked in a fixed preparation by artificial application of the neuromodulator octopamine (Jung *et al.*, 2011) or by stimulating octopamine-secreting neurons in the central brain (Suver *et al.*, 2012).

Lobula plate and behavior

In order to assess the requirement of lobula plate tangential cells for the optomotor response, Heisenberg *et al.* (1978) investigated the anatomy of the mutant omb^{H31} (*optomotor blind*^{H31}) which had been isolated in a mutation screen for optomotor deficits (Heisenberg and Götz, 1975). It was found that in omb^{H31}-mutant flies lobula plate tangential cells were absent or significantly degenerated, indicating their necessity for optomotor behavior. Interestingly, these flies were still able to perform closed-loop bar fixation, suggesting that this behavior can be realized via a lobula plate-independent pathway. Further, it has been shown that sustained unilateral activation of HS cells via a bistable channelrhodopsin induces a turning response to the side of stimulation, in blind flies, implying that HS cells are sufficient for the optomotor turning response (Haikala *et al.*, 2013).

Lobula

While the lobula plate has been studied for decades, the neighboring neuropil, the lobula, has received much less attention. No electrophysiological recordings exist, nor any imaging data, and hence, almost nothing is known about its physiology and function. Detailed anatomical studies have revealed a six-layered structure with numerous lobula columnar neurons (LCNs) (Fischbach and Dittrich, 1989; Strausfeld, 1976). Characterization of lobula projection neurons (Otsuna and Ito, 2006) suggested a functional role of the lobula for color vision (Otsuna *et al.*, 2014) as well as for processing of certain second-order motion stimuli (Zhang *et al.*, 2013). Moreover, the lobula has been speculated to be used during fixation behavior because activity labeling via deoxyglucose mapping showed that the two most anterior layers are more responsive to front-to-back than to back-to-front motion (Buchner *et al.*, 1984) and because the lobula was labeled when visually stimulating flies with a rotating stripe (Bausenwein *et al.*, 1994).

Beside the well-characterized HS and VS cells in the lobula plate, little is known about the many other neuron types which reside in the lobula complex. Several kinds of large-field looming-sensitive neurons (Foma-1) have been identified in the lobula plate and lobula of *Drosophila* (de Vries and Clandinin, 2012). Genetic silencing of these neurons abolished escape behavior in response to visual stimulation. In contrast, optogenetic stimulation was sufficient to induce take-off in blind flies. Moreover, electrophysiological recordings revealed that the firing rate of Foma-1 neurons increases upon stimulation with looming discs with similar dynamics as had been found in locust looming-sensitive neurons (Hatsopoulos *et al.*, 1995). In the blowfly, a set of figure detection cells has been found (Egelhaaf, 1985a,b,c). Other small-target motion detector neurons have been identified and characterized in the lobula of hoverflies (Nordström *et al.*, 2006; Nordström and O'Carroll, 2006). These neurons respond to moving small-field objects but are inhibited by large-field motion and have therefore been considered to be important for figure tracking. However, it is unclear whether such cells exist in *Drosophila*.

1.6 MODELING

Behavioral and electrophysiological experiments indicate that visual processing in insects is highly deterministic and follows relatively simple mathematical rules. Hence, the insect can be considered as a computational device which transforms sensory input into behavioral output. It should therefore be possible to apply strategies from systems analysis and electrical engineering to uncover the computations performed by the insect brain. Such a cybernetic approach was first applied by Hassenstein and Reichardt (1956) who developed a computational framework to understand the optomotor behavior of the beetle *Cholorphanus viridis*. Later, similar strategies were used to investigate visual fixation behavior in *Drosophila* (Poggio and Reichardt, 1973).

1.6.1 Optomotor response

First systematic characterization

In the initial experiments performed by Hassenstein (1951), he positioned a tethered beetle in the center of a rotating grating and placed a light straw-made "Y-maze globe" under the legs of the animal, allowing him to precisely record walking dynamics. He observed a robust optomotor response. Whenever the walking beetle arrived at a Y-junction of the globe, it turned in the direction of the moving surround. How the animal obtained the information about the directionality of the stimulus remained unclear. This robust essay allowed Hassenstein to explore several kinds of simple visual stimuli to systematically dissect the detailed mechanisms underlying motion vision. Specifically, he performed experiments in which the animal could see the moving grating only through a set of vertical slits, which reduced the visual stimulus to spatially and temporally separated luminance changes. When the first and second pulse were both brightness increments (ON–ON), the beetle turned in the direction of the apparent motion. The same was true when both pulses were brightness decrements (OFF–OFF). However, in the case of mixed luminance changes (ON–OFF or OFF–ON) the turning response of the beetle was inverted.

In order to understand these results, Hassenstein teamed-up with Werner Reichardt (whom he had met during the Second World War when both were working as air-force radio operators near Potsdam). Together, they realized that the behavioral result could be explained by a computation involving a sign-correct multiplication. They further explored how the behavioral response depends on the temporal dynamics of the stimulus and of the spatial separation of the slits. They found that the response strength is tuned to a certain time delay of the apparent motion signal and that the optimal slit distance matches the interommatidial angle of the animal.

The Reichardt detector

Based on these results, Hassenstein and Reichardt (1956) succeeded in developing a simple, yet influential, computational model of motion vision, the Reichardt detector. Two neighboring receptors measure the luminance at a specific location in the environment. One of the inputs is linearly low-pass filtered, therefore delayed in time, while the other is not and both signals are subsequently multiplied (Fig. 5a). Subtracting the output of another, mirror-symmetrical detector leads to a direction-selective signal (Fig. 5b). When

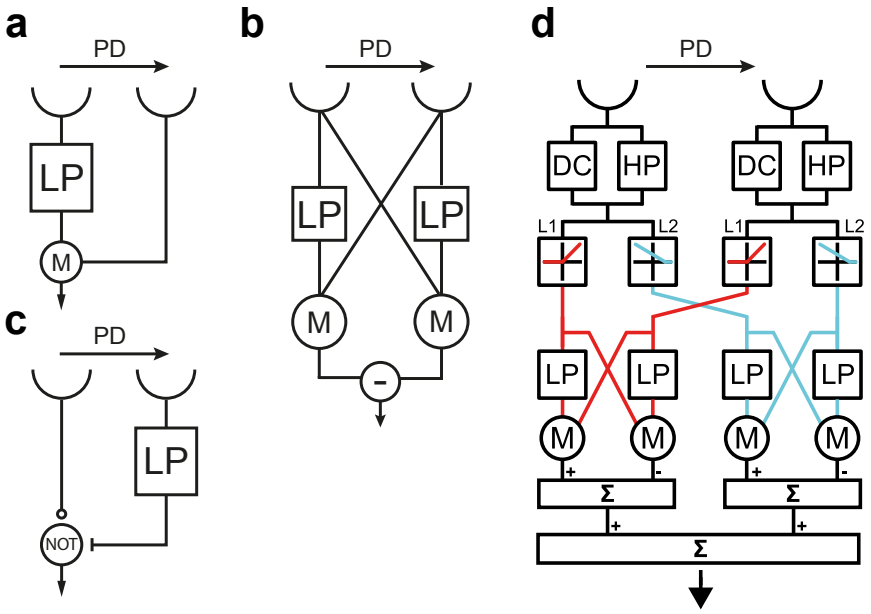

Figure 5: Models of motion vision. (**a**) Reichardt half-detector. Two neighboring signals are asymmetrically delayed and subsequently multiplied. (**b**) Mirror-symmetrical Reichardt detector. (**c**) Barlow-Levick half-detector. One signal leads to a delayed inhibition of the other and only positive signals are transmitted. (**d**) Variant of the Reichardt detector with independent ON and OFF channels (Eichner *et al.*, 2011). All models are direction-selective and prefer motion to the right.

stimulated with moving patterns in the preferred direction of motion, the model responds positively, while null-direction motion induces a negative response.

The Reichardt detector has proven to explain many of the behavioral observations in the beetle and was later shown to quantitatively predict in great detail the optomotor behavior of bees (Kunze, 1961) and different kinds of flies (Fermi and Reichardt, 1963; Götz, 1964) as well as direction-selective responses in fly lobula plate tangential cells (Egelhaaf and Borst, 1989; Joesch *et al.*, 2008). A very similar model, the Barlow-Levick motion detector, originated from early work on the rabbit retina (Barlow and Levick, 1965). It differs from the Reichardt model in the form of the non-linearity and in the arrangement of the delays (Fig. 5c). Further, the Reichardt detector has been influential in the development of more elaborated variants (van Santen and Sperling, 1985) as well as other classes of motion-detectors such as motion energy models (Adelson and Bergen, 1985), all of which were applied to vertebrate and human motion psychophysics.

Extension to ON and OFF pathways

With the discovery of separate contrast polarity-specific ON and OFF pathways for motion vision (Joesch *et al.*, 2010), the internal structure of the Reichardt detector needed to be extended to account for these independent processing pathways (Eichner *et al.*, 2011). One solution is to use four parallel detectors which cover all four possible input conditions (ON–ON, ON–OFF, OFF–ON, and OFF–OFF) and sum their outputs. Such a "4-quadrant detector" would have a suitable internal structure and would be mathematically equivalent to the original Reichardt model. Alternatively, two of such units could form a "2-quadrant detector", dealing only with

ON–ON and OFF–OFF input signals (Franceschini *et al.*, 1989) (Fig. 5d). By using apparent motion steps and pulses and recording direction-selective responses in lobula plate tangential cells, Eichner *et al.* (2011) could show that the latter structure is implemented in the visual system of the fly. Nevertheless, using behavioral experiments, Clark *et al.* (2011) developed a different model: Eight Reichardt half-detectors analyze all combinations of luminance changes whose outputs are differentially weighted and summed. These alternative models make several predictions about direction-selective responses to apparent motion steps when either the ON or the OFF pathway is blocked. Corresponding experiments have indicated a better match with the 2-quadrant detector (Joesch *et al.*, 2013).

Biophysical implementation

The structural simplicity of the Reichardt model suggests a corresponding biophysical implementation in the visual system of the fly: rectification in order to isolate ON from OFF signals, a low-pass filter in order to delay one of the input streams, a multiplication and a subtraction stage. Indeed, anatomical studies have shown that two pathways, starting at L1 and L2, converge onto lobula plate tangential cells and might therefore constitute independent detector units dealing with moving ON and OFF edges, respectively. Mi1, Tm3 neurons are postsynaptic to L1 and respond to brightness increments while Tm1–Tm3 neurons are postsynaptic to L2 and respond to brightness decrements (Behnia *et al.*, 2014; Meier *et al.*, 2014; Strother *et al.*, 2014) but none of these cells are direction-selective.

Using detailed electromicroscopic reconstructions of the medulla network, it has been possible to start at a direction-selective layer of the lobula plate and trace back anatomical connections within the ON pathway (Takemura *et al.*, 2013). It was found that the resulting photoreceptor input arrangement is spatially offset and, if Mi1 is considered to implement the low-pass filter, matches the preferred axis of cardinal motion of the chosen layer. A later study performed electrophysiological recordings from Mi1, Tm3 as well as from Tm1, Tm2 (Behnia *et al.*, 2014). It was found that the temporal dynamics are in agreement with the notion that Mi1 and Tm1 implement the low-pass filters within the ON and OFF pathways, respectively, and that Tm3 and Tm2 constitute the corresponding direct lines. As none of these neurons are direction-selective, the computation of direction-selectivity must occur afterwards. Finally, the outputs of the two arms of the Reichardt detector need to be subtracted. This is likely to be implemented at the level of the lobula plate via local inhibitory interneurons (Mauss *et al.*, 2014).

1.6.2 Fixation response

Motion and position system

When flies are given control over a vertical bar in closed-loop configuration, they quickly bring the bar to the front and keep it there (Reichardt and Wenking, 1969). The response is innate and robust, and has therefore stimulated a systematic dissection of the underlying mechanisms. Poggio and Reichardt (1973) started with open-loop experiments where they moved a single bar around the fly or showed an oscillating bar at a specific angular location. They found that the behavioral responses could be well-described by linear superposition of a motion detection system (r) and position detection system (D). Both systems were weighted depending on the angular horizontal position of the bar (ψ). The function $r(\psi)$ was always positive

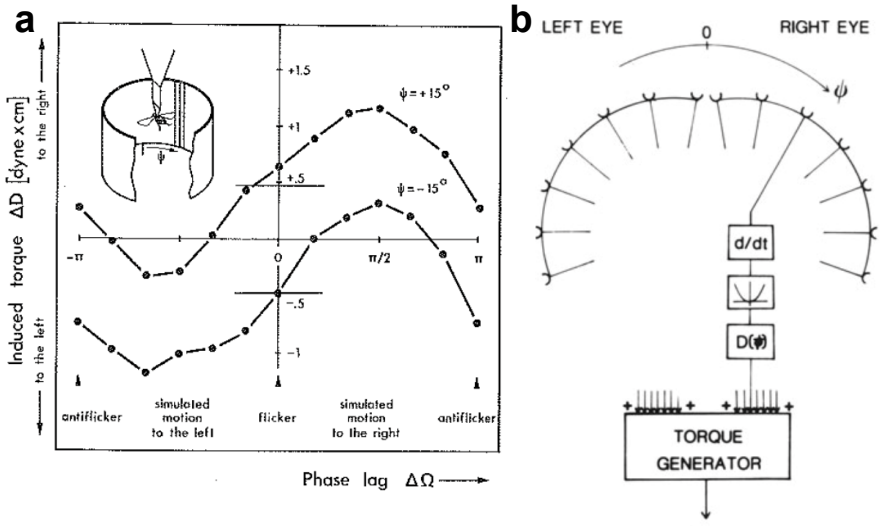

Figure 6: Position detection mechanism. (**a**) Experiments with two neighboring stripes flickering with the same frequency but with different phases (Pick, 1974). Variation of the phase produces directional responses in different directions and flies turn towards the position of the stripes for phase shifts 0° and 180°. The former result can readily be explained by the Reichardt model while the latter cannot, which suggests the presence of an independent flicker-sensitive position system. (**b**) A potential implementation of such a flicker system calculates the derivative of the signal and applies a subsequent squaring operation (Buchner, 1984).

(flies turn syn-directionally to bar movement), while $D(\psi)$ was positive on the right side of the fly and negative on the other (flies turns towards the position of the bar). These relatively simple findings led to the creation of an elaborate theoretical framework which could quantitatively describe closed-loop fixation behavior of one or multiple bars (Reichardt and Poggio, 1975).

Position detection via motion asymmetry

In order to initiate a directed turn towards an object or landmark in the environment, flies need to compute the position of such cues. Such a computation might theoretically be implemented at the level of single photoreceptors which measure the luminance distribution in the environment and trigger a rotational response towards the darkest point in space, for example. However, it was shown that stationary objects do not induce a turning tendency but that locally oscillating bars do (Reichardt, 1973). Moreover, it was shown that rotating bars produce responses of different amplitudes when moving progressively (front-to-back) or regressively (back-to-front) (Poggio and Reichardt, 1973). These findings have resulted in the notion that the position detection system requires motion detection and that progressive motion induces stronger turning responses than regressive motion. Such an asymmetry would, on average, lead to a turning tendency towards oscillating stripes during open-loop or to bar fixation during closed-loop experiments while it would not initiate responses towards static landmarks.

Position detection via flicker detectors

An alternative model was proposed by Pick (1974). Instead of using spatially oscillating bars he used bars with oscillation in luminance in order to characterize the position detection system (Fig. 6a). He found that flickering bars induce a robust turning responses towards the location of the flicker and concluded that a set of motion-independent flicker detectors must exist. These detectors could simply be modeled by taking the high-pass-filtered

signals from photoreceptors followed by a squaring operation, subsequent weighting and summation (Buchner, 1984) (Fig. 6b). Further characterization indicated that the positional weighting function of these detectors was almost identical to the one which was found for spatially oscillating bars. Pick (1974) realized that moving the bar in the environment not only creates a motion stimulus, it also induces local luminance decreases and increases. Hence, oscillating bars might simply stimulate local flicker detectors. Such a system would induce turning towards the position of a flicker and hence towards any moving bar and could therefore explain the apparent behavioral asymmetries without assuming differential processing of front-to-back and back-to-front motion.

However, oscillating and flickering stripes did not always produce the same responses: Pick (1976) tested different sizes of the flicker stimulus as well as varying amplitudes of the spatial oscillation. He found that responses towards oscillating stripes monotonically increased as a function of size while the response to the flicker was tuned to a specific bar width. He concluded that lateral interactions seem to play an important role for computation within the position detection system. Later, Wehrhahn and Hausen (1980) argued that the characterization of the position detection system with slowly moving, oscillating or flickering bars is based on time scales which are much slower than the ones flies would encounter during realistic flight maneuvers. Using transient stimuli, the authors could not confirm the existence of a flicker-sensitive system, but rather argued for a computation which relies on fast motion detection mechanisms similar to a front-to-back and back-to-front asymmetry (Wehrhahn, 1981).

Biophysical implementation

In contrast to the detailed knowledge of neuronal networks involved in motion computation, almost nothing is known about cells involved in fixation behavior. One study recorded from the internal chiasm of *Musca* and found units responding positively to brightness increments and decrements (Arnett, 1972) which might constitute the flicker detectors proposed by Pick (1974). Other studies have provided evidence for a motion-based tracking system by characterizing in detail a set of interneurons (FD-cells) in the lobula plate of *Musca* (Egelhaaf, 1985a,b,c). These cells are direction-selective, tuned to small objects, and are inhibited by large-field motion. This response was modeled based on an appropriate network of Reichardt detectors, which explained several behavioral measurements during figure-ground discrimination experiments. However, other studies testing mutant flies with missing or size-reduced lobula plates found that fixation behavior remained largely intact (Heisenberg *et al.*, 1978). This suggested that direction-selective units in the lobula plate are not essential for the behavior and that another visual pathway must constitute the position detection system.

In conclusion, despite quantitatively precise descriptions of fixation behavior, the literature does not currently provide a coherent picture of position detection. It is not known which neuronal elements are important and it remains unclear which role lateral interactions play and to what extent motion detection is essential for the computation of positional cues.

1.7 INSECT-INSPIRED ROBOTICS

Insects have tiny and relatively simple brains. Yet, they show astonishingly robust hard-wired visual orientation behaviors. These facts have long stimulated engineers from early on to implement some of the underlying principles in autonomously moving robots. Theoretical work showed that simple vehicles equipped with Reichardt detectors can perform surprisingly complex orientation maneuvers (Braitenberg, 1986). Accumulation of knowledge about details of visual processing in insects together with minimization in the size and cost of electrical circuit elements has made it possible to design realistic insect-inspired artificial systems.

The reasons for a such a cybernetic approach are two-fold: First, the design of such robots permits thorough testing and systematic manipulation of the system under real-world conditions. Hence, it allows assessing the degree of completeness of our understanding of how insects use visual cues for orientation. Second, insects have evolved over millions of years and have been under strong evolutionary pressure. One can therefore expect that nature has equipped them with visual systems that implement simple, robust, efficient and possibly even optimal solutions for vision-based spatial orientation. Thus, engineers and computer vision researchers might learn a lesson from exploring the solutions that insect evolution has found for a particular problem.

1.7.1 Unmanned micro aerial vehicles

Unmanned micro aerial vehicles (MAVs) are autonomously flying lightweight robots with diameters of $\approx 20\,\text{cm}$ or less and are used for surveillance or exploration. For example, they can be used to inspect areas which are too small or too dangerous to be accessed by humans and can even aid military during infantry operations. Due to their small size, they not only often resemble insects, they also face the same challenges: First, they have to be light and energy-efficient. Second, even small turbulences will change their flight path, and hence, they require systems for course stabilization.

Classical aerial engines and stabilization based on gyroscopic or GPS sensors are often too heavy and consume too much energy, and therefore, considerable effort is put into the development of insect-inspired flight motors (Ma *et al.*, 2013) and insect-inspired visual sensors (Song *et al.*, 2013). However, most vision-based algorithms are computationally expensive, yielding low-frame rates and are therefore performed off-board in many cases. This approach leaves the MAV with the sensory acquisition and motor control but requires efficient transmission to the external computing unit. Yet, wires limit the operational radius of the robot and wireless transmission is often not reliable enough. The solution to this problem is to simplify the computational algorithms such that they can be solved by processing elements on-board. Here, it is often technologically easier to first develop a robot-independent circuit architecture, then to adopt the system for terrestrial vehicles or for larger flying robots and then to move to miniaturization of MAVs.

1.7.2 Examples

Bees integrate optic flow in the environment during flight and implement a visually-driven odometer which is well-suited for estimating distance of travel (Srinivasan *et al.*, 1996). Such a system has been implemented in an autonomous vehicle: Integration of translatory and rotatory optic flow allowed the robot to compute its location in space and to automatically find its starting position (Chahl and Srinivasan, 1996). Moreover, bees have been shown to maintain distance from walls and regulate their flight speed by balancing optic flow in the two lateral hemispheres (Srinivasan *et al.*, 1991). A similar system was able to move through a tunnel, around corners and through narrow passages and was able to control its velocity based on optic flow (Humbert and Hyslop, 2010).

Maintaining constant height during flight normally requires heavy GPS-based sensors or altimeters on-board which are not feasible for MAVs. When flying with constant velocity, bees regulate distance to the ground by adjusting the ventral optic flow (Portelli *et al.*, 2010), a strategy which was implemented in a small flying helicopter and which enabled the robot to maintain its distance to the ground (Garratt and Chahl, 2008). Conversely, ventral optic flow can also be maintained by reducing flight speed during landing maneuvers. Such behavior is observed in bees (Chahl *et al.*, 2004) and was successfully implemented in a small flying airplane (Beyeler *et al.*, 2009). It ensures a safe landing operation in both bees and robots. Another design project, the DelFly project, has focused on creating a flying robot with flapping wings which has relatively low energy consumption while producing sufficient lift for takeoff (de Croon *et al.*, 2009). In its recent version, the DelFly only spans $\approx 10\,\text{cm}$ in diameter and weighs only $\approx 3\,\text{g}$, yet it is equipped with two small cameras, a small embedded computer and batteries. Thanks to efficient software algorithms, the system can process information from the cameras on-board in real-time, enabling the robot to fly autonomously for up to three minutes while avoiding obstacles in the environment.

1.7.3 Reichardt detector-based ego-motion sensors

In robotics, traditional approaches to estimate motion in the environment rely on computationally expensive algorithms which correlate image sections between successive frames. Yet, flies with their tiny brains perform such tasks with impressive speed and precision. The Reichardt detector has been shown to be a reliable model of fly orientation behavior and it is therefore tempting to apply this model to motion computation in robots. For example, a blimp-type flying robot was equipped with a full-field camera, wireless video link and radio receiver. Images from the cameras were transferred to a computer and analyzed by an array of vertically and horizontally arranged Reichardt detectors. Their outputs were subsequently added and generated a motor signal which was sent back to the blimp in order to control rotation, elevation and thrust (Iida, 2003).

In order to overcome the need of outsourcing computing power, O'Carroll *et al.* (2007) designed a microprocessor (analog VLSI) which was optimized

to compute the elementary operations of the Reichardt detector. Further, complexity was significantly reduced by using a circular ring array of 40 photodiodes instead of a full-field camera. The output of this simple system showed reliable correlation with the speed of several natural scenes rotating around the sensor. Similarly, Köhler *et al.* (2009) designed a system with a much increased resolution of 10 000 Reichardt detector elements, which approximates the value present in flies. The system was based on a field-programmable gate array (FPGA) which offers virtual implementations of logical circuits and makes the design process fast, flexible and modular. Hence, it allowed vigorous testing of several variants of the Reichardt model and different integration schemes and would, for example, be easily transformable into an efficient looming detector. Such systems use very little current, they are light-weight and can be small and are therefore ideal for implementing Reichardt detector arrays directly on-board MAVs.

1.8 CONCLUDING REMARKS

Drosophila is an ideal model organism for the fundamental questions in systems neuroscience as it permits simultaneous application of various tools. Specifically, significant progress in the field has been made by focusing on motion vision. The reasons for this focus are two-fold: First, motion vision is intuitive for the human researcher because it is also relevant to us. Second, the corresponding visual behavior, the optomotor response, is innate, robust, and has been well characterized for decades. It was formalized mathematically by the Reichardt detector, which provided the backbone for subsequent studies of the cellular components underlying motion computation.

These explorations were supported tremendously by recent tool developments. First, genetic manipulation techniques have evolved with an impressive pace, permit targeting of single cell types and can be used to express virtually any protein of choice. Second, anatomical studies have provided detailed maps of connectivity, morphology and neurotransmitter systems within the visual system. Third, physiological tools such as whole-cell patch clamp electrophysiology and two-photon calcium imaging allow in vivo recordings from single cells or populations of cell types. For these reasons, the visual system of the fly is probably the best-studied circuit for neuronal computation and could soon provide the first complete functional description of a biological system transforming sensory input into meaningful behavioral output.

However, such a functional loop can only provide a partial understanding of behavior under naturalistic conditions because other visual behaviors such as fixation of landmarks or avoiding looming objects, for example, are equally relevant for orientation. Yet, these behaviors have been much less studied and very little is known about their underlying computational rules and neuronal elements.

2 PAPER I: OBJECT TRACKING IN MOTION-BLIND FLIES

In this article the visual orientation performance of T4/T5-silenced flies has been studied. This is the main paper of my thesis and was published in Nature Neuroscience in April 2013[1].

Summary

The presented work contains a detailed description of a new kind of behavioral setup which I have designed and built and which permits precise measurements of behavioral visual responses of walking *Drosophilae*. We used this setup in combination with genetic silencing of T4 and T5 neurons in order to characterize the role of these cells in visual orientation behavior. We found that these flies were completely blind to motion but that they could still fixate a black bar, though at a reduced performance. We investigated in detail why motion-blind flies could still fixate the object and why their fixation performance was reduced. We found that the fixation response is mainly controlled by a T4/T5-independent flicker-sensitive position system. Additionally, we found that the motion response in control flies is asymmetric, i.e. it is stronger for front-to-back than for back-to-front motion, which further improves fixation performance.

The following people contributed to this work:

Author contributions

Armin Bahl[*], Tabea Schilling, Georg Ammer and Alexander Borst. — **A.Ba.**[*] and A.Bo. designed the study. **A.Ba.**[*] set up the locomotion recorder and the stimulus display, and wrote the software for reading the behavioral output and displaying the stimulus. **A.Ba.**[*] and T.S. performed all of the behavioral experiments and evaluated the data. G.A. performed the electrophysiological recordings from LPTCs and analyzed the data. A.Bo. carried out modeling work. A.Bo. and **A.Ba.**[*] wrote the manuscript with the help of the other authors.

The work in this paper has been highlighted in a News & Views article in Nature Neuroscience (Masson and Goffart, 2013).

1 Nature Neuroscience 16, 730–738 (2013) doi:10.1038/nn.3386

Object tracking in motion-blind flies

Armin Bahl, Georg Ammer, Tabea Schilling & Alexander Borst

Different visual features of an object, such as its position and direction of motion, are important elements for animal orientation, but the neural circuits extracting them are generally not well understood. We analyzed this problem in *Drosophila*, focusing on two well-studied behaviors known as optomotor response and fixation response. In the neural circuit controlling the optomotor response, columnar T4 and T5 cells are thought to be crucial. We found that blocking T4 and T5 cells resulted in a complete loss of the optomotor response. Nevertheless, these flies were still able to fixate a black bar, although at a reduced performance level. Further analysis revealed that flies in which T4 and T5 cells were blocked possess an intact position circuit that is implemented in parallel to the motion circuit; the optomotor response is exclusively controlled by the motion circuit, whereas the fixation response is supported by both the position and the motion circuit.

Optomotor and fixation responses of flies have been studied extensively. Experiments on tethered *Drosophila* walking or flying inside a rotating drum revealed a strong and persistent optomotor response along the direction of the rotating drum[1–3] (open loop). The effect of large-field stimuli on visual course control can also be seen in free flight, where the structure of the flight path of *Drosophila* depends on the visual pattern of the surrounding environment[4]. When the pattern is rotating, the fly's behavior exhibits distinct, circular flight paths around the center of the arena[5]. Fixation behavior was first observed in tethered flying house flies in which the fly's torque was fed back into a servo motor controlling the position of a black bar[6,7] (closed loop). Under these conditions, flies keep the bar in front of them most of the time. Moreover, it was shown that bar fixation interacts with the expansion avoidance reaction of *Drosophila* when presented with translatory full-field optic flow[8]. Fixation behavior has also been studied in freely walking and flying *Drosophila*[9–12]. On the basis of their different dynamics and spatial sensitivity, the optomotor and fixation responses were proposed to represent the output of different visual processing pathways[13]. Similar conclusions were drawn from experiments in which the tangential cells of the lobula plate were either genetically or surgically removed[14–17], or in mutants with reduced optic lobes[18]; in general, flies seem to be impaired more strongly in their response to large-field rotating patterns than in their reaction to single, moving bars. However, none of the techniques used provided a sufficiently high resolution to make any definitive statements about the involvement of individual cell types of the fly optic lobe in one or the other pathway.

To dissect the neural circuits underlying the optomotor and fixation responses, we built on recent progress in our understanding of the visual processing stream[19] leading from the photoreceptors R1–6 via lamina and medulla to directionally selective motion responses in the lobula plate tangential cells (LPTCs; **Fig. 1a**). Recording from LPTCs via whole-cell patch[20,21] combined with selective blockade of individual columnar cells revealed that lamina cells L1 and L2 provide the main input to the motion detection circuit, functionally segregating into an ON and an OFF pathway, respectively[22,23]. The L1 and L2 pathways, which have been described anatomically[24,25], converge again on the dendrites of the tangential cells in the lobula plate via T4 and T5 cells; blocking the synaptic output from T4 and T5 cells completely abolishes the motion response in tangential cells, but leaves some residual response to full-field flicker[26]. To test the behavioral performance of these flies, we used a procedure in which a tethered fly walks on a small sphere supported by an air stream[2,27]. A computer reads the movement of the sphere, controls the visual stimulus presented to the fly and adjusts the ambient temperature. Moreover, we used the *Gal4-UAS* system[28] to genetically express a temperature-sensitive allele of *shibire*[29] in a small subset of neurons in the fly brain. This permitted a selective shut down of the desired part of the neuronal circuit during the experiment by switching from the permissive temperature for *shibire^{ts}* (25 °C) to its restrictive one (34 °C).

RESULTS

Optomotor and fixation response

We tested the optomotor and fixation response of flies in which *shibire^{ts}* was expressed in T4 and T5 cells (T4/T5 block flies). As the behavior of flies turned out to be highly dependent on temperature (**Supplementary Fig. 1**), all of our control experiments were carried out with flies of a different genotype using the same temperature protocol. For controls, we used flies with two different genotypes: flies that carried the *shibire^{ts}* effector allele, but no *Gal4* driver gene (*shi^{ts}* control), and flies that carried the *Gal4* driver gene, but no *shibire^{ts}* effector gene (T4/T5 control). We examined the temperature dependency of the block: T4/T5 block flies behaved similar to control flies at 25 °C, as well as when the temperature was slowly elevated to 34 °C. However, clear differences emerged approximately 5 min after reaching 34 °C (**Supplementary Fig. 1**). To exclude any motor deficits in T4/T5 block flies, we analyzed their general walking and turning activity, which were not different from those of control flies (**Supplementary Fig. 2**).

Max Planck Institute of Neurobiology, Martinsried, Germany. Correspondence should be addressed to A. Bahl (bahl@neuro.mpg.de) or A. Borst (borst@neuro.mpg.de).

Received 6 February; accepted 28 March; published online 28 April 2013; doi:10.1038/nn.3386

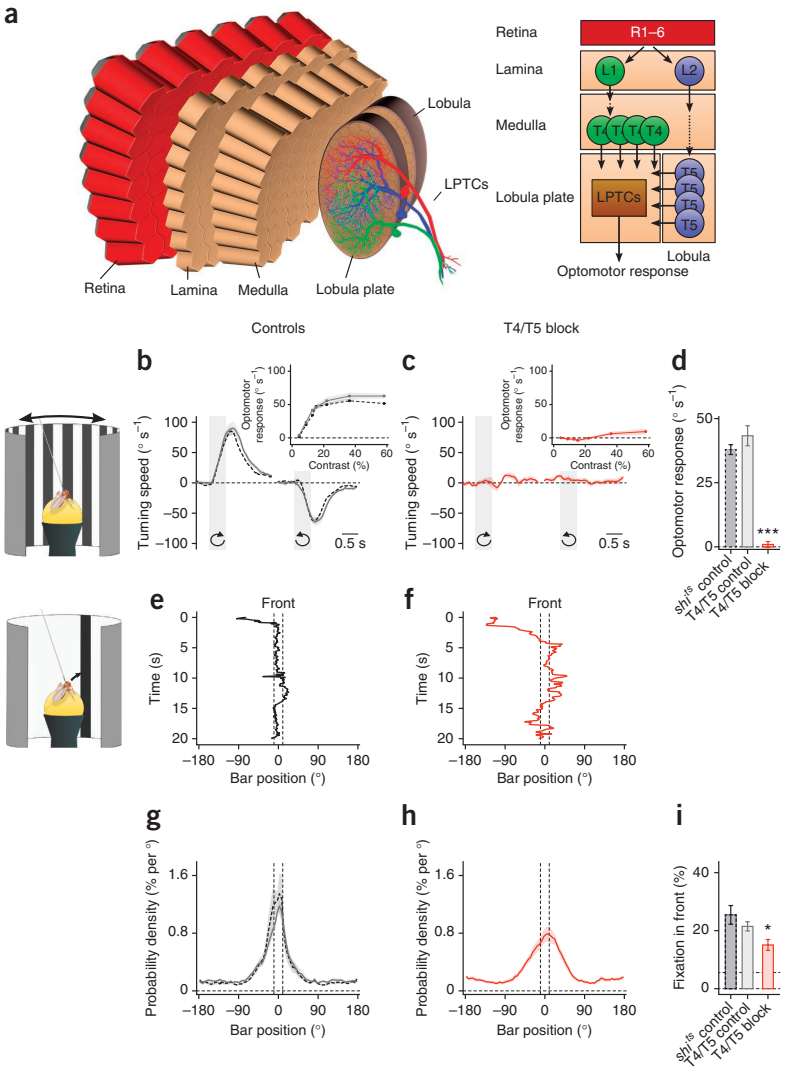

Figure 1 Optomotor response and fixation response of control and T4/T5 block flies. (**a**) Schematic of the fly's optic lobe. In each lamina column, photoreceptors R1–6 synapse onto lamina cells L1 and L2, forming parallel pathways for motion detection. The output signals of both pathways converge via T4 and T5 cells on the dendrites of LPTCs. (**b**,**c**) Turning speed of control (shi^{ts} control (dashed black line) and T4/T5 control (solid gray line); **b**) and T4/T5 block (solid red line; **c**) flies in response to clockwise and counterclockwise rotation of a grating pattern (contrast = 22%, gray shaded areas; 20 trials per fly, $n = 10$ flies per group). Inset, optomotor response as function of grating contrast (clockwise minus counterclockwise rotation response divided by 2; averaged in 1 s after stimulus onset). (**d**) Average optomotor response (average over contrasts). $^{***}P < 0.001$, two-sided t test compared with both control groups. The response of the T4/T5 block group was not significantly different from zero ($P = 0.47$, two-sided t test). (**e**,**f**) Bar position over time during closed-loop fixation (single trial of one shi^{ts} control fly (**e**), single trial for one T4/T5 block fly (**f**)). Vertical dashed lines indicate the frontal area (±10°). (**g**,**h**) Average probability density as function of bar position for control (40 trials per fly, $n = 10$ flies per group; **g**) and T4/T5 block (40 trials per fly, $n = 12$ flies; **h**) flies. (**i**) Integration of the probability density curves between ±10° gives the percentage of time the bar is held in the frontal visual field (fixation in front). Upper horizontal dashed line represents the chance level (5.6%, no fixation). $^{*}P < 0.05$, two-sided t test compared with both control groups. The value of the T4/T5 block group was significantly different from chance ($P < 0.001$, two-sided t test). All data represent mean ± s.e.m.

We first confronted the flies with a large-field grating moving clockwise and counterclockwise (**Fig. 1b–d**). Both types of control flies exhibited a strong and reliable optomotor response over a wide range of pattern contrasts (**Fig. 1b**,**d**). Instead, T4/T5 block flies no longer followed the motion of the panorama, no matter how high the pattern contrast (**Fig. 1c**,**d**). We next performed closed-loop fixation experiments and coupled the flies' turning tendency to the position of a single black bar such that whenever the fly turned into one direction, the bar moved into the other (**Fig. 1e–i**). Control flies robustly moved the bar to the front and kept it there (**Fig. 1e**,**g**,**i**). When we tested the flies in which the output from T4 and T5 cells was blocked, we were surprised that they were still clearly able to fixate the bar, although with a somewhat broader position distribution than control flies (**Fig. 1f**,**h**,**i**). Taken together, these results indicate that T4 and T5 cells are a necessary part of the neural circuit controlling the optomotor response to large-field motion, but are not needed for fixation behavior.

Dissection of motion and position system

Does that mean that fixation behavior relies on a separate set of motion-sensitive neurons tuned specifically to small moving objects, or does fixation behavior rely on a purely position-dependent system that is insensitive to motion? To tease apart the response to the direction and the response to the position of a moving bar, we used a classical approach[30] and moved a single bar in open loop around the fly, first in a clockwise and then in a counterclockwise direction, and measured both responses (R_{cw} and R_{ccw}, respectively) as a function of bar position (Ψ)[31].

Assuming that the turning response R of the fly to the rotating bar reflects a superposition of a position system P and a motion system M (with $v = d\Psi/dt$ denoting the angular velocity of the bar), we can write

$$R = P(\Psi, v) + M(\Psi, v)$$

For the two directions of bar rotations, we obtain

$$R_{cw} = P(\Psi, v) + M(\Psi, v)$$
$$R_{ccw} = P(\Psi, -v) + M(\Psi, -v)$$

To simplify these equations, two classical assumptions can be made[30]. First, the position system is velocity independent ($P(\Psi,v) = P(\Psi)$). Second, the motion system is linear in v ($M(\Psi,v) = M(\Psi)\cdot v$). Following

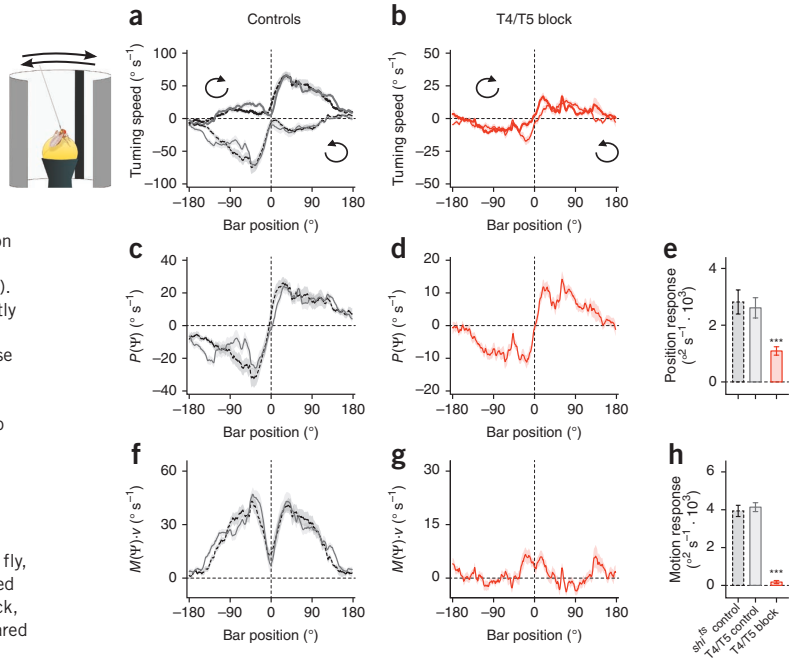

Figure 2 Open-loop analysis of the fixation response. (**a**,**b**) Responses of control (**a**) and T4/T5 block (**b**) flies to a single black bar moving clockwise (thicker lines) and counterclockwise around the fly. Responses are plotted as a function of the azimuth position of the bar; that is, during counterclockwise rotation, time progresses from right to left. (**c**,**d**) Summation of the clockwise and counterclockwise responses divided by 2 revealed the position-dependent response component, $P(\Psi)$, of control (**c**) and T4/T5 block (**d**) flies. (**e**) The position response (the integral of the curve $P(0° < \Psi < 180°)$ minus the integral of $P(-180° < \Psi < 0°)$ divided by 2). The response of the T4/T5 block group was significantly greater than zero ($P < 0.001$, two-sided t test). (**f**,**g**) Subtraction of the clockwise and counterclockwise responses divided by 2 yielded the motion-dependent response component, $M(\Psi)\cdot v$, of control (**f**) and T4/T5 block (**g**) flies (a positive value indicates a tendency to turn with the stimulus). (**h**) The motion response (the integral of the curve $M(0° < \Psi < 180°)\cdot v$ plus the integral of $M(-180° < \Psi < 0°)\cdot v$ divided by 2). The response of the T4/T5 block group was not significantly different than zero ($P = 0.06$, two-sided t test). All data represent mean ± s.e.m.; 35 trials per fly, $n = 10$, 11 and 14 flies per group (shi^{ts} control, dashed black lines; T4/T5 control, solid gray lines; T4/T5 block, solid red lines). $^{***}P < 0.001$, two-sided t test compared with both control groups.

these assumptions, the position system as well as the motion system can be recovered

$$P(\Psi) = (R_{cw} + R_{ccw})/2$$
$$M(\Psi)\cdot v = (R_{cw} - R_{ccw})/2$$

We performed such experiments on control and T4/T5 block flies (**Fig. 2**). With a starting position behind the flies, control flies followed the direction of motion of the bar, turning clockwise (+) during clockwise motion and counterclockwise (−) during counterclockwise motion (**Fig. 2a**), which is slightly different from what has been measured in flying *Drosophila* under similar conditions[8]. According to the formal decomposition outlined above, we recovered a position-dependent response component, $P(\Psi)$ (**Fig. 2c**,**e**), and a motion-dependent response component, $M(\Psi)$ (**Fig. 2f**,**h**). The responses of T4/T5 block flies to such stimuli were markedly different from those of control flies; in general, T4/T5 block fly responses had smaller amplitudes and were almost identical for both directions of bar motion (**Fig. 2b**). Decomposing the reaction into the position- and motion-dependent components revealed that the response of these flies to the position of the bar, $P(\Psi)$, was still present, although reduced in amplitude (**Fig. 2d**,**e**). However, the response to the motion of the moving bar, $M(\Psi)$, was completely abolished (**Fig. 2g**,**h**). We conclude that T4/T5 block flies are blind to the motion of a single bar, but can still detect its position. Thus, the ability of motion-blind flies to fixate a bar in closed loop (**Fig. 1f**,**h**,**i**) is a result of the remaining position response.

What is the visual cue used by the position system that allows the detection of bar position: is it mere stationary contrast, its temporal change or its local motion? To address these questions, we presented control flies with an appearing black bar (10° width) at +90° azimuth which stayed there for 4 s before disappearing again (**Fig. 3**). The time during which the bar appeared and disappeared amounted to 0.5 s approximating the local luminance change when a black bar (width = 10° and $v = 20\ ° s^{-1}$) moves into a 10°-wide window and, after 4 s, moves out again. Control flies exhibited a strong, but transient, response toward the position at which the bar was appearing as well as where it was disappearing, but, during the stationary phase of the bar, no response was detectable (**Fig. 3a**). We then determined the response values as function of bar position. In control flies, the shape of the resulting response functions (**Fig. 3c**,**i**) looked similar to $P(\Psi)$ as obtained in the previous experiment (**Fig. 2c**,**d**). We next repeated the experiments on T4/T5 block flies. Like control flies, T4/T5 block flies responded transiently to both the appearance as well as to the disappearance of the bar, but not when the bar was stationary (**Fig. 3b**). Moreover, the shape of the position-dependent response functions was almost identical to the ones of control flies (**Fig. 3d**,**g**,**j**). We conclude that the position system is insensitive to a stationary image but uses the change of luminance over time as its input signal[32]. Furthermore, the position system is not affected by blocking the output of T4 and T5 cells.

Turning responses to local motion and luminance changes

We observed a clear reduction of the performance of T4/T5 block flies compared to controls when we characterized their position response under closed-loop fixation conditions (**Fig. 1e–i**) and when we used a rotating bar (**Fig. 2**). However when we used local luminance changes, we found no difference between T4/T5 block and control flies (**Fig. 3**). This discrepancy suggests that the detection of motion somehow enhances the fly's response toward the position of the bar. We considered two possible mechanisms. First, the motion and position system may not be fully separable on the neuronal level. In this case, local motion might directly modify the position system to enhance the position response. Second, the motion system may have a stronger response to front-to-back than back-to-front motion. In the behaving fly, this would lead to a stronger compensation of bar motion away from the front, thereby improving fixation[33]. In both cases, T4/T5 block flies would no longer be able to detect the motion of the bar and their position response would be reduced. Furthermore, both arguments indicate that our assumptions (**Fig. 2**), which were adopted from classical experiments[30], might not be fully correct.

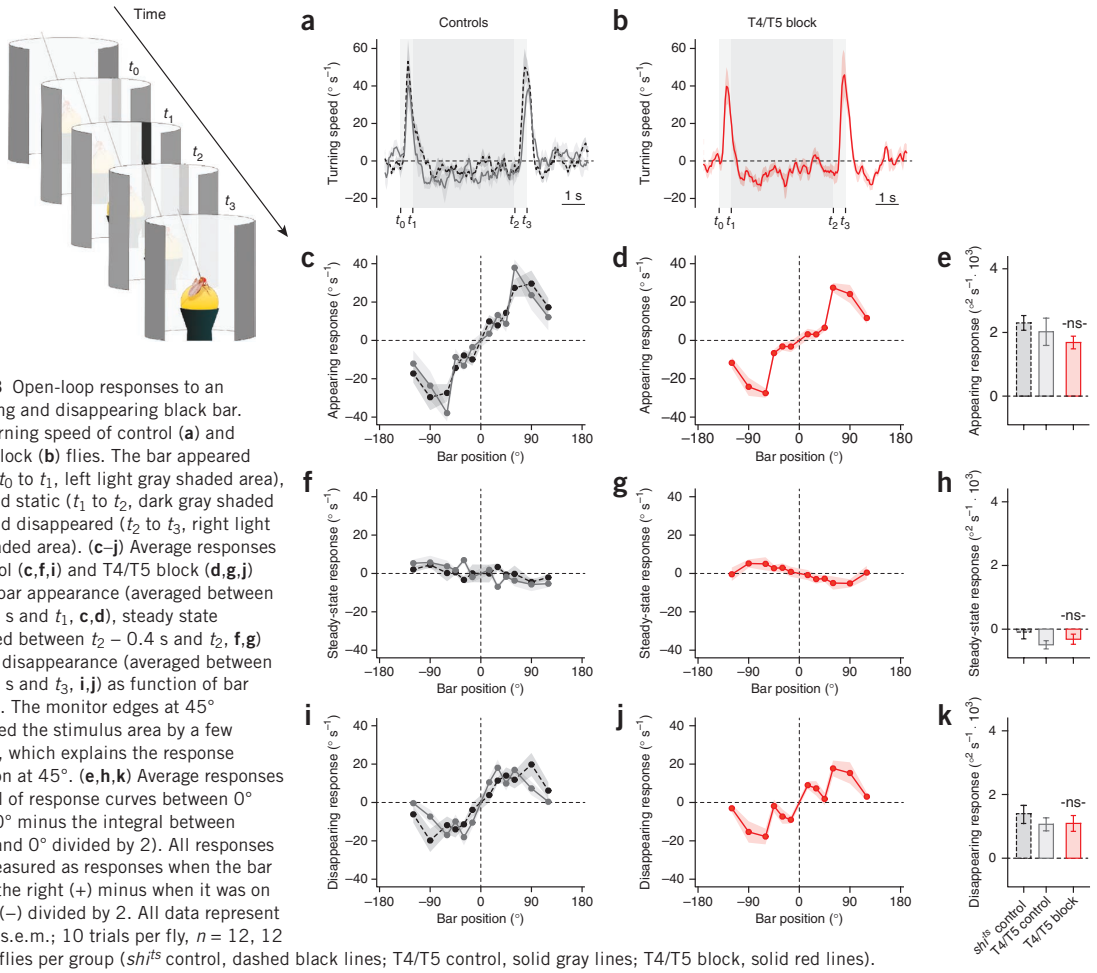

Figure 3 Open-loop responses to an appearing and disappearing black bar. (**a**,**b**) Turning speed of control (**a**) and T4/T5 block (**b**) flies. The bar appeared at 90° (t_0 to t_1, left light gray shaded area), remained static (t_1 to t_2, dark gray shaded area) and disappeared (t_2 to t_3, right light gray shaded area). (**c**–**j**) Average responses of control (**c**,**f**,**i**) and T4/T5 block (**d**,**g**,**j**) flies to bar appearance (averaged between t_0 + 0.1 s and t_1, **c**,**d**), steady state (averaged between t_2 – 0.4 s and t_2, **f**,**g**) and bar disappearance (averaged between t_2 + 0.1 s and t_3, **i**,**j**) as function of bar position. The monitor edges at 45° decreased the stimulus area by a few degrees, which explains the response reduction at 45°. (**e**,**h**,**k**) Average responses (integral of response curves between 0° and 120° minus the integral between –120° and 0° divided by 2). All responses were measured as responses when the bar was on the right (+) minus when it was on the left (–) divided by 2. All data represent mean ± s.e.m.; 10 trials per fly, n = 12, 12 and 16 flies per group (*shi^{ts}* control, dashed black lines; T4/T5 control, solid gray lines; T4/T5 block, solid red lines). ns indicates not significant, $P \geq 0.05$, two-sided t test compared with both control groups. Responses of T4/T5 block flies at 45° were not significantly different to control responses ($P \geq 0.05$; two-sided t test compared with both control groups). Responses of *shi^{ts}* control and T4/T5 block flies during steady state were not significantly different from zero, but the response of T4/T5 control flies was (P = 0.37, 0.11, 0.02, respectively; two-sided t test).

To test these ideas, we investigated the turning responses to local front-to-back motion, back-to-front motion and luminance changes in isolation (**Fig. 4**). We created a virtual environment consisting of a gray cylinder with a 10° window at two azimuthal positions (either Ψ = 30° or Ψ = 60°). Outside, a 10° black bar rotates at 40 ° s^{-1} around the cylinder. Whenever the bar passes the window, it briefly allows the fly's motion system to detect the direction of bar motion (either front to back or back to front), inducing a turning tendency (M_{FTB} and M_{BTF}) in the same direction. Moreover, when the bar passes through the window, it produces local luminance changes such that luminance first decreases and then increases again. This change in luminance is detected by the fly's position system, leading to an additional turning tendency toward that position (P_{FTB} and P_{BTF}). Thus, the turning response to local front-to-back and back-to-front motion can be described as the sum of both turning tendencies.

$$R_{FTB} = M_{FTB} + P_{FTB}$$
$$R_{BTF} = M_{BTF} + P_{BTF}$$

To tease apart the different response components, we need the response of the position system alone. We approximated the local luminance change when the rotating bar passes the window with a non-moving stimulus. The whole window starts at background luminance, darkens and then brightens again. This stimulus should only activate the position system, resulting in a turning tendency toward the position of the local luminance change ($R_L = P_L$).

When measuring the turning response of control flies to the three different stimulus conditions, all turning responses were found to be different. The response to the front-to-back stimulus (R_{FTB}) was positive and large in amplitude (**Fig. 4a**,**c**), the response to the back-to-front stimulus (R_{BTF}) was biphasic and weak (**Fig. 4d**,**f**), and the response to local luminance changes (R_L) was positive and weak (**Fig. 4g**,**i**). In contrast, the responses of T4/T5 block flies to front-to-back motion, back-to-front motion and local luminance changes were all identical (**Fig. 4b**,**e**,**h**,**j**). We found no differences in the responses to local luminance changes of controls and T4/T5 block flies (**Fig. 4i**), which is consistent with our earlier observations (**Fig. 3**). Taken together, these results indicate that the position system only detects changes in local luminance and that local motion does not influence its response properties. Thus,

$$R_L = P_L = P_{FTB} = P_{BTF}$$

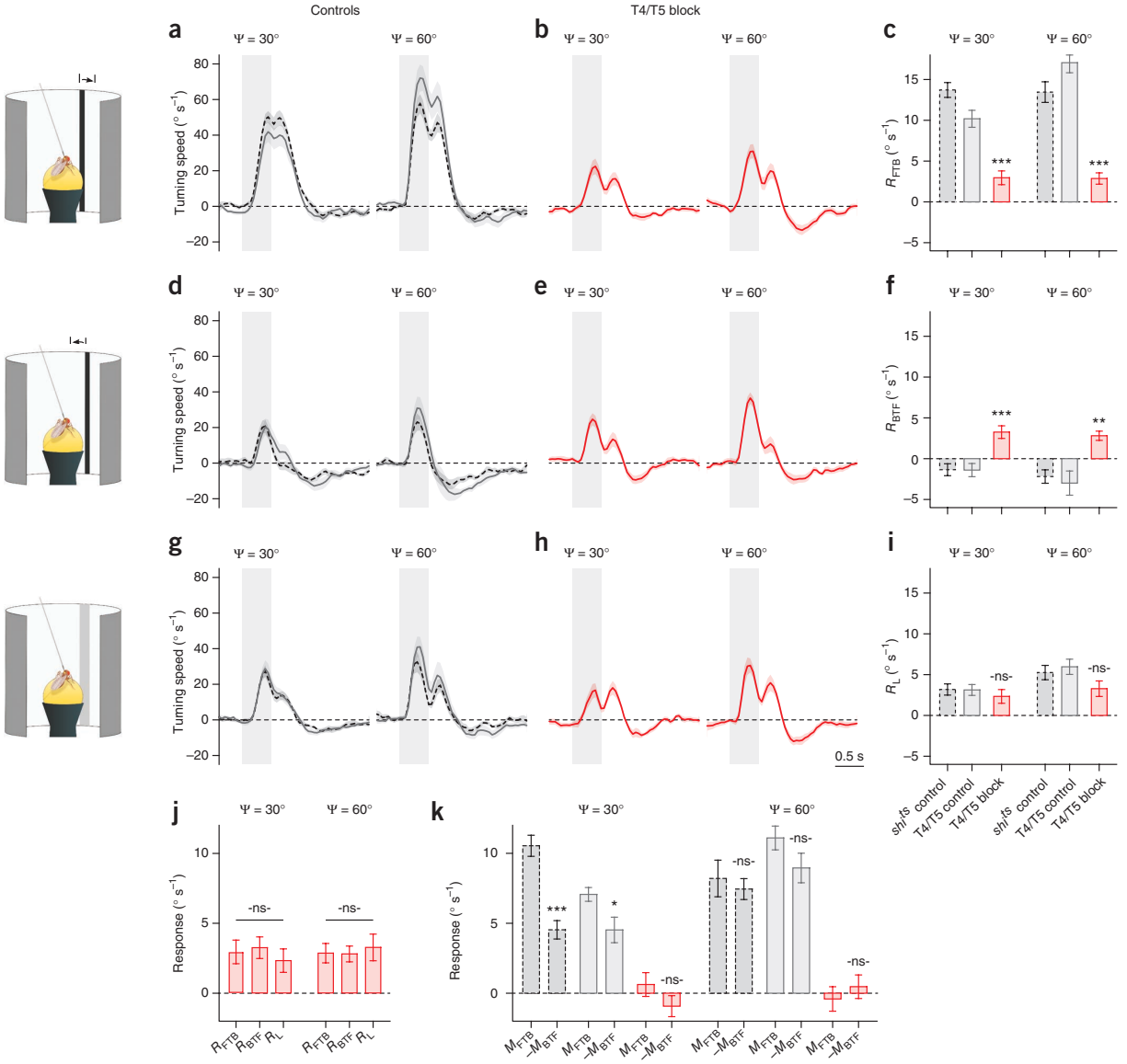

Figure 4 Open-loop responses to local bar motion and to local luminance changes. (**a**–**i**) Turning responses of control (**a**,**d**,**g**) and T4/T5 block (**b**,**e**,**h**) flies to local front-to-back motion (**a**,**b**), local back-to-front motion (**d**,**e**) and local luminance changes (**g**,**h**) at $\Psi = 30°$ and $\Psi = 60°$ (gray shaded areas). The corresponding average turning responses are shown in **c**, **f** and **i** (R_{FTB}, R_{BTF} and R_L, respectively; averaged between $t = 0.1$ s and $t = 2.1$ s after stimulus onset). (**j**) Comparison of responses to the different stimuli of T4/T5 block flies. (**k**) Comparison of isolated motion responses ($M_{FTB} = R_{FTB} - R_L$ and $M_{BTF} = R_{BTF} - R_L$). Motion responses of T4/T5 block flies were not significantly different from zero ($P \geq 0.05$, two-sided t test). All responses were measured as the response with the bar at $\Psi = +30°$ or $\Psi = +60°$ minus the response with the bar at $\Psi = -30°$ or $\Psi = -60°$, respectively, divided by 2. All data represent mean ± s.e.m.; 60 trials per fly of $n = 10$, 12 and 11 flies (at $\Psi = 30°$) and of $n = 10$, 11 and 11 flies (at $\Psi = 60°$) per group (shi^{ts} control, dashed black lines; T4/T5 control, solid gray lines; T4/T5 block, solid red lines). ns indicates not significant ($P \geq 0.05$), $^*P < 0.05$, $^{**}P < 0.01$ and $^{***}P < 0.001$; two-sided t-test compared with both controls (**c**,**f**,**i**) or comparing M_{FTB} to $-M_{BTF}$ within the groups (**k**); one-way ANOVA in **j**.

This finding allowed us to isolate the responses of the motion system to front-to-back and back-to-front stimulation.

$$M_{FTB} = R_{FTB} - R_L$$
$$M_{BTF} = R_{BTF} - R_L$$

Analyzing the data of control flies in this way revealed a strong asymmetry in the motion system for the frontal part of the visual field ($\Psi = 30°$), where its response to front-to-back was approximately twice as strong as that to back-to-front motion (**Fig. 4k**). In the lateral part ($\Psi = 60°$), we observed a similar tendency (**Fig. 4k**). This finding implies that $M(\Psi, v) \neq -M(\Psi, -v)$ and suggests that it is

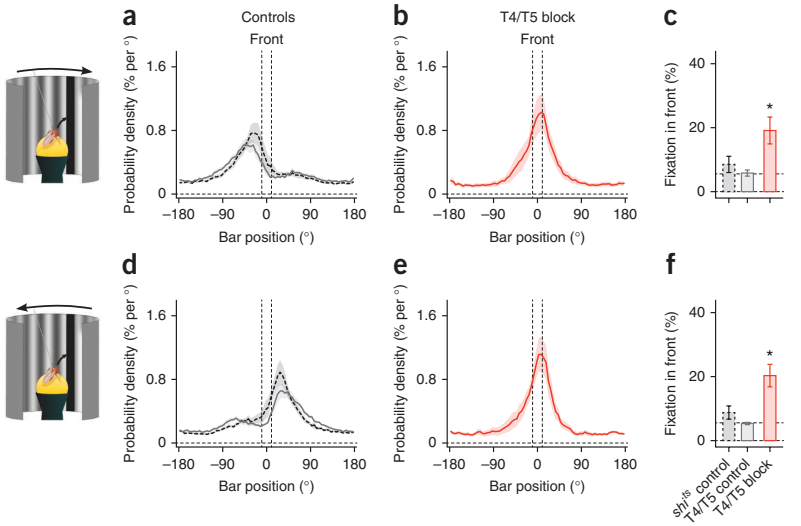

Figure 5 Closed-loop fixation response during open-loop background motion. (**a**–**f**) Fixation responses of control (**a**,**d**) and T4/T5 block (**b**,**e**) flies during clockwise (**a**,**b**) and counterclockwise (**d**,**e**) rotation of the sine-grating. The ability to keep the bar in front is shown in **c** and **f** (same measure as in **Fig. 1i**). Upper horizontal dashed lines represent the chance level (5.6%, no fixation). All data represent mean ± s.e.m.; 30 trials of $n = 11$, 9 and 9 flies per group (shi^{ts} control, dashed black lines; T4/T5 control, solid gray lines; T4/T5 block, solid red lines). $^*P < 0.05$, two-sided t test compared with both controls.

necessary to omit the classical assumption of velocity linearity of the motion system[30]. Consequently, we revised the interpretation of $P(\Psi)$ obtained in the previous experiment with the rotating bar (**Fig. 2**). Thus, $P(\Psi)$ actually overestimates the response of the pure position system (P_L) in control flies.

$$P(\Psi)^{\text{controls}} = (R_{cw} + R_{ccw})/2$$
$$= (M(\Psi, v) + M(\Psi, -v) + 2 \cdot P_L)/2$$
$$> P_L$$

On the other hand, for T4/T5 block flies, the motion responses were zero (**Figs. 2h** and **4k**). Under these conditions, $P(\Psi)$ corresponds to the response of the position system alone (P_L).

$$P(\Psi)^{\text{T4/T5 block}} = (R_{cw} + R_{ccw})/2$$
$$= (M(\Psi, v) + M(\Psi, -v) + 2 \cdot P_L)/2$$
$$= P_L$$

Taken together, these results indicate that the visual pathways of the motion and position system are indeed separable at the neuronal level. However, fixation is shaped by an interaction of both systems at the level of behavior.

Object tracking with background motion

Do both control systems also superimpose when the fly encounters a more natural situation where it has to track an object while the whole background is in motion? To answer this question, we fed back the fly's turning tendency on the position of the black bar, as in the usual fixation procedure (closed loop), and displayed a large-field sine-grating rotating in one or the other direction without giving the fly control over it (open loop) (**Fig. 5**). If both responses superimpose at the level of the fly's turning tendency, the large field stimulus should create a permanent offset, leading to a shift of the position where the fly fixates the bar.

We tested whether the presence of the sine-grating alone would alter the fixation response. To our surprise, the fixation response clearly improved for both control and T4/T5 block flies when the background was a static sine-grating (**Supplementary Fig. 3**), although the grating had the same average luminance as the uniformly gray background used in previous fixation experiments (**Fig. 1e**–**i**). This indicates that the fixation response is modulated by the spatial properties of the background, yet the detailed mechanism of this effect remains unknown.

With the sine-grating background moving clockwise or counterclockwise, control flies were still able to fixate the bar, but the peak of the position histogram was shifted in the direction opposite to the direction of the moving large-field stimulus (**Fig. 5a**,**d**). The motion system produced a tendency to turn in the direction of the moving background, whereas the position system induced turning toward the position of the bar. When the bar was shifted opposite to the direction of background motion, both responses summed to zero. Under the same conditions, T4/T5 block flies did not shift the fixation peak, but rather kept the bar in front of them, regardless of whether the large-field stimulus was moving clockwise or counterclockwise (**Fig. 5b**,**e**). These results suggest a superposition of the large-field motion system and the position system at the level of behavioral output, as has been proposed[30].

Electrophysiology in horizontal and vertical system cells

In our behavioral experiments, we found that a turning response could be elicited by local luminance changes and that this response was not changed when blocking T4 and T5 cell output (**Figs. 3** and **4**). In electrophysiological recordings from LPTCs sensitive to horizontal and vertical motion (horizontal and vertical system cells, respectively), the response to full-field flicker is only moderately reduced when T4 and T5 cell output is blocked[26], indicating that horizontal system and vertical system cells receive additional input from an unidentified flicker pathway. To investigate whether horizontal system or vertical system cells use this information to mediate the position response, we performed electrophysiological recordings from horizontal system and vertical system cells in the immobilized fly (**Fig. 6**). We presented gratings moving in different directions, full-field OFF and ON flicker, as well as appearing and disappearing black bars at different positions along the azimuth. Vertical system cells responded strongly in a direction-selective manner to vertical motion (**Fig. 6a**), whereas horizontal system cells responded most strongly to horizontal motion (**Fig. 6b**). Both cell types also responded strongly to full-field OFF and ON flicker. However, cellular responses to appearing and disappearing vertical bars were orders of magnitude weaker. Moreover, horizontal system cells slightly hyperpolarized when the black bar appeared, but depolarized when it disappeared.

These recordings conflict with the behavioral responses that we observed in several ways. First, flies robustly turned toward the

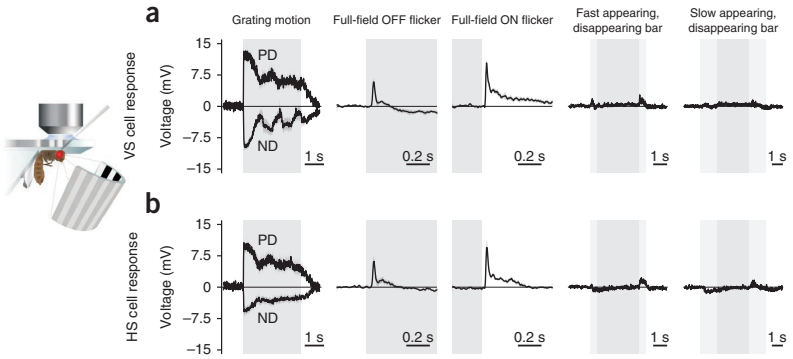

Figure 6 *In vivo* electrophysiological recordings from vertical system (VS) and horizontal system (HS) cells in the immobilized fly. (**a**,**b**) Voltage traces obtained from vertical system (**a**) and horizontal system cells (**b**) while presenting vertical (**a**) or horizontal (**b**) grating motion into the preferred direction (PD) and the null direction (ND) of the cell, full-field OFF and ON flicker, and a vertical dark bar that appeared and disappeared (fast or slow in 0.5 s or 1.5 s, respectively) at $\Psi = 30°$ in the front of the fly (responses at $\Psi = 60°$ and $\Psi = 90°$ were similar in amplitude; data not shown). All data represent mean ± s.e.m. obtained from $n = 8$ vertical system cells and $n = 6$ horizontal system cells from wild-type Canton S flies.

location of an appearing and a disappearing black bar, and this position response was on the same order of magnitude as the optomotor response to full-field grating motion (**Figs. 1b** and **3a**). Second, assuming that horizontal system and vertical system cells convey position information, we would not expect the fly to remain capable of tracking objects when the background is moving (**Fig. 5**); the tiny voltage responses to local luminance changes would vanish in the much stronger voltage response to the background motion. These discrepancies between electrophysiological responses of horizontal system and vertical system cells and behavioral responses render it unlikely that horizontal system and vertical system cells are part of the fly's position circuit.

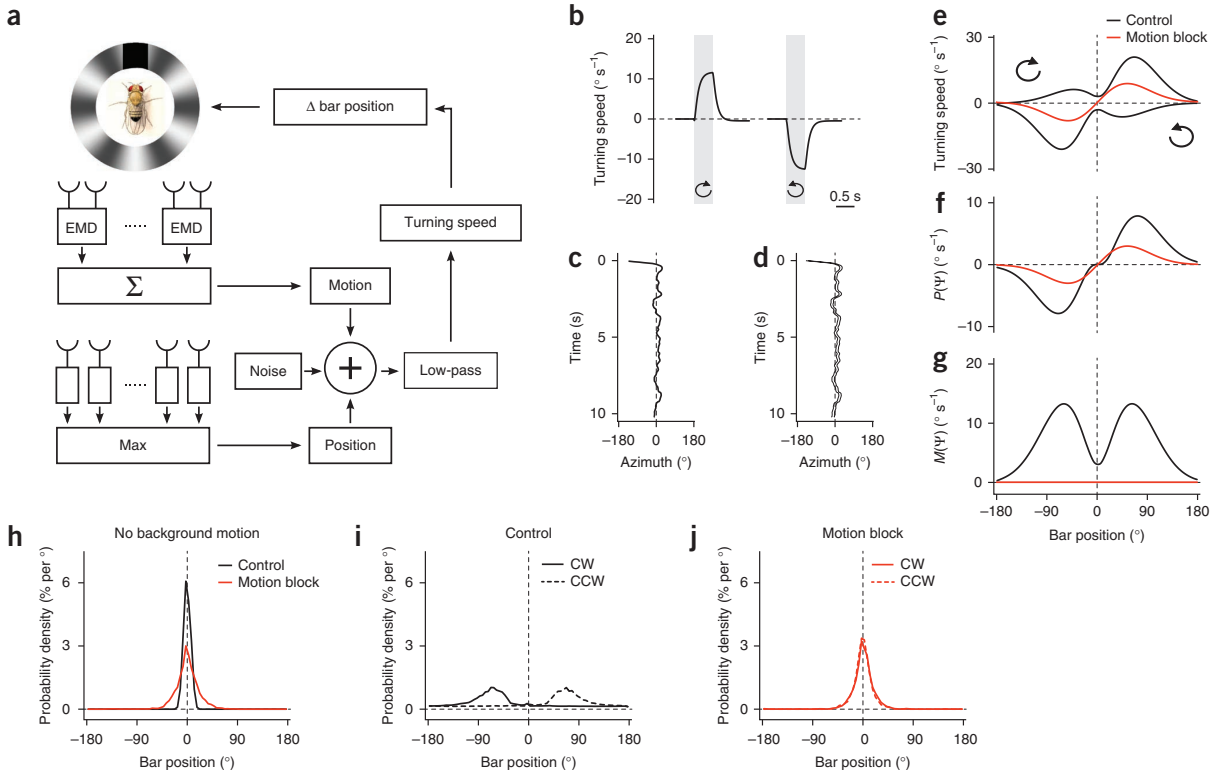

Figure 7 Model simulations of the fly's course control system. (**a**) Outline of the model. The visual scene was analyzed in parallel by a motion and a position system. Their output signals, plus noise, were summated and low-pass filtered to yield the fly's turning speed. To simulate closed-loop fixation behavior, this signal was used to control the bar position. (**b**) Turning responses of the model to full-field clockwise and counterclockwise grating rotation. (**c**,**d**) Bar position over time (**c**) and the resulting activity pattern of the array of position detectors (**d**) during a single run of closed-loop fixation. (**e**) Model responses to a bar rotating in open-loop clockwise, followed by counterclockwise. (**f**) Position component, $P(\Psi)$ (calculated by summing the two responses obtained in **e** and dividing them by 2). (**g**) Motion component, $M(\Psi)$ (calculated by subtracting the two responses obtained in **e** and dividing by 2). (**h**) Probability density as function of bar position obtained from 20 runs of closed-loop bar fixation. (**i**,**j**) Closed-loop fixation behavior during superimposed open-loop background sine-grating motion (solid lines, 10 ° s^{-1} clockwise (CW) rotation of the grating; dashed lines, −10 ° s^{-1} counterclockwise (CCW) rotation of the grating). Model responses were calculated with an intact motion system (black lines) and with the gain of the motion system set to zero (red lines).

Modeling

Our results suggest the existence of two course control systems operating in parallel. Can such a system track a single object effectively and quantitatively account for the observed behavior of the flies? To address this question, we modeled the two course control systems and tested them under the conditions that were used in the experiments (**Fig. 7**). We implemented the large-field motion system as an array of elementary motion detectors of the Reichardt type[34] weighted by a spatial sensitivity profile similar to $M(\Psi)$, as obtained in the experiments (**Fig. 2f**), and with a 50% stronger weight on front-to-back than on back-to-front motion, as we observed (**Fig. 4k**). The output signals of all motion detectors were summated. The position system was modeled as an array of squared high-pass filters. From the array, the location of the maximum response was extracted at each time point. The response amplitude toward this position was determined from a spatial sensitivity profile similar to the experimentally determined one (**Fig. 2c**,**d**). Both signals were multiplied by a gain factor, added together with white noise and low-pass filtered to obtain a turning signal. This could either be interpreted as the output signal under open-loop conditions or fed back into the bar position when simulating closed-loop fixation behavior (**Fig. 7a**).

Stimulating the model with grating motion under open-loop conditions resulted in a syndirectional optomotor response (**Fig. 7b**). When tested under closed-loop conditions, the model revealed a pronounced fixation behavior, bringing and keeping the bar in a frontal position (**Fig. 7c**,**h**). Comparing the bar position (**Fig. 7c**) with the output of the squared high-pass filters over time (**Fig. 7d**) revealed the effective detection of bar position. Moving the bar in open loop, first clockwise, then counterclockwise, led to a response profile that was consistent with the respective experimental data (**Fig. 7e**). We added and subtracted both responses to reveal the position-dependent and motion-dependent components ($P(\Psi)$ and $M(\Psi)$, respectively) and obtained similar profiles as in our experiments (**Fig. 7f**,**g**). We then tested the system for closed-loop fixation during open-loop background grating motion. As seen in the experiments, the maximum of the fixation histograms moved opposite to the direction of the drifting grating and the histograms became broader (**Fig. 7i**).

We then tested the model with the gain of the large-field motion system set to zero, simulating the blockage of T4 and T5 cell output; the model was still able to keep the bar in front, yet with a broader distribution (**Fig. 7h**). When the model was presented with the clockwise and counterclockwise rotating bar, the responses were identical for both directions of bar motion and only depended on the bar's position (**Fig. 7e**). Moreover, the resulting position-dependent response function, $P(\Psi)$, was reduced in amplitude compared with the control (**Fig. 7f**). Finally, in the case of closed-loop fixation with background motion, the model kept the bar in front, no matter the direction in which the background was moving (**Fig. 7j**). In summary, all of the effects that we observed in the experiments were reproduced by the model with one set of parameters.

DISCUSSION

Behavioral and electrophysiological studies in larger fly species have proposed that fixation behavior is mediated by a special class of lobula plate neurons that are selective for small moving objects[35–38]. These cells are thought to receive retinotopic input from the same set of columnar, motion-sensitive neurons as the large field–sensitive tangential cells. Their selectivity for small moving objects arises from additional inhibition that they receive from other large-field neurons of the lobula plate[39–41]. In contrast, we found that transgenic *Drosophila* in which the T4 and T5 cells were blocked were still able to fixate and track individual objects, even though their lobula plate tangential cells were motion blind and flies consequently did not show an optomotor response[26]. Our genetic and behavioral experiments revealed a control system that is purely sensitive to the position of the object and not to the direction in which it is moving, with the exact same spatial sensitivity profile as that revealed by the mathematical examination of behavioral results in wild-type houseflies performed many years ago[30]. Although the reduction in fixation strength observed in T4/T5 block flies might, at first sight, be interpreted as a partial overlap between the motion and the position circuit at the neuronal level, our analysis indicates that this is not the case; as a result of its asymmetry with respect to the direction of motion (front to back as compared to back to front), the motion circuit contributes to the fixation response at the behavioral level, but is separate from the position circuit at the neuronal level. An asymmetry in turning was also observed in the responses to rotating stripes[8,30] (**Fig. 2**), but, from these findings, one cannot conclude that the response of the motion circuit is asymmetrical. Even a perfectly symmetrical motion response, combined with the position response, would lead to the very same behavior. Our investigation of the two response components revealed that the asymmetrical turning response has two sources: a turning response to the position of the rotating bar and an asymmetrical motion response to its direction of motion. The powerful genetic tools available in *Drosophila*[42] will allow the future identification of the specific neural components of the position circuit.

METHODS

Methods and any associated references are available in the online version of the paper.

Note: Supplementary information is available in the online version of the paper.

ACKNOWLEDGMENTS

We wish to thank G. Rubin and A. Nern for providing the T4/T5 cell–specific driver line *R42F06-Gal4* and V. Jayaraman for advice on setting up the locomotion recorder. We are also grateful to J. Haag, A. Mauss, A. Arenz and A. Leonhardt for many helpful discussions and critically reading the manuscript, S. Prech for help with the design of the Peltier temperature control system, C. Theile for fly work, and F. Foerstner for reconstructing the three horizontal system cells shown in **Figure 1a**. A. Bahl and A. Borst are members of the Bernstein Center for Computational Neuroscience and the Graduate School of Systemic Neurosciences.

AUTHOR CONTRIBUTIONS

A. Bahl set up the locomotion recorder and the stimulus display, and wrote the software for reading the behavioral output and displaying the stimulus. A. Bahl and T.S. performed all of the behavioral experiments and evaluated the data. G.A. performed the electrophysiological recordings and analyzed the data. A. Bahl and A. Borst designed the study. A. Borst carried out the modeling work. A. Borst and A. Bahl wrote the manuscript with the help of the other authors.

COMPETING FINANCIAL INTERESTS

The authors declare no competing financial interests.

1. Götz, K.G. Optomotorische Untersuchung des visuellen Systems einiger Augenmutanten der Fruchtfliege *Drosophila*. *Kybernetik* **2**, 77–92 (1964).
2. Buchner, E. Elementary movement detectors in an insect visual system. *Biol. Cybern.* **24**, 85–101 (1976).
3. Blondeau, J. & Heisenberg, M. The three-dimensional optomotor torque system of *Drosophila melanogaster*. Studies on wild type and the mutant optomotor blind H31. *J. Comp. Physiol. A* **145**, 321–329 (1982).
4. Tammero, L.F. & Dickinson, M.H. The influence of visual landscape on the free flight behavior of the fruit fly *Drosophila melanogaster*. *J. Exp. Biol.* **205**, 327–343 (2002).

5. Mronz, M. & Lehmann, F.-O. The free-flight response of *Drosophila* to motion of the visual environment. *J. Exp. Biol.* **211**, 2026–2045 (2008).
6. Reichardt, W. & Wenking, H. Optical detection and fixation of objects by fixed flying flies. *Naturwissenschaften* **56**, 424–425 (1969).
7. Heisenberg, M. & Wolf, R. *Vision in Drosophila: Genetics of Microbehavior* (Springer-Verlag, Berlin, 1984).
8. Reiser, M.B. & Dickinson, M.H. *Drosophila* fly straight by fixating objects in the face of expanding optic flow. *J. Exp. Biol.* **213**, 1771–1781 (2010).
9. Rister, J. *et al.* Dissection of the peripheral motion channel in the visual system of *Drosophila melanogaster*. *Neuron* **56**, 155–170 (2007).
10. Götz, K.G. Visual guidance in *Drosophila*. in *Development and Neurobiology of Drosophila* (eds. Siddiqi, O., Babu, P., Hall, M.L. & Hall, J.C.) 391–407 (Plenum Press, New York, 1980).
11. Strauss, R. & Pichler, J. Persistence of orientation toward a temporarily invisible landmark in *Drosophila melanogaster*. *J. Comp. Physiol. A* **182**, 411–423 (1998).
12. Maimon, G., Straw, A.D. & Dickinson, M.H. A simple vision-based algorithm for decision making in flying *Drosophila*. *Curr. Biol.* **18**, 464–470 (2008).
13. Aptekar, J.W., Shoemaker, P.A. & Frye, M.A. Figure tracking by flies is supported by parallel visual streams. *Curr. Biol.* **22**, 482–487 (2012).
14. Heisenberg, M., Wonneberger, R. & Wolf, R. Optomotor-blind (H31): a *Drosophila* mutant of the lobula plate giant neurons. *J. Comp. Physiol. A* **124**, 287–296 (1978).
15. Geiger, G. & Nässel, D.R. Visual orientation behavior of flies after selective laser beam ablation of interneurones. *Nature* **293**, 398–399 (1981).
16. Hausen, K. & Wehrhahn, C. Neural circuits mediating visual flight control in flies. II. Separation of two control systems by microsurgical brain lesions. *J. Neurosci.* **10**, 351–360 (1990).
17. Bausenwein, B., Wolf, R. & Heisenberg, M. Genetic dissection of optomotor behavior in *Drosophila melanogaster*. Studies on wild-type and the mutant optomotor-blind (H31). *J. Neurogenet.* **3**, 87–109 (1986).
18. Wolf, R. & Heisenberg, M. Visual orientation in motion-blind flies is an operant behavior. *Nature* **323**, 154–156 (1986).
19. Meinertzhagen, I.A. & O'Neil, S.D. Synaptic organization of columnar elements in the lamina of the wild type in *Drosophila melanogaster*. *J. Comp. Neurol.* **305**, 232–263 (1991).
20. Joesch, M., Plett, J., Borst, A. & Reiff, D.F. Response properties of motion-sensitive visual interneurons in the lobula plate of *Drosophila melanogaster*. *Curr. Biol.* **18**, 368–374 (2008).
21. Schnell, B. *et al.* Processing of horizontal optic flow in three visual interneurons of the *Drosophila* brain. *J. Neurophysiol.* **103**, 1646–1657 (2010).
22. Joesch, M., Schnell, B., Raghu, S.V., Reiff, D.F. & Borst, A. ON and OFF pathways in *Drosophila* motion vision. *Nature* **468**, 300–304 (2010).
23. Eichner, H., Joesch, M., Schnell, B., Reiff, D.F. & Borst, A. Internal structure of the fly elementary motion detector. *Neuron* **70**, 1155–1164 (2011).
24. Bausenwein, B. & Fischbach, K. Activity labeling patterns in the medulla of *Drosophila melanogaster* caused by motion stimuli. *Cell Tissue Res.* **270**, 25–35 (1992).
25. Bausenwein, B., Dittrich, A.P. & Fischbach, K.F. The optic lobe of *Drosophila melanogaster*. II. Sorting of retinotopic pathways in the medulla. *Cell Tissue Res.* **267**, 17–28 (1992).
26. Schnell, B., Raghu, S.V., Nern, A. & Borst, A. Columnar cells necessary for motion responses of wide-field visual interneurons in *Drosophila*. *J. Comp. Physiol. A* **198**, 389–395 (2012).
27. Seelig, J.D. *et al.* Two-photon calcium imaging from head-fixed *Drosophila* during optomotor walking behavior. *Nat. Methods* **7**, 535–540 (2010).
28. Brand, A.H. & Perrimon, N. Targeted gene expression as a means of altering cell fates and generating dominant phenotypes. *Development* **118**, 401–415 (1993).
29. Kitamoto, T. Conditional modification of behavior in *Drosophila* by targeted expression of a temperature-sensitive *shibire* allele in defined neurons. *J. Neurobiol.* **47**, 81–92 (2001).
30. Poggio, T. & Reichardt, W. A theory of the pattern induced flight orientation of the fly *Musca domestica*. *Kybernetik* **12**, 185–203 (1973).
31. Wehrhahn, C. Flight torque and lift responses of the housefly (*Musca domestica*) to a single stripe moving in different parts of the visual field. *Biol. Cybern.* **29**, 237–247 (1978).
32. Pick, B. Visual flicker induces orientation behavior in the fly *Musca*. *Z. Naturforsch. C* **29c**, 310–312 (1974).
33. Wehrhahn, C. Fast and slow flight torque responses in flies and their possible role in visual orientation behavior. *Biol. Cybern.* **40**, 213–221 (1981).
34. Reichardt, W. Evaluation of optical motion information by movement detectors. *J. Comp. Physiol. A* **161**, 533–547 (1987).
35. Reichardt, W. & Poggio, T.A. Figure-ground discrimination by relative movement in the visual system of the fly. Part I: Experimental Results. *Biol. Cybern.* **35**, 81–100 (1979).
36. Egelhaaf, M. On the neuronal basis of figure-ground discrimination by relative motion in the visual system of the fly. I. Behavioral constraints imposed on the neuronal network and the role of the optomotor system. *Biol. Cybern.* **52**, 123–140 (1985).
37. Egelhaaf, M. On the neuronal basis of figure-ground discrimination by relative motion in the visual system of the fly. II. Figure-detection cells, a new class of visual interneurones. *Biol. Cybern.* **52**, 195–209 (1985).
38. Liang, P., Heitwerth, J., Kern, R., Kurtz, R. & Egelhaaf, M. Object representation and distance encoding in three-dimensional environments by a neural circuit in the visual system of the blowfly. *J. Neurophysiol.* **107**, 3446–3457 (2012).
39. Egelhaaf, M. On the neuronal basis of figure-ground discrimination by relative motion in the visual system of the fly. III. Possible input circuitries and behavioral significance of the FD cells. *Biol. Cybern.* **52**, 267–280 (1985).
40. Warzecha, A.K., Borst, A. & Egelhaaf, M. Photo-ablation of single neurons in the fly visual system reveals neural circuit for the detection of small moving objects. *Neurosci. Lett.* **141**, 119–122 (1992).
41. Cuntz, H., Haag, J. & Borst, A. Neural image processing by dendritic networks. *Proc. Natl. Acad. Sci. USA* **100**, 11082–11085 (2003).
42. Borst, A. *Drosophila*'s view on insect vision. *Curr. Biol.* **19**, R36–R47 (2009).

ONLINE METHODS

Behavioral experiments. The locomotion recorder[2,27] consisted of an air-suspended sphere floating in a bowl-shaped sphere holder. The sphere had a diameter of 6 mm and a weight of 40 mg; it was made from polyurethane foam and coated with polyurethane spray (spheres were kindly provided by V. Jayaraman, Janelia Farm). The airflow is adjusted to ~0.7 l min^{-1} by a rotary vane pump (G6/01-K-EB9L Gardner Denver Thomas GmbH) such that the sphere rotated freely in the holder, but did not jump out. A high-power infrared LED (800 nm, JET series, 90 mW, Roithner Electronics) was located in the back to illuminate the fly and the sphere surface. Two optical tracking sensors were equipped with lens and aperture systems to focus two 1-mm^2 equatorial spots (at ±30°) on the sphere at a distance 15 cm behind the fly. The tracking data were processed in a custom-designed circuit[27] at 4 kHz internally, read out via a USB interface and processed by a computer at ~200 Hz. This allowed real-time calculation of the instantaneous rotation axis of the sphere. A third camera (GRAS-20S4M-C, Point Grey Research) was located in the back, which is essential for proper positioning of the fly and allowed real-time observation and video recording of the fly during experiments. The bottom of the sphere holder was surrounded by an open plastic funnel connected to a metal fan with an aluminum tube. A self-designed Peltier controlling system read out the temperature of a thermometer placed just below the sphere and controlled the fan temperature such that the air temperature around the fly was regulated precisely (±0.1 °C). In all experiments, the temperature started at the permissive temperature level for *shibire^{ts}* (25 °C) and was raised linearly to the restrictive temperature of 34 °C in 10–20 min. Three 120-Hz LCD screens (Samsung 2233 RZ) were vertically arranged and formed a U-shaped visual arena (31 × 31 × 47 cm) with the fly in the center. We removed the monitor covers to minimize the borders between the screens in the corners of the arena and glued thin sheets of parchment paper onto the screens to scatter and evenly distribute the emitted light. The visual arena had a luminance ranging from 0–131 cd m^{-2} and covered almost the whole visual field of the fly (horizontal, ± 135°; vertical, ± 57°; resolution < 0.1°). The three LCD screens were controlled via NVIDIA 3D Vision Surround Technology on Windows 7 64 bit, allowing a synchronized update of the screens at 120 frames per s. For visual stimulation, we use Panda3D, an open-source gaming engine, and Python 2.7, which simultaneously controlled the frame rendering in Panda3D, read out the tracking data and temperature, and streamed data to the hard disk.

Time-position plots for the visual stimuli are illustrated in **Supplementary Figure 4** for all experiments. The large-field open-loop optomotor stimulus (**Fig. 1b–d** and **Supplementary Fig. 4a**,**b**) consisted of a striped grating (λ = 20°) rotating clockwise (+) or counterclockwise (−) at a velocity of 20 ° s^{-1} for 0.5 s. Seven contrasts were tested. The dark stripes always had a luminance value of 27 cd m^{-2}, whereas the luminance values of the brighter stripes ranged from 30–104 cd m^{-2}, resulting in contrast values between 4 and 58%, measured as $(I_{max}-I_{min})/(I_{max}+I_{min})$. In the open- and closed-loop fixation experiments, we showed a single black bar (10° wide, 114° high, 9 cd m^{-2}) on a gray background (58 cd m^{-2}). In the first set of open-loop fixation experiments (**Fig. 2** and **Supplementary Fig. 4d**,**e**), the bar started in the back and rotated at velocities of ±18 ° s^{-1} around the fly. In another set of experiments (**Fig. 3** and **Supplementary Fig. 4f**), the bar did not move, but slowly appeared (in 0.5 s), remained static for 4 s and disappeared (in 0.5 s) at well-defined locations (±120°, ±90°, ±60°, ±45°, ±30° and ±15°). In another experiment (**Fig. 4** and **Supplementary Fig. 4g–i**), we chose two locations (Ψ = 30° and Ψ = 60°) to show local motion (front to back and back to front) and local luminance change. Here, the local luminance change dynamics were chosen such that they approximated the luminance change when the local motion was shown. In the case of closed-loop fixation, the bar was placed at a random position (between −180° and +180°) around the fly before each trial and the fly was then given 20 s control of the angular position of that bar (Δbar = −fly turning, updated approximately every 9 ms). This was done either in front of a gray background (**Fig. 1e–i** and **Supplementary Figs. 3a–c** and **4c**) or a large-field sine-grating (λ = 30°, the luminance values of the pattern were between 27 and 104 cd m^{-2}). The sine-grating was either static (**Supplementary Figs. 3d–f** and **4j**) or rotated at ±15 ° s^{-1} (**Fig. 5** and **Supplementary Fig. 4k**,**l**).

Flies were raised on standard cornmeal-agar medium at 18 °C and 60% humidity throughout development on a 12-h light, 12-h dark cycle. We used *shi^{ts}* control flies (*w^+; +; +/UAS-shi^{ts}*), T4/T5 control flies (*w^+/w^-; +; R42F06-Gal4/+*) and T4/T5 block flies (*w^+/w^-; +; R42F06-Gal4/UAS-shi^{ts}*). The T4 and T5 cell–specific driver line *R42F06-Gal4* was kindly provided by A. Nern and G. Rubin (Janelia Farm) and was generated[43] using a 4.0-kb DNA fragment of the *bab2* gene amplified from genomic DNA with primers CGGCTGATCCAACAAAGGATG CACC and CTCAGTGTAGCCGCACCTTGTTCCT. The *shibire^{ts}* effector has multiple insertions on the third chromosome. We used wild-type Canton S flies for the control crosses. Only female flies aged 2–10 d were used in experiments. Flies were taken from 18 °C just before the experiment and immediately cold anesthetized. The head, thorax and wings were glued to a needle using near-ultraviolet bonding glue (Sinfony Opaque Dentin) and strong blue LED light (440 nm, dental curing light, New Woodpecker).

For each fly, the experiment lasted approximately 50 min and was split into 50–200 trials depending on the length and the number of visual stimuli. Stimuli in one trial were presented in random order. For data analysis, we chose a range of trials (same for control and T4/T5 block flies per experiment) during which the temperature was constant at 34 °C and during which flies had a constant average turning and walking speed. The experimental raw data were first downsampled (interpolated from 120 to 20 Hz). Turning speed traces were then determined by taking the average over trials and low-pass filtering the resulting trace (τ = 0.1 s in all experiments, except those shown in **Fig. 2**, where τ = 0.4 s). Probability density functions of bar position were calculated separately for each trial with a bin size of 5° and then averaged over trials and flies. The measure 'fixation in front' was determined by integrating the probability density function of one trial between −10° and 10°, which resulted in a percentage value for how probable it was to find the bar in that area during that trial. These values were then averaged over trials and flies. Flies were excluded from data analysis when the average walking speed during the whole experiment was below 0.1 cm s^{-1}, indicating severe walking problems, or (only in closed-loop fixation experiments with static background) when the average turning speed was either larger than +10 ° s^{-1} or smaller than −10 ° s^{-1}, indicating an asymmetry in walking behavior that led to a substantially reduced fixation performance. All data analysis was performed in Python 2.7 using NumPy and SciPy on Mac OSX 10.8.

P values were obtained using different statistical tests. To test the hypothesis that a group had a certain mean, we performed a two-sided *t* test. When two groups were compared (**Fig. 4k**), we performed a two-sided *t* test. When T4/T5 block flies were compared with *shi^{ts}* control and T4/T5 control flies, we performed a two-sided *t* test comparing each control with the block flies and chose the larger *P* value. When three groups were compared (**Fig. 4j**), we performed a one-way ANOVA. We used approximately the same sample size (smallest n = 9 flies, largest n = 16 flies) per group and experiment, which permitted a statistical comparison between the different experiments. This sample size was considered as sufficiently large because the optomotor response of T4/T5 block flies shown in **Figure 1b–d** was highly significantly reduced at n = 10 flies ($P < 0.001$, two-sided *t* test compared with both controls). See **Supplementary Statistics** for a detailed list of group sizes, statistical tests and *P* values.

Electrophysiology. Patch-clamp recordings were performed as described previously[20] with minor modifications. All electrophysiological experiments were performed with female wild-type Canton S flies 6–24 h post-eclosion. Flies were raised on standard cornmeal-agar medium and kept at 25 °C and 60% humidity on a 12-h dark/light cycle.

Flies were anesthetized on ice and immobilized on a plexiglas holder with wax. The head was bent downwards and fixed by waxing the proboscis to the thorax. The fly was then inserted into an opening cut into a piece of aluminum foil mounted in a recording chamber. A part of the posterior side of the head cuticle and the muscle that covers the cell bodies of LPTCs was removed with fine forceps. Extracellular saline (103 mM NaCl, 3 mM KCl, 5 mM TES, 10 mM trehalose, 10 mM glucose, 7 mM sucrose, 26 mM $NaHCO_3$, 1 mM NaH_2PO_4, 1.5 mM $CaCl_2$ and 4 mM $MgCl_2$, pH 7.3, 280 mOsm) was bubbled with 95% O_2 and 5% CO_2 and continuously perfused over the preparation. The brain of the fly was visualized with an upright microscope (Axiotech Vario 100, Zeiss) equipped with a 40× water-immersion objective (LumPlanFL, NA 0.8, Olympus) and an Hg-light source (HXP-120, Visitron Systems). For contrast enhancement, we used two polarization filters that were slightly shifted with respect to their polarization plane. The health of the flies was checked regularly by monitoring periodic movements of the brain. A glass electrode filled with collagenase (Collagenase IV, Gibco, 0.5 mg ml^{-1} in extracellular saline) was used to weaken the perineural sheath and expose the somata of LPTCs.

doi:10.1038/nn.3386

Somata of vertical system and horizontal system cells were patched with a glass electrode (6–9 MΩ) filled with internal solution (140 mM potassium aspartate, 10 mM HEPES, 4mM Mg-ATP, 0.5 mM Na-GTP, 1 mM EGTA, 1 mM KCl and 0.03 mM Alexa 568–hydrazide sodium, pH 7.26, 265 mOsm). All recordings were performed in current-clamp bridge mode with an NPI BA-1S amplifier (NPI electronics), low-pass filtered at 3 kHz and digitized at 10 kHz. Data acquisition was performed with Matlab (version R2011a, MathWorks). Cells had an average resting membrane potential of −51.6 ± 0.7 mV (corrected for a liquid junction potential of 12 mV) and an average input resistance of 204.5 ± 16.7 MΩ. Cell types were identified on the basis of their typical response profiles to moving gratings. In addition, fluorescence images of each cell were taken after the recording with a CCD camera (Spot Pursuit, Visitron Systems) to verify their identity.

Visual stimuli were presented on a custom-built LED arena that subtended 170° in azimuth and 85° in elevation with a resolution of approximately 1.4° per LED. The arena allowed refresh rates of up to 600 Hz and had a maximum luminance of 80 cd m^{-2}. Motion stimuli consisted of square-wave gratings with a wavelength of 20° moving at 1 Hz. Stimuli lasted for 3 s with an interstimulus interval of 5 s and were repeated three times. For bar flicker stimuli, the arena background was set to full luminance. After 1.5 s, a dark bar that had a width of 10° and was centered at 30°, 60° or 90° along the azimuth appeared. The contrast of that bar was increased linearly to a maximum of 66% over 0.5 s or 1.5 s. After an interval of 3 s, the dark bar disappeared again in the same time period. Bar flicker stimuli were presented five times. For full-field flicker stimuli, the arena was stepped to full luminance for 3 s and then back to zero again for 3 s. Full-field flicker stimuli were presented ten times per cell.

Data analysis was performed with Matlab (version R2011b, MathWorks) using custom-written scripts. For all stimuli, we averaged voltage traces over sweeps and calculated the mean and s.e.m. over cells. The baseline membrane potential was calculated by averaging over a period of 500 ms preceding the stimulus onset and subtracted from the responses. For horizontal system cells, we pooled responses of all three horizontal system cell types. To properly match the receptive field of vertical system cells[20], we averaged the responses of vertical system cells with frontal receptive fields (VS1–VS3) to obtain the responses to the appearing and disappearing bar at 30° and 60°. Responses of vertical system cells with lateral receptive fields (VS5–6) were averaged to determine the responses at 90°.

Modeling. Visual patterns were modeled as one-dimensional luminance functions at a spatial resolution of 0.01° and a temporal resolution of 1 ms. They were covered by 360 elementary motion detectors of the Reichardt type[34]. Briefly, the luminance value at one location was low-pass filtered (first-order, 20-ms time constant) and subsequently multiplied with the instantaneous value derived from the neighboring location, separated by 1° of visual angle. This was done twice in a mirror-symmetrical fashion, and the output signals of both operations were subtracted. All elementary motion detectors were weighted according to the $M(\Psi)$ sensitivity profile and subsequently summated. In each hemisphere, motion detection subunits tuned to back-to-front motion were given half the response amplitude of those tuned to front-to-back motion. The visual pattern was also viewed by an array of 360 position detectors. These were modeled as high-pass filters (first-order, 10-ms time constant), the outputs of which were squared. From this array, the location of the maximum was determined. If this maximum was below a certain threshold, the location decayed back to zero with a 20-ms time constant. The output of the position system was calculated as the value of the $P(\Psi)$ function at this location. The $M(\Psi)$ and $P(\Psi)$ functions were approximated in the following way, with $Z(\Psi)$ describing the shape of their profiles, g_P being the gain factor of the position system (= 3) and g_M being the gain factor of the motion system (= 5).

$$Z(\Psi) = -\frac{d}{d\Psi} e^{-(\Psi/75)^2}$$
$$P(\Psi) = g_P \cdot Z(\Psi)$$
$$M(\Psi) = g_M \cdot |Z(\Psi)|$$

$M(\Psi)$ was subsequently smoothed by a box filter of 20° width. As a noise function we used Gaussian white noise that was filtered by a first-order low-pass filter with 100-ms time constant and multiplied with a noise-gain factor (g_N = 15). The sum of noise, motion and position system was then fed through a first-order low-pass filter with 100-ms time-constant to result in the turning speed. In closed-loop simulations, the turning speed was used to update the bar position each millisecond.

$$\text{bar position}(t+1) = \text{bar position}(t) - 0.1 \cdot \text{turning speed}(t)$$

Fixation histograms were obtained from 20 simulation runs, each 30 s long. At the beginning of each run, the bar was positioned in front of the fly. As large field pattern, we used a sine-grating with a spatial wavelength of 22.5°, a mean luminance of 0.5 and a contrast of 1. When activated, it moved at 10 ° s^{-1}, resulting in a temporal frequency of 0.44 Hz. The black bar was simulated as zero luminance from −5° to + 5° around the bar location, replacing the luminance value of either the grating or the one of a uniform background of luminance value 1. The model was simulated in IDL (Exelis) on 64-bit Windows 7.

43. Pfeiffer, B.D. *et al.* Tools for neuroanatomy and neurogenetics in *Drosophila*. *Proc. Natl. Acad. Sci. USA* **105**, 9715–9720 (2008).

Object Tracking in Motion-Blind Flies

Armin Bahl, Georg Ammer, Tabea Schilling and Alexander Borst*

Max-Planck-Institute of Neurobiology, Am Klopferspitz 18, 82152 Martinsried, Germany

* Corresponding author: borst@neuro.mpg.de

Supplemental Material

Nature Neuroscience: doi:10.1038/nn.3386

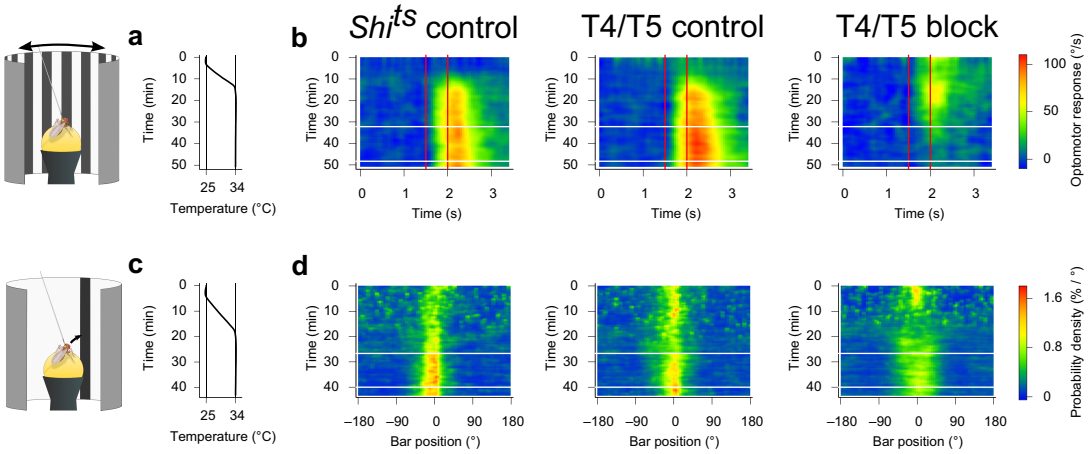

Fig. S1 Temperature control data for the optomotor response and fixation response. **a** Temperature protocol during the full-field grating motion experiment (Fig. 1b-d). The temperature around the fly starts at 25 °C and rises slowly to 34 °C within 10 minutes. **b** The optomotor response – defined as the turning speed in response to clockwise motion minus the turning speed in response to counterclockwise motion divided by two – as a function of stimulus time (x-axis) and overall experimental time (y-axis) for the three groups. Red vertical lines illustrate the time points when grating motion starts and ends. White horizontal lines indicate the time span during which the trials were used for detailed data analysis (Fig. 1). **c** Temperature protocol for closed-loop bar fixation (Fig. 1e-i). **d** Probability density of bar positions (x-axis) as function of overall experimental time (y-axis). All data represent mean of N = 10,10,10 (b) and N = 10,10,12 (d) flies per group (left to right). Same flies as in Fig. 1.

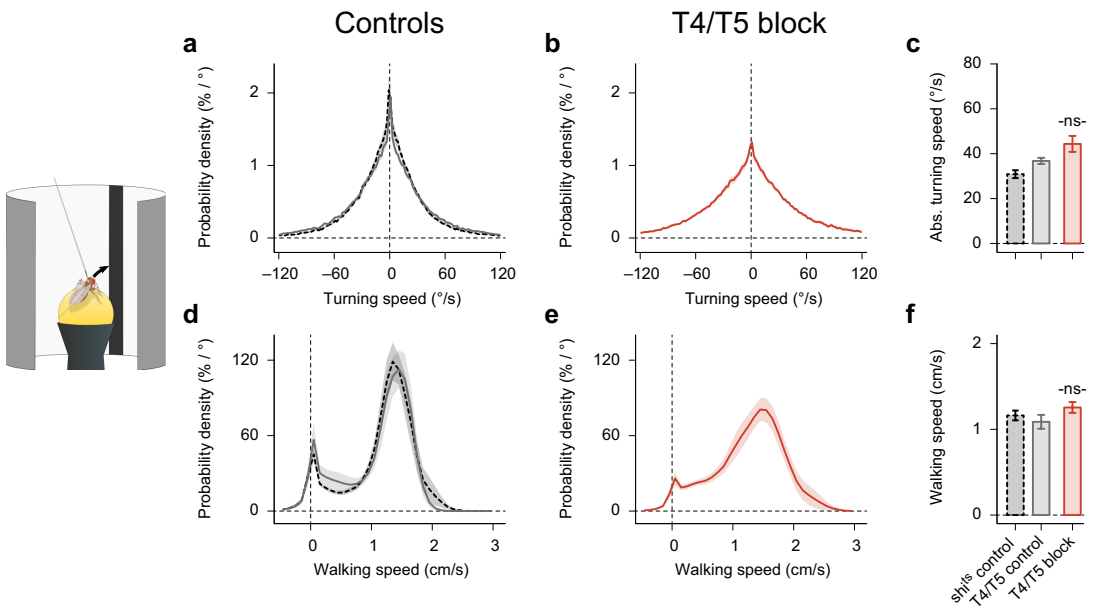

Fig. S2 Walking and turning speed of control and T4/T5 block flies during closed-loop fixation. **a** Probability density functions for turning speed (bin size = 2 °/s) of control flies. **d** Probability density functions for walking speeds (bin size = 0.1 cm/s) of control flies. **b,e** Same as in (a,d), but obtained from flies in which the output from T4 and T5 cells was blocked. **c** Average absolute turning speed. **f** Average walking speed. All data represent mean ± SEM; 40 trials per fly of N = 11,9,9 flies per group (*shi*^{ts} control, dashed black lines; T4/T5 control, solid gray lines; T4/T5 block, solid red lines). $^{-ns-}$p >= 0.05; two-sided t-test comparing to both controls. Same flies as in Fig. 1e-i.

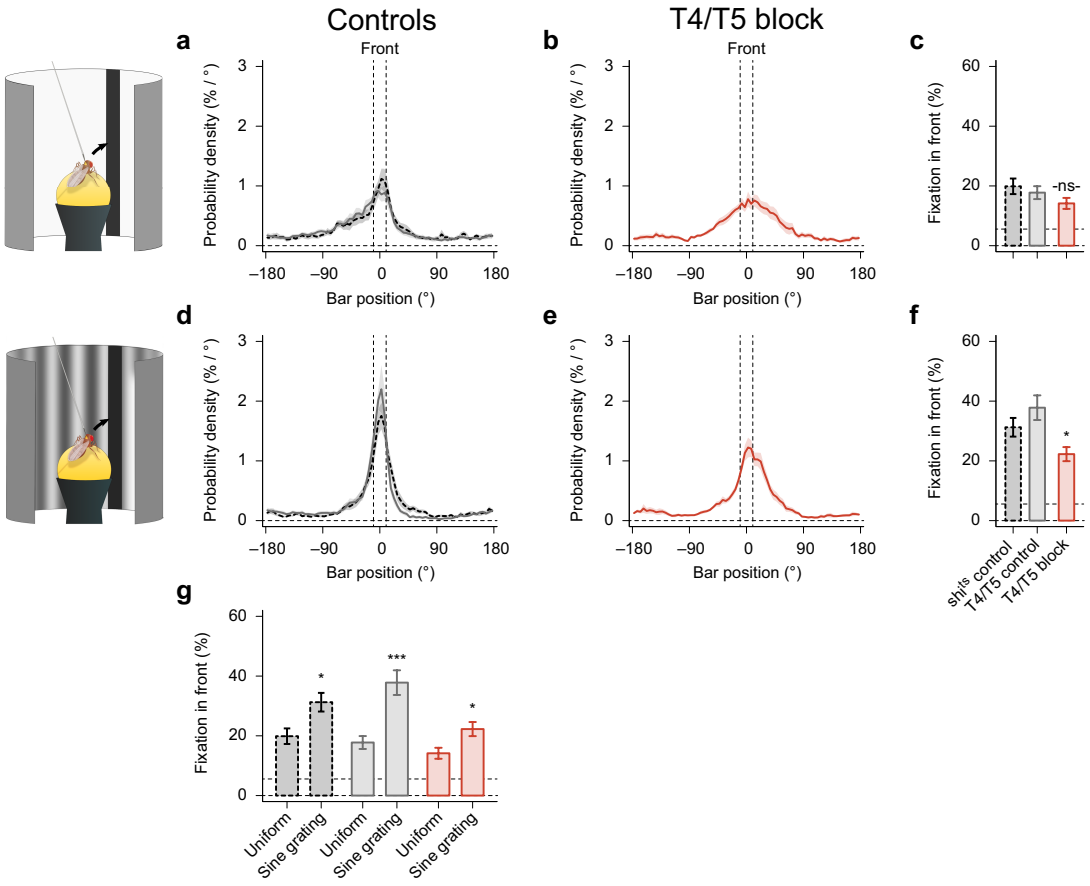

Fig. S3 The fixation response improves with a static background pattern. **a,d** Average probability density as function of bar position for the two controls when the background is gray (a) and when it is a static sine-grating pattern with the same average luminance (d). **b,e** Same as in (a,d) but for flies in which the output of T4/T5 cells was blocked. **c,f** Ability to keep the stripe in the frontal field (same measure as in Fig. 1i) when the background is gray (c) or when it is a static sine-grating background (f). **g** Comparison of the ability to keep the bar in the frontal field between uniform and sine-grating background for all groups. Upper horizontal dashed lines in (c,f,g) indicate the chance level (= 5.6 %; no fixation). All data represent mean ± SEM; 15 trials per fly of N = 10,10,9 flies per group (*shi*^{ts} control, dashed black lines; T4/T5 control, solid gray lines; T4/T5 block, solid red lines). $^{-ns-}$p >= 0.05, *p < 0.05, ***p < 0.001; two-sided t-test comparing to both controls (c,f) or comparing uniform to sine-grating within the groups (g).

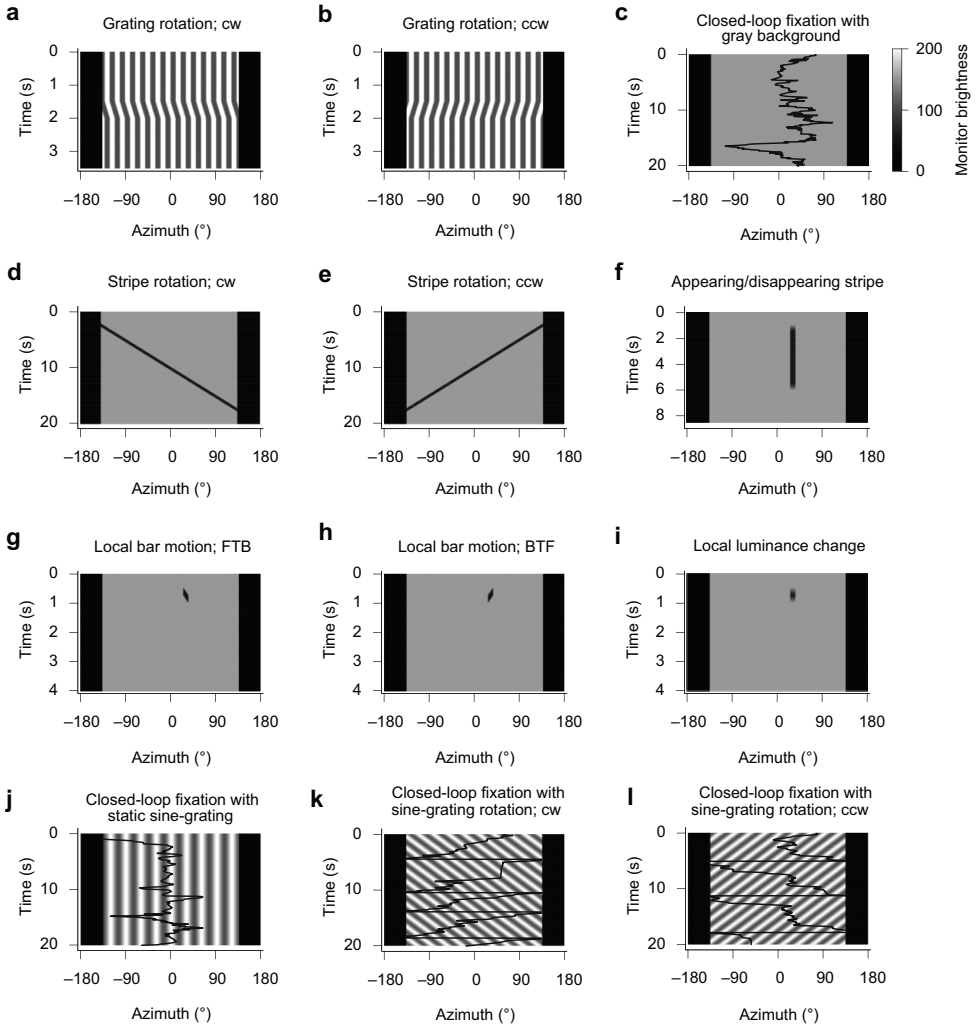

Fig. S4 Position-time plots of all visual stimuli in all experiments. **a,b** Full-field grating moving clockwise (cw) or countclockwise (ccw). **c** Closed-loop fixation of a black bar on an uniformly gray background. **d,e** Rotating black bar (cw, ccw). **f** Slowly appearing and disappearing black bar at Ψ = +60° (other locations were ±15°, ±30°, ±45°, –60°, ±90°, ±120°). **g,h** A localized black bar moves front-to-back (g) and back-to-front (h) at Ψ = +60° (other locations were Ψ = ±30°, Ψ = –60°). **i** Approximation of the local luminance dynamics in (g,h). **j** Closed-loop fixation of a black bar on a static sine-grating with the same average brightness as in (c). **k,l** Closed-loop bar fixation during background motion (cw, ccw, respectively); the black traces in (c,j-l) are experimental example traces of bar position for a single trial of a *shi*^{ts} control fly. Monitor position 0° is directly in front of the fly. The black areas indicate the region of no visual stimulation behind the fly (–180° < x < –135° and +135° < x < +180° in azimuth).

Detailed statistics (list of group sizes, statistical tests and p-values)

The degree of significance was given as follows: not significant (-ns-) when p >= 0.05; * when p < 0.05; ** when p < 0.01; *** when p < 0.001.

Figure 1

Fig. 1d

20 trials per fly; $N^{shi\ control}$ = 10 flies, $N^{T4/T5\ control}$ = 10 flies, $N^{T4/T5\ block}$ = 10 flies.
Shi^{ts} control ↔ T4/T5 control: **p = 0.254, t = –1.177** (two-sided t-test)
Shi^{ts} control ↔ T4/T5 block: **p < 0.001, t = 15.663** (two-sided t-test)
T4/T5 control ↔ T4/T5 block: **p < 0.001, t = 9.882** (two-sided t-test)
T4/T5 block ↔ zero: **p = 0.473, t = 0.749** (two-sided t-test)

Fig. 1i

40 trials per fly; $N^{shi\ control}$ = 10 flies, $N^{T4/T5\ control}$ = 10 flies, $N^{T4/T5\ block}$ = 12 flies.
Shi^{ts} control ↔ T4/T5 control: **p = 0.307, t = 1.052** (two-sided t-test)
Shi^{ts} control ↔ T4/T5 block: **p = 0.012, t = 2.759** (two-sided t-test)
T4/T5 control ↔ T4/T5 block: **p = 0.025, t = 2.427** (two-sided t-test)
T4/T5 block ↔ chance: **p < 0.001, t = 5.862** (two-sided t-test)

Figure 2

35 trials per fly; $N^{shi\ control}$ = 10 flies, $N^{T4/T5\ control}$ = 11 flies, $N^{T4/T5\ block}$ = 14 flies.

Fig. 2e

Shi^{ts} control ↔ T4/T5 control: **p = 0.725, t = 0.356** (two-sided t-test)
Shi^{ts} control ↔ T4/T5 block: **p < 0.001, t = 4.136** (two-sided t-test)
T4/T5 control ↔ T4/T5 block: **p < 0.001, t = 4.068** (two-sided t-test)
T4/T5 block ↔ zero: **p < 0.001, t = 7.086** (two-sided t-test)

Fig. 2h

Shi^{ts} control ↔ T4/T5 control: **p = 0.618, t = 0.507** (two-sided t-test)
Shi^{ts} control ↔ T4/T5 block: **p < 0.001, t = 13.408** (two-sided t-test)
T4/T5 control ↔ T4/T5 block: **p < 0.001, t = 16.735** (two-sided t-test)
T4/T5 block ↔ zero: **p = 0.056, t = 2.098** (two-sided t-test)

Figure 3

10 trials per fly; $N^{shi\ control}$ = 12 flies, $N^{T4/T5\ control}$ = 12 flies, $N^{T4/T5\ block}$ = 16 flies. Half of each group was used to measure responses at positions ±15°, ±60°, ±120°, the other half at ±30°, ±45°, ±90°.

Fig. 3e

Shi^{ts} control ↔ T4/T5 control: **p = 0.611, t = 0.524** (two-sided t-test)
Shi^{ts} control ↔ T4/T5 block: **p = 0.086, t = 1.872** (two-sided t-test)
T4/T5 control ↔ T4/T5 block: **p = 0.489, t = 0.713** (two-sided t-test)

Fig. 3h

Shi^{ts} control ↔ T4/T5 control: **p = 0.151, t = 1.553** (two-sided t-test)

Shi^{ts} control ↔ T4/T5 block: **p = 0.527, t = 0.650** (two-sided t-test)
T4/T5 control ↔ T4/T5 block: **p = 0.465, t = –0.753** (two-sided t-test)
Shi^{ts} control ↔ zero: **p = 0.368, t = –0.990** (two-sided t-test)
T4/T5 control ↔ zero: **p = 0.018, t = –3.451** (two-sided t-test)
T4/T5 block ↔ zero: **p = 0.107, t = –1.851** (two-sided t-test)

Fig. 3i,j
At 45°:
Shi^{ts} control ↔ T4/T5 block: **p = 0.054, t = 2.137** (two-sided t-test)
T4/T5 control ↔ T4/T5 block: **p = 0.155, t = 1.517** (two-sided t-test)

Fig. 3k
Shi^{ts} control ↔ T4/T5 control: **p = 0.407, t = 0.865** (two-sided t-test)
Shi^{ts} control ↔ T4/T5 block: **p = 0.470, t = 0.745** (two-sided t-test)
T4/T5 control ↔ T4/T5 block: **p = 0.939, t = –0.077** (two-sided t-test)

Figure 4
60 trials per fly; At Ψ = 30°: $N^{shi\ control}$ = 10 flies, $N^{T4/T5\ control}$ = 12 flies, $N^{T4/T5\ block}$ = 11 flies. At Ψ = 60°: Additional $N^{shi\ control}$ = 10 flies, $N^{T4/T5\ control}$ = 11 flies, $N^{T4/T5\ block}$ = 11 flies.

Fig. 4c
At 30°
Shi^{ts} control ↔ T4/T5 control: **p = 0.027, t = 2.390** (two-sided t-test)
Shi^{ts} control ↔ T4/T5 block: **p < 0.001, t = 8.262** (two-sided t-test)
T4/T5 control ↔ T4/T5 block: **p < 0.001, t = 5.103** (two-sided t-test)
At 60°:
Shi^{ts} control ↔ T4/T5 control: **p = 0.067, t = –1.939** (two-sided t-test)
Shi^{ts} control ↔ T4/T5 block: **p < 0.001, t = 7.148** (two-sided t-test)
T4/T5 control ↔ T4/T5 block: **p < 0.001, t = 9.596** (two-sided t-test)

Fig. 4f
At 30°
Shi^{ts} control ↔ T4/T5 control: **p = 0.969, t = 0.039** (two-sided t-test)
Shi^{ts} control ↔ T4/T5 block: **p < 0.001, t = –4.101** (two-sided t-test)
T4/T5 control ↔ T4/T5 block: **p < 0.001, t = –3.962** (two-sided t-test)
At 60°
Shi^{ts} control ↔ T4/T5 control: **p = 0.666, t = 0.438** (two-sided t-test)
Shi^{ts} control ↔ T4/T5 block: **p < 0.001, t = –4.842** (two-sided t-test)
T4/T5 control ↔ T4/T5 block: **p = 0.002, t = –3.488** (two-sided t-test)

Fig. 4i
At 30°
Shi^{ts} control ↔ T4/T5 control: **p = 0.955, t = 0.057** (two-sided t-test)
Shi^{ts} control ↔ T4/T5 block: **p = 0.471, t = 0.736** (two-sided t-test)
T4/T5 control ↔ T4/T5 block: **p = 0.485, t = 0.711** (two-sided t-test)
At 60°:
Shi^{ts} control ↔ T4/T5 control: **p = 0.609, t = –0.518** (two-sided t-test)

Shi^{ts} control ↔ T4/T5 block: **p = 0.165, t = 1.443** (two-sided t-test)
T4/T5 control ↔ T4/T5 block: **p = 0.069, t = 1.916** (two-sided t-test)

Fig. 4j
At 30°
R_{FTB} ↔ R_{BTF} ↔ R_L (T4/T5 block): **p = 0.742, F = 0.300** (one-way ANOVA)
At 60°
R_{FTB} ↔ R_{BTF} ↔ R_L (T4/T5 block): **p = 0.902, F = 0.103** (one-way ANOVA)

Fig. 4k
At 30°
M_{FTB} ↔ $-M_{BTF}$ (*shi*^{ts} control): **p < 0.001, t = 5.696** (two-sided t-test)
M_{FTB} ↔ $-M_{BTF}$ (T4/T5 control): **p = 0.028, t = 2.346** (two-sided t-test)
M_{FTB} ↔ $-M_{BTF}$ (T4/T5 block): **p = 0.209, t = 1.299** (two-sided t-test)
M_{FTB} ↔ zero (T4/T5 block): **p = 0.447, t = 0.790** (two-sided t-test)
M_{BTF} ↔ zero (T4/T5 block): **p = 0.325, t = –1.035** (two-sided t-test)
At 60°
M_{FTB} ↔ $-M_{BTF}$ (*shi*^{ts} control): **p = 0.639, t = 0.476** (two-sided t-test)
M_{FTB} ↔ $-M_{BTF}$ (T4/T5 control): **p = 0.147, t = 1.508** (two-sided t-test)
M_{FTB} ↔ $-M_{BTF}$ (T4/T5 block): **p = 0.499, t = –0.687** (two-sided t-test)
M_{FTB} ↔ zero (T4/T5 block): **p = 0.653, t = –0.463** (two-sided t-test)
M_{BTF} ↔ zero (T4/T5 block): **p = 0.622, t = 0.508** (two-sided t-test)

Figure 5
30 trials per fly; $N^{shi\ control}$ = 11 flies, $N^{T4/T5\ control}$ = 9 flies, $N^{T4/T5\ block}$ = 9 flies.

Fig. 5c
Shi^{ts} control ↔ T4/T5 control: **p = 0.394, t = 0.874** (two-sided t-test)
Shi^{ts} control ↔ T4/T5 block: **p = 0.047, t = –2.127** (two-sided t-test)
T4/T5 control ↔ T4/T5 block: **p = 0.010, t = –2.908** (two-sided t-test)

Fig. 5f
Shi^{ts} control ↔ T4/T5 control: **p = 0.176, t = 1.410** (two-sided t-test)
Shi^{ts} control ↔ T4/T5 block: **p = 0.012, t = –2.797** (two-sided t-test)
T4/T5 control ↔ T4/T5 block: **p = 0.001, t = –3.999** (two-sided t-test)

Figure S1
Fig. S1b
$N^{shi\ control}$ = 10 flies, $N^{T4/T5\ control}$ = 10 flies, $N^{T4/T5\ block}$ = 10 flies. Same flies as in Fig. 1b-d.

Fig. S1d
$N^{shi\ control}$ = 10 flies, $N^{T4/T5\ control}$ = 10 flies, $N^{T4/T5\ block}$ = 12 flies. Same flies as in Fig. 1e-i.

Figure S2
40 trials per fly; $N^{shi\ control}$ = 10 flies, $N^{T4/T5\ control}$ = 10 flies, $N^{T4/T5\ block}$ = 12 flies. Same flies as in Fig. 1e-i.

Fig. S2c

Shi^{ts} control ↔ T4/T5 control: **p = 0.023, t = –2.490** (two-sided t-test)
Shi^{ts} control ↔ T4/T5 block: **p = 0.006, t = –3.049** (two-sided t-test)
T4/T5 control ↔ T4/T5 block: **p = 0.095, t = –1.767** (two-sided t-test)

Fig. S2f

Shi^{ts} control ↔ T4/T5 control: **p = 0.486, t = 0.710** (two-sided t-test)
Shi^{ts} control ↔ T4/T5 block: **p = 0.319, t = –1.021** (two-sided t-test)
T4/T5 control ↔ T4/T5 block: **p = 0.131, t = –1.575** (two-sided t-test)

Figure S3

15 trials per fly; $N^{shi\ control}$ = 10 flies $N^{T4/T5\ control}$ = 10 flies, $N^{T4/T5\ block}$ = 9 flies.

Fig. S3c

Shi^{ts} control ↔ T4/T5 control: **p = 0.561, t = 0.591** (two-sided t-test)
Shi^{ts} control ↔ T4/T5 block: **p = 0.115, t = 1.659** (two-sided t-test)
T4/T5 control ↔ T4/T5 block: **p = 0.252, t = 1.186** (two-sided t-test)

Fig. S3f

Shi^{ts} control ↔ T4/T5 control: **p = 0.246, t = –1.200** (two-sided t-test)
Shi^{ts} control ↔ T4/T5 block: **p = 0.047, t = 2.136** (two-sided t-test)
T4/T5 control ↔ T4/T5 block: **p = 0.008, t = 3.004** (two-sided t-test)

Fig. S3g

Uniform ↔ Sine grating (*shi*^{ts} control): **p = 0.016, t = –2.651** (two-sided t-test)
Uniform ↔ Sine grating (T4/T5 control): **p < 0.001, t = –4.079** (two-sided t-test)
Uniform ↔ Sine grating (T4/T5 block): **p = 0.021, t = –2.553** (two-sided t-test)

3 PAPER II: A DIRECTIONAL TUNING MAP OF DROSOPHILA ELEMENTARY MOTION DETECTORS

In this article, neural activity in T4 and T5 neurons was imaged via two-photon microscopy. These cells were further characterized according to their differential role in motion processing and related motion behavior. The paper was published in Nature in August 2013[1].

Summary

The work presented here shows that T4 and T5 neurons form local direction-selective units which respond in a contrast polarity-specific manner: T4 neurons respond only to moving bright edges (ON) and T5 neurons respond only to moving dark edges (OFF). Moreover, we found that both cell types fall into four neuronal subclasses according to their tuning to one of the four cardinal directions of motion. Each class targets a specific layer in the lobula plate, which gives rise to a directional tuning map. Further, we assessed the functional role of T4 and T5 neurons in motion processing: When silencing T4 neurons, ON motion responses in lobula plate tangential cells were impaired while blocking T5 neurons reduced OFF motion responses. Similarly, in behavioral experiments with T4 block flies, direction-selective responses to moving ON edges were more impaired than to moving OFF edges and the opposite was true for the T5 block.

The following authors contributed to this work:

Author contributions

Matthew S. Maisak, Jürgen Haag, Georg Ammer, Etienne Serbe, Matthias Meier, Aljoscha Leonhardt, Tabea Schilling, **Armin Bahl**[*], Gerald M. Rubin, Aljoscha Nern, Barry J. Dickson, Dierk F. Reiff, Elisabeth Hopp and Alexander Borst. — M.S.M. and J.H. jointly performed and, together with A.Bo., evaluated all calcium imaging experiments. G.A., E.S. and M.M. recorded from tangential cells. A.L., T.S. and **A.Ba.**[*] performed the behavioral experiments and analyzed the data. G.R., B.D. and A.N. generated the driver lines and characterized their expression pattern. D.F.R. performed preliminary imaging experiments. E.H. helped with programming and developed the PMT shielding for the two-photon microscope. A.Bo. designed the study and wrote the manuscript with the help of all authors.

The work in this paper has been highlighted in several journals (Flight, 2013; Gilbert, 2013; Masland, 2013; Yonehara and Roska, 2013).

1 Nature 500, 212–216 (08 August 2013) doi:10.1038/nature12320

LETTER

doi:10.1038/nature12320

A directional tuning map of *Drosophila* elementary motion detectors

Matthew S. Maisak[1]*, Juergen Haag[1]*, Georg Ammer[1], Etienne Serbe[1], Matthias Meier[1], Aljoscha Leonhardt[1], Tabea Schilling[1], Armin Bahl[1], Gerald M. Rubin[2], Aljoscha Nern[2], Barry J. Dickson[3], Dierk F. Reiff[1]†, Elisabeth Hopp[1] & Alexander Borst[1]

The extraction of directional motion information from changing retinal images is one of the earliest and most important processing steps in any visual system. In the fly optic lobe, two parallel processing streams have been anatomically described, leading from two first-order interneurons, L1 and L2, via T4 and T5 cells onto large, wide-field motion-sensitive interneurons of the lobula plate[1]. Therefore, T4 and T5 cells are thought to have a pivotal role in motion processing; however, owing to their small size, it is difficult to obtain electrical recordings of T4 and T5 cells, leaving their visual response properties largely unknown. We circumvent this problem by means of optical recording from these cells in *Drosophila*, using the genetically encoded calcium indicator GCaMP5 (ref. 2). Here we find that specific subpopulations of T4 and T5 cells are directionally tuned to one of the four cardinal directions; that is, front-to-back, back-to-front, upwards and downwards. Depending on their preferred direction, T4 and T5 cells terminate in specific sublayers of the lobula plate. T4 and T5 functionally segregate with respect to contrast polarity: whereas T4 cells selectively respond to moving brightness increments (ON edges), T5 cells only respond to moving brightness decrements (OFF edges). When the output from T4 or T5 cells is blocked, the responses of postsynaptic lobula plate neurons to moving ON (T4 block) or OFF edges (T5 block) are selectively compromised. The same effects are seen in turning responses of tethered walking flies. Thus, starting with L1 and L2, the visual input is split into separate ON and OFF pathways, and motion along all four cardinal directions is computed separately within each pathway. The output of these eight different motion detectors is then sorted such that ON (T4) and OFF (T5) motion detectors with the same directional tuning converge in the same layer of the lobula plate, jointly providing the input to downstream circuits and motion-driven behaviours.

Most of the neurons in the fly brain are dedicated to image processing. The respective part of the head ganglion, called the optic lobe, consists of several layers of neuropile called lamina, medulla, lobula and lobula plate, all built from repetitive columns arranged in a retinotopic way (Fig. 1a). Each column houses a set of identified neurons that, on the basis of Golgi staining, have been described anatomically in great detail[3–5]. Owing to their small size, however, most of these columnar neurons have never been recorded from electrophysiologically. Therefore, their specific functional role in visual processing is still largely unknown. This fact is contrasted by rather detailed functional models about visual processing inferred from behavioural studies and recordings from the large, electrophysiologically accessible output neurons of the fly lobula plate (tangential cells). As the most prominent example of such models, the Reichardt detector derives directional motion information from primary sensory signals by multiplying the output from adjacent photoreceptors after asymmetric temporal filtering[6]. This model makes a number of rather counter-intuitive predictions all of which have been confirmed experimentally (for review, see ref. 7). Yet, the neurons corresponding to most

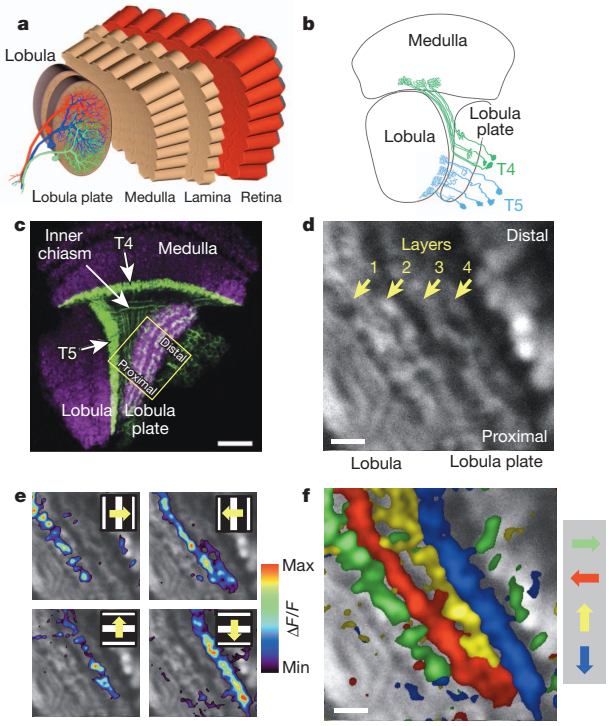

Figure 1 | Directional tuning and layer-specific projection of T4 and T5 cells. **a**, Schematic diagram of the fly optic lobe. In the lobula plate, motion-sensitive tangential cells extend their large dendrites over many hundreds of columns. Shown are the reconstructions of the three cells of the horizontal system[22]. **b**, Anatomy of T4 and T5 cells, as drawn from Golgi-impregnated material (from ref. 5). **c**, Confocal image of the Gal4-driver line R42F06, shown in a horizontal cross-section (from ref. 10). Neurons are marked in green (Kir2.1–EGFP labelled), whereas the neuropile is stained in purple by an antibody against the postsynaptic protein Dlg. Scale bar, 20 μm. **d**, Two-photon image of the lobula plate of a fly expressing GCaMP5 under the control of the same driver line R42F06. Scale bar, 5 μm. The size and orientation of the image approximately corresponds to the yellow square in **c**. **e**, Relative fluorescence changes ($\Delta F/F$) obtained during 4-s grating motion along the four cardinal directions, overlaid on the greyscale image. Each motion direction leads to activity in a different layer. Minimum and maximum $\Delta F/F$ values were 0.3 and 1.0 (horizontal motion), and 0.15 and 0.6 (vertical motion). **f**, Compound representation of the results obtained from the same set of experiments. Scale bar, 5 μm. Results in **e** and **f** represent the data obtained from a single fly averaged over four stimulus repetitions. Similar results were obtained from six other flies.

[1]Max Planck Institute of Neurobiology, 82152 Martinsried, Germany. [2]Janelia Farm Research Campus, Ashburn, Virginia 20147, USA. [3]Institute of Molecular Pathology, 1030 Vienna, Austria. †Present address: Institute Biology 1, Albert-Ludwigs University, 79085 Freiburg, Germany.
*These authors contributed equally to this work.

of the circuit elements of the Reichardt detector have not been identified so far. Here, we focus on a set of neurons called T4 and T5 cells (Fig. 1b) which, on the basis of circumstantial evidence, have long been speculated to be involved in motion detection[1,8–10]. However, it is unclear to what extent T4 and T5 cells are directionally selective or whether direction selectivity is computed or enhanced within the dendrites of the tangential cells. Another important question concerns the functional separation between T4 and T5 cells; that is, whether they carry equivalent signals, maybe one being excitatory and the other inhibitory on the tangential cells, or whether they segregate into directional- and non-directional pathways[11] or into separate ON- and OFF-motion channels[12,13].

To answer these questions, we combined Gal4-driver lines specific for T4 and T5 cells[14] with GCaMP5 (ref. 2) and optically recorded the visual response properties using two-photon fluorescence microscopy[15]. In a first series of experiments, we used a driver line labelling both T4 and T5 cells. A confocal image (Fig. 1c, modified from ref. 10) revealed clear labelling (in green) in the medulla (T4 cell dendrites), in the lobula (T5 cell dendrites), as well as in four distinct layers of the lobula plate, representing the terminal arborizations of the four subpopulations of both T4 and T5 cells. These four layers of the lobula plate can also be seen in the two-photon microscope when the calcium indicator GCaMP5 is expressed (Fig. 1d). After stimulation of the fly with grating motion along four cardinal directions (front-to-back, back-to-front, upwards and downwards), activity is confined to mostly one of the four layers, depending on the direction in which the grating is moving (Fig. 1e). The outcome of all four stimulus conditions can be combined into a single image by assigning a particular colour to each pixel depending on the stimulus direction to which it responded most strongly (Fig. 1f). From these experiments it is clear that the four subpopulations of T4 and T5 cells produce selective calcium signals depending on the stimulus direction, in agreement with previous deoxyglucose labelling[8]. Sudden changes of the overall luminance evokes no responses in any of the layers (field flicker; $n = 4$ experiments, data not shown). However, gratings flickering in counter-phase lead to layer-specific responses, depending on the orientation of the grating (Supplementary Fig. 1).

The retinotopic arrangement of this input to the lobula plate is demonstrated by experiments where a dark edge was moved within a small area of the visual field only. Depending on the position of this area, activity of T4 and T5 cells is confined to different positions within the lobula plate (Fig. 2a). Consequently, when moving a bright vertical edge horizontally from back to front, activity of T4 and T5 cells is elicited sequentially in layer 2 of the lobula plate (Fig. 2b). These two experiments also demonstrate that T4 and T5 cells indeed signal motion locally. We next investigated the question of where direction selectivity of T4 and T5 cells arises; that is, whether it is already present in the dendrite, or whether it is generated by synaptic interactions within the lobula plate. This question is hard to answer, as the dendrites of both T4 and T5 cells form a dense mesh within the proximal layer of the medulla (T4) and the lobula (T5), respectively. However, signals within the inner chiasm where individual processes of T4 and T5 cells can be resolved in some preparations show a clear selectivity for motion in one over the other directions (Fig. 2c). Such signals are as directionally selective as the ones measured within the lobula plate, demonstrating that the signals delivered from the dendrites of T4 and T5 cells are already directionally selective.

To assess the particular contribution of T4 and T5 cells to the signals observed in the above experiments, we used driver lines specific for T4 and T5 cells, respectively. Applying the same stimulus protocol and data evaluation as in Fig. 1, identical results were obtained as before for both the T4- as well as the T5-specific driver line (Fig. 3a, b). We conclude that T4 and T5 cells each provide directionally selective signals to the lobula plate, in contrast to previous reports[11]. Thus, both T4 and T5 cells can be grouped, according to their preferred direction, into four subclasses covering all four cardinal directions, reminiscent of ON–OFF ganglion cells of the rabbit retina[16].

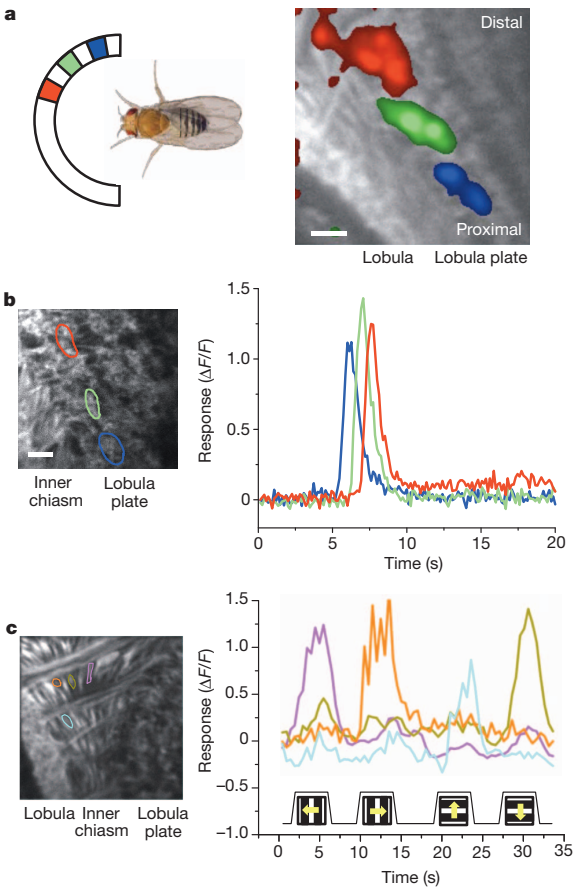

Figure 2 | Local signals of T4 and T5 cells. **a**, Retinotopic arrangement of T4 and T5 cells. A dark edge was moving repeatedly from front-to-back within a 15° wide area at different azimuthal positions (left). This leads to relative fluorescence changes at different positions along the proximal–distal axis within layer 1 of the lobula plate (right). Scale bar, 5 µm. Similar results have been obtained in four other flies. **b**, Sequential activation of T4 and T5 cells. A bright edge was moving from back-to-front at 15° s^{-1}. Scale bar, 5 µm. Similar results have been obtained in six other flies. **c**, Signals recorded from individual fibres within the inner chiasm (left) reveal a high degree of direction selectivity (right). Scale bar, 5 µm. Similar results were obtained from four other flies, including both lines specific for T4 and T5 cells. Response traces in **b** and **c** are derived from the region of interest encircled in the image with the same colour.

We next addressed whether T4 cells respond differently to T5 cells. To answer this question, we used, instead of gratings, moving edges with either positive (ON edge, brightness increment) or negative (OFF edge, brightness decrement) contrast polarity as visual stimuli. We found that T4 cells strongly responded to moving ON edges, but showed little or no response to moving OFF edges (Fig. 3c). This is true for T4 cells terminating in each of the four layers. We found the opposite for T5 cells. T5 cells selectively responded to moving OFF edges and mostly failed to respond to moving ON edges (Fig. 3d). Again, we found this for T5 cells in each of the four layers. We next addressed whether there are any other differences in the response properties between T4 and T5 cells by testing the velocity tuning of both cell populations by means of stimulating flies with grating motion along the horizontal axis from the front to the back at various velocities covering two orders of magnitude. T4 cells revealed a maximum response at a stimulus velocity of 30° s^{-1}, corresponding to a temporal frequency of 1 Hz (Fig. 3e). T5 cell responses showed a similar dependency on stimulus velocity, again with a peak at a temporal frequency of

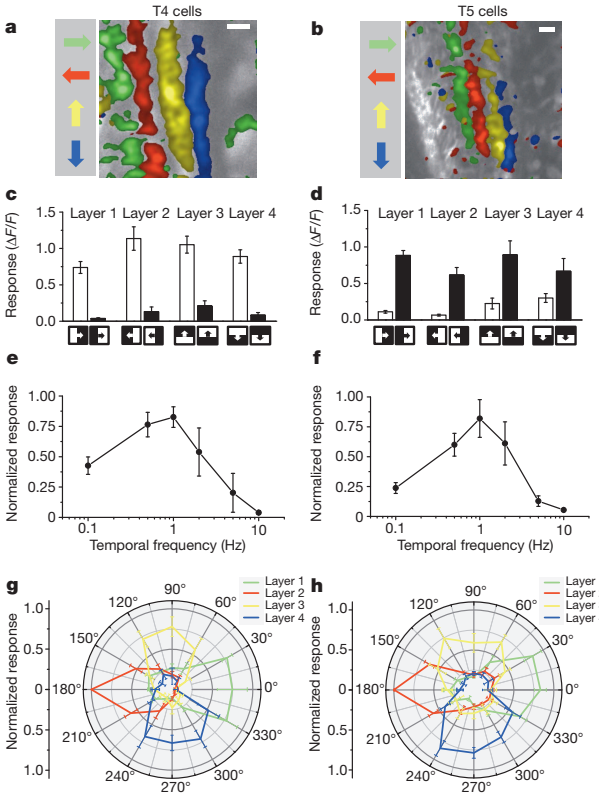

Figure 3 | Comparison of visual response properties between T4 and T5 cells. **a**, **b**, Relative fluorescence changes ($\Delta F/F$) of the lobula plate terminals of T4 (**a**) and T5 (**b**) cells obtained during grating motion along the four cardinal directions. Results represent the data obtained from a single fly each, averaged over two stimulus repetitions. Scale bars, 5 μm. Similar results have been obtained in ten other flies. **c**, **d**, Responses of T4 (**c**) and T5 (**d**) cells to ON and OFF edges moving along all four cardinal directions. ON (white) and OFF (black) responses within each layer are significantly different from each other, with $P < 0.005$ except for layers 3 and 4 in T5 cells, where $P < 0.05$. **e**, **f**, Responses of T4 (**e**) and T5 (**f**) cells to gratings moving horizontally at different temporal frequencies. Relative fluorescence changes were evaluated from layer 1 of the lobula plate and normalized to the maximum response before averaging. **g**, **h**, Responses of T4 (**g**) and T5 (**h**) cells to gratings moving in 12 different directions. Relative fluorescence changes were evaluated from all four layers of the lobula plate normalized to the maximum response before averaging. Data represent the mean ± s.e.m. of the results obtained in $n = 8$ (**c**), $n = 7$ (**d**), $n = 6$ (**e**), $n = 7$ (**f**), $n = 6$ (**g**) and $n = 5$ (**h**) different flies. Significances indicated are based on two-sample *t*-test.

1 Hz (Fig. 3f). Thus, there is no obvious difference in the velocity tuning between T4 and T5 cells. As another possibility, T4 cells might functionally differ from T5 cells with respect to their directional tuning width. To test this, we stimulated flies with gratings moving into 12 different directions and evaluated the relative change of fluorescence in all four layers of the lobula plate. Using the T4-specific driver line, we found an approximate half width of 60–90° of the tuning curve, with the peak responses in each layer shifted by 90° (Fig. 3g). No decrease of calcium was detectable for grating motion opposite to the preferred direction of the respective layer. When we repeated the experiments using the T5-specific driver line, we found a similar dependence of the relative change of fluorescence on the stimulus direction (Fig. 3h). We conclude that T4 cells have the same velocity and orientation tuning as T5 cells. The only functional difference we were able to detect remains their selectivity for contrast polarity.

Our finding about the different preference of T4 and T5 cells for the polarity of a moving contrast makes the strong prediction that selective blockade of T4 or T5 cells should selectively compromise the responses of downstream lobula plate tangential cells to either ON or OFF edges. To test this prediction, we blocked the output of either T4 or T5 cells via expression of the light chain of tetanus toxin[17] and recorded the responses of tangential cells via somatic whole-cell patch to moving ON and OFF edges. In response to moving ON edges, strong and reliable directional responses were observed in all control flies (Fig. 4a). However, T4-block flies showed a strongly reduced response to ON edges, whereas the responses of T5-block flies were at the level of control flies (Fig. 4b, c). When we used moving OFF edges, control flies again responded with a large amplitude (Fig. 4d). However, the responses of T4-block flies were at the level of control flies, whereas the responses of T5-block flies were strongly reduced (Fig. 4e, f). These findings are reminiscent on the phenotypes obtained from blocking lamina cells L1 and L2 (ref. 13) and demonstrate that T4 and T5 cells are indeed the motion-coding intermediaries for these contrast polarities on their way to the tangential cells of the lobula plate. Whether the residual responses to ON edges in T4-block flies and to OFF edges in T5-block flies are due to an incomplete signal separation between the two pathways or due to an incomplete genetic block in both fly lines is currently unclear.

To address the question of whether T4 and T5 cells are the only motion detectors of the fly visual system, or whether they represent one cell class, in parallel to other motion-sensitive elements, we used tethered flies walking on an air-suspended sphere[18] and stimulated them by ON and OFF edges moving in opposite directions[19]. As in the previous experiments, we blocked T4 and T5 cells specifically by selective expression of the light chain of tetanus toxin. During balanced motion, control flies did not show significant turning responses to either side (Fig. 4g). T4-block flies, however, strongly followed the direction of the moving OFF edges, whereas T5-block flies followed the direction of the moving ON edges (Fig. 4h, i). In summary, the selective preference of T4-block flies for OFF edges and of T5-block flies for ON edges not only corroborates our findings about the selective preference of T4 and T5 cells for different contrast polarities, but also demonstrates that the signals of T4 and T5 cells are indeed the major, if not exclusive, inputs to downstream circuits and motion-driven behaviours.

Almost a hundred years after T4 and T5 cells have been anatomically described[3], this study reports their functional properties in a systematic way. Using calcium as a proxy for membrane voltage[20], we found that both T4 and T5 cells respond to visual motion in a directionally selective manner and provide these signals to each of the four layers of the lobula plate, depending on their preferred direction. Both cell types show identical velocity and orientation tuning which matches the one of the tangential cells[21,22]. The strong direction selectivity of both T4 and T5 cells is unexpected, as previous studies had concluded that the high degree of direction selectivity of tangential cells is due to a push–pull configuration of weakly directional input with opposite preferred direction[23,24]. Furthermore, as the preferred direction of T4 and T5 cells matches the preferred direction of the tangential cells branching within corresponding layers, it is currently unclear which neurons are responsible for the null-direction response of the tangential cells. As for the functional separation between T4 and T5 cells, we found that T4 cells selectively respond to brightness increments, whereas T5 cells exclusively respond to moving brightness decrements. Interestingly, parallel ON and OFF motion pathways had been previously postulated on the basis of selective silencing of lamina neurons L1 and L2 (ref. 13). Studies using apparent motion stimuli to probe the underlying computational structure arrived at controversial conclusions: whereas some studies concluded that there was a separate handling of ON and OFF events by motion detectors[12,25,26], others did not favour such a strict separation[19,27]. The present study directly demonstrates the existence of separate ON and OFF motion detectors, as represented by T4 and T5 cells, respectively. Furthermore, our results anatomically confine the essential processing steps of elementary

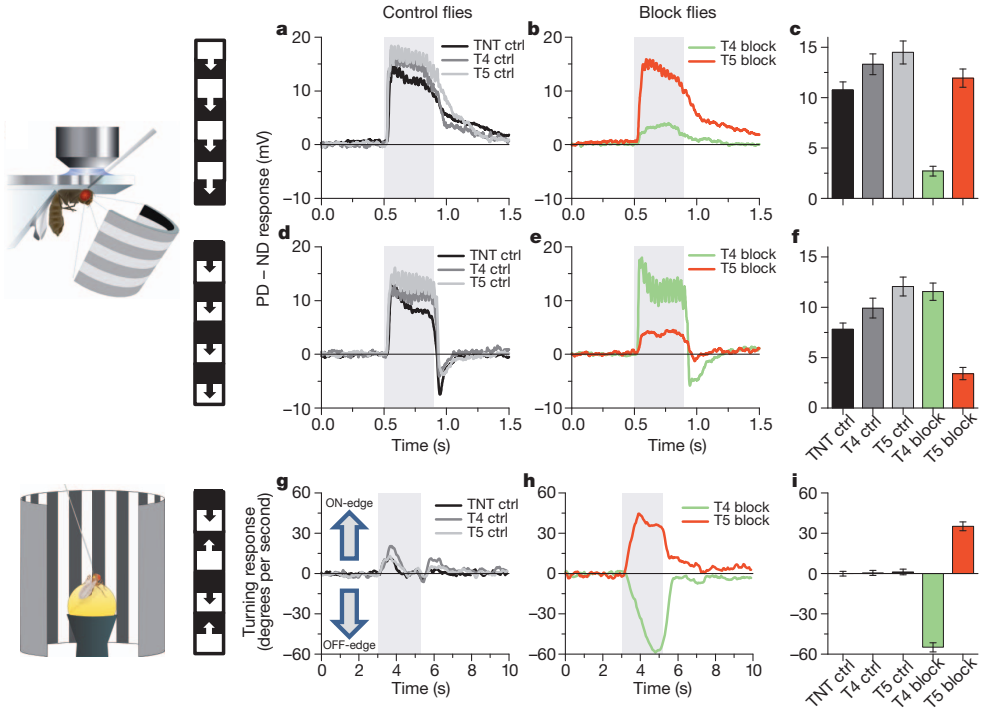

Figure 4 | Voltage responses of lobula plate tangential cells and turning responses of walking flies to moving ON and OFF edges. **a**, **d**, Average time course of the membrane potential in response to preferred direction motion minus the response to null direction motion (PD − ND response) as recorded in three types of control flies (stimulation period indicated by shaded area). **b**, **e**, Same as in **a**, **d**, but recorded in T4-block flies (green) and T5-block flies (red). The stimulus pattern, shown to the left, consisted of multiple ON- (**a**) or OFF-edges (**d**). **c**, **f**, Mean voltage responses (PD − ND) of tangential cells in the five groups of flies. Recordings were done from cells of the vertical[21] and the horizontal[22] system. Because no difference was detected between them, data were pooled. Data comprise recordings from $n = 20$ (TNT control), $n = 12$ (T4 control), $n = 16$ (T5 control), $n = 17$ (T4 block) and $n = 18$ (T5 block) cells. In both T4 and T5-block flies, ON and OFF responses are significantly different from each other with $P < 0.001$. In T4-block flies, ON responses are significantly reduced compared to all three types of control flies, whereas in T5-block flies, OFF responses are significantly reduced, both with $P < 0.001$. **g**, Average time course of the turning response of three types of control flies to ON and OFF edges moving simultaneously to opposite directions (stimulation period indicated by shaded area). **h**, Same as in **g**, but recorded from T4-block flies (green) and T5-block flies (red). **i**, Mean turning tendency (±s.e.m.) during the last second of the stimulation period averaged across all flies within each group. Data comprise average values obtained in $n = 12$ (TNT controls), $n = 11$ (T4 controls), $n = 11$ (T5 controls), $n = 13$ (T4 block) and $n = 12$ (T5 block) flies. Values of T4 and T5-block flies are highly significantly different from zero with $P < 0.001$. Significances indicated are based on two-sample t-test.

motion detection—that is, asymmetric temporal filtering and non-linear interaction—to the neuropile between the axon terminals of lamina neurons L1 and L2 (ref. 28) and the dendrites of directionally selective T4 and T5 cells (Supplementary Fig. 2). The dendrites of T4 and T5 cells might well be the place where signals from neighbouring columns interact in a nonlinear way, similar to the dendrites of starburst amacrine cells of the vertebrate retina[29].

METHODS SUMMARY

Flies. Flies used in calcium imaging experiments (Figs 1–3) had the following genotypes: T4/T5 line (w^-; +/+; *UAS-GCaMP5,R42F06-GAL4/UAS-GCaMP5, R42F06-GAL4*), T4 line (w^-; +/+; *UAS-GCaMP5,R54A03-GAL4/UAS-GCaMP5, R54A03-GAL4*), T5 line (w^-; +/+; *UAS-GCaMP5,R42H07-GAL4/UAS-GCaMP5, R42H07-GAL4*). Flies used in electrophysiological and behavioural experiments (Fig. 4) had identical genotypes of the following kind: TNT control flies (w^+/w^+; *UAS-TNT-E/UAS-TNT-E*; +/+), T4 control flies (w^+/w^-; + /+; *VT37588-GAL4/+*), T5 control flies (w^+/w^-; +/+; *R42H07-GAL4/+*), T4-block flies (w^+/w^-; *UAS-TNT-E/+*; *VT37588-GAL4/+*), T5-block flies (w^+/w^-; *UAS-TNT-E/+*; *R42H07-GAL4/+*).

Two-photon microscopy. We used a custom-built two-photon laser scanning microscope [29] equipped with a ×40 water immersion objective and a mode locked Ti:sapphire laser. To shield the photomultipliers from the stimulus light, two separate barriers were used: the first was placed directly over the LEDs, the second extended from the fly holder over the arena. Images were acquired at a resolution of 256 × 256 pixels and a frame rate of 1.87 Hz, except where indicated, using ScanImage software[30].

Electrophysiology. Recordings were established under visual control using a Zeiss Microscope and a ×40 water immersion objective.

Behavioural analysis. The locomotion recorder was custom-designed according to ref. 18. It consisted of an air-suspended sphere floating in a bowl-shaped sphere holder. Motion of the sphere was recorded by two optical tracking sensors.

Visual stimulation. For calcium imaging and electrophysiological experiments, we used a custom-built LED arena covering 180° and 90° of the visual field along the horizontal and the vertical axis, respectively, at 1.5° resolution. For the behavioural experiments, three 120-Hz LCD screens formed a U-shaped visual arena with the fly in the centre, covering 270° and 114° of the visual field along the horizontal and the vertical axes, respectively, at 0.1° resolution.

Data evaluation. Data were evaluated off-line using custom-written software (Matlab and IDL).

Full Methods and any associated references are available in the online version of the paper.

Received 16 April; accepted 20 May 2013.

1. Bausenwein, B., Dittrich, A. P. M. & Fischbach, K. F. The optic lobe of *Drosophila melanogaster* II. Sorting of retinotopic pathways in the medulla. *Cell Tissue Res.* **267,** 17–28 (1992).
2. Akerboom, J. *et al.* Optimization of a GCaMP calcium indicator for neural activity imaging. *J. Neurosci.* **32,** 13819–13840 (2012).
3. Cajal, S. R. & Sanchez, D. *Contribucion al conocimiento de los centros nerviosos de los insectos* (Imprenta de Hijos de Nicholas Moja, 1915).
4. Strausfeld, N. J. *Atlas of an Insect Brain* (Springer, 1976).
5. Fischbach, K. F. & Dittrich, A. P. M. The optic lobe of *Drosophila melanogaster*. I. A Golgi analysis of wild-type structure. *Cell Tissue Res.* **258,** 441–475 (1989).

6. Reichardt, W. Autocorrelation, a principle for the evaluation of sensory information by the central nervous system. In *Sensory Communication* (ed. Rosenblith, W. A.) 303–317 (MIT Press and John Wiley & Sons, 1961).
7. Borst, A., Haag, J. & Reiff, D. F. Fly motion vision. *Annu. Rev. Neurosci.* **33,** 49–70 (2010).
8. Buchner, E., Buchner. S. & Buelthoff, I. Deoxyglucose mapping of nervous activity induced in *Drosophila* brain by visual movement. 1. Wildtype. *J. Comp. Physiol.* **155,** 471–483 (1984).
9. Strausfeld, N. J. & Lee, J. K. Neuronal basis for parallel visual processing in the fly. *Vis. Neurosci.* **7,** 13–33 (1991).
10. Schnell, B., Raghu, V. S., Nern, A. & Borst, A. Columnar cells necessary for motion responses of wide-field visual interneurons in *Drosophila*. *J. Comp. Physiol. A* **198,** 389–395 (2012).
11. Douglass, J. K. & Strausfeld, N. J. Visual motion-detection circuits in flies: Parallel direction- and non-direction-sensitive pathways between the medulla and lobula plate. *J. Neurosci.* **16,** 4551–4562 (1996).
12. Franceschini, N., Riehle, A. & Le Nestour, A. Directionally selective motion detection by insect neurons. In *Facets of Vision* (ed. Stavenga, H.) 360–390 (Springer, 1989).
13. Joesch, M., Schnell, B., Raghu, S. V., Reiff, D. F. & Borst, A. ON and OFF pathways in *Drosophila* motion vision. *Nature* **468,** 300–304 (2010).
14. Pfeiffer, B. D. *et al.* Tools for neuroanatomy and neurogenetics in *Drosophila*. *Proc. Natl Acad. Sci. USA* **105,** 9715–9720 (2008).
15. Denk, W., Strickler, J. H. & Webb, W. W. Two-photon laser scanning fluorescence microscopy. *Science* **248,** 73–76 (1990).
16. Oyster, C. W. & Barlow, H. B. Direction-selective units in rabbit retina: distribution of preferred directions. *Science* **155,** 841–842 (1967).
17. Sweeney, S. T., Broadie, K., Keane, J., Niemann, H. & O'Kane, C. J. Targeted expression of tetanus toxin light chain in *Drosophila* specifically eliminates synaptic transmission and causes behavioral defects. *Neuron* **14,** 341–351 (1995).
18. Seelig, J. D. *et al.* Two-photon calcium imaging from head-fixed *Drosophila* during optomotor walking behavior. *Nature Methods* **7,** 535–540 (2010).
19. Clark, D. A., Bursztyn, L., Horowitz, M. A., Schnitzer, M. J. & Clandinin, T. R. Defining the computational structure of the motion detector in *Drosophila*. *Neuron* **70,** 1165–1177 (2011).
20. Egelhaaf, M. & Borst, A. Calcium accumulation in visual interneurons of the fly: Stimulus dependence and relationship to membrane potential. *J. Neurophysiol.* **73,** 2540–2552 (1995).
21. Joesch, M., Plett, J., Borst, A. & Reiff, D. F. Response properties of motion-sensitive visual interneurons in the lobula plate of *Drosophila melanogaster*. *Curr. Biol.* **18,** 368–374 (2008).
22. Schnell, B. *et al.* Processing of horizontal optic flow in three visual interneurons of the *Drosophila* brain. *J. Neurophysiol.* **103,** 1646–1657 (2010).
23. Borst, A. & Egelhaaf, M. Direction selectivity of fly motion-sensitive neurons is computed in a two-stage process. *Proc. Natl Acad. Sci. USA* **87,** 9363–9367 (1990).
24. Single, S., Haag, J. & Borst, A. Dendritic computation of direction selectivity and gain control in visual interneurons. *J. Neurosci.* **17,** 6023–6030 (1997).
25. Eichner, H., Joesch, M., Schnell, B., Reiff, D. F. & Borst, A. Internal structure of the fly elementary motion detector. *Neuron* **70,** 1155–1164 (2011).
26. Joesch, M., Weber, F., Eichner, H. & Borst, A. Functional specialization of parallel motion detection circuits in the fly. *J. Neurosci.* **33,** 902–905 (2013).
27. Egelhaaf, M. & Borst, A. Are there separate ON and OFF channels in fly motion vision? *Vis. Neurosci.* **8,** 151–164 (1992).
28. Takemura, S. Y., Lu, Z. & Meinertzhagen, I. A. Synaptic circuits of the *Drosophila* optic lobe: the input terminals to the medulla. *J. Comp. Neurol.* **509,** 493–513 (2008).
29. Euler, T., Detwiler, P. B. & Denk, W. Directionally selective calcium signals in dendrites of starburst amacrine cells. *Nature* **418,** 845–852 (2002).
30. Pologruto, T. A., Sabatini, B. L. & Svoboda, K. ScanImage: Flexible software for operating laser scanning microscopes. *Biomed. Eng. Online* **2,** 13 (2003).

Supplementary Information is available in the online version of the paper.

Acknowledgements We thank L. Looger, J. Simpson, V. Jayaraman and the Janelia GECI team for making and providing us with the GCaMP5 flies before publication; J. Plett for designing and engineering the LED arena; C. Theile, W. Essbauer and M. Sauter for fly work; and A. Mauss, F. Gabbiani and T. Bonhoeffer for critically reading the manuscript. This work was in part supported by the Deutsche Forschungsgemeinschaft (SFB 870). M.S.M., G.A., E.S., M.M., A.L., A.Ba and A.Bo are members of the Graduate School of Systemic Neurosciences.

Author Contributions M.S.M. and J.H. jointly performed and, together with A.Bo., evaluated all calcium imaging experiments. G.A., E.S. and M.M. recorded from tangential cells. A.L., T.S. and A.Ba. performed the behavioural experiments. G.R., B.D. and A.N. generated the driver lines and characterized their expression pattern. D.F.R. performed preliminary imaging experiments. E.H. helped with programming and developed the PMT shielding for the two-photon microscope. A.Bo. designed the study and wrote the manuscript with the help of all authors.

Author Information Reprints and permissions information is available at www.nature.com/reprints. The authors declare no competing financial interests. Readers are welcome to comment on the online version of the paper. Correspondence and requests for materials should be addressed to A.Bo. (borst@neuro.mpg.de).

METHODS

Flies. Flies were raised on standard cornmeal-agar medium at 25 °C and 60% humidity throughout development on a 12 h light/12 h dark cycle. For calcium imaging, we used the genetically encoded single-wavelength indicator GCaMP5, variant G, with the following mutations: T302L, R303P and D380Y (ref. 2). Expression of GCaMP5 was directed by three different Gal4 lines, all from the Janelia Farm collection[14]. Flies used in calcium imaging experiments (Figs 1–3) had the following genotypes: T4/T5 line (*w*$^-$; +/+; *UAS-GCaMP5,R42F06-GAL4/UAS-GCaMP5,R42F06-GAL4*), T4 line (*w*$^-$; +/+; *UAS-GCaMP5,R54A03-GAL4/UAS-GCaMP5,R54A03-GAL4*), T5 line (*w*$^-$; +/+; *UAS-GCaMP5,R42H07-GAL4/UAS-GCaMP5,R42H07-GAL4*). All driver lines were generated by the methods described in ref. 14 and were identified by screening a database of imaged lines, followed by reimaging of selected lines[31]. As homozygous for both the Gal4-driver and the UAS-GCaMP5 genes, T4 flies also showed some residual expression in T5 cells, and T5 flies also in T4 cells. This unspecific expression, however, was in general less than 25% of the expression in the specific cells. Flies used in electrophysiological and behavioural experiments (Fig. 4) had identical genotypes of the following kind: TNT control flies (*w*$^+$/*w*$^+$; *UAS-TNT-E/UAS-TNT-E*; +/+), T4 control flies (*w*$^+$/*w*$^-$; + /+; *VT37588-GAL4/+*), T5 control flies (*w*$^+$/*w*$^-$; +/+; *R42H07-GAL4/+*), T4-block flies (*w*$^+$/*w*$^-$; *UAS-TNT-E/+*; *VT37588-GAL4/+*), T5-block flies (*w*$^+$/*w*$^-$; *UAS-TNT-E/+*; *R42H07-GAL4/+*). UAS-TNT-E flies were derived from the Bloomington Stock Center (stock no. 28837) and VT37588-Gal4 flies were derived from the VDRC (stock no. 205893). Before electrophysiological experiments, flies were anaesthetized on ice and waxed on a Plexiglas holder using bees wax. The dissection of the fly cuticle and exposure of the lobula plate were performed as described previously (for imaging experiments, see ref. 32; for electrophysiology, see ref. 21). Flies used in behavioural experiments were taken from 18 °C just before the experiment and immediately cold-anaesthetized. The head, the thorax and the wings were glued to a needle using near-ultraviolet bonding glue (Sinfony Opaque Dentin) and strong blue LED light (440 nm, dental curing-light, New Woodpecker).

Two-photon microscopy. We used a custom-built two-photon laser scanning microscope[33] equipped with a ×40 water immersion objective (0.80 NA, IR-Achroplan; Zeiss). Fluorescence was excited by a mode locked Ti:sapphire laser (<100 fs, 80 MHz, 700–1,020 nm; pumped by a 10 W CW laser; both Mai Tai; Spectraphysics) with a DeepSee accessory module attached for dispersion compensation control resulting in better pulse compression and fluorescence at the target sample. Laser power was adjusted to 10–20 mW at the sample, and an excitation wavelength of 910 nm was used. The photomultiplier tube (H10770PB-40, Hamamatsu) was equipped with a dichroic band-pass mirror (520/35, Brightline). Images were acquired at a resolution of 256 × 256 pixels and a frame rate of 1.87 Hz, except in Fig. 2 (7.5 Hz), using the ScanImage software[30].

Electrophysiology. Recordings were established under visual control using a ×40 water immersion objective (LumplanF, Olympus), a Zeiss microscope (Axiotech vario 100, Zeiss), and illumination (100 W fluorescence lamp, hot mirror, neutral density filter OD 0.3; all from Zeiss). To enhance tissue contrast, we used two polarization filters, one located as an excitation filter and the other as an emission filter, with slight deviation on their polarization plane. For eye protection, we additionally used a 420-nm LP filter on the light path.

Behavioural analysis. The locomotion recorder was custom-designed according to ref. 18. Briefly, it consists of an air-suspended sphere floating in a bowl-shaped sphere holder. A high-power infrared LED (800 nm, JET series, 90 mW, Roithner Electronics) is located in the back to illuminate the fly and the sphere surface. Two optical tracking sensors are equipped with lens and aperture systems to focus on the sphere behind the fly. The tracking data are processed at 4 kHz internally, read out via a USB interface and processed by a computer at ≈200 Hz. This allows real-time calculation of the instantaneous rotation axis of the sphere. A third camera (GRAS-20S4M-C, Point Grey Research) is located in the back which is essential for proper positioning of the fly and allows real-time observation and video recording of the fly during experiments.

Visual stimulation. For calcium imaging and electrophysiological experiments, we used a custom-built LED arena that allowed refresh rates of up to 550 Hz and 16 intensity levels. It covered 180° (1.5° resolution) and 90° (1.5° resolution) of the visual field along the horizontal and the vertical axis, respectively. The LED arena was engineered and modified based upon ref. 34. The LED array consists of 7 × 4 individual TA08-81GWA dot-matrix displays (Kingbright), each harbouring 8 × 8 individual green (568 nm) LEDs. Each dot-matrix display is controlled by an ATmega168 microcontroller (Atmel) combined with a ULN2804 line driver (Toshiba America) acting as a current sink. All panels are in turn controlled via an I2C interface by an ATmega128 (Atmel)-based main controller board, which reads in pattern information from a compact flash (CF) memory card. Matlab was used for programming and generation of the patterns as well as for sending the serial command sequences via RS-232 to the main controller board. The luminance range of the stimuli was 0.5–33 cd m^{-2}. For the calcium imaging experiments, two separate barriers were used to shield the photomultipliers from the stimulus light coming from the LED arena. The first was a spectral filter with transparency to wavelengths >540 nm placed directly over the LEDs (ASF SFG 10, Microchemicals). The second was a layer of black PVC extending from the fly holder over the arena. Square wave gratings had a spatial wavelength of 30° of visual angle and a contrast of 88%. Unless otherwise stated, they were moving at 30° s^{-1}. Edges had the same contrast and were also moving at 30° s^{-1}. For the experiments shown in Figs 1, 2b and 3, each grating or edge motion was shown twice within a single sweep, resulting in a total of eight stimulation periods. Each stimulus period lasted 4 s, and subsequent stimuli were preceded by a 3-s pause. In the experiment shown in Fig. 2a, a dark edge of 88% contrast was moved for 1 s at 15° s^{-1} from the front to the back at three different positions (22°, 44°, 66°, from frontal to lateral). At each position, edge motion was repeated 15 times. For the experiment shown in Fig. 2b, a bright edge of 88% contrast was moving at 15° s^{-1} from the back to the front, and images were acquired at a frame rate of 7.5 Hz. For the experiments shown in Figs 3e, f, all six stimulus velocities were presented once within one sweep, with the stimulus lasting 4 s, and different stimuli being separated by 2 s. In the experiments shown in Figs 3g, h, a single sweep contained all 12 grating orientations with the same stimulus and pause length as above. For the electrophysiology experiments (Fig. 4a–f), multiple edges were used as stimuli moving simultaneously at 50° s^{-1}. To stimulate cells of horizontal system (HS cells), a vertical, stationary square-wave grating with 45° spatial wavelength was presented. For ON-edge motion, the right (preferred direction, PD) or the left edge (null direction, ND) of each light bar started moving until it merged with the neighbouring bar. For OFF-edge motion, the right or the left edge of each dark bar was moving. To stimulate cells of the vertical system (VS cells), the pattern was rotated by 90° clockwise. For the behavioural experiments (Fig. 4g–i), three 120-Hz LCD screens (Samsung 2233 RZ) were vertically arranged to form a U-shaped visual arena (w = 31 cm × d = 31 cm × h = 47 cm) with the fly in the centre. The luminance ranged from 0 to 131 cd m^{-2} and covered large parts of the flies' visual field (horizontal, ±135°; vertical, ±57°; resolution, <0.1°). The three LCD screens were controlled via NVIDIA 3D Vision Surround Technology on Windows 7 64-bit allowing a synchronized update of the screens at 120 frames per second. Visual stimuli were created using Panda3D, an open-source gaming engine, and Python 2.7, which simultaneously controlled the frame rendering in Panda3D, read out the tracking data and temperature and streamed data to the hard disk. The balanced motion stimulus consisted of a square-wave grating with 45° spatial wavelength and a contrast of 63%. Upon stimulation onset, dark and bright edges moved into opposite directions at 10° s^{-1} for 2.25 s. This stimulation was performed for both possible edge directions and two initial grating positions shifted by half a wavelength, yielding a total of four stimulus conditions.

Data evaluation. Data were evaluated off-line using custom-written software (Matlab and IDL). For the images shown in Figs 1e, f, 2a and 3a, b, the raw image series was converted into four images representing the relative fluorescence change during each direction of grating motion: $(\Delta F/F)_{stim} = (F_{stim} - F_{ref})/F_{ref}$. The image representing the stimulus fluorescence (F_{stim}) was obtained by averaging all images during stimulation; the image representing the reference fluorescence (F_{ref}) was obtained by averaging three images before stimulation. Both images were smoothed using a Gaussian filter of 10 pixel half-width. For the images shown in Figs 1f and 3a, b, $\Delta F/F$ images were normalized by their maximum value. Then, a particular colour was assigned to each pixel according to the stimulus direction during which it reached maximum value, provided it passed a threshold of 25%. Otherwise, it was assigned to background. The response strength of each pixel was coded as the saturation of that particular colour. For the data shown in Figs 2b, c and 3c–h, the raw image series was first converted into a $\Delta F/F$ series by using the first three images as reference. Then, a region was defined within a raw image, and average $\Delta F/F$ values were determined within that region for each image, resulting in a $\Delta F/F$ signal over time. Responses were defined as the maximum $\Delta F/F$ value reached during each stimulus presentation minus the average $\Delta F/F$ value during the two images preceding the stimulus. For the bar graphs shown in Fig. 4c, f, the average voltage responses during edge motion (0.45 s) along the cell's preferred (PD) and null direction (ND) were calculated. For each recorded tangential cell, the difference between the PD and the ND response was determined, and these values were averaged across all recorded cells. The data shown in Fig. 4g, h were obtained from the four stimulus conditions by averaging the turning responses for the two starting positions of the grating and calculating the mean difference between the turning responses for the two edge directions. For the bar graph shown in Fig. 4i, the average turning response of each fly during the last second of balanced motion stimulation was calculated. These values were averaged across all recorded flies within each genotype.

31. Jenett, A. *et al.* A Gal4-driver line resource for *Drosophila* neurobiology. *Cell Rep.* **2,** 991–1001 (2012).
32. Reiff, D. F., Plett, J., Mank, M., Griesbeck, O. & Borst, A. Visualizing retinotopic half-wave rectified input to the motion detection circuitry of *Drosophila. Nature Neurosci.* **13,** 973–978 (2010).
33. Euler, T. *et al.* Eyecup scope—optical recording of light stimulus-evoked fluorescence signals in the retina. *Pfluger Arch.* **457,** 1393–1414 (2009).
34. Reiser, M. B. & Dickinson, M. H. A modular display system for insect behavioral neuroscience. *J. Neurosci. Methods* **167,** 127–139 (2008).

SUPPLEMENTARY INFORMATION

doi:10.1038/nature12320

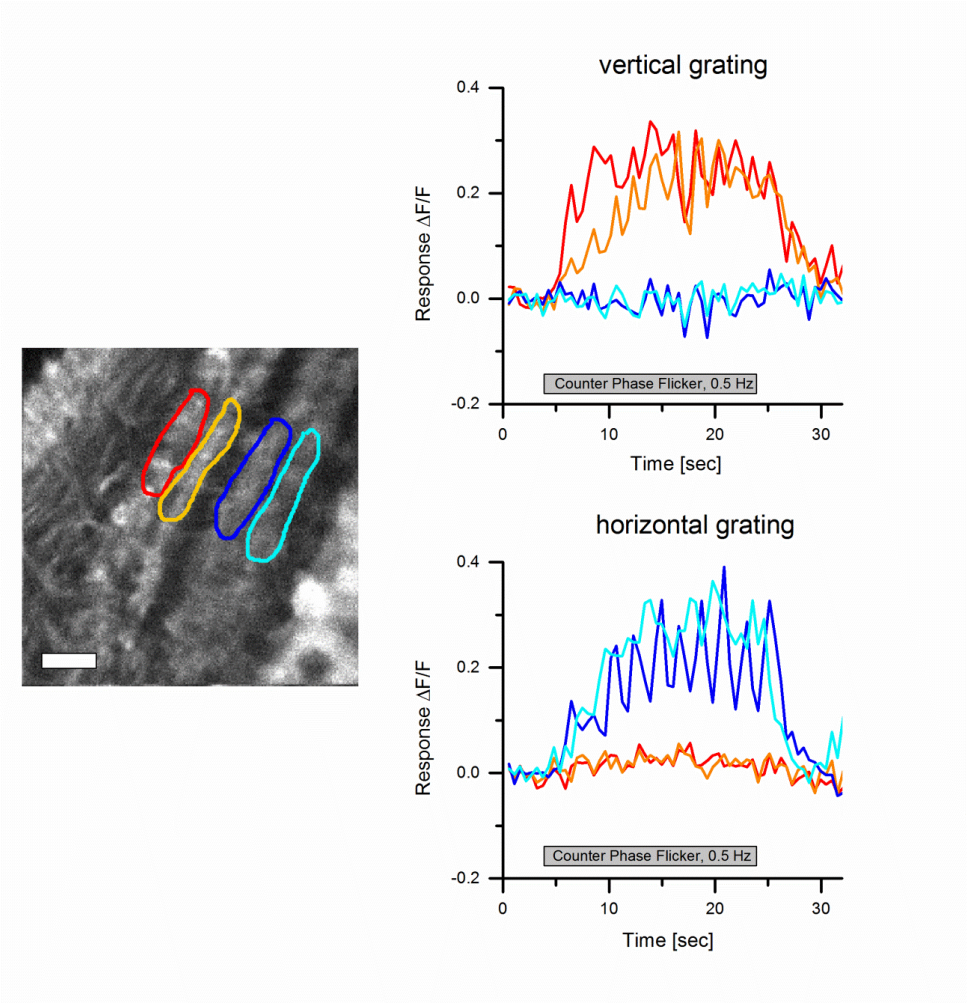

Supplemental Fig.1 Responses of T4 and T5 cells to counter-phase flicker. Square-wave gratings (15 deg spatial wavelength and 88% contrast) with vertical (top) and horizontal (bottom) orientation were phase-shifted every second by 180 deg for 20 seconds. Response traces are derived from the region of interest encircled in the image to the left with the same color from a single stimulation period. T4 and T5 cells in layers 1 and 2 only respond to the vertical grating, cells in layers 3 and 4 selectively respond to the horizontal grating. Similar results were obtained in n=4 flies. Scale bar = 5 μm. Together with the missing response of T4 and T5 cells to full-field flicker, these findings suggest that T4 and T5 cells receive input signals from neurons with different orientation tuning , depending on whether they respond to motion along the horizontal (layers 1 and 2) or the vertical (layers 3 and 4) axis [1,2].

1 Pick, B. & Buchner, E. Visual movement detection under light- and dark-adaptation in the fly, *Musca domestica*. *J. Comp. Physiol.* **134**, 45-54 (1979).
2 Srinivasan, M.V. & Dvorak, D.R. Spatial processing of visual information in the movement-detecting pathway of the fly. *J. Comp. Physiol.* **140**, 1-23 (1980).

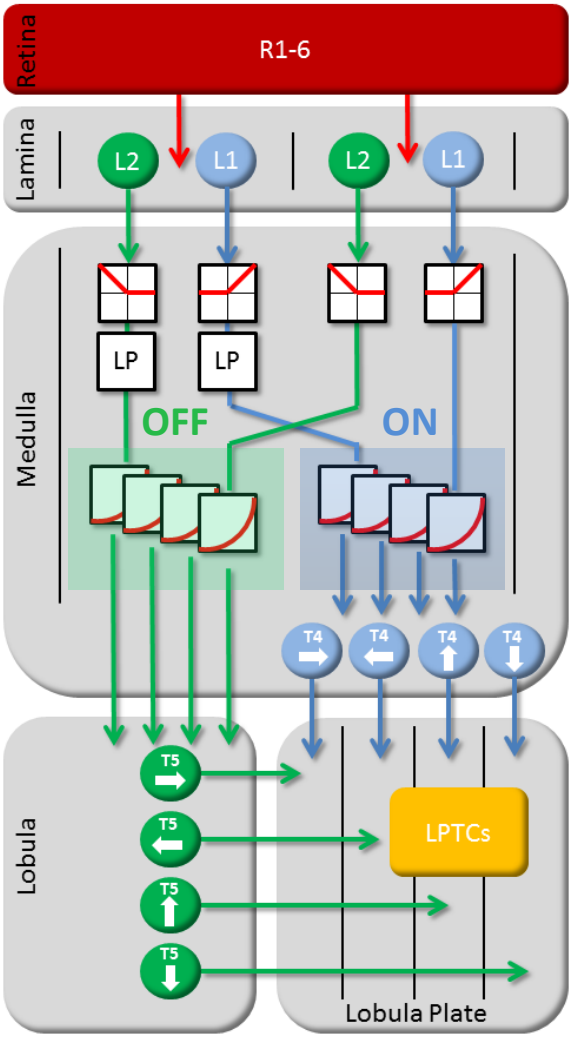

Supplemental Fig.2 Circuit diagram of the fly elementary motion detector. Visual input from photoreceptors R1-6 is split into parallel pathways, L1 and L2, at the level of the lamina. Two neighboring columns are shown. The outputs from both L1 and L2 are half-wave rectified, such that downstream elements carry information about ON (L1-pathway) and OFF (L2-pathway) signals separately. After temporal low-pass filtering ('LP') the signals from one column, they interact in a supra-linear way with the instantaneous signals derived from the other column. This interaction takes place, separately in both pathways, along all four cardinal directions. Directionally selective signals are carried via T4 and T5 cells to the four layers of the lobula plate where T4 and T5 cells with the same preferred direction converge again on the dendrites of the tangential cells ('LPTCs').

4 PAPER III: BIO-INSPIRED VISUAL EGO-ROTATION SENSOR FOR MAVS

This paper describes the design and function of a lobula plate-inspired microcircuit for motion sensing and was published in the Journal of Biological Cybernetics in January 2012[1].

Summary

VS-cells in the lobula plate of the fly are tuned to specific optic flow fields corresponding to rotations along different body axes and it is thought that the fly uses this information to stabilize its orientation during flight. Much is known about how such optic flow fields arise from local motion detection and spatial integration. In this work, a FPGA-based microchip simulated an artificial lobula plate network. The system was equipped with a camera and a spherical fisheye lens and tested in a virtual environment with several natural images rotating along different axes. The fly-inspired electrical microcircuit provided reliable vision-based predictions of the axis of rotation and could be well-suited to stabilize the orientation of a micro aerial vehicle (MAV).

The following authors contributed to this work:

Author contributions

Johannes Plett, **Armin Bahl**[*], Martin Buss, Kolja Kühnlenz, Alexander Borst. — J.P. and A.Bo. designed the study. M.B., K.H. and A.Bo. supervised the study. J.P. did all microchip engineering, programming and data analysis. **A.Ba.**[*] built the virtual environment setup and programmed the visual stimuli. J.P. and A.Bo. wrote the paper with help of the other authors.

1 Biological Cybernetics January 2012, Volume 106, Issue 1, pp 51-63, doi:10.1007/s00422-012-0478-6

Biol Cybern (2012) 106:51–63
DOI 10.1007/s00422-012-0478-6

ORIGINAL PAPER

Biological Cybernetics

Bio-inspired visual ego-rotation sensor for MAVs

Johannes Plett · Armin Bahl · Martin Buss · Kolja Kühnlenz · Alexander Borst

Received: 27 July 2011 / Accepted: 31 January 2012 / Published online: 14 February 2012

Abstract Flies are capable of extraordinary flight maneuvers at very high speeds largely due to their highly elaborate visual system. In this work we present a fly-inspired FPGA based sensor system able to visually sense rotations around different body axes, for use on board micro aerial vehicles (MAVs). Rotation sensing is performed analogously to the fly's VS cell network using zero-crossing detection. An additional key feature of our system is the ease of adding new functionalities akin to the different tasks attributed to the fly's lobula plate tangential cell network, such as object avoidance or collision detection. Our implementation consists of a modified eneo SC-MVC01 SmartCam module and a custom built circuit board, weighing less than 200 g and consuming less than 4 W while featuring 57,600 individual two-dimensional elementary motion detectors, a 185° field of view and a frame rate of 350 frames per second. This makes our sensor system compact in terms of size, weight and power requirements for easy incorporation into MAV platforms, while autonomously performing all sensing and processing on-board and in real time.

Keywords Reichardt Detector · Rotation estimation · Motion detection · MAV · Fly vision · Biorobotics

J. Plett ( ) · A. Bahl · A. Borst
Department of Systems and Computational Neurobiology, Max Planck Institute of Neurobiology, 82152 Martinsried, Germany
e-mail: jplett@neuro.mpg.de

M. Buss · K. Kühnlenz
Institute of Automatic Control Engineering (LSR), Technische Universität München (TUM), 80290 Munich, Germany

1 Introduction

Perception of visual motion has been an intense and fruitful field of research over many decades. Especially studies of insects—and flies in particular—have revealed astoundingly simple, yet robust and elegant solutions of extracting motion information from noisy and complex environments. Flies are able to autonomously navigate at very high speeds through highly unstructured settings, by and large relying only on visual cues. Despite having only a few 100,000 neurons, they are able to achieve these feats because of the highly optimized way these neurons are interconnected and the ideally suited basic operation principles of motion vision. Flies extract cues about motion relative to the environment from the *optic flow* at remarkably high temporal resolution. The true optic flow is the velocity field of the projection of the relative motion between observer and visual surroundings onto the retina. Given that this true optic flow is not directly measurable it is estimated from spatiotemporal luminance patterns on the retina by dedicated neuronal circuits. Since these dedicated circuits are very effective, robust, and efficient in terms of implementation they lend themselves well for technical applications.

In recent years, unmanned aerial vehicles (UAVs) and micro aerial vehicles (MAVs) have become more and more common in tasks, such as aerial reconnaissance, surveillance, and exploration. To cope with the rising complexity of these challenges increasing levels of automation are needed. This usually leads to larger and computationally more intense solutions which require large on-board processing units (e.g., Franceschini et al. 1992) somewhat limiting their use on board small flying vehicles. One solution to this problem is "out-sourcing" of computational load to off-board computing platforms (e.g., Bermudez i Badia et al. 2007; Kendoul et al. 2009; Zhang et al. 2008). This, however, is often not

possible due to inadequacies of wireless transmission, such as low throughput, large delays, jitter, temporary loss of signal, etc. A promising way of solving these issues is the onboard use of highly efficient algorithms, such as those found in biological vision systems. In fact, over the past decades the insect visual system has inspired many studies towards visually guided autonomous vehicles. Much emphasis has been put on the implementation of collision avoidance strategies (e.g., Harrison 2005; Bermudez i Badia et al. 2007) and local navigation (e.g., Zufferey and Floreano 2006; Srinivasan et al. 2009; Conroy et al. 2009; Moeckel and Liu 2009; Beyeler et al. 2009; Hyslop et al. 2010). Moreover, considerable work has been put forth on autonomous height control (e.g., Netter and Franceschini 2002; Valette et al. 2010).

One aspect of fly motion vision that has received relatively little attention in technical implementations is rotation sensing. There have been studies on basic motion detection circuits for rotation detection (O'Carroll et al. 2006; Aubepart et al. 2004), but despite considerable advances in understanding of the fly neuronal rotation sensing circuitry (Krapp et al. 1998; Borst et al. 2010; Cuntz et al. 2007) there have been few biologically realistic practical applications involving these findings. O'Carroll et al. (2006) have put forth a rotation sensor using a custom aVLSI chip that relies on basic motion detection circuitry for a one-dimensional circular array of 40 input photodiodes. Aubepart et al. (2004) used a Field Programmable Gate Array (FPGA) based solution with a linear 12-photodiode array, theoretically capable of handling up to 245 input elements. Köhler et al. (2009) proposed a solution of higher spatial resolution at 120×100 input pixels over a 40° horizontal field of view and a temporal resolution of 100 frames per second (fps), expandable up to 200 fps in bright outdoor conditions. But despite promising results in artificially structured environments, the system did not work in naturalistic settings. A similarly oriented approach was used by Zhang et al. (2008). They successfully implemented 256×256 motion detection circuits operating at 350 fps and six motion templates for template matching based motion detection. However, their system architecture residing on a PCI-FPGA card in a host PC forfeits use on board small aerial vehicles. Also, to the authors' best knowledge there is currently no commercially available visual ego-rotation sensor for this specific purpose.

In this study we set out to implement a small and lightweight fly-inspired visual rotation sensor for MAVs, keeping algorithmically as close as possible to the biological model while maintaining similar spatial and temporal resolution over a similar field of view.

2 Fly motion vision

The fly motion vision system can be segmented into several distinct functional and anatomical units. The input layer is the compound eye, which consists of a hexagonal array of several hundreds to thousands of *ommatidia*, each harboring a lenslet and a set of photoreceptor cells. This stage constitutes the retina, from where information is passed retinotopically on to three successive neuropiles, the lamina, medulla, and lobula complex. In the medulla, local motion estimates are computed according to the detector model put forward by Hassenstein and Reichardt (1956), commonly known as the Reichardt Detector or elementary motion detector (EMD). As depicted in Fig. 1a, the simplest form of the Reichardt Detector consists of two mirror-symmetric subunits, each correlating two spatially adjacent input signals with each other by multiplying one input signal with a temporally low-pass filtered version of the other. The output of both subunits is then subtracted, yielding a direction-selective output while suppressing non-motion artifacts. This way of estimating motion is particularly well suited for applications in presence of noise, i.e., with poor signal to noise ratio (Potters and Bialek 1994; Borst 2007). However, it is not a perfect velocity estimator as it depends not only on velocity but also on local texture and contrast (Reichardt and Egelhaaf 1988; Egelhaaf et al. 1989). Furthermore, individual local motion estimators suffer from the *aperture problem* due to their limited field of view (Stumpf 1911).

To circumvent these problems flies spatially integrate local motion estimates over larger areas, thus to a large extent averaging out the aforementioned effects (Single and Borst 1988). This is done in the lobula plate by large interneurons called lobula plate tangential cells (LPTCs). These neurons form an ensemble of roughly 60 uniquely identifiable cells, out of which two prominent groups—the vertical system (VS) and horizontal system (HS) cells—are preferentially sensitive to vertical and horizontal motion, respectively. Per hemisphere, the blowfly *Calliphora erythrocephala* possesses ten VS cells VS 1 through VS 10, whose dendritic receptive fields sequentially cover narrow but overlapping vertical stripes of the visual field, going around the dorsoventral axis from frontal (VS 1) to caudal (VS 10). Each VS cell integrates the responses from local vertical motion detectors within its own specific receptive field. Strikingly, the response of VS cells in their axon terminal regions suggest much broader receptive fields (Elyada et al. 2009). This broadening of the axon terminal response has been shown to be caused by gap junctions interconnecting the VS cells (Haag and Borst 2004, 2005; Farrow et al. 2005). Furthermore, VS 1 and VS 10 cells mutually inhibit each other (Haag and Borst 2004, 2007). This gives rise to the VS cell network illustrated in Fig. 2a with its associated connection strength matrix given in Fig. 2b. The reason for this network scheme is thought to be strengthening of robustness to inhomogeneities of pattern contrast, i.e., making this system more suitable for use in naturalistic environments (Cuntz et al. 2007; Elyada et al. 2009; Wertz et al. 2009). We note that the model

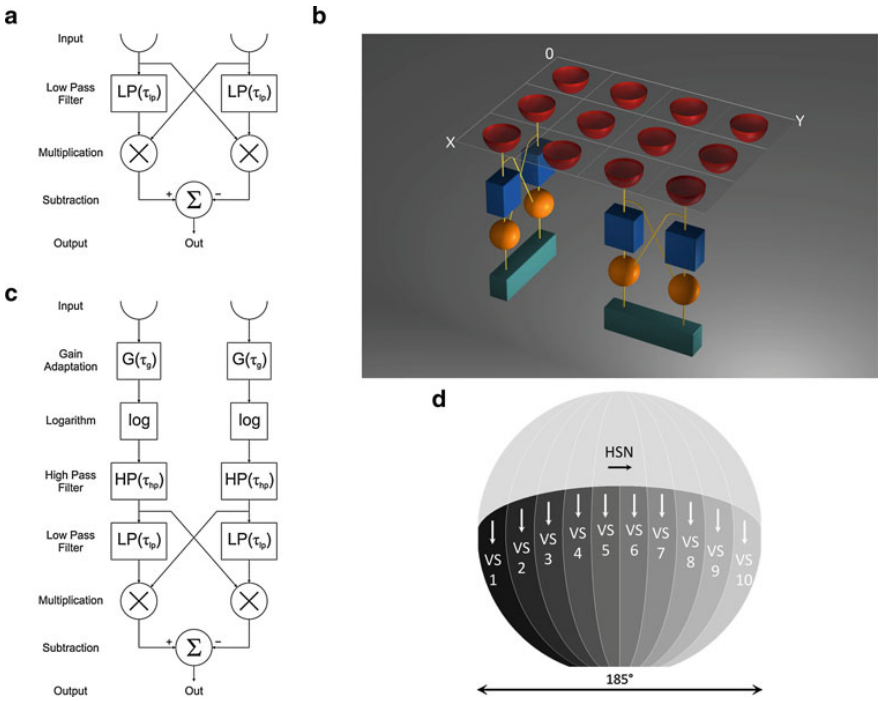

Fig. 1 **a** Basic Reichardt Detector consisting of two mirror-symmetric units, each correlating one input with a low-pass filtered version of the other. Final subtraction of both sub-unit outputs yields a directionally selective signal depending on stimulus velocity and direction. **b** Two-dimensional arrangement of Reichardt Detectors giving rise to 2D local motion estimates by estimating vertical and horizontal components of local motion. **c** Elaborated Reichardt Detector including automatic gain adaptation and a homomorphic filtering stage sequentially connected giving input to a basic Reichardt Detector. **d** VS and HSN cell dendritic field distribution over the half sphere captured by the 185° fisheye lens showing direction of motion sensitivity of each cell

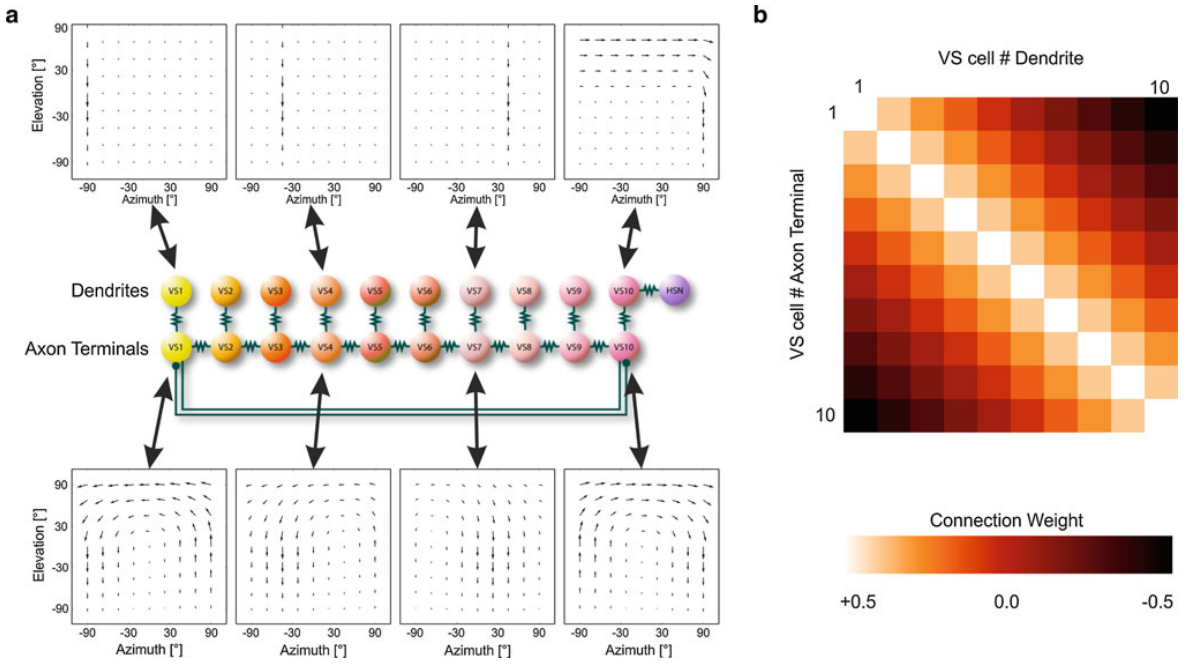

Fig. 2 VS cell network coupling. **a** VS cell network showing coupling between adjacent cells in their axon terminal regions, including bi-directional mutual inhibition between VS 1 and VS 10. HSN and VS 10 are connected directly in the dendritic regions. Ideal receptive fields of individual cells are shown for both the dendritic and the axon terminal regions. Whereas receptive fields in the dendritic regions exhibit but one narrow vertical stripe, the receptive fields in the axon terminals regions resemble matched filters for rotations around different axes along the equator. **b** Connection strength matrix for network coupling. The axon terminal output of a cell is exited strongly by its own dendritic input, slightly less by its immediate neighbors, little by more distal cells and even inhibited by most distal cells

analyzed here additionally includes the effect of the HSN cell on the dendritic compartment of VS 10, thereby accounting for reported responses to dorsal horizontal motion (Krapp et al. 1998; Haag and Borst 2003, 2007).

As proposed by Cuntz et al. (2007) the responses of the VS cell network in its axonally coupled form can be used to robustly infer the approximate center of rotation for rotations around axes lying on the equatorial plane. Due to their vertical directional sensitivity, the VS cells on one side of the center of rotation will respond by hyperpolarizing, while to the other side they will depolarize. The location where VS cell responses change signs, i.e., the *zero-crossing* location, indicates the approximate location of the center of rotation.

3 System design

3.1 Requirements and restrictions

The goal of this study was the construction of an optic flow based sensor system that is algorithmically as close as possible to the biological original of the fly visual system, in particular the VS cell network. Therefore the design requirements included similar spatiotemporal resolution and field of view (FOV) compared to a fly, as well as reasonable light weight, low power consumption, and compact size.

The blowfly *Calliphora* is able to detect flicker up to rates between 200 and 300 Hz (Autrum 1952) or even higher (Tatler et al. 2000). Thus, the design goal was set to achieve frame rates well above 300 fps, exceeding cutoff frequencies of 150 Hz. Each compound eye of *Calliphora* extends about 190° in the horizontal and 198° in the vertical plane (Seitz 1968). To achieve a large FOV the camera system was equipped with a fisheye lens covering a solid angle of approximately 2π sr, i.e., half of the unit sphere. The highest spatial resolution found in *Calliphora* amounts to inter-ommatidial angles of $\Delta\varphi = 1.07°$ (Land and Eckert 1985) and is reached in the frontal visual field (Petrowitz et al. 2000). Thus, to obtain a spatial resolution better than 1° per pixel in the frontal part while using a 185° fisheye lens the sensor system had to have a resolution of at least 185 × 185 pixels. Commonly found MAVs are able to carry payloads only up to a few hundred grams. The envisaged primary test platform for this sensor system, the AscTec Hummingbird quadrocopter (Ascending Technologies, Krailling, Germany), features a payload of up to 200 g. Hence, the weight restrictions of the sensor system were fixed to an upper limit of 200 g. Due to these weight restrictions, battery power on board is limited. We specified power consumption restrictions to a maximum of 4 W. In terms of size the system was required to be able to be mounted on such an MAV without interfering much with its aerodynamics.

3.2 Computations

The computation of rotational axis and velocity estimates was divided into the following five pipelined sequential steps:

Image acquisition is done by the image sensor in a row-wise fashion pixel by pixel at full frame rate,
Pre-processing suppresses illumination artifacts by automatic gain adaptation and homomorphic filtering,
Local motion detection is performed using a Reichardt Detector correlation model,
Global motion integration is achieved by wide-field integration of local motion estimates,
Rotation estimation is accomplished by calculating location and slope of the VS cell network zero-crossing.

The individual processing steps are described in more detail in the following sections.

3.2.1 Pre-processing

At the core of this sensor design lies the aforementioned Reichardt Detector or EMD. An EMD inherently displays a quadratic dependence on image contrast which makes it also sensitive to changes in overall lighting. To improve robustness against lighting changes a homomorphic filtering approach (Gonzalez and Woods 2007) was applied as a pre-processing stage to the EMD. In a visual scene, illumination and reflectance combine multiplicatively and are therefore not linearly separable. Nevertheless, they usually occupy distinct regions in the frequency domain since illumination tends to vary slowly in time and space while reflectance provides mostly high temporal frequency components due to reflections from objects. For a given pixel in an image its value is given by

$$I(x, y, t) = L(x, y, t) \cdot R(x, y, t) \tag{1}$$

where $I(x, y, t)$ represents the value of the pixel at location (x, y) at time point t, while $L(x, y, t)$ and $R(x, y, t)$ represent illumination and reflectance for that location and time point. By taking the logarithm of the pixel value these two components become additive (Eq. 2) and the low frequency illumination components can be filtered out using a high-pass filter, leaving only reflectance (Eq. 3).

$$\log\left(I(x, y, t)\right) = \log\left(L(x, y, t)\right) + \log\left(R(x, y, t)\right) \tag{2}$$

$$\mathrm{HP}\left(\log\left(I(x, y, t)\right)\right) \approx \log\left(R(x, y, t)\right) \tag{3}$$

Using this homomorphic filtering technique the elaborated Reichardt Detector used for final implementation effectively included a logarithmic stage via lookup table and a first-order

temporal high-pass filter acting together as an input stage to a basic EMD (Fig. 1c).

To further optimize the dynamic range of the image sensor pixel values over a large illumination range an automatic camera gain adaptation control was implemented. The temporally low-pass filtered mean pixel values of each frame ($\tau_g = 1s$) were utilized as a crude measure for overall illumination. A simple proportional controller was used to adjust the internal camera gain as to keep the mean pixel values reasonably centered within the sensor coding range.

3.2.2 Local and global motion detection

For local motion detection of each pixel the elementary Reichardt Detector of Fig. 1a was used in conjunction with a homomorphic pre-processing stage, constituting the elaborated EMD (Fig. 1c). Each incoming pixel value is thusly correlated with its immediate horizontal and vertical neighbor, giving rise to a two-dimensional local motion estimate (Fig. 1b).

For wide field integration of these local motion estimates a network akin to the Calliphora VS cell network was established. For all ten VS cell homologues the vertical components of local motion estimates within their respective receptive fields are linearly summed up. For the three HS cell homologues this was done for the respective horizontal components. The ten VS cells' receptive fields are linearly spaced along the equator, each covering a tenth of the fisheye lens projection on the image plane, ranging from VS 1 on the far left up to VS 10 on the far right (Fig. 1d). Similarly, the HSN receptive field covers the upper third of the lens projection (Fig. 1d), the HSE receptive field the middle third and the HSS receptive field the lower third. The HSE and HSS cells, however, were not used for rotation sensing and therefore included for future extensions only.

To improve robustness as in the biological original (Cuntz et al. 2007) the cells in the network were interconnected as outlined in Fig. 2. In this wiring scheme adjacent cells are strongly coupled while most distant cells are mutually inhibitory, as indicated by the connection matrix of Fig. 2b. This yielded a robust and symmetrical response pattern of the network.

3.2.3 Rotation estimation

Estimation of the axis of rotation based on the VS cell output relies on the fact that VS cells' receptive fields resemble matched filters for rotations around rotations sequentially arranged around the dorso-ventral axis on the equatorial plane (Krapp et al. 1998). As introduced in Sect. 2, by calculating the zero-crossing location of the VS cell network responses the center of rotation can be inferred. Furthermore, at that location the slope of the curve is strongly correlated with the rate and direction of rotation. If the curve has a positive slope going from a negative VS 1 response to a positive VS 10 response the rotation of the visual scene is clockwise. Accordingly, a negative slope indicates a counter-clockwise rotation. Also, a fast rotation would produce a steep slope, whereas slower rotations would yield a more shallow slope. Hence, this slope magnitude correlates directly with the rate of rotation, albeit in a nonlinear bell-shaped fashion.

3.3 Implementation

3.3.1 Components overview

The key challenges of the implementation of this sensor system were the high computation rate and small footprint required. For the computing platform the typical choices were off-board computation on a PC or on-board computation using microcontrollers, microprocessors, programmable logic, or fully custom designed chips. For the off-board computation the images would have to be first sent from the MAV to the PC, which with the current wireless transmission standards, such as WLAN, ZigBee, or Bluetooth is not yet possible at frame rates much higher than around 100 fps. Therefore, the choices were limited to on-board solutions, of which due to the high throughput requirements and size/weight constraints microcontrollers and sequential general purpose microprocessors were ruled out. Fully custom designed Application Specific Integrated Circuits (ASICs) were not an option due to their high cost and time consuming design cycles. Since optic flow calculations are highly parallel FPGAs were the ideal choice owing to their inherently parallel and pipelineable nature, thus permitting high throughputs.

As the core image capture and processing unit an eneo SmartCam SC-MVC01 module (Videor, Rödermark, Germany) was chosen, being able to provide a spatial resolution of 640 × 240 pixels at 370 fps and 8 bit resolution in row interlaced mode. It features a 1/2 inch Micron MT9V403 CMOS image sensor, an Intel XScale PXA255 processor running at 400 MHz, a Xilinx Spartan-3 series XC3S1000 FPGA and an Infineon HYB25L256160AF 256 Mbit Mobile-RAM module accessible freely from the FPGA. Using a 185° DSL215B-NIR miniature fisheye lens (Sunex, Carlsbad, USA) and a custom built light weight camera backplane the camera possessed a 72 mm × 45 mm × 45 mm footprint weighing 148 g. Additional processing was carried out on an Atmel AT91SAM7A3 ARM processor (Atmel, San Jose, USA) on a custom designed printed circuit board (PCB) also housing power conversion circuitry and communication interfaces. Overall hardware costs amounted to approximately 2,000.

In order to monitor the outcome of the optic flow calculation, ego motion estimation, and the captured camera images,

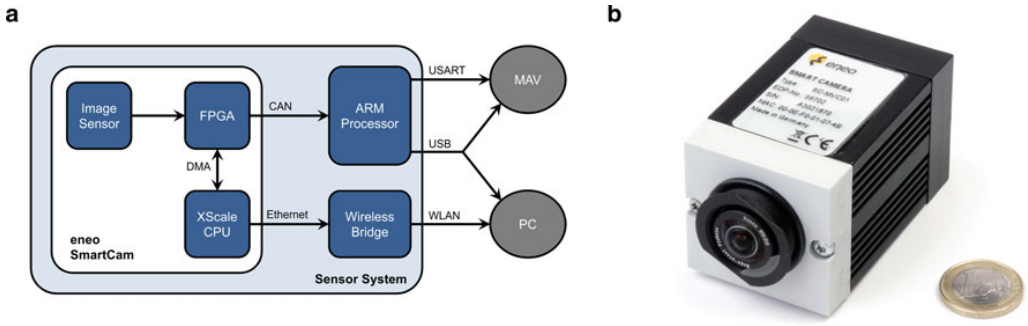

Fig. 3 **a** General system architecture. At the system core lies an eneo SmartCam with its embedded FPGA and XScale processor, weighing 148 g including the fisheye lens and consuming 1.69 W. Further processing and communication with the MAV and an optional real-time data acquisition PC is carried out using an ARM processor hosted on a custom PCB weighing 30 g and consuming 0.51 W. For wireless transmission of live images and processed data towards the PC ground station the eneo SmartCam Ethernet port is used via a wireless bridge weighing 15 g and consuming 1.47 W. Total system weight was 193 g while consuming a total of 3.67 W. **b** eneo SmartCam including 185° fisheye lens in size comparison with a 1 coin

a wireless communication system was used to communicate with an external laptop PC (Dell, Round Rock, USA) hosting a control and monitoring interface. A general schematic of the system hardware architecture is given in Fig. 3.

3.3.2 FPGA design

Pre-processing, computation of the local motion estimates, and subsequent spatial integration was implemented on board the Xilinx Spartan-3 FPGA using VHDL. The internal design was broken down into several modules dealing with specific tasks, such as image data acquisition from the image sensor, local motion estimation, external SDRAM communication and management, large field integration of local motion estimates, internal timing management, communication with the off-board ARM processor and monitoring PC, etc.

The fisheye lens projects a centered circular image onto the imager's row interlaced 640×240 pixels, but only the central 240×240 pixels were used. To estimate local motion, each pixel was correlated with the adjacent left and upper pixel, using the elaborated EMD, resulting in a two-dimensional local motion vector for each pixel. The distance between EMD input arms $\Delta\varphi$—equivalent to the fly's inter-ommatidial angle—is thus equal to 1 pixel, which in the frontal part of the the FOV equates to $\Delta\varphi = \frac{185°}{240} = 0.77°$.

Taking advantage of an FPGAs inherent parallel capabilities, the local motion estimate computation was implemented in a pipelined fashion, thus, reducing the elaborated EMD to 15 atomic instructions (such as memory fetch, table look up, multiplication, sum, and subtraction operations), each being executed in strictly less than 20 ns. For multiplication, dedicated hardware multipliers of the Spartan-3 series were used. EMD computations were carried out at 18 bit Q10.7 fixed point precision, thereby accounting for fractional results ensuring minimal loss of precision through truncation.

The elaborated EMD incorporates temporal low-pass and high-pass filters whose immediate results need to be stored between image cycles, yielding an amount of data of over four times the total internal Block RAM storage capacity of the Spartan-3 XC3S1000. Therefore, the external SDRAM attached to the FPGA needed to be used to store and retrieve inter-frame filter data. An SDRAM controller module loosely based on application notes by XILINX (1999, 2003) was implemented, operating in half-duplex mode at 100 MHz and a 16 bit data bus width.

A wide field integration module was written to calculate the dendritic part of the VS cell network output from the local motion estimates via Boolean map lookup, yielding one scalar value for each VS and HS cell.

Also a communication module was implemented for relaying the resulting wide field integration data at full frame rate towards the external ARM processor. The SmartCam hardware was modified in a way that its High Speed CAN bus output could be used directly by the FPGA. For establishing the communication with the ARM processor a custom CAN bus controller FPGA core operating at 1 Mbit/s was written. The communications module also handles data transfers from and towards the SmartCam internal Intel XScale processor via the shared 64 MByte SDRAM memory between FPGA and XScale processor using Direct Memory Access (DMA).

Using a speed optimized XST synthesizer the complete design occupied 47% of available slice flip flops, 69% of all 4-input look up tables (LUTs) and 83% of available block RAM of the Spartan-3 XC3S1000.

3.3.3 XScale firmware

The internal Intel XScale processor of the SmartCam module controls several variables and parameters of the image sensor, such as operation modes, buffer sizes, and frame rate. These

parameters along with incoming image data are transferred via DMA through the shared SDRAM memory. For communication towards an external PC the SmartCam features a 10/100 Mbit/s Ethernet MAC/PHY directly connected to the processor. Its operating system is an embedded Linux Kernel 2.6.6 for which a resident camera daemon application was written in C++ that takes care of initialization routines, handshaking protocols, and communication between XScale processor and FPGA as well as between XScale processor and the ground station PC. To communicate wirelessly between camera system and ground station PC the internal PCB of an Asus WL-330gE wireless bridge (Asus, Taipei, Taiwan) was used. One transmitted data frame consists of an image, local motion estimates, and the associated wide field integration results.

3.3.4 ARM firmware

For further processing of the raw wide field integration data computed on board of the FPGA the XScale processor was unsuitable because of the lack of interfaces towards the MAV and the difficulty of allotting well-defined time slots for real-time processing. Therefore, a custom 60 mm × 60 mm PCB featuring an AT91SAM7A3 ARM processor and interface logic has been developed. Its primary objective is the extraction of axis of rotation and rotation rate from the raw wide field integration data, calculated on the FPGA and transmitted towards the ARM processor via CAN bus at full frame rate in simplex mode. As shown by Cuntz et al. (2007) during rotations the fly's VS cell network and its lateral axo-axonal gap junction couplings provide a robust way of encoding the axis of rotation. This *zero-crossing* strategy was implemented on the ARM processor. The axon terminal output of each VS cell was calculated as the weighted sum of the incoming dendritic VS cell data according to the matrix and connection diagram given in Fig. 2. As dendritic VS 10 input into the network the simple sum of pure dendritic VS 10 and HSN values was used. Subsequently the axis of rotation is obtained by determining the zero-crossing location of the resulting ten axon terminal VS cell values. For a crude estimate of the rate and direction of rotation the slope at the zero-crossing location is calculated. Both rotation axis and rate are then further transmitted at full frame rate towards the MAVs flight controller via USART. A USB 2.0 link was also implemented for data transmission towards the MAV or an external PC, e.g., for data logging.

Thus, the interface array on board the PCB consists of two CAN bus ports for accepting incoming data from two independent SmartCam modules, a USART port for communication with the MAV and a microUSB port for MAV communication or optional data logging. An MMC/SD card slot is also provided for future on board data logging, e.g., during flight. For power conversion to the SmartCam's voltage requirements of 24 V a Traco Power THB 3-1215 converter (Traco Electronic AG, Zürich, Switzerland) has been included, which additionally strengthens robustness against voltage irregularities owing to motor noise and battery depletion. Total weight of the PCB was 30 g.

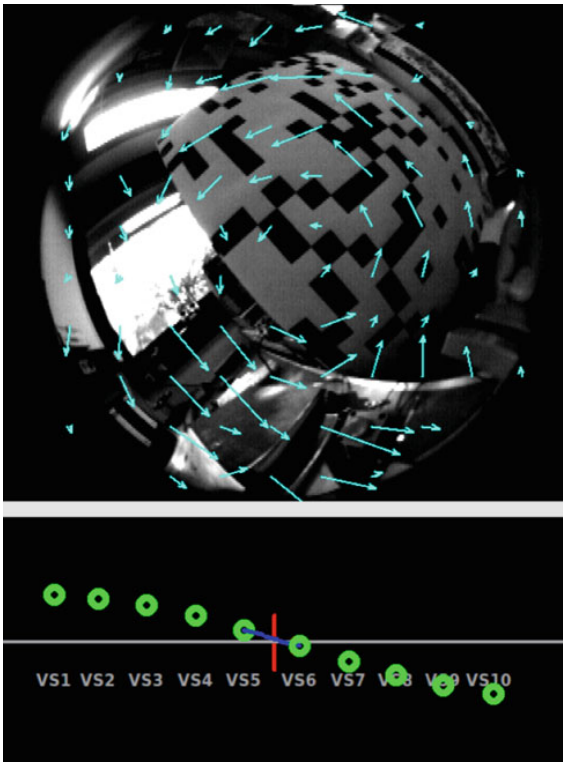

Fig. 4 Screenshot of the GUI on the ground station PC during a rotation around an axis close to zero. The *upper graph* shows the local motion estimates overlaid on top of the live video stream, while the corresponding VS cell network axon terminal responses are displayed in the *lower graph*

3.3.5 PC monitoring software

In order to display and monitor in real time the captured image data along with the estimated local motion and wide field integration data a Linux monitoring interface was written in C++ using the QT framework. For proper visualization in the Graphical User Interface (GUI) the optic flow vectors are scaled and overlaid onto the camera video stream while VS cell homologue data is shown in a corresponding plot (Fig. 4). Data is acquired via an IEEE 802.11g wireless link between the laptop and the sensor system. Due to the limited bandwidth of the wireless connection on average between 10 and 15 frames could be transmitted per second, which nevertheless is sufficient for a human observer to monitor the live image stream and the corresponding optic flow output of

the system. For recording wide field integration data at full frame rate the USB connection between the ARM PCB and the monitoring laptop could be used.

3.4 Design outcome

The final sensor system was able to compute 350 ego-motion estimates per second for transmission towards the MAV flight controller and/or data logging PC, while weighing a total of 193g and consuming less than 4 W off a standard three cell 12 V LiPo RC model battery. At the same time, real time images, flow fields and ego-motion estimates were sent to a control ground station PC at a reduced frame rate of roughly 12 fps. Using automatic gain adaptation the 8 bit image sensor produced pixel values roughly centered in its 0–255 coding range. In dim indoor lighting conditions between 10 and 30 cd/m^2 with an exposure time of 2.85 ms per frame temporal noise caused a typical standard deviation of 2.2% of this range.

4 Results

To test the functionality and reveal the characteristics of the sensor system two kinds of trials were conducted. On one hand, experiments were carried out to ascertain the resemblance with the biological original. On the other hand, essays to elucidate the actual sensor characteristics and accuracy of measurement were performed.

4.1 EMD output characteristics

A distinct feature of correlation type motion detectors is the existence of a velocity optimum in response to moving sine grating stimuli (Buchner 1976; Poggio and Reichardt 1976). As shown by Borst et al. (2003) for a Reichardt Detector configuration with a temporal high-pass filter in its input lines the velocity response curve for sinusoidal gratings is given by

$$\langle R_i \rangle_\varphi = \Delta I^2 \frac{\tau_{\mathrm{lp}} \tau_{\mathrm{hp}}^2 \omega^3}{(1+\tau_{\mathrm{lp}}^2\omega^2)(1+\tau_{\mathrm{hp}}^2\omega^2)} \sin(2\pi\,\Delta\varphi/\lambda), \qquad (4)$$

where ΔI is the pattern contrast, ω the angular frequency, $\Delta\varphi$ the inter-ommatidial angle, λ the wavelenth and τ_{lp} and τ_{hp} are the low-pass and high-pass time constants, respectively. The velocity optimum is a linear function of the spatial pattern wavelength leading to a constant temporal frequency optimum. This has been observed in behavioral and electrophysiological studies in resting, walking, and flying animals across various fly species. These studies have revealed frequency optima around 1 Hz for stationary *Drosophila*, *Phaenicia*, and *Calliphora* (see Joesch et al. 2008; Eckert 1980; Haag et al. 2004, respectively). For walking *Drosophila* optima from 2 to 3 Hz have been shown (Götz and Wenking 1973; Chiappe et al. 2010). In flying animals, optima have been reported between 3 and 10 Hz for *Drosophila* (Duistermars et al. 2007; Fry et al. 2009), 1 to 10 Hz for *Musca* (Borst and Bahde 1987) and 5 to 7 Hz for *Calliphora* (Hausen and Wehrhahn 1989; Jung et al. 2011). We chose to adjust the filter time constants to values yielding a theoretical frequency optimum similar to *Calliphora* during flight, i.e., at 7.3 Hz ($\tau_{\mathrm{lp}} = 45$ ms and $\tau_{\mathrm{hp}} = 33$ ms). For confirming the existence and location of the velocity optimum of our sensor system we measured the sensor output for vertically moving sine gratings at spatial wavelengths $\lambda = 12°$, 24°, and 48° at different velocities using a cylinder-shaped LED arena as described by Weber et al. (2010). The normalized mean response of VS 7 cells over $n = 23$ trials revealed velocity optima at 85, 175, and 350°/s for $\lambda = 12°$, 24°, and 48°, respectively (Fig. 5a). Dividing the velocity optima by the corresponding spatial wavelength, the frequency optima coincide around 7.3 Hz as predicted by the model calculations in Eq. 4 (Fig. 5b).

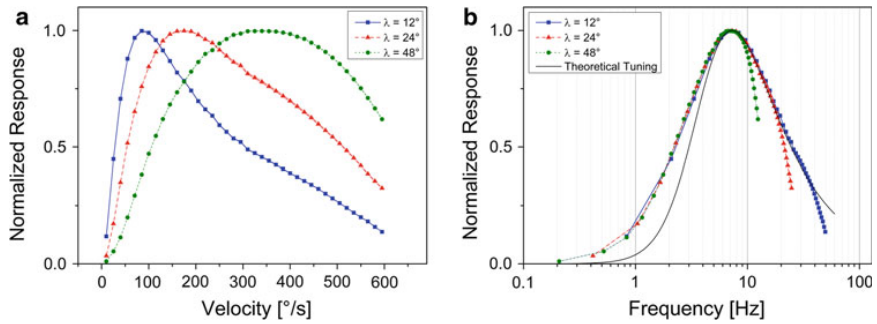

Fig. 5 VS cell velocity tuning. **a** Normalized VS cell response curves for sinusoidal gratings of spatial wavelengths $\lambda = 12°$, 24°, and 48° of visual angle as seen by the fly over a wide range of velocities, displaying optima at 85, 175, and 350°/s, respectively. Representative data from VS 7 cells over $n = 23$ trials are shown. Standard deviation is within symbol size. **b** VS cell frequency tuning. Data from **a** are plotted as a function of temporal frequency by dividing velocity by the respective pattern wavelength. Frequency optima for all three wavelengths lie around 7.3 Hz. Standard deviation is within symbol size

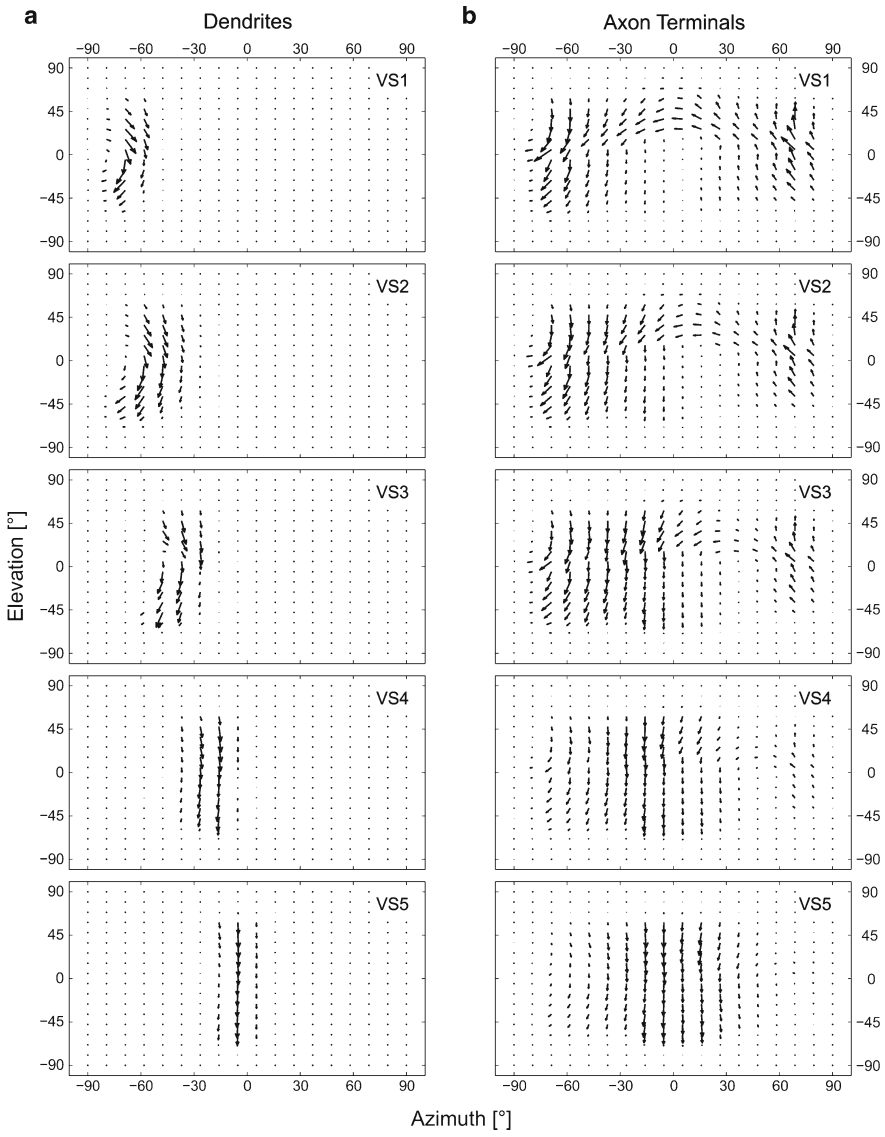

Fig. 6 Receptive fields of VS 1 to VS 5 for **a** dendritic and **b** axon terminal regions. Average data from $n = 21$ trials are shown. Note the resemblance between axon terminal receptive fields and rotations around axes sequentially arranged on the equator

4.2 Receptive fields

To measure our sensor's receptive fields, we used a custom built arena consisting of three 120 Hz SyncMaster 2233RZ monitors (Samsung, South Korea) in combination with NVIDIA GeForce GTX 480/580 graphics cards (NVIDIA Corp., California, USA) using NVIDIA 3D Vision Surround technology. The monitors were perpendicularly placed in front, left, and right of the sensor, covering the visual space from $-135°$ to $135°$ in equatorial azimuth and from $-58°$ to $58°$ in frontal elevation. Monitor radiance inhomogeneities were largely compensated by using diffusing filter paper. Stimuli were written in Python and rendered using the open source graphics engine Panda3D (Goslin and Mine, 2004). They consisted of a small $5.7° \times 5.7°$ white square moving at $120°/s$ on a dark background (92% Michelson contrast) sweeping the extent of the arena in the frontal hemisphere up and down to reveal the vertical components and left and right to reveal the horizontal components of the receptive fields. For $n = 21$ complete trials the response data was spatially divided into 36×36 equisolid angle bins covering the frontal hemisphere. Both dendritic and axon terminal responses from all implemented VS and HS cells were recorded at the camera frame rate of 350 measurements per second. As expected, the dendritic compartments respond to vertical motion in rather narrow stretches of the visual field (Figs. 6a, 7a), while in

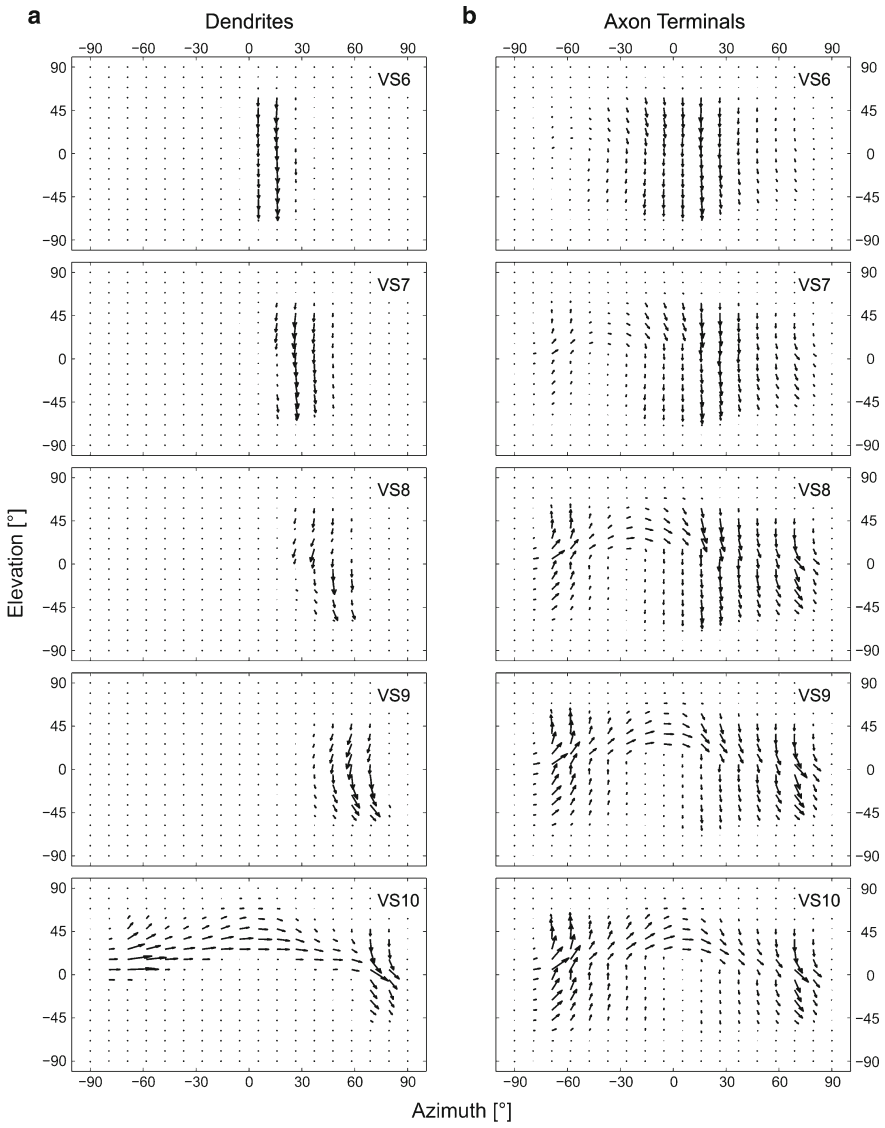

Fig. 7 Receptive fields of VS 6 to VS 10 for **a** dendritic and **b** axon terminal regions. Average data from $n = 21$ trials are shown. Note the resemblance between axon terminal receptive fields and rotations around axes sequentially arranged on the equator

the axon terminals the cells exhibit responses over a much broader area (Figs. 6b, 7b) owing to the lateral connections with their neighboring cells, as depicted in Fig. 2. Thus, the axon terminal output receptive fields resembled matched filters for optic flow generated by rotations around axes sequentially arranged along the equator (see Krapp et al. 1998; Franz and Krapp 2000).

4.3 Rotation axis estimation

The main objective of this sensor system is the estimation of the axis of rotation during ego-motion. In order to examine the measurement accuracy of the sensor system we tested it both in a simulation environment and in a real world scenario. The experimental setup used for the simulation environment was the same as for the receptive field analysis described in Sect. 4.2. For spatially correct stimulus presentation *cube mapping* was used (Greene 1986). The sensor system was mounted in the focal spot and the simulated environment was rotated around axes ranging from $\theta_{\text{ref}} = -60°$ to 60° along the equator in 15° steps at angular velocities from 30 to 100°/s in 5°/s steps for each axis. For performance evaluation the Root Mean Square Deviation (RMSD) between sensor axis estimate and reference angle was defined as

$$\text{RMSD}(\theta_{\text{est}}, \theta_{\text{ref}}) = \sqrt{\frac{\sum_{i=1}^{n} (\theta_{\text{est}}(i) - \theta_{\text{ref}}(i))^2}{n}}, \qquad (5)$$

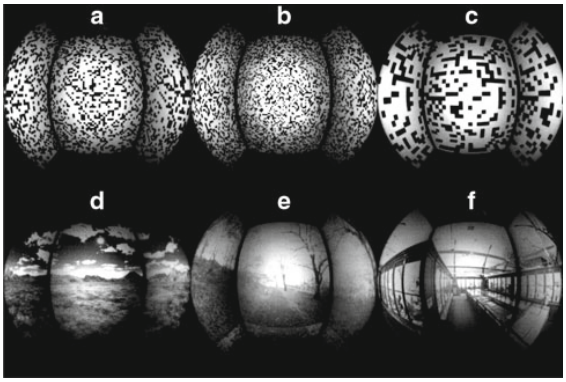

Fig. 8 Screenshots of visual scenarios used in the simulation environment for rotation estimation experiments. Scenes A, B, and C were artificially generated using random probability distributions while scenes D, E, and F were cube mapping projections of photographic scenes

Table 1 Contrast and RMSD for simulated scenes

Scene	Type	Contrast			Result
		C_{RMS}	C_{MAD}	C_{RAPS}	RMSD
A	Artificial	1.39	0.28	0.19	3.00°
B	Artificial	1.36	0.26	0.17	3.65°
C	Artificial	1.38	0.31	0.16	4.59°
D	Natural	1.70	0.17	0.06	9.01°
E	Natural	1.39	0.20	0.04	14.44°
F	Natural	1.42	0.20	0.07	18.42°

where θ_{est} is the sensor axis estimate and θ_{ref} the reference angle.

Three contrast metrics were defined for the presented images. RMS contrast (C_{RMS}) was defined as the standard deviation of pixel values divided by their mean. As a second metric MAD contrast (C_{MAD}) was defined as the Mean Absolute Deviation (MAD) of pixel values. These two metrics are global measures and therefore do not depend on the spatial frequency content or the spatial brightness distribution. Hence, radially averaged power spectrum contrast (C_{RAPS}) was defined as the square root of the mean of the radially averaged power spectra between 0.0649 cycles per degree and 0.6486 cycles per degree, thereby covering the spatial coding range of the sensor system up to its Nyquist limit.

Three artificial and three naturalistic scenarios were presented in the simulation environment (Fig. 8). Owing to their high contrast ratios the artificial scenarios yielded very robust and exact estimation of the rotational axes, on average deviating by less than 5° from the actual axis of rotation (see Table 1). Natural images displayed larger RMS deviations between 9° and 18° due to their lower contrast and the relatively low mean luminance values of available scenes in the experimental setup. In line with the motion detection model, the higher

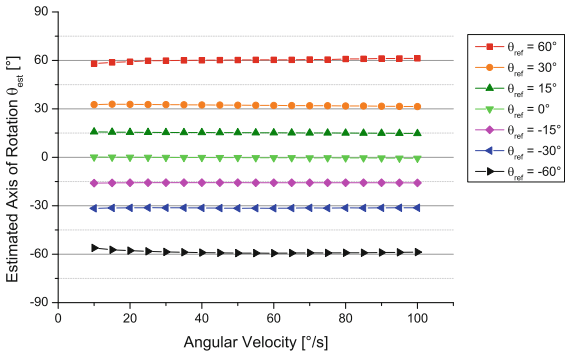

Fig. 9 Axis estimation during real world trials. The sensor system was rotated in a wide range of angular velocities around different reference axes, yielding highly accurate rotation axis estimates virtually regardless of angular velocity

the contrast the better the sensor system performed. To test an extreme case and an exception to this rule we included a scene with high rotational asymmetries (Table 1, row F). In this case the sensor generated the highest RMS deviations in the test set despite not having the lowest contrast. Remarkably, this worst case RMSD of 18.42° is almost identical to the 18.5° spacing between VS cell dendritic receptive fields. This means that the worst case sensor inaccuracy tends to be at most one cell to the left or to the right of the true center of rotation.

For recording data in a real world environment the sensor system was mounted axially on a PLE40 planetary gear with a 100:1 gear reduction ratio (Neugart, Kippenheim, Germany) and rotated using a PANdrive PD1-140-42-SE-232 motor with an integrated control unit (Trinamic, Hamburg, Germany). Situated in an indoor environment with both high and low visual contrast areas the sensor system was rotated around the axes $\theta_{ref} = -60°, -30°, -15°, 0°, 15°, 30°$, and 60° along the equator at angular velocities ranging from 10 to 100°/s in 5°/s steps. The actual angular velocity was monitored utilizing the integrated encoders. As can be observed in Fig. 9 rotation axis estimation by the sensor system accurately reflects the actual axis of rotation, basically regardless of rotational velocity. There tends to be, however, slightly higher accuracy towards higher velocities, as can also be seen in Fig. 9.

4.4 Rotation rate estimation

Concurrently with the rotation axis estimation, the sensor system also computes an estimate of the rate of rotation around that particular axis by calculating the slope at the zero-crossing location. To analyze the properties of these estimates, the camera system was subjected to $n = 22$ trials with rotations around the rostro-caudal axis at angular velocities ranging from 10 to 1,000°/s using the same scenes

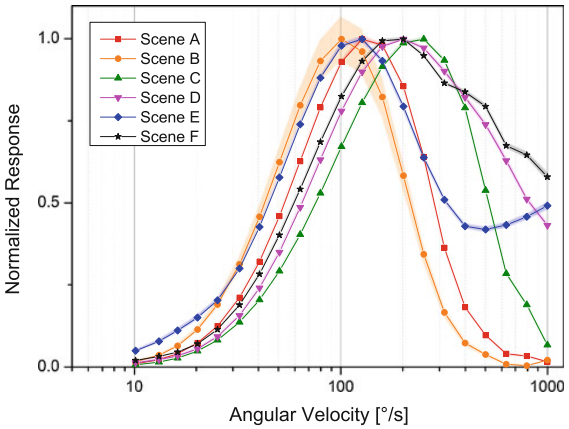

Fig. 10 Rotation rate estimation for naturalistic and artificial scenes. *Traces* show mean estimates while *shaded areas* indicate standard deviation between $n = 22$ trials. Velocity optima lie between 100 and 251°/s

as for the axis estimation trials in Sect. 4.3. Figure 10 presents the typical bell-shaped response curves of the system. Peak responses were found between 100 and 251°/s.

5 Discussion and conclusions

We have presented a fly-inspired visual rotation sensor capable of accurate measurements in a variety of visual scenes, while maintaining the tight restrictions of space, weight and power requirements necessary for use on board MAVs. The outcome of our experiments substantiates on one hand the close resemblance of our implementation with the biological original. On the other hand, our results demonstrate the good performance over a wide range of different visual environments. Our implementation was specifically designed to be used on-board MAVs and therefore features only a small footprint in terms of size, weight and power consumption while maintaining mechanical robustness.

One possible source of performance degradation is the inherent barrel distortion of fisheye lenses. We have therefore tested various correction algorithms on board the FPGA with slight, albeit not substantial performance improvements. This suggests that fisheye lens distortion does not decisively perturb sensor performance.

A particularly useful property of our FPGA- and ARM-based implementation is the versatility and ease of adding other functionalities. By adding different templates for global motion integration, new uses of this sensor system could arise. The simple sum of all VS cell templates for instance, could be used as a measure of global vertical motion for lift control. The sum of HS cells might be used for indication of global horizontal motion for yaw control. Using specialized horizontal templates, *tunnel centering* behavior (Srinivasan et al. 1999) could be implemented for autonomous robot navigation. Along these same lines, collision detection can be envisioned by using templates for radial expansion. The advantage of our system lies in the fact that there are sufficient free resources for all these computations to be implemented simultaneously, at full frame rate and resolution.

The system has been designed to be used with either one or two cameras, potentially covering the complete 4π sr unit sphere of visual space for true global motion integration and consequently added robustness of ego-motion estimates. Also multi-modal integration of other sensors, such as rate gyroscopes, accelerometers, etc., is supported. This is particularly useful for future studies on sensor fusion with inertial data, akin to integration of vision and inertial haltere measurements in the fly brain. The system we have presented here might therefore prove useful when employed complementarily to inertial measurement units.

In conclusion, we have shown a successful implementation of visual ego-rotation sensing based on the fly visual system, while keeping within tight space, weight and performance restriction boundaries.

Acknowledgments We wish to thank Väinö Haikala and Hubert Eichner for helpful discussions. This work was supported in part by the Deutsche Forschungsgemeinschaft (DFG) excellence initiative research cluster Cognition for Technical Systems (CoTeSys).

References

Aubepart F, El Farji M, Franceschini N (2004) FPGA implementation of elementary motion detectors for the visual guidance of micro-air-vehicles. In: Proc IEEE Int Symp Ind Electron, vol 1, pp 71–76

Autrum H (1952) Über zeitliches Auflösungsvermögen and Primärvorgänge im Insektenauge. Naturwissenschaften 39:290–297

Bermudezi Badia S, Pyk P, Verschure PFM (2007) A fly-locust based neuronal control system applied to an unmanned aerial vehicle: the invertebrate neuronal principles for course stabilization, altitude control and collision avoidance. Int J Robot Res 26:759–772

Beyeler A, Zufferey J, Floreano D (2009) Vision-based control of near-obstacle flight. Auton Robot 27:201–219

Borst A (2007) Correlation versus gradient type motion detectors: the pros and cons. Philos Trans R Soc Lond B 362:369–374

Borst A, Bahde S (1987) Comparison between the movement detection systems underlying the optomotor and the landing response in the housefly. Biol Cybern 56:217–224

Borst A, Reisenman C, Haag J (2003) Adaptation of response transients in fly motion vision. II: Model studies. Vis Res 43:1311–1324

Borst A, Haag J, Reiff DF (2010) Fly motion vision. Annu Rev Neurosci 33:49–70

Buchner E (1976) Elementary movement detectors in an insect visual system. Biol Cybern 24:85–101

Chiappe ME, Seelig JD, Reiser MB, Jayaraman V (2010) Walking modulates speed sensitivity in *Drosophila* motion vision. Curr Biol 20:1470–1475

Conroy J, Gremillion G, Ranganathan B, Humbert JS (2009) Implementation of wide-field integration of optic flow for autonomous quadrotor navigation. Auton Robot 27:189–198

Cuntz H, Haag J, Forstner F, Segev I, Borst A (2007) Robust coding of flow-field parameters by axo-axonal gap junctions between fly visual interneurons. Proc Natl Acad Sci USA 104:10229–10233

Duistermars BJ, Chow DM, Condro M, Frye MA (2007) The spatial, temporal and contrast properties of expansion and rotation flight optomotor responses in *Drosophila*. J Exp Biol 210:3218–3227

Eckert H (1980) Functional properties of the H1-neurone in the third optic ganglion of the blowfly, *Phaenicia*. J Comp Physiol A 135:29–39

Egelhaaf M, Borst A, Reichardt W (1989) Computational structure of a biological motion-detection system as revealed by local detector analysis in the fly's nervous system. J Opt Soc Am A 6:1070–1087

Elyada YM, Haag J, Borst A (2009) Different receptive fields in axons and dendrites underlie robust coding in motion-sensitive neurons. Nat Neurosci 12:327–332

Farrow K, Borst A, Haag J (2005) Sharing receptive fields with your neighbors: tuning the vertical system cells to wide field motion. J Neurosci 25:3985–3993

Franceschini N, Pichon JM, Blanes C, Brady JM (1992) From insect vision to robot vision. Philos Trans R Soc Lond B 337:283–294

Franz MO, Krapp HG (2000) Wide-field, motion-sensitive neurons and matched filters for optic flow fields. Biol Cybern 83:185–197

Fry SN, Rohrseitz N, Straw AD, Dickinson MH (2009) Visual control of flight speed in *Drosophila melanogaster*. J Exp Biol 212:1120–1130

Gonzalez RC, Woods RE (2007) Digital image processing, 3rd edn. Prentice Hall, Upper Saddle River, NJ

Goslin M, Mine MR (2004) The Panda3D graphics engine. Computer 37:112–114

Götz KG, Wenking H (1973) Visual control of locomotion in the walking fruitfly *Drosophila*. J Comp Physiol A 85:235–266

Greene N (1986) Environment mapping and other applications of world projections. IEEE Comput Graph Appl 6:21–29

Haag J, Borst A (2003) Orientation tuning of motion-sensitive neurons shaped by vertical–horizontal network interactions. J Comp Physiol A 189:363–370

Haag J, Borst A (2004) Neural mechanism underlying complex receptive field properties of motion-sensitive interneurons. Nat Neurosci 7:628–634

Haag J, Borst A (2005) Dye-coupling visualizes networks of large-field motion-sensitive neurons in the fly. J Comp Physiol A 191:445–454

Haag J, Borst A (2007) Reciprocal inhibitory connections within a neural network for rotational optic-flow processing. Front Neurosci 1:111–121

Haag J, Denk W, Borst A (2004) Fly motion vision is based on reichardt detectors regardless of the signal-to-noise ratio. Proc Natl Acad Sci USA 101:16333–16338

Harrison RR (2005) A biologically inspired analog IC for visual collision detection. IEEE Trans Circuits Syst I 52:2308–2318

Hassenstein B, Reichardt W (1956) Systemtheoretische Analyse der Zeit-, Reihenfolgen- und Vorzeichenauswertung bei der Bewegungsperzeption des Rüsselkäfers *Chlorophanus*. Z Naturforsch B 11:513–524

Hausen K, Wehrhahn C (1989) Neural circuits mediating visual flight control in flies. I. Quantitative comparison of neural and behavioral response characteristics. J Neurosci 9:3828–3836

Hyslop A, Krapp HG, Humbert JS (2010) Control theoretic interpretation of directional motion preferences in optic flow processing interneurons. Biol Cybern 103:353–364

Joesch M, Plett J, Borst A, Reiff DF (2008) Response properties of motion-sensitive visual interneurons in the lobula plate of *Drosophila melanogaster*. Curr Biol 18:368–374

Jung SN, Borst A, Haag J (2011) Flight activity alters velocity tuning of fly motion-sensitive neurons. J Neurosci 31:9231–9237

Kendoul F, Fantoni I, Nonami K (2009) Optic flow-based vision system for autonomous 3D localization and control of small aerial vehicles. Robot Auton Syst 57:591–602

Köhler T, Röchter F, Lindemann JP, Möller R (2009) Bio-inspired motion detection in an FPGA-based smart camera module. Bioinspir Biomim 4:015,008 (10 pp)

Krapp HG, Hengstenberg B, Hengstenberg R (1998) Dendritic structure and receptive-field organization of optic flow processing interneurons in the fly. J Neurophysiol 79:1902–1917

Land MF, Eckert H (1985) Maps of the acute zones of fly eyes. J Comp Physiol A 156:525–538

Moeckel R, Liu S (2009) Motion detection chips for robotic platforms. In: Floreano D, Zufferey J, Srinivasan MV, Ellington C (eds) Flying insects and robots. Springer, Berlin, pp 101–114

Netter T, Franceschini N (2002) A robotic aircraft that follows terrain using a neuromorphic eye. In: Proceedings of the International Conference on Intellectual Robotic System, vol 1, pp 129–134

O'Carroll DC, Shoemaker PA, Brinkworth RSA (2006) Bio-inspired optical rotation sensor. In: Proceedings of the SPIE Symposium on Smart Structures, Devices, and Systems III, vol 641418, pp 1–12

Petrowitz R, Dahmen H, Egelhaaf M, Krapp HG (2000) Arrangement of optical axes and spatial resolution in the compound eye of the female blowfly *Calliphora*. J Comp Physiol A 186:737–746

Poggio T, Reichardt W (1976) Visual control of orientation behaviour in the fly. Part II. Towards the underlying neural interactions. Q Rev Biophys 9:377–438

Potters M, Bialek W (1994) Statistical mechanics and visual signal processing. J Phys I 4:1755–1775

Reichardt W, Egelhaaf M (1988) Properties of individual movement detectors as derived from behavioural experiments on the visual system of the fly. Biol Cybern 58:287–294

Seitz G (1968) Der Strahlengang im Appositionsauge von *Calliphora erythrocephala* (Meig.). J Comp Physiol A 59(2):205–231

Single S, Borst A (1998) Dendritic integration and its role in computing image velocity. Science 281:1848–1850

Srinivasan MV, Chahl JS, Weber K, Venkatesh S, Nagle MG, Zhang SW (1999) Robot navigation inspired by principles of insect vision. Robot Auton Syst 26:203–216

Srinivasan M, Thurrowgood S, Soccol D (2009) Competent vision and navigation systems. IEEE Robot Autom Mag 16:59–71

Stumpf P (1911) Über die Abhängigkeit der visuellen Bewegungsrichtung und negativen Nachbildes von den Reizvorgängen auf der Netzhaut. Z Psychol 59:321–330

Tatler B, O'Carroll DC, Laughlin SB (2000) Temperature and the temporal resolving power of fly photoreceptors. J Comp Physiol A 186:399–407

Valette F, Ruffier F, Viollet S, Seidl T (2010) Biomimetic optic flow sensing applied to a lunar landing scenario. In: Proceedings of the IEEE International Conference on Robotics and Automation, pp 2253–2260

Weber F, Machens CK, Borst A (2010) Spatiotemporal response properties of optic-flow processing neurons. Neuron 67:629–642

Wertz A, Gaub B, Plett J, Haag J, Borst A (2009) Robust coding of ego-motion in descending neurons of the fly. J Neurosci 29:14993–15000

XILINX (1999) XAPP134: Virtex synthesizable high performance SDRAM controller. XILINX

XILINX (2003) XAPP394: Interfacing to mobile SDRAM with CoolRunner-II CPLDs. XILINX

Zhang T, Wu H, Borst A, Kühnlenz K, Buss M (2008) An FPGA implementation of insect-inspired motion detector for high-speed vision systems. In: Proceedings of the IEEE International Conference on Robotics and Automation, pp 335–340

Zufferey J, Floreano D (2006) Fly-inspired visual steering of an ultralight indoor aircraft. IEEE Trans Robot 22:137–146

5 DISCUSSION

Flies use visual cues for orientation during walking and while they perform impressive maneuvers during flight. In this cumulative thesis we studied the neuronal mechanisms underlying such visual orientation behaviors. In order to do this, we designed new behavioral setups which allow for measuring *Drosophila*'s walking behavior in a precisely controlled virtual environment. Using targeted genetic silencing experiments, we characterized the role of different sets of neurons in visual information processing. We concentrated on visual interneurons T4 and T5 which are major output elements from the medulla and project into the lobula plate.

In the first study, we silenced the output of both cell types and found that these flies were completely blind to motion. However, such motion-blind flies were still able to fixate a black bar, although at a reduced performance. Further quantification revealed a motion-independent flicker-sensitive visual subsystem which is implemented in parallel to the motion detection circuitry and which can mediate bar fixation behavior. We also found that motion responses are asymmetric, i.e. that they are stronger for front-to-back than for back-to-front motion. Hence, the motion system mediates bar fixation as well, which further improves performance in control flies.

In the second study, we investigated the response properties of T4 and T5 neurons via two-photon calcium imaging. Both cell types showed clear direction-selective contrast polarity-specific responses: T4 neurons only responded to motion of bright (ON) edges, while T5 neurons responded only to motion of dark (OFF) edges. Electrophysiological recordings from postsynaptic lobula plate tangential cells and behavioral experiments revealed that this separation is also functional: When blocking the output from T4 neurons, responses to ON edge motion were largely impaired while responses to OFF edge motion remained intact and the opposite was true for the T5 block.

In the third study, we tested an artificial FPGA-based microcircuit which simulates the lobula plate network of the fly. The system was equipped with a camera and spherical fisheye lens and placed in a virtual environment setup. When stimulated with various rotating natural scenes, the insect-inspired system predicted very well the axes of rotation.

5.1 BEHAVIORAL READOUT OF VISUAL PROCESSING

Bottom-up and top-down approaches

One way to explore neural computations in the brain is to study the connectivity and response properties of every single nerve cell in a dedicated

microcircuit. This approach is technically challenging but, if applied successfully, leads to a clear picture of local information processing. Still, with such a bottom-up approach it is difficult to deduce activity on larger neuronal scales, which is eventually required to fully understand how behavioral output is controlled. One solution is to combine all knowledge and to perform computer simulations. This allows one to systematically vary model parameters and to explore the resulting network activity and behavioral responses. Yet, this approach leads to highly complex models which are often difficult to tune.

Here, a prominent and very ambitious example is the Blue Brain Project which aims to build a realistic and complete column of the cat visual cortex (Markram, 2006). However, pharmacological, physiological and anatomical information about cortical neurons, the building blocks of the model, is far from complete and it remains to be shown whether the approach will be successful. The fly visual system is much simpler and much better understood than the mammalian visual system and it was possible to perform detailed computer simulations of the lobula plate network (Borst and Weber, 2011): All current knowledge about synaptic and electrical coupling within the lobula plate was combined, resulting in a model which predicted the optic flow tuning properties of lobula plate tangential cells.

Alternatively, one can choose a top-down approach and consider the entire animal as a black box which transforms visual stimuli into behavioral responses. The creation of an input-output map allows one to formulate simple mathematical rules without knowing the details of cellular processing. Such a cybernetic approach was pioneered by Hassenstein and Reichardt (1956): Based on behavioral experiments, they formulated the Reichardt detector, which tremendously helped to understand the computational operations underlying motion vision. Once such rules are established, one can then explore cellular activity and test how circuit manipulations affect behavior.

Relating behavior and neuronal circuits

The gold standard in systems neuroscience is to relate neuronal activity to behavioral output and to predict changes in behavior upon modifications of the circuit. However, this is often more challenging than expected, for at least two main reasons:

Defining behavior

First, it is very difficult to properly define what a delineated behavior actually is. In the bar fixation paradigm, for example, the fly has control over the position of a black bar in closed-loop configuration and brings it to the front and keeps it there. This entire response is called a behavior and can be interpreted as object tracking or orientation based on landmarks. During optomotor behavior the fly follows global and local motion cues and therefore, this behavior is thought to be essential for optic flow-based visual course control. Both behaviors are very much interpreted from a human perspective and it is generally unclear how meaningful these paradigms are for the fly when navigating in natural environments. It might, for example, be that the observed behaviors are simply artifacts of some other systems dedicated to processing specific kinds of, potentially unexplored, visual features and that the underlying circuits interplay in a complex fashion during real-world orientation.

The solution to this problem can come from two different sides. One can study the animals in more natural environments and test the hypotheses which have been designed during restricted lab experiments. For this, one needs proper tracking of freely walking (Branson *et al.*, 2009) or flying flies (Straw *et al.*, 2011) and to then silence specific neuronal elements. Alternatively, one can choose the opposite approach and design behavioral paradigms which are free from human-biased interpretations of behavior. Vogelstein *et al.* (2014) developed a computer algorithm which was used to analyze movies of more than 30 000 crawling larvae in order to create a tree of statistically distinguishable behaviors, called behaviotypes. Such unbiased strategies for describing behavior are just beginning to emerge and should be adapted to the study of adult flies. Combined with targeted circuit manipulations this could help to explore which set of neurons control which set of behaviotypes.

Modular organization and redundancy

Second, the brain is often considered to be organized in different modules. Each of these modules is dedicated to process specific features from visual space or to control a specific kind of behavior. However, the interpretations of blocking experiments become very unintuitive if such modules are coupled, if feedback connections exist or if modules show large degrees of redundancy. Moreover, many visual stimuli activate many modules at the same time, even when they appear to be very simple. The black bar fixation stimulus is a good example: It contains a moving OFF edge, a moving ON edge and local flicker when the bar moves through a certain region of the visual field. Hence, bar fixation could, in principle, be performed with any of these cues and blocking one part of the system might leave the behavior intact.

Simple visual stimuli and simple behaviors

In this study we tried to stay close to the strategy of using simple visual stimuli and simple behavioral readouts: In a first set of experiments we found that visual interneurons $T4$ and $T5$ are necessary for the optomotor response but that they are only partially needed for bar fixation. As the two behaviors are difficult to compare (open-loop vs. closed-loop, turning speed vs. fixation performance and full-field vs. local stimulus) we simplified both experiments: We used a small window in which we showed motion or flicker and turning speed was the behavioral readout during both kinds of stimuli. We found that blocking $T4/T5$ neurons abolished responses to motion but left flicker responses intact. Interestingly, turning responses of control flies were stronger for front-to-back motion than for back-to-front motion. These findings clearly speak in favor for two independent visual subsystems where one system is dedicated to motion processing while the other analyzes flicker. Importantly, this implies that the flicker-sensitive system and the asymmetric motion system both mediate closed-loop bar fixation in concert. Hence, this example shows that the outputs of apparently distinct neural circuits do not necessarily have to be restricted to controlling distinct behaviors but that they can converge in order to control more complex behaviors.

5.2 MOTION VISION

Detection of motion provides an animal with important cues for spatial orientation. We have shown with behavioral experiments that visual interneurons T4 and T5 are necessary for direction-selective responses to large-field motion stimuli as well as to small moving objects. This has two important implications. First, it shows that the visual pathways L1–T4 and L2–T5 are the only systems which can mediate direction-selective behaviors. Second, the computation of directionality of small-field motion and large-field motion happens via the same elements. The characterization of T4 and T5 neurons via two-photon imaging, which we performed in this study, revealed that T4 and T5 neurons are local motion detectors. They are directionally selective and converge onto distinct layers in the lobula plate where they synpase onto lobula plate tangential cells. Hence, T4 and T5 neurons with their small receptive field of just 2–3 ommatidia (Takemura *et al.*, 2013) sum up to give rise to the global receptive field of postsynpatic lobula plate tangential cells (Krapp and Hengstenberg, 1996).

5.2.1 Parallel ON and OFF channels

Physiological and behavioral experiments in flies have suggested that motion computation is split into separate ON and OFF pathways. This split starts at the level of the lamina where L1 output feeds into the ON pathway while L2 output feeds into the OFF pathway (Joesch *et al.*, 2010). Anatomical studies have suggested that these pathways remain separate and converge onto T4 and T5 neurons, respectively (Bausenwein and Fischbach, 1992). Hence, the separation should still be visible at the level of these neurons. Indeed, we could show that T4 neurons respond only to ON edge motion while T5 neurons respond only to OFF edge motion. We did electrophysiological recordings from postsynaptic lobula plate tangential cells and performed behavioral experiments: When blocking T4, only responses to ON edge motion were impaired and blocking T5 resulted in a response reduction to OFF edge motion. Hence, our data indicate that the split of motion vision still exists at the level of T4 and T5. This simplifies the search for the neural implementation of motion vision because it is now possible to focus on either of the pathways.

The split of motion computation into separate polarity-specific pathways is found in many visual systems (Sanes and Zipursky, 2010), yet, it is not fully clear why this occurs so frequently in nature. One explanation is that neural activity cannot be negative and hence, in order to transmit information about OFF signals, responses have to be inverted and fed into a distinct channel. Moreover, this allows a simple implementation of sign-correct multiplication as proposed by Hassenstein and Reichardt (1956) where ON–ON and OFF–OFF signals both yield positive responses. Motion vision could, in principle, work entirely with only one of the pathways. Yet, it could be shown that the use of both channels requires less energy in order to transmit the same amount of information (Gjorgjieva *et al.*, 2014), which is a clear evolutionary advantage.

5.2.2 Temporal delay

Any motion detector needs to implement spatial offset together with asymmetric temporal delay. The delay in the motion vision circuitry of the fly could be implemented in various ways. It might be a network phenomena which arises via an intermediate cell or it could be due to different membrane time constants. It could also arise via distinct receptor kinetics at the postsynaptic neuron. Hence, many different schemes are possible and perhaps a combination of all of the above occurs in the visual system of flies.

Short delay differences in T4/T5 input lines

We have found that T4 and T5 neurons are direction-selective. This tremendously simplifies the question how temporal delay is implemented and suggests that it is located before or within T4 and T5. Specifically, the ON pathway is a promising microcircuit as it is much simpler than its counterpart, the OFF pathway: L1 synapses onto Mi1 and Tm3 which, in turn, converge onto the dendrites of T4 neurons. The fact that T4 cells receive only two major input lines suggests that Mi1 and Tm3 convey asymmetrically delayed signals (Takemura *et al.*, 2013). Indeed, Behnia *et al.* (2014) recorded electrophysiologically from these cells and found distinct filter constants for Mi1 and Tm3, respectively. With the parameters obtained from these experiments the authors performed Reichardt detector simulations which could reproduce the temporal frequency tuning and direction-selectivity of lobula plate tangential cells. However, the time constant difference for Mi1 and Tm3 was as little as 18 ms, which resulted in weak orientation tuning before the subtraction stage. Thus, their model predicted that T4 neurons should show little orientation tuning. Yet, in our experiments we found that T4 neurons are well tuned to the direction of motion and hence, a 18 ms time constant difference is probably too small.

Potential mechanisms for longer delays

The question arises how larger temporal delays could be implemented. From anatomy, it is known that there is no additional interneuron in the ON pathway which could convey a delay via network mechanisms. Hence, a tempting alternative hypothesis is that asymmetric filtering could be implemented via different receptor types on the dendrites of T4 and T5 neurons, respectively. Shinomiya *et al.* (2014) started to characterize the receptor composition of T4 and T5 neurons and found different types of muscarinic and nicotinic cholinoreceptors. Importantly, muscarinic receptors are metabotropic and activate a G-protein-coupled biochemical cascade while nicotonic receptors are ionotropic and rapidly depolarize the neuron. This means that muscarinic receptors might, for example, slowly increase internal calcium levels which in turn could activate further ion channels and thereby provide a strongly delayed signal. It remains to be shown to what extent the input elements of T4 and T5 neurons use different neurotransmitters in order to differentially activate these classes of receptors and whether such a scheme could render T4 and T5 neurons direction-selective.

5.2.3 Nonlinearity

Reichardt detector

T4 and T5 neurons implement a nonlinearity in order to become direction-selective. In the Reichardt detector model, the nonlinearity is a sign-correct multiplication and amplifies two excitatory input signals which occur at the

same time (Fig. 5a). This happens when a pattern moves in the preferred direction and sequentially activates the delayed and direct input lines. A multiplication could be implemented biophysically via a log-exp-transform, for example, a mechanism which was shown experimentally to be present in lobula giant movement detector neurons in the locust (Gabbiani *et al.*, 2002). Yet, whether such mechanisms are also present in the dendrites of T4 and T5 in flies, remains unclear.

Barlow-Levick detector

However, several other nonlinearities can implement direction-selectivity as well (Grzywacz and Koch, 1987) and are often more biologically plausible than multiplication. Here, a prominent example is the Barlow-Levick detector (Barlow and Levick, 1965) which was developed as a model for direction-selectivity in the rabbit retina (Fig. 5c). Similarly to the Reichardt model, it consists of a delayed and a non-delayed input line. However, instead of multiplying these signals, they are subtracted and passed through a nonlinearity. In its original formulation, this is an AND–NOT gate which leads to so-called null-direction inhibition: When motion goes in the preferred direction of the cell, the inhibition is delayed and the neuron is activated but when motion goes in the opposite direction the delayed inhibitory signal can veto the direct input line.

Potential biophysical representation

Biophysically, excitatory and inhibitory signals can arise via different receptor types and a thresholding mechanism could simply be implemented by transmitting only positive signals. As muscarinic receptors are present in T4 and T5 (Shinomiya *et al.*, 2014), both the Barlow-Levick and the Reichardt nonlinearity could be implemented: In the case of the Barlow-Levick model, muscarinic receptors should lead to delayed activation of hyperpolarizing ion channels while for the Reichardt multiplication they should either activate additional depolarizing ion channels or inhibit hyperpolarizing membrane conductances. Which of the nonlinear integration schemes is present in T4 and T5 dendrites remains to be shown. Genetic manipulation or pharmacological activation of the different receptor types combined with two-photon imaging from T4 or T5 neurons could soon reveal some of the underlying principles.

5.2.4 Integration of local motion cues

T4 and T5 neurons target different layers in the lobula plate and each of these layers is tuned to one of the four cardinal directions of motion (Buchner *et al.*, 1984). We have established that this layered structure also becomes apparent when imaging the terminals of T4 and T5 neurons. Hence, T4 and T5 neurons fall into distinct subclasses according to their directional preference. This also means that lobula plate tangential cells which have their dendrites in these layers receive mixed inputs from the T4 and T5 channels. Hence, the two contrast polarity-specific pathways finally converge. Integrating local motion cues from different layers as well as coupling between lobula plate tangential cells give rise to the complex optic flow fields of neurons in the lobula plate (Krapp and Hengstenberg, 1996).

An important feature of lobula plate tangential cells is that they hyperpolarize upon motion in null direction (Joesch *et al.*, 2008). Yet, T4 and T5 are both cholinergic (Shinomiya *et al.*, 2014) and thus probably have an

excitatory effect on lobula plate tangential cells (S. V. Raghu *et al.*, 2011). Furthermore, our data indicate that T4 and T5 do not hyperpolarize upon motion in their non-preferred direction (however, definite statements are currently not possible as we used calcium-sensitive GCaMPs for imaging). Hence, it is likely that the hyperpolarization in lobula plate tangential cells is due to lobula plate-intrinsic inhibition. Indeed, recent data from Mauss *et al.* (2014) suggests that this seems to be the case. Using a combination of pharmacology, optogenetic stimulation and electrophysiological recordings in lobula plate tangential cells the authors concluded that lobula plate tangential cells receive a direct cholinergic excitatory input from T4 and T5 followed by indirect GABAergic inhibition via currently unknown neurons.

5.2.5 Lobula plate and motion behavior

Despite detailed knowledge of the response properties of HS and VS cells in the lobula plate, final proof was missing as to whether these neurons are really in charge of controlling motion vision-based course-control. To this end, one would have to block HS and VS cells and observe the fly during navigation, expecting that it would fail to maintain a straight course. However, such experiments have not been possible so far. Tracking freely walking and flying flies is becoming feasible (Branson *et al.*, 2009; Straw *et al.*, 2011) but there are currently no Gal4 lines which can be used to specifically silence HS and VS cells without generally affecting the fly's ability to move. Alternatively, one can test well-defined motion stimuli in tethered walking flies and use an indirect approach: Silencing T4 and T5 neurons, which renders HS and VS motion-insensitive (Schnell *et al.*, 2012).

We tested T4/T5 block flies for large-field moving gratings and for moving bars and found that these flies were completely blind to these motion stimuli. Given that T4 and T5 neurons potentially target many unknown cells in the lobula plate in addition to HS and VS cells, we can currently only conclude that some neurons in the lobula plate are necessary for motion-vision based behaviors. However, HS and VS cells are very likely some of the key players. Further evidence for this has recently come from sufficiency experiments. Haikala *et al.* (2013) used optogenetic stimulation in flying blind flies which expressed a channelrhodopsin in HS cells. When the neurons were activated unilaterally, flies responded with a directed turn towards the side of stimulation.

5.2.6 Higher-order motion vision

Flies see higher-order motion cues which are spatio-temporal correlations other than standard two-point correlations of luminance (Aptekar and Frye, 2013; Clark *et al.*, 2014; Theobald *et al.*, 2008). Such correlations occur in natural scenes and contain additional information about motion in the outside world. This could be, for example, an object with the same average luminance as the background but distinct internal contrast. It is generally thought that the processing of such cues requires higher cortical computation in mammals (Y. X. Zhou and Baker, 1993). However, the fact that flies can perform such computations suggests that the underlying computa-

tional principles are much simpler. The classical Reichardt detector model does not respond to higher-order motion correlations and hence, it would be very interesting to block T4 and T5 neurons and test the behavioral performance of flies for such stimuli. If they can still see higher-order motion stimuli, one could then investigate which other neuronal structures are processing such features. If they cannot, it would be interesting to explore the response properties of T4 and T5 neurons for such stimuli, which might help to facilitate an understanding of the underlying higher-order computations.

5.2.7 Comparison to other organisms

Apart from many insects, optomotor behavior is present in numerous other species including rabbits, dogs, pigs, reptiles (Tauber and Atkin, 1968), fish (Fleisch and Neuhauss, 2006), and even echolocating bats (Suthers, 1966). Hence, these animals must be able to compute motion cues and can therefore serve as distinct model systems for the study of the underlying neuronal principles. Specifically, the mammalian retina is an area of intense research as it is easy to access experimentally with physiological tools. Almost a century ago, Ramón y Cajal described astonishing anatomical similarities between the visual systems of flies and vertebrates (Cajal and Sánchez, 1915). It is known today that these systems also share many functional and developmental features (Borst and Euler, 2011; Sanes and Zipursky, 2010).

Mouse retina

Direction-selective responses in the retina were first described by Barlow and Levick (1965) in the rabbit but more recent work has focused an retinal circuits in the mouse. The mouse retina consists of several layers (Euler *et al.*, 2014): the outer nuclear layer (ONL), the outer plexiform layer (OPL), the inner nuclear layer (INL), the inner plexiform layer (IPL) and the ganglion cell layer (GCL). The ONL houses photoreceptors, rods and cones, which project into the OPL where horizontal and bipolar cells have their dendrites and receive their signals. Bipolar cells pass through the INL and project to the IPL where they interact with starbust amacrine and retinal ganglion cells.

Separate pathways for ON and OFF signals are present directly after the photoreceptor output. OFF bipolar cells target the upper layers of the IPL while ON bipolar cells target the lower layers. Lateral interaction with horizontal and starbust amacrine cells are mostly polarity-specific as well. Bipolar cells acquire their contrast polarity-specificity via distinct glutamate receptors: In the dark, mammalian photoreceptors constantly release glutamate, which is suppressed by illumination. OFF bipolar cells have ionotropic glutamate receptors and hence, they are depolarized in the dark. Instead, ON bipolar cells have metabotropic glutamate receptors which indirectly trigger the closing of a cation channel. This means that illumination reduces photoreceptor glutamate release, which reduces the suppression of the cation channel and hence depolarizes the neuron.

More than 20 types of retinal ganglion cells have been identified in the mouse retina out of which three are known to be direction-selective: ON/OFF direction-selective ganglion cells respond to local motion of both ON and OFF edges. According to its preferred direction, this type of ganglion cell is further divided into four subtypes which roughly

correspond to the four cardinal directions of motion (Oyster and Barlow, 1967). Another type is the ON ganglion cell which only responds to moving ON edges and has larger receptive fields. A third type, the JAM-B retinal ganglion cell, has a peculiar anatomy with asymmetric dendrites which are mostly oriented towards the ventral side (I.-J. Kim *et al.*, 2008). This cell type is activated by motion towards the distal dendritic tips (downwards) and hence, taking into account that the lens inverts the retinal image, it is tuned to upwards motion.

Starbust amacrine cells are key players for the computation of motion cues (Yoshida *et al.*, 2001). These neurons have mostly an inhibitory effect on retinal ganglion cells as well as on bipolar cells. This interaction, in combination with the remaining excitatory signal from bipolar cells, then shapes direction-selective responses in retinal ganglion cells (Euler *et al.*, 2014). Interestingly, starbust amacrine cells themselves are direction-selective (Euler *et al.*, 2002), which shifts the question of how direction-selectivity is computed towards these neurons. It has been shown, at least for OFF starbust amacrine cells, that they receive excitatory input from different types of bipolar cells that have different kinetics and synapse onto distinct dendritic locations (J. S. Kim *et al.*, 2014). Hence, the input structure of starbust amacrine cells resembles the circuit motif expected from a Reichardt-type correlator where signals are excitatory, spatially offset and temporally delayed.

Cortical representation

A general feature in many visual systems is that motion cues are first computed locally and then integrated into a global and more abstract representation of motion (Adelson and Movshon, 1982). Such a hierarchical organization solves, for example, the aperture problem which is that the direction of motion for larger moving patterns cannot be inferred only from local motion cues (Wallach, 1935). After having computed local motion cues, retinal ganglion cells project into different areas of the brain. In mammals, this is mainly the lateral geniculate nucleus (LGN) which forms a major relay station on the way towards higher visual centers (Huberman *et al.*, 2009).

Many neurons in primary visual cortex (V1) are orientation- and direction-selective and can be grouped according to their receptive field properties into simple cells and complex cells (Hubel and Wiesel, 1962). It is not well understood how direction-selective responses arise in these cells but it is likely that direction-selectivity is both computed de novo within the intracortical circuitry (S.-H. Lee *et al.*, 2012; Livingstone, 1998) as well as inherited from retinal ganglion cells (Cruz-Martín *et al.*, 2014). Direction-selective responses from V1 are further transmitted to higher visual areas, such as the middle temporal visual area (area MT) (Born and Bradley, 2005).

Thus, neurons in area MT inherit parts of the response properties from V1 neurons (Movshon and Newsome, 1996). Yet, MT neurons can be tuned to more abstract features of directionality such as, for example, motion coherence within clouds of randomly moving dots (Newsome *et al.*, 1989). Moreover, when stimulated with superimposed gratings moving in different directions (plaids), some MT neurons respond to the movement of either grating and some to the movement of the resulting plaid pattern (Rust *et al.*, 2006). Area MT was shown to be important for motion vision in humans: A patient with lesions in area MT (the "motion-blind" patient) had severe deficits in several visual motion-related tasks but was not entirely blind

(Baker *et al.*, 1991; Hess *et al.*, 1989; Zihl *et al.*, 1983). The medial superior temporal area (area MST) receives most of its inputs from area MT (Komatsu and Wurtz, 1988) and contains neurons which are tuned to specific kinds of optic flow fields (Duffy, 1998).

In summary, the mammalian and fly visual systems show large functional and structural similarities: First, visual processing is split into polarity-specific pathways which remain separate until the computation of direction-selective responses is finalized. Second, mammals and flies use temporally delayed and spatially separated signals in order to compute direction-selective responses. Third, a hierarchical organization is evident where local motion cues are integrated into global ones. These astonishing analogies speak in favor of convergent evolution, namely that the solutions which were found independently by mammals and flies seem to be optimal for motion processing.

Differences

However, implementation details differ. For example, fly photoreceptors depolarize upon illumination. As they use histamine, an inhibitory neurotransmitter, this leads to hyperpolarization of lamina cells. Lobula plate tangential cells are equipped with complex receptive fields even though they are just one synapse away from T4 and T5 neurons. This indicates that the fly visual system does not seem to require intermediate motion processing. Many of the questions which have been tackled in the mammalian retina remain unsolved in the fly. For example, it is currently unclear how neurotransmitter systems of lamina neurons and receptors in postsynaptic cells interact in order to establish functional polarity-specific pathways. T4 and T5 neurons are considered to be the first neurons in the fly visual system which are direction-selective and can therefore be seen as analogues of mammalian starbust amacrine cells. It would be interesting to investigate in detail whether similar spatial and temporal interactions occur on the dendrites of T4 and T5 as have been found for their retinal counterparts (J. S. Kim *et al.*, 2014).

5.3 OBJECT FIXATION

In order to track or fixate an object, flies must determine the position of the object in the environment and its direction of motion. This is a challenging task when the object is located on a patterned background as any turning maneuver towards the object creates large-field optic flow in the opposite direction. This, in turn, stimulates an optomotor response away from the object and would therefore prevent object fixation. On the other hand, not every object should be used for orientation or tracking because this would mean that the fly would constantly collide with any object in its surround. Hence, in order to generate an appropriate behavioral response, the fly visual system must effectively separate features of the object from the background (Trischler *et al.*, 2010).

Parallel pathways

Given the complexity of such a computation, it has long been a matter of debate to what extent optomotor behavior and fixation response are mediated by different pathways in the visual system of flies and how such systems would interact. Mutant *Drosophilae* in which the lobula plate was

absent or significantly reduced in size showed a severe reduction in their optomotor response but still performed well in bar tracking experiments (Bausenwein *et al.*, 1986; Heisenberg *et al.*, 1978). Thus, a motion vision-independent pathway can mediate the behavior. Similar conclusions were drawn from experiments with *Musca* in which lobula plate tangential cells were unilaterally laser-ablated (Geiger and Nässel, 1981). Further evidence for separate pathways were derived from behavioral experiments (Aptekar *et al.*, 2012; Fox *et al.*, 2014; Fox and Frye, 2014): Tethered flying *Drosophilae* were stimulated with randomly moving figures on randomly moving backgrounds. Via a reverse-correlation approach, it was found that the temporal dynamics of the fly turning tendency were different for the two kinds of visual stimuli.

Results from studies with mutated flies or laser ablations should be taken with caution. It is possible, for example, that brain structures were changed which were not meant to be altered, that the desired structures were incompletely affected or that compensatory mechanisms take place during development. In order to properly test the hypothesis of different pathways for the optomotor and fixation response, it is required to perform clean genetic blocking experiments combined with a thorough exploration of behavior.

In this study we used the Gal4-UAS system to silence the output of T4 and T5 neurons via temperature-sensitive shibire. This allowed us to raise flies at room temperature with an intact neuronal circuit. At a desired time point during the experiment lobula plate tangential cells could then be rendered motion-insensitive by increasing the temperature. Even though these flies were completely blind to motion of large-field gratings and elongated vertical bars, they still performed well in closed-loop bar fixation experiments. Hence, this finding provides clean evidence for the existence of a separate visual pathway which can mediate bar fixation but is independent of motion processing via T4 and T5. Yet, we have found that the fixation performance of motion-blind flies was significantly reduced compared to control flies. This, in turn, implies that motion-processing via T4 and T5 improves fixation performance.

5.3.1 Mechanism of fixation behavior

The first detailed explorations of the mechanism of bar fixation behavior were performed by Reichardt and Wenking (1969). When the authors stimulated flies with fast flickering stationary bars, they did not observe a bias in the fly's turning tendency. However, when they used bars which oscillated around a certain location flies turned towards the side of the stimulus. The authors concluded that positional information is conveyed by motion detectors which respond in an asymmetric manner rather than by flicker detectors which analyze local luminance change. These findings stimulated the development of an elaborate theoretical framework of bar fixation (Poggio and Reichardt, 1973, 1976; Reichardt, 1973; Reichardt and Poggio, 1976): Two hypothetical complementary systems were introduced, a position system which calculates the position of the bar and a motion system which analyzes its motion. A superposition of the two systems along with noise predicted closed-loop fixation behavior with one or multiple bars.

Flicker system and motion asymmetry

However, it remained controversial whether the calculation of the positional cues would in fact depend on asymmetrically tuned motion detectors. By using bars which flickered more slowly and for longer durations, Pick (1974) discovered that such stimuli can induce a directed turning response. Hence, information about position could be conveyed by flicker detectors and might not require motion processing. Moreover, Pick (1976) also found that responses to flickering stripes did combine linearly when two neighboring ommatidia were stimulated simultaneously and postulated an important role for lateral interactions. Yet, it was noted by Wehrhahn and Hausen (1980) that the turning response to flickering bars was only visible when stimulating the fly for several minutes and that such time scales are orders of magnitude away from the ones which are required for object fixation under realistic conditions. In order to test attractiveness to flicker on shorter time scales, the authors stimulated flies with gratings which unilaterally moved into different directions. Even though any kind of motion contains temporal flicker, upwards and downwards motion did not induce an attraction to the side of the stimulus. In contrast, motion from front to back resulted in much stronger turning responses than motion from back to front. These results indicated that the flicker components are negligible and spoke in favor of the originally proposed asymmetric motion processing mechanism.

Our investigation revealed strong, robust and immediate responses to flicker in both control as well as in T4/T5 block flies. Whenever a non-moving elongated vertical bar darkened or brightened, flies turned towards its location. Varying the position of the stimulus revealed that response strength was highest for positions around 60° in azimuth and declined towards the frontal and distal visual field. Interestingly, the resulting sensitivity profile was very similar to the ones which have been described in former characterizations of the positional response to oscillating and flickering bars (Pick, 1974; Poggio and Reichardt, 1973). In order to test for asymmetry in the motion system, we used moving bars which were visible only within a narrow window. Additionally, we approximated the flicker component of motion stimuli by quickly darkening and brightening the entire window. We found that T4/T5 block flies responded with exactly the same turning dynamics towards the location of the stimulus irrespective of whether we showed motion or flicker. In contrast, control flies responded much stronger to front-to-back than to back-to-front motion, which could not be explained by a superposition of a motion-sensitive and a flicker-sensitive visual subsystem. We concluded that the motion response is indeed asymmetric. Hence, our findings implicate that positional cues can be computed via alternative mechanisms within a flicker-sensitive motion-independent subsystem and within an asymmetric motion system. This means that during closed-loop bar fixation experiments both systems analyze different features of the visual stimulus but converge at the level of behavioral output (Fig. 7).

Our findings also indicate that care should be taken when searching for the neuronal pathways underlying fixation behavior. Blocking parts of the visual system might affect processing of only particular features of the stimulus. Silencing T4 and T5, for examples, abolished motion computation but flies could still use the flicker-sensitive system for bar fixation. Conversely, if one would silence the flicker-sensitive pathway only, flies would be expected to still perform well in the behavior because they still have their asymmetric motion system. Thus, each system can realize fixation behav-

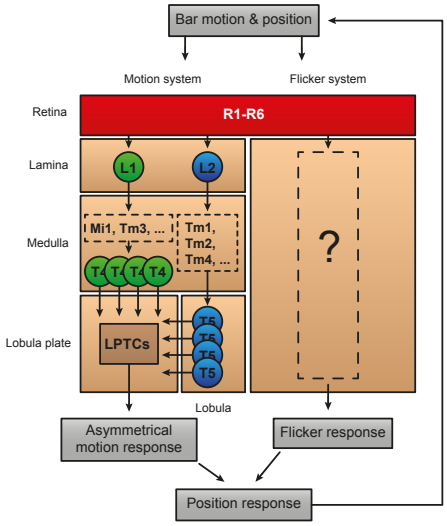

Figure 7: Schematic of bar fixation mechanism. During bar fixation, the stimulus has a motion and a flicker component. Bar motion is analyzed by the well-studied L1 and L2 pathways of the motion system. However, the behavioral response is asymmetric, compensating local motion from front to back more strongly than from back to front. This, on average, produces a turning bias. The other system, a flicker-sensitive parallel subsystem analyzes the flicker component of the bar. Whenever local flicker is detected, it creates a turning spike towards that location. Hence, both systems together induce a position response towards the bar, which moves it to the frontal visual field.

ior on its own and one would potentially miss important phenotypes in a screen for bar fixation. Hence, it is preferable to work with stimuli that contain fewer visual features, such as, for example, flickering bars, or explore bar fixation performance when blocking candidate neurons simultaneously with silencing T4 and T5.

5.3.2 Potential implementation of the position system

In order to model the flicker-sensitive system, we calculated the squared high-pass-filtered signal from the photoreceptors and determined the one with maximal response. The asymmetric motion system was modeled by using standard Reichardt detectors whose outputs were multiplied with 0.5 whenever negative which corresponds to back-to-front motion. Both systems together quantitatively reproduced our open-loop and closed-loop experiments with control and motion-blind flies.

Flicker-sensitive system

Biophysically, the squaring operation of the flicker-sensitive system may be approximated by summation of neuronal responses after rectification within the ON and OFF pathways. It is very likely that the flicker-sensitive system is mediated via circuits postsynpatic to R1–R6 because blocking these neurons abolishes orientation behavior towards bars and edges (Rister *et al.*, 2007; Y. Zhou *et al.*, 2012). Except for this finding, virtually nothing is known about its potential pathways. Rister *et al.* (2007) also found that blocking L1 and L2 leaves some residual fixation performance. However, it is known today that the visual pathway which starts at L3 converges onto T5 (Shinomiya *et al.*, 2014). Thus, it remains unclear whether the signal from L3 feeds into the flicker-sensitive system or into the asymmetric motion system. The determination of the maximum signal in our model could be implemented by a network of cells with recurrent inhibitory connections which establish a winner-take-all mechanism. However, whether such strategies are used in the fly brain remains speculative (Seeds *et al.*, 2014).

Asymmetric motion system

The asymmetry in the motion system could be implemented in various ways. First, the two types of horizontally-tuned T4 and T5 neurons could

respond with different amplitudes for front-to-back and back-to-front motion. However, our two-photon imaging data suggest that this seems not to be the case. Second, it could be due to an asymmetry in the HS cell voltage response which is indeed stronger for motion in preferred direction (ipsilateral front-to-back) than for motion in null direction (ipsilateral back-to-front). However, while it is known that HS cell depolarization induces turning in the direction of the cell's preferred direction (Haikala *et al.*, 2013), it remains unclear whether hyperpolarization has the opposite effect. It could well be that only depolarization elicits a behavioral response. Instead, other types of neurons, such as *Calliphora* H1, are known to be excited by ipsilateral back-to-front motion (Borst and Haag, 2002; Eckert, 1980). These cells project into the other hemisphere where they activate contralateral HS cells which, in turn, initiate a turning response in the direction of motion. Hence, a motion asymmetry could simply be implemented by having different cellular dynamics in H1 and HS cells, for example, or by using a weak synapse between H1 and HS. Third, small field-tuned object detection neurons have been identified in the lobula plate of larger fly species (Egelhaaf, 1985b; Nordström and O'Carroll, 2006; O'Carroll, 1993). These neurons might be well suited to bias the directional response to bar motion but it is not known whether they exist in *Drosophila*. Moreover, such cells cannot explain the asymmetric responses which have been found for larger patches of motion (Wehrhahn and Hausen, 1980).

5.3.3 Flicker responses in tangential cells

We have found that an unknown flicker-sensitive visual pathway which can mediate fixation behavior diverges before T4 and T5. However, we cannot fully exclude that it enters the lobula plate. Various cell types other than T4 and T5 project from the medulla or lobula into the lobula plate and could convey flicker signals (Fischbach and Dittrich, 1989). Indeed, it was found that lobula plate tangential cells respond to ON and OFF full-field flicker even when T4 and T5 neurons were silenced (Schnell *et al.*, 2012). Given their sufficiency for behavior this should induce a behavioral response towards the side of the flicker. However, it seems unlikely that such flicker responses are relevant for the flicker-sensitive behaviors we observe. In our behavioral experiments we used elongated bars which slowly changed their luminance and observed strong turning responses towards the stimulus. However, in electrophysiological experiments we found that HS and VS cell voltage responses to such stimuli were negligible. Nevertheless, it is critical to further characterize the flicker responses in lobula plate tangential cells because an exploration of the underlying T4/T5-independent pathways might improve our understanding of how motion cues are integrated within these neurons.

5.3.4 Role of other brain structures

During the last few decades studies on visual processing in *Drosophila* have mainly focused on the neuronal circuits going from lamina to lobula plate. Other brain structures have received much less attention even though activity labeling studies by Bausenwein *et al.* (1994) identified various regions which are active during visual orientation. For example, closed-loop bar fix-

ation experiments revealed strong labeling in the central brain and in certain layers of the lobula. Some lobula projection neurons have recently been associated with the processing of higher-order motion cues. Yet, the response properties of these cells are unknown and it remains speculative whether they play a role during fixation behavior (Zhang *et al.*, 2013). Moreover, ring neurons in the ellipsoid body of the central complex were shown to respond in a retinotopic manner to the position of moving bars (Seelig and Jayaraman, 2013) and seem to be needed for spatial orientation behavior (Neuser *et al.*, 2008; Ofstad *et al.*, 2011; Xiong *et al.*, 2010). However, it is unknown how these cells acquire their response properties by pooling signals from the visual system.

5.3.5 Comparison to other organisms

Tracking an object in the environment is not only important for fies but also for primates and many other vertebrates (Land, 1999). Following quickly moving objects such as, for example, the ball during a baseball game is challenging as it requires fast visual processing and extrapolation of the object's flight path (McBeath *et al.*, 1995). Here, tracking responses of the eye are of particular importance because they allow us to keep the image of the moving object in the foveal region of the retina where acuity is highest.

Eye tracking experiments

Eye tracking experiments are technically simple and free of many complications in other motor systems and have thus been performed in humans and monkeys for more than a century. The first attempts to systematically study human eye movements in response to visual stimuli were done by Dodge (1903) who discovered several types of slow and fast eye movements. In principle, responses can be grouped into two main categories, the optokinetic nystagmus and pursuit (Masson and Perrinet, 2012). The optokinetic nystagmus is a reflexive following movement of the eyes in response to large-field moving patterns which function is to stabilize the image on the retina. Pursuit responses on the other hand can be voluntary and lead to tracking of small objects. If such an object is moving slowly (up to $40\,^\circ\,s^{-1}$), pursuit is characterized by a smooth following trajectory. However, when the object moves faster, the eye cannot keep up with the velocity any more and responses are interleaved with rapid jumps of the eye, so-called catch-up saccades, towards the position of the object. Moreover, saccades can also be elicited by non-moving stationary and flickering objects. While smooth pursuit eye movements correlate well with the velocity of the object, the amplitude of saccades can be described as a function of object distance to the fovea.

Motion and position pathways

Due and to these inherently different properties of smooth pursuit and saccadic eye movements, it has long been thought that both behaviors are controlled by two different systems, a motion and a position pathway (Orban de Xivry and Lefèvre, 2007). As the motion pathway analyzes only the velocity of the object, it accumulates positional error. This is especially problematic if the object accelerates or moves in an unpredictable manner. Instead, the position pathway rapidly directs the eye towards the position of the object and thereby aids the motion pathway in realizing smooth object tracking.

Indeed, a neuronal representation of such pathways was found in the brain of monkeys: Newsome *et al.* (1985) did an experiment where they lesioned area MT, the center of global motion processing, and found that smooth pursuit responses and catch-up saccades were severely impaired. Yet, saccades to stationary objects remained intact, which speaks in favor of the existence of a MT-independent neuronal circuit which can analyze positional cues. Catch-up saccades need to account for relative motion of the eye with respect to the object (de Brouwer *et al.*, 2001). Hence, this kind of following behavior requires motion processing in order to be accurate and was therefore impaired in Newsome's experiments. In contrast, the superior colliculus (SC) seems to be part of the position pathway. Recording from several sites in this brain area revealed neuronal activity which was coupled to the positional error of the moving object during tracking experiments (Keller *et al.*, 1996) and electrical stimulation could even trigger saccades (Missal *et al.*, 1996).

In summary, research in humans and monkeys has revealed surprisingly similar strategies as found for *Drosophila*: two different neuronal pathways, one for motion and the other for position calculation which converge at the level of behavior in order to shape smooth object tracking.

5.4 COURSE STABILIZATION IN ROBOTS

Reliable and fast course control is essential for small flying systems because without it, air turbulence or the slightest asymmetry during a flight maneuver would inevitably lead to a crash. This is true for flies as well as for robots, such as micro aerial vehicles (MAVs). However, the small size of flies and MAVs require their control systems to be as light-weight and energy-efficient as possible. Evolution has solved this problem for flies by equipping them with an intricate network of VS cells which are known to be well-suited for estimation of the rotational axes during flight. Hence, gaining inspiration from the visual system of flies might help engineers to design better course control systems for robots. We have presented such a fly-inspired approach by implementing the lobula plate VS cell network on a field programmable gate array (FPGA). When testing the system in a virtual environment, it showed reliable estimation of the axes of rotation and should therefore be well-suited for on-board use in MAVs.

However, a flying robot would require further control elements to be fully operational. In order not to bump into walls or other obstacles, one should implement an avoidance response system. Moreover, goal-directed flight would require the implementation of an object tracking system. The addition of such systems in parallel to the course stabilization strategy would then render the MAV suitable for autonomous surveillance even in complex environments. Here, again, insects might be an inspiration: The lobula giant movement detector of the locust performs essential computations for the avoidance response (Fotowat and Gabbiani, 2011). It can be modeled with an array of Reichardt detectors and has indeed been implemented in robots, resulting in successful obstacle avoidance (Bermúdez i Badia *et al.*, 2007; Bermúdez i Badia and Verschure, 2004; Harrison, 2005). On the other hand, object tracking algorithms for MAVs have so far largely relied on com-

putationally expensive algorithms (Azrad *et al.*, 2009; Bachrach *et al.*, 2009). This requires wireless transmission and image processing on a ground station, which limits the operational radius of the robot. It would be very interesting to see whether our simple flicker-based model of object tracking could be implemented on an FPGA chip and how well it would work in more natural environments.

5.5 CONCLUSION AND OUTLOOK

How do neural circuits process signals from photoreceptors and arrive at a meaningful representation of the visual surround in order to orchestrate vision-based navigation? In this cumulative thesis, I have presented three published studies which deal with this fascinating question. We found that interneurons T4 and T5 in the visual system of *Drosophila* play a pivotal role for motion vision. We found that they are direction-selective, fall into contrast polarity-specific subgroups, and that they are necessary for the optomotor response. Moreover, we also found that motion vision is not the only cue for visual course control and that flies can perform object fixation or landmark-based orientation without T4 and T5 neurons. Thus, multiple separate pathways exist which analyze different features of the outside world but converge on the level of behavior.

Several open questions remain. One of them is how T4 and T5 neurons become direction-selective. As the known presynaptic partners of these cells are not direction-selective, the essential computations are likely to occur on the dendrites of T4 and T5 neurons. It is suggestive that the mechanism for this involves differentially delayed input lines, distinct receptor types and kinetics, or both. Moreover, such signals have to be integrated in a nonlinear fashion within T4 and T5 cells. The study of each of these points requires a combination of detailed anatomical and functional connectivity analyses, pharmacology, receptor profiling and more imaging. In principle, all necessary tools exist for *Drosophila* in order to tackle this, and thus, we will probably soon witness the answer to this question.

Another open question is how objects are segregated from the background. Here, it remains unclear to what extent lateral or feedback connections in the medulla play a role and whether lobula plate-intrinsic circuits further shape object-specific tuning responses. To this end, it will be required to better characterize receptive fields of medulla neurons and to continue exploring the neuronal network of the lobula plate.

Finally, it remains unclear which computations are performed by the flicker-sensitive pathway and which neuronal substrate is involved. Here, further behavioral characterization of flicker responses should shed more light on the mechanisms of this behavior. Additionally, systematic silencing of lamina and medulla neurons might produce specific behavioral phenotypes and help identify key players in this circuit. Once such neurons are found, they can be further characterized with two-photon imaging or electrophysiology.

Eventually, it will be required to investigate in detail where and how the neuronal pathways for motion and flicker computation converge and how this information is read out by the fly motor control centers. Having this, would pave the way towards a complete picture of the stimulus-response loop of fly visual course control, an important goal in systems neuroscience.

BIBLIOGRAPHY

Adelson, E. H. and Bergen, J. R. (1985), "Spatiotemporal energy models for the perception of motion." *Journal of the Optical Society of America A*, vol. 2 (2), 284-99.

Adelson, E. H. and Movshon, J. A. (1982), "Phenomenal coherence of moving visual patterns." *Nature*, vol. 300 (5892), 523-5.

Akerboom, J., Chen, T.-W., *et al.* (2012), "Optimization of a GCaMP calcium indicator for neural activity imaging." *Journal of Neuroscience*, vol. 32 (40), 13819-40.

Alderson, T. (1965), "Chemically induced delayed germinal mutation in *Drosophila*." *Nature*, vol. 207 (993), 164-7.

Aptekar, J. W. and Frye, M. A. (2013), "Higher-order figure discrimination in fly and human vision." *Current Biology*, vol. 23 (16), R694-700.

Aptekar, J. W., Shoemaker, P. A., and Frye, M. A. (2012), "Figure tracking by flies is supported by parallel visual streams." *Current Biology*, vol. 22 (6), 482-7.

Arnett, D. W. (1972), "Spatial and temporal integration properties of units in first optic ganglion of dipterans." Vol. 35 (4), 429-44.

Autrum, H. (1950), "Die Belichtungspotentiale und das Sehen der Insekten (Untersuchungen an *Calliphora* und *Dixippus*)." *Zeitschrift für vergleichende Physiologie*, vol. 32 (3), 176-227.

Azrad, S., Kendoul, F., Perbrianti, D., and Nonami, K. (2009), "Visual servoing of an autonomous Micro Air Vehicle for ground object tracking." In *Proceedings of the 2009 IEEE/RSJ International Conference on Intelligent Robots and Systems*, St. Louis, MO, 5321-6.

Bachrach, A., Geramifard, A., Gurdan, D., He, R., Prentice, S., Stumpf, J., and Roy, N. (2009), "Co-ordinated tracking and planning using air and ground vehicles." In *Experimental Robotics*, ed. by B. Siciliano, O. Khatib, F. Groen, V. Kumar, and G. J. Pappas, Springer, Berlin, Heidelberg, 137-46.

Bahl, A., Ammer, G., Schilling, T., and Borst, A. (2013), "Object tracking in motion-blind flies." *Nature Neuroscience*, vol. 16 (6), 730-8.

Baines, R. A., Uhler, J. P., Thompson, A., Sweeney, S. T., and Bate, M. (2001), "Altered electrical properties in *Drosophila* neurons developing without synaptic transmission." *Journal of Neuroscience*, vol. 21 (5), 1523-31.

Baker, C. L., Hess, R. F., and Zihl, J. (1991), "Residual motion perception in a "motion-blind" patient, assessed with limited-lifetime random dot stimuli." *Journal of Neuroscience*, vol. 11 (2), 454-61.

Barlow, H. B. and Levick, W. R. (1965), "The mechanism of directionally selective units in rabbit's retina." *Journal of Physiology-London*, vol. 178 (3), 477-504.

Bausenwein, B., Dittrich, A. P., and Fischbach, K. F. (1992), "The optic lobe of *Drosophila melanogaster*. II. Sorting of retinotopic pathways in the medulla." *Cell and Tissue Research*, vol. 267 (1), 17-28.

Bausenwein, B. and Fischbach, K. F. (1992), "Activity labeling patterns in the medulla of *Drosophila melanogaster* caused by motion stimuli." *Cell and Tissue Research*, vol. 270 (1), 25-35.

Bausenwein, B., Müller, N. R., and Heisenberg, M. (1994), "Behavior-dependent activity labeling in the central complex of *Drosophila* during controlled visual stimulation." *Journal of Comparative Neurology*, vol. 340 (2), 255-68.

Bausenwein, B., Wolf, R., and Heisenberg, M. (1986), "Genetic dissection of optomotor behavior in *Drosophila melanogaster*. Studies on wild-type and the mutant *optomotor-blind*^{H31}." *Journal of Neurogenetics*, vol. 3 (2), 87-109.

Behnia, R., Clark, D. A., Carter, A. G., Clandinin, T. R., and Desplan, C. (2014), "Processing properties of ON and OFF pathways for *Drosophila* motion detection." *Nature*, vol. 512 (7515), 427-30.

Benzer, S. (1967), "Behavioral mutants of *Drosophila* isolated by countercurrent distribution." *Proceedings of the National Academy of Sciences of the United States of America*, vol. 58 (3), 1112-9.

Bermúdez i Badia, S., Pyk, P., and Verschure, P. F. M. J. (2007), "A fly-locust based neuronal control system applied to an unmanned aerial vehicle: the invertebrate neuronal principles for course stabilization, altitude control and collision avoidance." *The International Journal of Robotics Research*, vol. 26 (7), 759-72.

Bermúdez i Badia, S. and Verschure, P. F. M. J. (2004), "A collision avoidance model based on the lobula giant movement detector (LGMD) neuron of the locust." In *Proceedings of the 2004 IEEE International Joint Conference on Neural Networks*, Budapest, 1757-61.

Berndt, A., Lee, S. Y., Ramakrishnan, C., and Deisseroth, K. (2014), "Structure-guided transformation of channelrhodopsin into a light-activated chloride channel." *Science*, vol. 344 (6182), 420-4.

Berndt, A., Yizhar, O., Gunaydin, L. A., Hegemann, P., and Deisseroth, K. (2009), "Bi-stable neural state switches." *Nature Neuroscience*, vol. 12 (2), 229-34.

Beyeler, A., Zufferey, J. C., and Floreano, D. (2009), "optiPilot: control of take-off and landing using optic flow." In *Proceedings of the 2009 European Micro Air Vehicle Conference and Competition*, Delft, 1-8.

Blondeau, J. and Heisenberg, M. (1982), "The three-dimensional optomotor torque system of *Drosophila melanogaster*. Studies on wildtype and

the mutant *optomotor-blind*^{H31}." *Journal of Comparative Physiology A*, vol. 145 (3), 321-9.

Bloomquist, B. T., Shortridge, R. D., *et al.* (1988), "Isolation of a putative phospholipase C gene of *Drosophila*, *norpA*, and its role in phototransduction." *Cell*, vol. 54 (5), 723-33.

Born, R. T. and Bradley, D. C. (2005), "Structure and function of visual area MT." *Annual Review of Neuroscience*, vol. 28 (1), 157-89.

Borst, A. (1986), "Time course of the houseflies' landing response." *Biological Cybernetics*, vol. 54 (6), 379-83.

Borst, A. (2009), "*Drosophila*'s view on insect vision." *Current Biology*, vol. 19 (1), R36-R47.

Borst, A. (2013), "Neurobiology of movement-sensitive behavior in flies." In *New Visual Neurosciences*, ed. by J. S. Werner and L. M. Chalupa, MIT Press, Cambridge, MA, 1191-205.

Borst, A. and Bahde, S. (1986), "What kind of movement detector is triggering the landing response of the housefly?" *Biological Cybernetics*, vol. 55 (1), 59-69.

Borst, A. and Euler, T. (2011), "Seeing things in motion: Models, circuits, and mechanisms." *Neuron*, vol. 71 (6), 974-94.

Borst, A. and Haag, J. (2002), "Neural networks in the cockpit of the fly." *Journal of Comparative Physiology A*, vol. 188 (6), 419-37.

Borst, A., Haag, J., and Reiff, D. F. (2010), "Fly motion vision." *Annual Review of Neuroscience*, vol. 33 (1), 49-70.

Borst, A. and Weber, F. (2011), "Neural action fields for optic flow based navigation: A simulation study of the fly lobula plate network." *PLoS ONE*, vol. 6 (1), 1-19.

Boyden, E. S., Zhang, F., Bamberg, E., Nagel, G., and Deisseroth, K. (2005), "Millisecond-timescale, genetically targeted optical control of neural activity." *Nature Neuroscience*, vol. 8 (9), 1263-8.

Braitenberg, V. (1967), "Patterns of projection in the visual system of the fly. I. Retina-lamina projections." *Experimental Brain Research*, vol. 3 (3), 271-98.

Braitenberg, V. (1986), *Vehicles: Experiments in Synthetic Psychology*, MIT press, Cambridge, London.

Brand, A. H. and Perrimon, N. (1993), "Targeted gene expression as a means of altering cell fates and generating dominant phenotypes." *Development*, vol. 118 (2), 401-15.

Branson, K., Robie, A. A., Bender, J., Perona, P., and Dickinson, M. H. (2009), "High-throughput ethomics in large groups of *Drosophila*." *Nature Methods*, vol. 6 (6), 451-7.

Buchner, E. (1971), *Dunkelanregung des stationären Flugs der Fruchtfliege Drosophila*. PhD thesis, University of Tübingen, Tübingen, Germany.

Buchner, E. (1976), "Elementary movement detectors in an insect visual system." *Biological Cybernetics*, vol. 24 (2), 85-101.

Buchner, E. (1984), "Behavioural analysis of spatial vision in insects." In *Photoreception and Vision in Invertebrates*, ed. by M. A. Ali, Plenum Press, 561-621.

Buchner, E., Buchner, S., and Bülthoff, I. (1984), "Deoxyglucose mapping of nervous activity induced in *Drosophila* brain by visual movement. I. Wildtype." *Journal of Comparative Physiology A*, vol. 155 (4), 471-83.

Buchner, E. and Wu, C.-F. (2009), "Editorial: *Drosophila* neurogenetics - The Heisenberg impact. Photo gallary." *Journal of Neurogenetics*, vol. 23 (1), 127-35.

Bülthoff, H. (1982), "*Drosophila* mutants disturbed in visual orientation. II. mutants affected in movement and position computation." *Biological Cybernetics*, vol. 45 (1), 71-7.

Bülthoff, H., Götz, K. G., and Herre, M. (1982), "Recurrent inversion of visual orientation in the walking fly, *Drosophila melanogaster.*" *Journal of Comparative Physiology A*, vol. 148 (4), 471-81.

Cajal, S. R. and Sánchez, D. (1915), "Contribución al conocimiento de los centros nerviosos de los insectos: Parte I, Retina y centros ópticos." *Trab Lab Invest Bil Univ Madr*, vol. 13, 1-168.

Cao, G., Platisa, J., Pieribone, V. A., Raccuglia, D., Kunst, M., and Nitabach, M. N. (2013), "Genetically targeted optical electrophysiology in intact neural circuits." *Cell*, vol. 154 (4), 904-13.

Card, G. and Dickinson, M. H. (2008), "Visually mediated motor planning in the escape response of *Drosophila*." *Current Biology*, vol. 18 (17), 1300-7.

Carpenter, F. W. (1905), "The reactions of the pomace fly (*Drosophila ampelophila* Loew) to light gravity, and mechanical stimulation." *American Naturalist*, vol. 39 (459), 157-71.

Chahl, J. S. and Srinivasan, M. V. (1996), "Visual computation of egomotion using an image interpolation technique." *Biological Cybernetics*, vol. 74 (5), 405-11.

Chahl, J. S., Srinivasan, M. V., and Zhang, S.-W. (2004), "Landing strategies in honeybees and applications to uninhabited airborne vehicles." *The International Journal of Robotics Research*, vol. 23 (2), 101-10.

Chalfie, M., Tu, Y., Euskirchen, G., Ward, W. W., and Prasher, D. C. (1994), "Green fluorescent protein as a marker for gene expression." *Science*, vol. 263 (5148), 802-5.

Chen, T.-W., Wardill, T. J., *et al.* (2013), "Ultrasensitive fluorescent proteins for imaging neuronal activity." *Nature*, vol. 499 (7458), 295-300.

Chiappe, M. E., Seelig, J. D., Reiser, M. B., and Jayaraman, V. (2010), "Walking modulates speed sensitivity in *Drosophila* motion vision." *Current Biology*, vol. 20 (16), 1470-5.

Clark, D. A., Bursztyn, L., Horowitz, M. A., Schnitzer, M. J., and Clandinin, T. R. (2011), "Defining the computational structure of the motion detector in *Drosophila*." *Neuron*, vol. 70 (6), 1165-77.

Clark, D. A., Fitzgerald, J. E., Ales, J. M., Gohl, D. M., Silies, M. A., Norcia, A. M., and Clandinin, T. R. (2014), "Flies and humans share a motion estimation strategy that exploits natural scene statistics." *Nature Neuroscience*, vol. 17 (2), 296-303.

Cruz-Martín, A., El-Danaf, R. N., *et al.* (2014), "A dedicated circuit links direction-selective retinal ganglion cells to the primary visual cortex." *Nature*, vol. 507 (7492), 358-61.

De Brouwer, S., Missal, M., and Lefevre, P. (2001), "Role of retinal slip in the prediction of target motion during smooth and saccadic pursuit." Vol. 86 (2), 550-8.

De Croon, G. C. H. E., de Clercq, K. M. E., Ruijsink, R., Remes, B., and de Wagter, C. (2009), "Design, aerodynamics, and vision-based control of the DelFly." *International Journal of Micro Air Vehicles*, vol. 1 (2), 71-97.

De Vries, S. E. J. and Clandinin, T. R. (2012), "Loom-sensitive neurons link computation to action in the *Drosophila* visual system." *Current Biology*, vol. 22 (5), 353-62.

Denk, W., Strickler, J. H., and Webb, W. W. (1990), "Two-photon laser scanning fluorescence microscopy." *Science*, vol. 248 (4951), 73-6.

Denk, W. and Horstmann, H. (2004), "Serial block-face scanning electron microscopy to reconstruct three-dimensional tissue nanostructure." *PLoS Biology*, vol. 2 (11), 1900-9.

Dickinson, M. H. (2014), "Death Valley, *Drosophila*, and the Devonian toolkit." *Annual Review of Entomology*, vol. 59 (1), 51-72.

Dickson, B. J. (2008), "Wired for sex: the neurobiology of *Drosophila* mating decisions." *Science*, vol. 322 (5903), 904-9.

Dodge, R. (1903), "Five types of eye movement in the horizontal meridian plane of the field of regard." *American Journal of Physiology*, vol. 8, 307-29.

Douglass, J. K. and Strausfeld, N. J. (1996), "Visual motion-detection circuits in flies: parallel direction- and non-direction-sensitive pathways between the medulla and lobula plate." *Journal of Neuroscience*, vol. 16 (15), 4551-62.

Duffy, C. J. (1998), "MST neurons respond to optic flow and translational movement." Vol. 80 (4), 1816-27.

Eckert, H. (1980), "Functional properties of the H1-neurone in the third optic ganglion of the blowfly, *Phaenicia*." *Journal of Comparative Physiology A*, vol. 135 (1), 29-39.

Egelhaaf, M. (1985a), "On the neuronal basis of figure-ground discrimination by relative motion in the visual system of the fly. I. Behavioural constraints imposed on the neuronal network and the role of the optomotor system." *Biological Cybernetics*, vol. 52 (2), 123-40.

Egelhaaf, M. (1985b), "On the neuronal basis of figure-ground discrimination by relative motion in the visual system of the fly. II. Figure-detection cells, a new class of visual interneurones." *Biological Cybernetics*, vol. 52 (2), 195-209.

Egelhaaf, M. (1985c), "On the neuronal basis of figure-ground discrimination by relative motion in the visual system of the fly. III. Possible input circuitries and behavioural significance of the FD-cells." *Biological Cybernetics*, vol. 52 (2), 267-80.

Egelhaaf, M. and Borst, A. (1989), "Transient and steady-state response properties of movement detectors." *Journal of the Optical Society of America A*, vol. 6 (1), 116-27.

Eichner, H., Joesch, M., Schnell, B., Reiff, D. F., and Borst, A. (2011), "Internal structure of the fly elementary motion detector." *Neuron*, vol. 70 (6), 1155-64.

Euler, T., Detwiler, P. B., and Denk, W. (2002), "Directionally selective calcium signals in dendrites of starburst amacrine cells." *Nature*, vol. 418 (6900), 845-52.

Euler, T., Haverkamp, S., Schubert, T., and Baden, T. (2014), "Retinal bipolar cells: elementary building blocks of vision." *Nature Reviews Neuroscience*, vol. 15 (8), 507-19.

Feiler, R., Bjornson, R., *et al.* (1992), "Ectopic expression of ultraviolet-rhodopsins in the blue photoreceptor cells of *Drosophila*: Visual physiology and photochemistry of transgenic animals." *Journal of Neuroscience*, vol. 12 (10), 3862-8.

Fenno, L., Yizhar, O., and Deisseroth, K. (2011), "The development and application of optogenetics." *Annual Review of Neuroscience*, vol. 34, 389-412.

Fermi, G. and Reichardt, W. (1963), "Optomotorische Reaktionen der Fliege *Musca domestica*: Abhängigkeit der Reaktion von der Wellenlänge, der Geschwindigkeit, dem Kontrast und der mittleren Leuchtdichte bewegter periodischer Muster." *Kybernetik*, vol. 2 (1), 15-28.

Fischbach, K. F. and Dittrich, A. (1989), "The optic lobe of *Drosophila melanogaster*. I: A Golgi analysis of wild-type structure." *Cell and Tissue Research*, vol. 258 (3), 441-75.

Fleisch, V. C. and Neuhauss, S. C. F. (2006), "Visual behavior in zebrafish." *Zebrafish*, vol. 3 (2), 191-201.

Flight, M. H. (2013), "Visual system: Mapping motion detection." *Nature Reviews Neuroscience*, vol. 14 (10), 669-9.

Fotowat, H. and Gabbiani, F. (2011), "Collision detection as a model for sensory-motor integration." *Annual Review of Neuroscience*, vol. 34, 1-19.

Fox, J. L., Aptekar, J. W., Zolotova, N. M., Shoemaker, P. A., and Frye, M. A. (2014), "Figure-ground discrimination behavior in *Drosophila*. I. Spatial organization of wing-steering responses." *Journal of Experimental Biology*, vol. 217 (4), 558-69.

Fox, J. L. and Frye, M. A. (2014), "Figure-ground discrimination behavior in *Drosophila*. II. Visual influences on head movement behavior." *Journal of Experimental Biology*, vol. 217 (4), 570-9.

Franceschini, N., Kirschfeld, K., and Minke, B. (1981), "Fluorescence of photoreceptor cells observed in vivo." *Science*, vol. 213 (4513), 1264-7.

Franceschini, N., Riehle, A., and Le Nestour, A. (1989), "Directionally selective motion detection by insect neurons." In *Facets of Vision*, ed. by D. G. Stavenga and R. C. Hardie, Springer, Berlin, Heidelberg, 360-90.

Freifeld, L., Clark, D. A., Schnitzer, M. J., Horowitz, M. A., and Clandinin, T. R. (2013), "GABAergic lateral interactions tune the early stages of visual processing in *Drosophila*." *Neuron*, vol. 78 (6), 1075-89.

Gabbiani, F., Krapp, H. G., Koch, C., and Laurent, G. (2002), "Multiplicative computation in a visual neuron sensitive to looming." *Nature*, vol. 420 (6913), 320-4.

Gao, S., Takemura, S.-Y., *et al.* (2008), "The neural substrate of spectral preference in *Drosophila*." *Neuron*, vol. 60 (2), 328-42.

Garratt, M. A. and Chahl, J. S. (2008), "Vision-based terrain following for an unmanned rotorcraft." *Journal of Field Robotics*, vol. 25 (4-5), 284-301.

Geiger, G. and Nässel, D. (1981), "Visual orientation behaviour of flies after selective laser beam ablation of interneurones." *Nature*, vol. 293 (5831), 398-9.

Gengs, C., Leung, H.-T., *et al.* (2002), "The target of *Drosophila* photoreceptor synaptic transmission is a histamine-gated chloride channel encoded by *ort* (*hclA*)." *The Journal of Biological Chemistry*, vol. 277 (44), 42113-20.

Gilbert, C. (2013), "Brain connectivity: Revealing the fly visual motion circuit." *Current Biology*, vol. 23 (18), R851-3.

Gjorgjieva, J., Sompolinsky, H., and Meister, M. (2014), "Benefits of pathway splitting in sensory coding." *Journal of Neuroscience*, vol. 34 (36), 12127-44.

Golic, K. G. and Lindquist, S. (1989), "The FLP recombinase of yeast catalyzes site-specific recombination in the *Drosophila* genome." *Cell*, vol. 59 (3), 499-509.

Goodman, L. J. (1960), "The landing responses of insects. I. The landing response of the fly, *Lucilia sericata*, and other Calliphorinae." *Journal of Experimental Biology*, vol. 37 (4), 854-78.

Götz, K. G. (1964), "Optomotorische Untersuchung des visuellen Systems einiger Augenmutanten der Fruchtfliege *Drosophila*." *Kybernetik*, vol. 2 (2), 77-92.

Götz, K. G. (1970), "Fractionation of *Drosophila* populations according to optomotor traits." *Journal of Experimental Biology*, vol. 52 (2), 419-36.

Götz, K. G. (1975), "The optomotor equilibrium of the *Drosophila* navigation system." *Journal of Comparative Physiology*, vol. 99 (3), 187-210.

Götz, K. G. (1980), "Visual guidance in *Drosophila*." In *Development and Neurobiology of Drosophila*, ed. by O. Siddiqi, P. Babu, L. M. Hall, and J. C. Hall, Springer, New York, 391-407.

Götz, K. G. (1987), "Course-control, metabolism and wing interference during ultralong tethered flight in *Drosophila melanogaster*." *Journal of Experimental Biology*, vol. 128 (1), 35-46.

Götz, K. G. and Wenking, H. (1973), "Visual control of locomotion in walking fruitfly *Drosophila*." *Journal of Comparative Physiology*, vol. 85 (3), 235-66.

Gradinaru, V., Thompson, K. R., and Deisseroth, K. (2008), "eNpHR: a Natronomonas halorhodopsin enhanced for optogenetic applications." *Brain Cell Biology*, vol. 36 (1-4), 129-39.

Greenspan, R. J. (2008), "The origins of behavioral genetics." *Current Biology*, vol. 18 (5), R192-8.

Grether, M. E., Abrams, J. M., Agapite, J., White, K., and Steller, H. (1995), "The *head involution defective* gene of *Drosophila melanogaster* functions in programmed cell death." *Genes & Development*, vol. 9 (14), 1694-708.

Grzywacz, N. M. and Koch, C. (1987), "Functional properties of models for direction selectivity in the retina." *Synapse*, vol. 1 (5), 417-34.

Haag, J. and Borst, A. (2001), "Recurrent network interactions underlying flow-field selectivity of visual interneurons." *Journal of Neuroscience*, vol. 21 (15), 5685-92.

Haag, J. and Borst, A. (2004), "Neural mechanism underlying complex receptive field properties of motion-sensitive interneurons." *Nature Neuroscience*, vol. 7 (6), 628-34.

Haikala, V., Joesch, M., Borst, A., and Mauss, A. S. (2013), "Optogenetic control of fly optomotor responses." *Journal of Neuroscience*, vol. 33 (34), 13927-34.

Hamada, F. N., Rosenzweig, M., Kang, K., Pulver, S. R., Ghezzi, A., Jegla, T. J., and Garrity, P. A. (2008), "An internal thermal sensor controlling temperature preference in *Drosophila*." *Nature*, vol. 454 (7201), 217-20.

Hardie, R. C. (1989), "A histamine-activated chloride channel involved in neurotransmission at a photoreceptor synapse." *Nature*, vol. 339 (6227), 704-6.

Hardie, R. C. (1991), "Whole-cell recordings of the light-induced current in dissociated *Drosophila* photoreceptors: Evidence for feedback by calcium permeating the light-sensitive channels." *Proceedings: Biological Sciences*, vol. 245 (1314), 203-10.

Hardie, R. C. and Franze, K. (2012), "Photomechanical responses in *Drosophila* photoreceptors." *Science*, vol. 338 (6104), 260-3.

Hardie, R. C. and Raghu, P. (2001), "Visual transduction in *Drosophila*." *Nature*, vol. 413 (6852), 186-93.

Harris, W. A., Stark, W. S., and Walker, J. A. (1976), "Genetic dissection of the photoreceptor system in the compound eye of *Drosophila melanogaster*." *Journal of Physiology-London*, vol. 256 (2), 415-39.

Harrison, R. R. (2005), "A biologically inspired analog IC for visual collision detection," *Circuits and Systems I: Regular Papers, IEEE Transactions on*, vol. 52 (11), 2308-18.

Hassenstein, B. (1951), "Ommatidienraster und afferente Bewegungsintegration." *Zeitschrift für vergleichende Physiologie*, vol. 33 (4), 301-26.

Hassenstein, B. (1991), "Erzählte Erfahrungen I: Der Biologe Bernhard Hassenstein." In *Freiburger Universitätsblätter*, Rombach Verlag, Freiburg, 85-112.

Hassenstein, B. and Reichardt, W. (1956), "Systemtheoretische Analyse der Zeit, Reihenfolgen und Vorzeichenauswertung bei der Bewegungsperzeption des Rüsselkäfers *Chlorophanus*." *Zeitschrift für Naturforschung B*, vol. 11 (9), 513-24.

Hatsopoulos, N., Gabbiani, F., and Laurent, G. (1995), "Elementary computation of object approach by a wide-field visual neuron." *Science*, vol. 270 (5238), 1000-3.

Hausen, K. (1976), "Functional characterization and anatomical identification of motion sensitive neurons in the lobula plate of the blowfly *Calliphora erythrocephala*." *Zeitschrift für Naturforschung C*, vol. 31, 629-33.

Hausen, K. (1982a), "Motion sensitive interneurons in the optomotor system of the fly: I. The horizontal cells: Structure and signals." *Biological Cybernetics*, vol. 45 (2), 143-56.

Hausen, K. (1982b), "Motion sensitive interneurons in the optomotor system of the fly. II. The horizontal cells: Receptive field organization and response characteristics." *Biological Cybernetics*, vol. 46, 67-79.

Heisenberg, M. and Buchner, E. (1977), "Role of retinula cell-types in visual behavior of *Drosophila melanogaster*." *Journal of Comparative Physiology A*, vol. 117 (2), 127-62.

Heisenberg, M. and Götz, K. G. (1975), "The use of mutations for the partial degradation of vision in *Drosophila melanogaster.*" *Journal of Comparative Physiology*, vol. 98 (3), 217-41.

Heisenberg, M. and Wolf, R. (1984), *Vision in Drosophila*, ed. by V. Braitenberg, H. B. Barlow, T. H. Bullock, E. Florey, O. J. Grüsser, and A. Peters, Springer, Berlin, Heidelberg, New York, Tokyo.

Heisenberg, M., Wonneberger, R., and Wolf, R. (1978), "*Optomotor-blind*^{H31}: a *Drosophila* mutant of the lobula plate giant neurons." *Journal of Comparative Physiology A*, vol. 124 (4), 287-96.

Hengstenberg, R. (1982), "Common visual response properties of giant vertical cells in the lobula plate of the blowfly *Calliphora*." *Journal of Comparative Physiology A*, vol. 149 (2), 179-93.

Hengstenberg, R. (1988), "Mechanosensory control of compensatory head roll during flight in the blowfly *Calliphora erythrocephala* Meig." *Journal of Comparative Physiology A*, vol. 163 (2), 151-65.

Hess, R. H., Baker, C. L., and Zihl, J. (1989), "The "motion-blind" patient: low-level spatial and temporal filters." *Journal of Neuroscience*, vol. 9 (5), 1628-40.

Hidalgo, A., Urban, J., and Brand, A. H. (1995), "Targeted ablation of glia disrupts axon tract formation in the *Drosophila* CNS." *Development*, vol. 121 (11), 3703-12.

Hofbauer, A. and Campos-Ortega, J. A. (1990), "Proliferation pattern and early differentiation of the optic lobes in *Drosophila melanogaster.*" *Roux's archives of developmental biology*, vol. 198 (5), 264-74.

Horn, E. (1978), "The mechanism of object fixation and its relation to spontaneous pattern preferences in *Drosophila melanogaster.*" *Biological Cybernetics*, vol. 31 (3), 145-58.

Horn, E. and Wehner, R. (1975), "Mechanism of visual pattern fixation in walking fly, *Drosophila melanogaster*." *Journal of Comparative Physiology*, vol. 101 (1), 39-56.

Hubel, D. H. and Wiesel, T. N. (1962), "Receptive fields, binocular interaction and functional architecture in the cat's visual cortex." *Journal of Physiology-London*, vol. 160, 106-54.

Huberman, A. D., Wei, W., Elstrott, J., Stafford, B. K., Feller, M. B., and Barres, B. A. (2009), "Genetic identification of an On-Off direction-selective retinal ganglion cell subtype reveals a layer-specific subcortical map of posterior motion." *Neuron*, vol. 62 (3), 327-34.

Humbert, J. S. and Hyslop, A. M. (2010), "Bioinspired visuomotor convergence." *IEEE Transactions on Robotics*, vol. 26 (1), 121-30.

Iida, F. (2003), "Biologically inspired visual odometer for navigation of a flying robot." *Robotics and Autonomous Systems*, vol. 44 (3), 201-8.

Inagaki, H. K., Jung, Y., *et al.* (2014), "Optogenetic control of *Drosophila* using a red-shifted channelrhodopsin reveals experience-dependent influences on courtship." *Nature Methods*, vol. 11 (3), 325-32.

Jenett, A., Rubin, G. M., *et al.* (2012), "A GAL4-driver line resource for *Drosophila* neurobiology." *Cell Reports*, vol. 2 (4), 991-1001.

Jennings, B. H. (2011), "*Drosophila* - a versatile model in biology & medicine." *Materials Today*, vol. 14 (5), 190-5.

Joesch, M., Plett, J., Borst, A., and Reiff, D. F. (2008), "Response properties of motion-sensitive visual interneurons in the lobula plate of *Drosophila melanogaster.*" *Current Biology*, vol. 18 (5), 368-74.

Joesch, M., Schnell, B., Raghu, S. V., Reiff, D. F., and Borst, A. (2010), "ON and OFF pathways in *Drosophila* motion vision." *Nature*, vol. 468 (7321), 300-4.

Joesch, M., Weber, F., Eichner, H., and Borst, A. (2013), "Functional specialization of parallel motion detection circuits in the fly." *Journal of Neuroscience*, vol. 33 (3), 902-5.

Jung, S. N., Borst, A., and Haag, J. (2011), "Flight activity alters velocity tuning of fly motion-sensitive neurons." *Journal of Neuroscience*, vol. 31 (25), 9231-7.

Katsov, A. Y. and Clandinin, T. R. (2008), "Motion processing streams in *Drosophila* are behaviorally specialized." *Neuron*, vol. 59 (2), 322-35.

Keller, E. L., Gandhi, N. J., and Weir, P. T. (1996), "Discharge of superior collicular neurons during saccades made to moving targets." Vol. 76 (5), 3573-7.

Kim, J. S., Greene, M. J., *et al.* (2014), "Space-time wiring specificity supports direction selectivity in the retina." *Nature*, vol. 509 (7500), 331-6.

Kim, I.-J., Zhang, Y., Yamagata, M., Meister, M., and Sanes, J. R. (2008), "Molecular identification of a retinal cell type that responds to upward motion." *Nature*, vol. 452 (7186), 478-82.

Kirschfeld, K. (1967), "Die Projektion der optischen Umwelt auf das Raster der Rhabdomere im Komplexauge von *Musca*." *Experimental Brain Research*, vol. 3 (3), 248-70.

Kitamoto, T. (2001), "Conditional modification of behavior in *Drosophila* by targeted expression of a temperature-sensitive *shibire* allele in defined neurons." *Journal of Neurobiology*, vol. 47 (2), 81-92.

Klapoetke, N. C., Murata, Y., *et al.* (2014), "Independent optical excitation of distinct neural populations." *Nature Methods*, vol. 11 (3), 338-46.

Knoll, M. and Ruska, E. (1932), "Das Elektronenmikroskop." *Zeitschrift für Physik*, vol. 78 (5-6), 318-39.

Köhler, T., Röchter, F., Lindemann, J. P., and Möller, R. (2009), "Bio-inspired motion detection in an FPGA-based smart camera module." *Bioinspiration & biomimetics*, vol. 4 (1), 1-10.

Komatsu, H. and Wurtz, R. H. (1988), "Relation of cortical areas MT and MST to pursuit eye movements. I. Localization and visual properties of neurons." Vol. 60 (2), 580-603.

Krapp, H. G., Hengstenberg, B., and Hengstenberg, R. (1998), "Dendritic structure and receptive-field organization of optic flow processing interneurons in the fly." Vol. 79 (4), 1902-17.

Krapp, H. G. and Hengstenberg, R. (1996), "Estimation of self-motion by optic flow processing in single visual interneurons." *Nature*, vol. 384 (6608), 463-6.

Kunze, P. (1961), "Untersuchung des Bewegungssehens fixiert fliegender Bienen." *Zeitschrift für vergleichende Physiologie*, vol. 44 (6), 656-84.

Lai, S.-L. and Lee, T. (2006), "Genetic mosaic with dual binary transcriptional systems in *Drosophila*." *Nature Neuroscience*, vol. 9 (5), 703-9.

Land, M. F. (1997), "Visual acuity in insects." *Annual Review of Entomology*, vol. 42 (1), 147-77.

Land, M. F. (1999), "Motion and vision: Why animals move their eyes." *Journal of Comparative Physiology A*, vol. 185 (4), 341-52.

Land, M. F. and Collett, T. S. (1974), "Chasing behavior of houseflies (*Fannia canicularis*): A description and analysis." *Journal of Comparative Physiology*, vol. 89 (4), 331-57.

Laughlin, S. B. and Hardie, R. C. (1978), "Common strategies for light adaptation in the peripheral visual systems of fly and dragonfly." *Journal of Comparative Physiology A*, vol. 128 (4), 319-40.

Laughlin, S. B. and Osorio, D. (1989), "Mechanisms for neural signal enhancement in the blowfly compound eye." *Journal of Experimental Biology*, vol. 144 (1), 113-46.

Lee, S.-H., Kwan, A. C., *et al.* (2012), "Activation of specific interneurons improves V1 feature selectivity and visual perception." *Nature*, vol. 488 (7411), 379-83.

Livingstone, M. S. (1998), "Mechanisms of direction selectivity in macaque V1." *Neuron*, vol. 20 (3), 509-26.

Lott, G. K., Rosen, M. J., and Hoy, R. R. (2007), "An inexpensive submillisecond system for walking measurements of small animals based on optical computer mouse technology." *Journal of Neuroscience Methods*, vol. 161 (1), 55-61.

Luan, H., Peabody, N. C., Vinson, C. R., and White, B. H. (2006), "Refined spatial manipulation of neuronal function by combinatorial restriction of transgene expression." *Neuron*, vol. 52 (3), 425-36.

Ma, K. Y., Chirarattananon, P., Fuller, S. B., and Wood, R. J. (2013), "Controlled flight of a biologically inspired, insect-scale robot." *Science*, vol. 340 (6132), 603-7.

Maimon, G., Straw, A. D., and Dickinson, M. H. (2008), "A simple vision-based algorithm for decision making in flying *Drosophila*." *Current Biology*, vol. 18 (6), 464-70.

Maimon, G., Straw, A. D., and Dickinson, M. H. (2010), "Active flight increases the gain of visual motion processing in *Drosophila*." *Nature Neuroscience*, vol. 13 (3), 393-9.

Mank, M., Santos, A. F., *et al.* (2008), "A genetically encoded calcium indicator for chronic in vivo two-photon imaging." *Nature Methods*, vol. 5 (9), 805-11.

Markram, H. (2006), "The blue brain project." *Nature Reviews Neuroscience*, vol. 7 (2), 153-60.

Masland, R. H. (2013), "Neuroscience: Accurate maps of visual circuitry." *Nature*, vol. 500 (7461), 154-5.

Masson, G. S. and Goffart, L. (2013), "Fixate and stabilize: Shall the twain meet?" *Nature Neuroscience*, vol. 16 (6), 663-4.

Masson, G. S. and Perrinet, L. U. (2012), "The behavioral receptive field underlying motion integration for primate tracking eye movements." *Neuroscience and Biobehavioral Reviews*, vol. 36 (1), 1-25.

Mauss, A. S., Meier, M., Serbe, E., and Borst, A. (2014), "Optogenetic and pharmacologic dissection of feedforward inhibition in *Drosophila* motion vision." *Journal of Neuroscience*, vol. 34 (6), 2254-63.

McBeath, M. K., Shaffer, D. M., and Kaiser, M. K. (1995), "How baseball outfielders determine where to run to catch fly balls." *Science*, vol. 268 (5210), 569-73.

McGuire, S. E., Le, P. T., Osborn, A. J., Matsumoto, K., and Davis, R. L. (2003), "Spatiotemporal rescue of memory dysfunction in *Drosophila*." *Science*, vol. 302 (5651), 1765-8.

Meier, M., Serbe, E., Maisak, M. S., Haag, J., Dickson, B. J., and Borst, A. (2014), "Neural circuit components of the *Drosophila* OFF motion vision pathway." *Current Biology*, vol. 24 (4), 385-92.

Meinertzhagen, I. A. and O'Neil, S. D. (1991), "Synaptic organization of columnar elements in the lamina of the wild type in *Drosophila melanogaster.*" *Journal of Comparative Neurology*, vol. 305 (2), 232-63.

Menne, D. and Spatz, H.-C. (1977), "Colour vision in *Drosophila melanogaster.*" *Journal of Comparative Physiology A*, vol. 114 (3), 301-12.

Missal, M., Lefevre, P., Delinte, A., Crommelinck, M., and Roucoux, A. (1996), "Smooth eye movements evoked by electrical stimulation of

the cat's superior colliculus." *Experimental Brain Research*, vol. 107 (3), 382-90.

Morgan, T. H. (1910), "Sex limited inheritance in *Drosophila*." *Science*, vol. 32 (1), 120-2.

Movshon, J. A. and Newsome, W. T. (1996), "Visual response properties of striate cortical neurons projecting to area MT in macaque monkeys." *Journal of Neuroscience*, vol. 16 (23), 7733-41.

Mronz, M. and Lehmann, F.-O. (2008), "The free-flight response of *Drosophila* to motion of the visual environment." *Journal of Experimental Biology*, vol. 211 (13), 2026-45.

Muijres, F. T., Elzinga, M. J., Melis, J. M., and Dickinson, M. H. (2014), "Flies evade looming targets by executing rapid visually directed banked turns." *Science*, vol. 344 (6180), 172-7.

Muller, H. J. (1928), "The production of mutations by x-rays." *Proceedings of the National Academy of Sciences of the United States of America*, vol. 14 (9), 714-26.

Nagel, G., Brauner, M., Liewald, J. F., Adeishvili, N., Bamberg, E., and Gottschalk, A. (2005), "Light activation of channelrhodopsin-2 in excitable cells of *Caenorhabditis elegans* triggers rapid behavioral responses." *Current Biology*, vol. 15 (24), 2279-84.

Nagel, G., Szellas, T., *et al.* (2003), "Channelrhodopsin-2, a directly light-gated cation-selective membrane channel." *Proceedings of the National Academy of Sciences of the United States of America*, vol. 100 (24), 13940-5.

Nakai, J., Ohkura, M., and Imoto, K. (2001), "A high signal-to-noise Ca(2+) probe composed of a single green fluorescent protein." *Nature biotechnology*, vol. 19 (2), 137-41.

Neuser, K., Triphan, T., Mronz, M., Poeck, B., and Strauss, R. (2008), "Analysis of a spatial orientation memory in *Drosophila*." *Nature*, vol. 453 (7199), 1244-8.

Newsome, W. T., Britten, K. H., and Movshon, J. A. (1989), "Neuronal correlates of a perceptual decision." *Nature*, vol. 341 (6237), 52-4.

Newsome, W. T., Wurtz, R. H., Dürsteler, M. R., and Mikami, A. (1985), "Deficits in visual motion processing following ibotenic acid lesions of the middle temporal visual area of the macaque monkey." *Journal of Neuroscience*, vol. 5 (3), 825-40.

Nordström, K., Barnett, P. D., and O'Carroll, D. C. (2006), "Insect detection of small targets moving in visual clutter." *PLoS Biology*, vol. 4 (3), e54.

Nordström, K. and O'Carroll, D. C. (2006), "Small object detection neurons in female hoverflies." *Proceedings of the Royal Society B: Biological Sciences*, vol. 273 (1591), 1211-6.

O'Carroll, D. C. (1993), "Feature-detecting neurons in dragonflies." *Nature*, vol. 362 (6420), 541-3.

O'Carroll, D. C., Shoemaker, P. A., and Brinkworth, R. S. A. (2007), "Bioinspired optical rotation sensor." In *Proceedings of the SPIE Symposium on Smart Structures, Devices, and Systems III*, ed. by S. F. Al-Sarawi, 1-12.

Ofstad, T. A., Zuker, C. S., and Reiser, M. B. (2011), "Visual place learning in *Drosophila melanogaster*." *Nature*, vol. 474 (7350), 204-7.

Orban de Xivry, J.-J. and Lefèvre, P. (2007), "Saccades and pursuit: two outcomes of a single sensorimotor process." *Journal of Physiology-London*, vol. 584 (1), 11-23.

O'Tousa, J. E., Baehr, W., Martin, R. L., Hirsh, J., Pak, W. L., and Applebury, M. L. (1985), "The *Drosophila ninaE* gene encodes an opsin." *Cell*, vol. 40 (4), 839-50.

Otsuna, H. and Ito, K. (2006), "Systematic analysis of the visual projection neurons of *Drosophila melanogaster*. I. Lobula-specific pathways." *Journal of Comparative Neurology*, vol. 497 (6), 928-58.

Otsuna, H., Shinomiya, K., and Ito, K. (2014), "Parallel neural pathways in higher visual centers of the *Drosophila* brain that mediate wavelength-specific behavior." *Frontiers in Neural Circuits*, vol. 8, 1-12.

Oyster, C. W. and Barlow, H. B. (1967), "Direction-selective units in rabbit retina: distribution of preferred directions." *Science*, vol. 155 (3764), 841-2.

Pfeiffer, B. D., Ngo, T.-T. B., Hibbard, K. L., Murphy, C., Jenett, A., Truman, J. W., and Rubin, G. M. (2010), "Refinement of tools for targeted gene expression in *Drosophila*." *Genetics*, vol. 186 (2), 735-55.

Pfeiffer, B. D., Truman, J. W., and Rubin, G. M. (2012), "Using translational enhancers to increase transgene expression in *Drosophila*." *Proceedings of the National Academy of Sciences of the United States of America*, vol. 109 (17), 6626-31.

Pick, B. (1974), "Visual flicker induces orientation behaviour in the fly *Musca*." *Zeitschrift für Naturforschung C*, vol. 29, 310-2.

Pick, B. (1976), "Visual pattern discrimination as an element of the fly's orientation behaviour." *Biological Cybernetics*, vol. 23 (3), 171-80.

Poggio, T. A. and Reichardt, W. (1973), "A theory of the pattern induced flight orientation of the fly *Musca domestica*." *Kybernetik*, vol. 12 (4), 185-203.

Poggio, T. A. and Reichardt, W. (1976), "Visual control of orientation behaviour in the fly. Part II. Towards the underlying neural interactions." *Quarterly Reviews of Biophysics*, vol. 9 (3), 377-438.

Portelli, G., Ruffier, F., and Franceschini, N. (2010), "Honeybees change their height to restore their optic flow." *Journal of Comparative Physiology A*, vol. 196 (4), 307-13.

Potter, C. J., Tasic, B., Russler, E. V., Liang, L., and Luo, L. (2010), "The Q system: a repressible binary system for transgene expression, lineage tracing, and mosaic analysis." *Cell*, vol. 141 (3), 536-48.

Raghu, S. V. and Borst, A. (2011), "Candidate glutamatergic neurons in the visual system of *Drosophila*." *PLoS ONE*, vol. 6 (5), 1-11.

Raghu, S. V., Reiff, D. F., and Borst, A. (2011), "Neurons with cholinergic phenotype in the visual system of *Drosophila*." *Journal of Comparative Neurology*, vol. 519 (1), 162-76.

Reichardt, W. (1973), "Musterinduzierte Flugorientierung: Verhaltens-Versuche an der Fliege *Musca domestica*." *Die Naturwissenschaften*, vol. 60 (3), 122-38.

Reichardt, W. and Poggio, T. A. (1975), "A theory of the pattern induced flight orientation of the fly *Musca domestica* II." *Biological Cybernetics*, vol. 18 (2), 69-80.

Reichardt, W. and Poggio, T. A. (1976), "Visual control of orientation behaviour in the fly. Part I. A quantitative analysis." *Quarterly Reviews of Biophysics*, vol. 9 (3), 311-75.

Reichardt, W. and Wenking, H. (1969), "Optical detection and fixation of objects by fixed flying flies." *Die Naturwissenschaften*, vol. 56 (8), 424-5.

Reiff, D. F., Plett, J., Mank, M., Griesbeck, O., and Borst, A. (2010), "Visualizing retinotopic half-wave rectified input to the motion detection circuitry of *Drosophila*." *Nature Neuroscience*, vol. 13 (8), 973-8.

Reiser, M. B. and Dickinson, M. H. (2010), "*Drosophila* fly straight by fixating objects in the face of expanding optic flow." *Journal of Experimental Biology*, vol. 213 (10), 1771-81.

Rister, J., Pauls, D., *et al.* (2007), "Dissection of the peripheral motion channel in the visual system of *Drosophila melanogaster*." *Neuron*, vol. 56 (1), 155-70.

Rubin, G. M. and Spradling, A. C. (1982), "Genetic transformation of *Drosophila* with transposable element vectors." *Science*, vol. 218 (4570), 348-53.

Rust, N. C., Mante, V., Simoncelli, E. P., and Movshon, J. A. (2006), "How MT cells analyze the motion of visual patterns." *Nature Neuroscience*, vol. 9 (11), 1421-31.

Sanes, J. R. and Zipursky, S. L. (2010), "Design principles of insect and vertebrate visual systems." *Neuron*, vol. 66 (1), 15-36.

Schnaitmann, C., Garbers, C., Wachtler, T., and Tanimoto, H. (2013), "Color discrimination with broadband photoreceptors." *Current Biology*, vol. 23 (23), 2375-82.

Schnell, B., Joesch, M., *et al.* (2010), "Processing of horizontal optic flow in three visual interneurons of the *Drosophila* brain." Vol. 103 (3), 1646-57.

Schnell, B., Raghu, S. V., Nern, A., and Borst, A. (2012), "Columnar cells necessary for motion responses of wide-field visual interneurons in *Drosophila*." *Journal of Comparative Physiology A*, vol. 198 (5), 389-95.

Schümperli, R. A. (1973), "Evidence for colour vision in *Drosophila melanogaster* through spontaneous phototactic choice behaviour." *Journal of Comparative Physiology*, vol. 86 (1), 77-94.

Scott, E. K., Raabe, T., and Luo, L. (2002), "Structure of the vertical and horizontal system neurons of the lobula plate in *Drosophila*." *Journal of Comparative Neurology*, vol. 454 (4), 470-81.

Seeds, A. M., Ravbar, P., Chung, P., Hampel, S., Midgley, F. M., Mensh, B. D., and Simpson, J. H. (2014), "A suppression hierarchy among competing motor programs drives sequential grooming in *Drosophila*." *eLife*, vol. 3, 1-23.

Seelig, J. D., Chiappe, M. E., Lott, G. K., Dutta, A., Osborne, J. E., Reiser, M. B., and Jayaraman, V. (2010), "Two-photon calcium imaging from head-fixed *Drosophila* during optomotor walking behavior." *Nature Methods*, vol. 7 (7), 535-40.

Seelig, J. D. and Jayaraman, V. (2013), "Feature detection and orientation tuning in the *Drosophila* central complex." *Nature*, vol. 503 (7475), 262-6.

Shaw, S. R., Fröhlich, A., and Meinertzhagen, I. A. (1989), "Direct connections between the R7/8 and R1-6 photoreceptor subsystems in the dipteran visual system." *Cell and Tissue Research*, vol. 257 (2), 295-302.

Shinomiya, K., Karuppudurai, T., Lin, T.-Y., Lu, Z., Lee, C.-H., and Meinertzhagen, I. A. (2014), "Candidate neural substrates for off-edge motion detection in *Drosophila*." *Current Biology*, vol. 24 (10), 1062-70.

Silies, M., Gohl, D. M., Fisher, Y. E., Freifeld, L., Clark, D. A., and Clandinin, T. R. (2013), "Modular use of peripheral input channels tunes motion-detecting circuitry." *Neuron*, vol. 79 (1), 111-27.

Simpson, J. H. (2009), "Mapping and manipulating neural circuits in the fly brain." In *Genetic Dissection of Neural Circuits and Behavior*, ed. by S. F. Goodwin, Elsevier, 79-143.

Song, Y. M., Xie, Y., *et al.* (2013), "Digital cameras with designs inspired by the arthropod eye." *Nature*, vol. 497 (7447), 95-9.

Srinivasan, M. V., Lehrer, M., Kirchner, W. H., and Zhang, S. W. (1991), "Range perception through apparent image speed in freely flying honeybees." *Visual Neuroscience*, vol. 6 (5), 519-35.

Srinivasan, M. V., Zhang, S., Lehrer, M., and Collett, T. S. (1996), "Honeybee navigation en route to the goal: Visual flight control and odometry." *Journal of Experimental Biology*, vol. 199 (1), 237-44.

St Johnston, D. (2002), "The art and design of genetic screens: *Drosophila melanogaster*." *Nature Reviews Genetics*, vol. 3 (3), 176-88.

Strausfeld, N. J. (1976), *Atlas of an Insect Brain*, Springer, New York.

Straw, A. D., Branson, K., Neumann, T. R., and Dickinson, M. H. (2011), "Multi-camera real-time three-dimensional tracking of multiple flying animals." *Journal of the Royal Society Interface*, vol. 8 (56), 395-409.

Strother, J. A., Nern, A., and Reiser, M. B. (2014), "Direct observation of ON and OFF pathways in the *Drosophila* visual system." *Current Biology*, vol. 24 (9), 976-83.

Suthers, R. A. (1966), "Optomotor responses by echolocating bats." *Science*, vol. 152 (3725), 1102-4.

Suver, M. P., Mamiya, A., and Dickinson, M. H. (2012), "Octopamine neurons mediate flight-induced modulation of visual processing in *Drosophila*." *Current Biology*, vol. 22 (24), 2294-302.

Sweeney, S. T., Broadie, K., Keane, J., Niemann, H., and O'Kane, C. J. (1995), "Targeted expression of tetanus toxin light chain in *Drosophila* specifically eliminates synaptic transmission and causes behavioral defects." *Neuron*, vol. 14 (2), 341-51.

Takemura, S.-Y., Bharioke, A., *et al.* (2013), "A visual motion detection circuit suggested by *Drosophila* connectomics." *Nature*, vol. 500 (7461), 175-81.

Takemura, S.-Y., Karuppudurai, T., Ting, C.-Y., Lu, Z., Lee, C.-H., and Meinertzhagen, I. A. (2011), "Cholinergic circuits integrate neighboring visual signals in a *Drosophila* motion detection pathway." *Current Biology*, vol. 21 (24), 2077-84.

Takemura, S.-Y., Lu, Z., and Meinertzhagen, I. A. (2008), "Synaptic circuits of the *Drosophila* optic lobe: The input terminals to the medulla." *Journal of Comparative Neurology*, vol. 509 (5), 493-513.

Tammero, L. F., Frye, M. A., and Dickinson, M. H. (2004), "Spatial organization of visuomotor reflexes in *Drosophila*." *Journal of Experimental Biology*, vol. 207 (1), 113-22.

Tauber, E. S. and Atkin, A. (1968), "Optomotor responses to monocular stimulation: relation to visual system organization." *Science*, vol. 160 (3834), 1365-7.

Theobald, J. C., Duistermars, B. J., Ringach, D. L., and Frye, M. A. (2008), "Flies see second-order motion." *Current Biology*, vol. 18 (11), R464-5.

Trischler, C., Kern, R., and Egelhaaf, M. (2010), "Chasing behavior and optomotor following in free-flying male blowflies: Flight performance and interactions of the underlying control systems." *Frontiers in Behavioral Neuroscience*, vol. 4, 1-13.

Tuthill, J. C., Nern, A., Holtz, S. L., Rubin, G. M., and Reiser, M. B. (2013), "Contributions of the 12 neuron classes in the fly lamina to motion vision." *Neuron*, vol. 79 (1), 128-40.

Tuthill, J. C., Nern, A., Rubin, G. M., and Reiser, M. B. (2014), "Wide-field feedback neurons dynamically tune early visual processing." *Neuron*, vol. 82 (4), 887-95.

Van Santen, J. P. and Sperling, G. (1985), "Elaborated Reichardt detectors." *Journal of the Optical Society of America A*, vol. 2 (2), 300-21.

Velez, M. M., Wernet, M. F., Clark, D. A., and Clandinin, T. R. (2014), "Walking *Drosophila* align with the e-vector of linearly polarized light through directed modulation of angular acceleration." *Journal of Comparative Physiology A*, vol. 200 (6), 603-14.

Venken, K. J. T., Simpson, J. H., and Bellen, H. J. (2011), "Genetic manipulation of genes and cells in the nervous system of the fruit fly." *Neuron*, vol. 72 (2), 202-30.

Vogelstein, J. T., Park, Y., Ohyama, T., Kerr, R. A., Truman, J. W., Priebe, C. E., and Zlatic, M. (2014), "Discovery of brainwide neural-behavioral maps via multiscale unsupervised structure learning." *Science*, vol. 344 (6182), 386-92.

Wallach, H. (1935), "Über visuell wahrgenommene Bewegungsrichtung." *Psychologische Forschung*, vol. 20 (1), 325-80.

Wardill, T. J., List, O., *et al.* (2012), "Multiple spectral inputs improve motion discrimination in the *Drosophila* visual system." *Science*, vol. 336 (6083), 925-31.

Wehner, R. (1972), "Spontaneous pattern preferences of *Drosophila melanogaster* to black areas in various parts of the visual field." *Journal of Insect Physiology*, vol. 18 (8), 1531-43.

Wehner, R. (2001), "Polarization vision - A uniform sensory capacity?" *Journal of Experimental Biology*, vol. 204 (14), 2589-96.

Wehrhahn, C. (1981), "Fast and slow flight torque responses in flies and their possible role in visual orientation behaviour." *Biological Cybernetics*, vol. 40 (3), 213-21.

Wehrhahn, C. and Hausen, K. (1980), "How is tracking and fixation accomplished in the nervous system of the fly?" *Biological Cybernetics*, vol. 38 (3), 179-86.

Weir, P. T. and Dickinson, M. H. (2012), "Flying *Drosophila* orient to sky polarization." *Current Biology*, vol. 22 (1), 21-7.

Wernet, M. F., Velez, M. M., *et al.* (2012), "Genetic dissection reveals two separate retinal substrates for polarization vision in *Drosophila*." *Current Biology*, vol. 22 (1), 12-20.

Wietek, J., Wiegert, J. S., *et al.* (2014), "Conversion of channelrhodopsin into a light-gated chloride channel." *Science*, vol. 344 (6182), 409-12.

Wilson, R. I., Turner, G. C., and Laurent, G. (2004), "Transformation of olfactory representations in the *Drosophila* antennal lobe." *Science*, vol. 303 (5656), 366-70.

Wolf, R., Gebhardt, B., Gademann, R., and Heisenberg, M. (1980), "Polarization sensitivity of course control in *Drosophila melanogaster*." *Journal of Comparative Physiology A*, vol. 139 (3), 177-91.

Wolf, R. and Heisenberg, M. (1986), "Visual orientation in motion-blind flies is an operant behavior." *Nature*, vol. 323 (6084), 154-6.

Xiong, Y., Lv, H., Gong, Z., and Liu, L. (2010), "Fixation and locomotor activity are impaired by inducing tetanus toxin expression in adult *Drosophila* brain." *Fly*, vol. 4 (3), 194-203.

Yamaguchi, S., Desplan, C., and Heisenberg, M. (2010), "Contribution of photoreceptor subtypes to spectral wavelength preference in *Drosophila*." *Proceedings of the National Academy of Sciences of the United States of America*, vol. 107 (12), 5634-9.

Yamaguchi, S., Wolf, R., Desplan, C., and Heisenberg, M. (2008), "Motion vision is independent of color in *Drosophila*." *Proceedings of the National Academy of Sciences of the United States of America*, vol. 105 (12), 4910-5.

Yonehara, K. and Roska, B. (2013), "Motion detection: Neuronal circuit meets theory." *Cell*, vol. 154 (6), 1188-9.

Yoshida, K., Watanabe, D., Ishikane, H., Tachibana, M., Pastan, I., and Nakanishi, S. (2001), "A key role of starburst amacrine cells in originating retinal directional selectivity and optokinetic eye movement." *Neuron*, vol. 30 (3), 771-80.

Zhang, X., Liu, H., Lei, Z., Wu, Z., and Guo, A. (2013), "Lobula-specific visual projection neurons are involved in perception of motion-defined second-order motion in *Drosophila*." *Journal of Experimental Biology*, vol. 216 (3), 524-34.

Zhou, Y. X. and Baker, C. L. (1993), "A processing stream in mammalian visual cortex neurons for non-Fourier responses." *Science*, vol. 261 (5117), 98-101.

Zhou, Y., Ji, X., Gong, H., Gong, Z., and Liu, L. (2012), "Edge detection depends on achromatic channel in *Drosophila melanogaster*." *Journal of Experimental Biology*, vol. 215 (19), 3478-87.

Zhu, Y., Nern, A., Zipursky, S. L., and Frye, M. A. (2009), "Peripheral visual circuits functionally segregate motion and phototaxis behaviors in the fly." *Current Biology*, vol. 19 (7), 613-9.

Zihl, J., von Cramon, D., and Mai, N. (1983), "Selective disturbance of movement vision after bilateral brain damage." *Brain: A Journal of Neurology*, vol. 106 (2), 313-40.

AUTHOR CONTRIBUTIONS

The author contributions to the papers presented in this cumulative thesis were as follows:

- Paper I: "Object tracking in motion-blind flies." **Armin Bahl**[*], Tabea Schilling, Georg Ammer and Alexander Borst. — **A.Ba.**[*] and A.Bo. designed the study. **A.Ba.**[*] set up the locomotion recorder and the stimulus display, and wrote the software for reading the behavioral output and displaying the stimulus. **A.Ba.**[*] and T.S. performed all of the behavioral experiments and evaluated the data. G.A. performed the electrophysiological recordings from LPTCs and analyzed the data. A.Bo. carried out modeling work. A.Bo. and **A.Ba.**[*] wrote the manuscript with the help of the other authors.

- Paper II: "A directional tuning map of *Drosophila* elementary motion detectors." Matthew S. Maisak, Jürgen Haag, Georg Ammer, Etienne Serbe, Matthias Meier, Aljoscha Leonhardt, Tabea Schilling, **Armin Bahl**[*], Gerald M. Rubin, Aljoscha Nern, Barry J. Dickson, Dierk F. Reiff, Elisabeth Hopp and Alexander Borst. — M.S.M. and J.H. jointly performed and, together with A.Bo., evaluated all calcium imaging experiments. G.A., E.S. and M.M. recorded from tangential cells. A.L., T.S. and **A.Ba.**[*] performed the behavioral experiments and analyzed the data. G.R., B.D. and A.N. generated the driver lines and characterized their expression pattern. D.F.R. performed preliminary imaging experiments. E.H. helped with programming and developed the PMT shielding for the two-photon microscope. A.Bo. designed the study and wrote the manuscript with the help of all authors.

- Paper III: "Bio-inspired visual ego-rotation sensor for MAVs." Johannes Plett, **Armin Bahl**[*], Martin Buss, Kolja Kühnlenz, Alexander Borst. — J.P. and A.Bo. designed the study. M.B., K.H. and A.Bo. supervised the study. J.P. did all microchip engineering, programming and data analysis. **A.Ba.**[*] built the virtual environment setup and programmed the visual stimuli. J.P. and A.Bo. wrote the paper with help of the other authors.

I hereby certify that the information above is true and accurate.

Munich, 21st of November 2014,

Armin Bahl

.....

Alexander Borst

.....

EIDESSTATTLICHE VERSICHERUNG (AFFIDAVIT)

Hiermit versichere ich an Eides statt, dass ich die vorliegende Dissertation "The role of direction-selective visual interneurons T4 and T5 in *Drosophila* orientation behavior" selbstständig angefertigt habe, mich außer der angegebenen keiner weiteren Hilfsmittel bedient und alle Erkenntnisse, die aus dem Schrifttum ganz oder annähernd übernommen sind, als solche kenntlich gemacht und nach ihrer Herkunft unter Bezeichnung der Fundstelle einzeln nachgewiesen habe.

I hereby confirm that the dissertation "The role of direction-selective visual interneurons T4 and T5 in *Drosophila* orientation behavior" is the result of my own work and that I have only used sources or materials listed and specified in the dissertation.

München, den 21. November 2014,

Munich, 21st of November 2014,

Armin Bahl

.....